ABSTRACT

KUMAR, PRABHAT. Development of Bio-nanocomposite Films with Enhanced Mechanical and Barrier Properties Using Extrusion Processing. (Under the direction of Dr. K.P. Sandeep and Dr. V.D. Truong.)

Recently, a new class of materials represented by bio-nanocomposites (biopolymer matrix reinforced with nanoparticles) has proven to be a promising option in improving mechanical and barrier properties of biopolymers derived from renewable sources. Therefore, the current study was undertaken with the main objective of developing bio-nanocomposite films based on soy protein isolate (SPI) and montmorillonite (MMT) with enhanced mechanical and barrier properties by melt intercalation using extrusion processing. Effects of extrusion processing parameters (screw speed and barrel temperature distribution) and type (natural and modified) and content (0-15%) of MMT on the structure (degree of intercalation and exfoliation) and properties (mechanical, dynamic mechanical, thermal stability, and water vapor permeability) of SPI-MMT bio-nanocomposites were studied.

The arrangement of MMT in the bio-nanocomposite matrix ranged from exfoliated to intercalated depending on the type (natural and modified) and content of MMT. The results showed that extrusion of SPI and MMTs resulted in bio-nanocomposites with exfoliated structures at lower MMT content (5%) for natural (Cloisite Na^+) as well as modified MMTs (Cloisite 20A and Cloisite 30B). At higher MMT content (15%), structure of bio-nanocomposites ranged from intercalated for Cloisite Na^+ and Cloisite 20A to disordered intercalated for Cloisite 30B.

Higher screw speed and barrel temperature resulted in films with improved mechanical and dynamic mechanical properties. Higher screw speed also resulted in films with lower water vapor permeability (WVP). However, the effect of barrel temperature

distribution on WVP was insignificant. There was a significant improvement in mechanical and dynamic mechanical properties, thermal stability, and WVP of the films with the addition of natural and modified MMTs. At a MMT content of 5%, bio-nanocomposite films based on modified MMTs had better mechanical, dynamic mechanical, and water barrier properties as compared to those based on natural MMT. However, films based on modified MMTs were thermally less stable at temperatures higher than 500 °C as compared to films based on natural MMT.

This study shows the potential of films based on SPI and Cloisite 30B to replace some of the existing plastics such as LDPE and PVDC. However, much higher WVP values of these films as compared to those of LDPE and PVDC might limit the application of these bio-nanocomposite films to packaging of high moisture foods such as fresh fruits and vegetables. Further research is required to improve the properties of these SPI-MMT bio-nanocomposite films for commercial application.

Development of Bio-nanocomposite Films with Enhanced Mechanical and Barrier Properties Using Extrusion Processing

by
Prabhat Kumar

A dissertation submitted to the Graduate Faculty of
North Carolina State University
In partial fulfillment of the
Requirements for the degree of
Doctor of Philosophy

Food Science

Raleigh, North Carolina

2009

APPROVED BY:

Dr. E. Allen Foegeding	Dr. Russell E. Gorga
Dr. Van Den Truong (Co-chair of Advisory Committee)	Dr. K.P. Sandeep (Chair of Advisory Committee)

DEDICATION

Dedicated to

the most important persons

in my life,

my parents

for giving me this life

and

my wife

for making this life wonderful

BIOGRAPHY

Prabhat Kumar was born on June 9, 1982 in Patna, India. He graduated from Indian Institute of Technology (IIT), Kharagpur in 2003, with a Bachelor of Technology (Honors) degree in Agricultural and Food Engineering. After his graduation, he worked for Coca Cola India as a Graduate Engineer Trainee for 1 year. In the fall of 2004, he began his MS degree in the Department of Food Science at North Carolina State University under the guidance of Dr. K.P. Sandeep and Dr. Josip Simunovic. His research during MS focused on aseptic processing of low-acid multiphase foods using a continuous flow microwave system. Upon completion of MS degree, Prabhat started Ph.D. under the guidance of Dr. K.P. Sandeep and Dr. Van-Den Truong. His Ph.D. research focuses on development of bio-nanocomposite films with enhanced properties using extrusion processing. During his Ph.D., Prabhat got married to Pallavi in February 2008. Upon completion of Ph.D., he will join Frito Lay, Inc. as a research scientist in Plano, Texas.

ACKNOWLEDGMENTS

There are many people to be mentioned by name, but you know who you are. Teachers, colleagues, friends, and family members – your investment in me is partly responsible for everything I accomplish. However, the role of certain individuals was crucial in completing this work.

First and foremost, I am deeply indebted to my advisor, Dr. K.P. Sandeep, for his guidance, support, and encouragement throughout this work. He understands the individual needs of his students and generates thoughtful insight about every aspect of science. His expert advice and wisdom helped me finish this work and made my study under his supervision enjoyable. I would like to thank Dr. Sajid Alavi for all the helpful discussions and advice. I would also like to thank my co-chair, Dr. Van-Den Truong, for his guidance and valuable suggestions.

I am grateful to my committee member and college bowl coach, Dr. Allen Foegeding, for his guidance and encouragement. His belief in my abilities helped me finish this work. He did a great job in coaching our college bowl team to win the college bowl national championship. I would like to thank my other committee member, Dr. Russell Gorga, for his suggestions and support during the course of this work. He also provided me access to use instruments in his lab, for which I am thankful.

Special thanks to Dr. Josip Simunovic for his constant advice, encouragement, and support during the course of this work. I really appreciate everything he has done for me. I would also like to thank Harry Reinitz, Joanna Foegeding, Gary Cartwright, Jack Canady,

Sharon Ramsey, Birgit Anderson, Nagarajan, Gail Liston, Roberto Garcia, Chuck Mooney, and Jonathan Pierce for their assistance in one way or the other.

I wish to thank all my friends and colleagues who have helped me and made my stay here such a pleasure. In particular, I thank Saurabh Sharma for his constant encouragement and his confidence in me to do well in life.

I thank my parents, sisters, and brother for their love, affection, and support. I also thank my amazing wife for her love, continuous support, patience, and confidence in me. I certainly didn't deserve such a special person. Without her, this work would not have been the same. I would also like to thank her dad who has been the greatest source of inspiration for us.

TABLE OF CONTENTS

LIST OF TABLES

LIST OF FIGURES

Chapter 1

INTRODUCTION

Foods are packaged to protect them from the environment and to maintain them in proper condition during shipping, distribution, retailing, and home storage. However, food packaging must balance protection of food with other issues such as impact on environment. There has been a 37% increase in municipal solid waste (MSW) from 179.6 million tons in 1988 to 245.7 million tons in 2005. Packaging has maximum contribution to total solid wastes at 31.2%. Food packaging alone accounts for almost two-thirds of total packaging wastes by volume. Therefore, food packaging has become a focus of waste reduction efforts because proper waste management is important to protect human health and environment (Marsh and Bugusu 2007).

Glass, metal, paper and paperboard, and plastics have been traditionally used in food packaging. The use of plastics over glass and metals has continued to increase because they offer several advantages over other materials. Plastics are inexpensive, light-weight, and chemically inert. Plastics are heat sealable, easy to print, and offer flexibility in fabricating different shapes of containers. Plastics are made by condensation polymerization or addition polymerization of monomers of hydrocarbons or hydrocarbon-like materials. Thus, they find their origin in the petrochemical industry making them non-biodegradable and non-renewable. The non-biodegradable and non-renewable nature of plastics overshadows its merits (Marsh and Bugusu 2007).

The non-degradable and non-renewable nature of plastic packaging has led to a renewed interest in packaging materials based on biopolymers derived from renewable

sources. The use of biopolymer-based packaging materials can solve the waste disposal problem to a certain extent. Such biopolymers include naturally occurring proteins, cellulose, starches, and other polysaccharides and those synthesized chemically from naturally derived monomers such as lactic acid. Commercialization of biopolymer-based packaging materials has already started. Natureworks, LLC (Minnetonka, MN) manufactures polylactide from corn sugar. The polymer can be hydrolyzed back to lactic acid. Wal-Mart stores, Inc. is already using polylactide to package fresh-cut produce (Marsh and Bugusu 2007). Currently, bio-based packaging materials constitutes about 1-2% of the food packaging market even though food packaging accounts for about 40 percent of the $460 billion global packaging industry (Jahangir and Leber 2007). According to a report, bio-based packaging materials will grow at an annual rate of 17.3% between 2007 and 2012. The report predicts that the current capacity of bio-based packaging materials will increase from about 0.185 million tons annually to 0.545 million tons by 2012 (Schlechter 2007).

Protein-based films have become a research focus because of their better film forming properties, low cost, and biodegradable nature. Protein films have been developed from soy protein, whey protein, casein, collagen, corn zein, gelatin, and wheat gluten. Among all the protein sources, soy proteins have attracted attention as a potential source for bio-based packaging materials because it has excellent film forming properties. Soy protein isolate (SPI) is a commercial form of soy protein that contains more than 90% protein. However, materials based on soy proteins cannot meet the requirements of a cost-effective film with mechanical and barrier properties similar to those of plastics.

Mechanical properties of interest in food packaging are tensile modulus (TM), tensile strength (TS), and percent elongation (%E) at break. Tensile modulus is a measure of stiffness of a material. Tensile strength is the maximum tensile stress a film can sustain whereas %E is an indication of flexibility of a film. Barrier properties of interest are water vapor permeability (WVP) and oxygen permeability (OP). Biopolymers made from SPI alone are extremely brittle. Plasticizers such as glycerol and polyethylene glycol impart flexibility to SPI-based biopolymer films. However, the use of plasticizers leads to significant decrease in TS of the films (Wang and others 1996). Soy protein-based films have been reported to have oxygen permeability (OP) similar to that of plastic films (Brandenburg and others 1993). However, they have higher water vapor permeability (WVP) as compared to plastic films due to the hydrophilic nature of proteins. Therefore, research has been geared to develop techniques to improve mechanical and water vapor barrier properties of soy protein-based packaging materials. Some of the techniques developed include chemical modification of biopolymers, addition of plasticizers such as glycerol, incorporation of other biodegradable polymers (with better properties) into biopolymers to produce material with intermediate properties, and addition of compatibilizers to increase miscibility of incompatible polymers to decrease interfacial energy and stabilize polymer blends. None of the above mentioned methods can produce a cost-effective film with mechanical and barrier properties similar to those of plastics. Therefore, there is a need to explore new techniques to produce biopolymer-based films with improved mechanical and barrier properties.

Nanotechnology involves study and use of materials at a scale of 1 to 100 nanometers. Nanotechnology exploits the fact that material properties could be very different

at a nanometer scale than at a macro level. Recently, a new class of materials represented by bio-nanocomposites has proven to be a promising option in improving mechanical and barrier properties. The bio-nanocomposites consist of a biopolymer matrix reinforced with particles (nanoparticles) having at least one dimension in the nanometer range (1-100 nm) and exhibit much improved properties due to high aspect ratio and high surface area of nanoparticles (Ray and Bousmina 2005; Rhim and Ng 2007; Zhao and others 2008). Clay minerals such as montmorillonite (MMT), hectorite, sapnotite, and laponite have proven to be very effective due to their unique structure and properties (Zeng and others 2005). MMT has very high surface area (750 m^2/g), high aspect ratio (> 50), and very high elastic modulus (178 GPa) (Dennis and others 2001; Fornes and Paul 2003). These unique properties of MMT can result in bio-nanocomposites with improved properties, which could potentially replace conventional packaging materials such as plastics. The bio-nanocomposites could be either thermoformed into trays and containers for food service or casted into films for food packaging applications.

There are four possible arrangements of layered clays dispersed in a polymer matrix – phase separated or immiscible (microcomposite), intercalated, exfoliated, and disordered intercalated (partially exfoliated). In an immiscible arrangement, platelets of layered clays exist as tactoids (stack of platelets) and the polymer encapsulates these tactoids. Intercalation occurs when a monolayer of extended polymer chains penetrates into the galleries (gap between layers of clay) of the layered silicates. Intercalation results in finite expansion (2-3 nm) of the silicate layers. However, these silicate layers remain parallel to each other. Extensive penetration of polymer chains into the galleries of layered silicate leads to

exfoliation or delamination of silicate layers. Clay platelets are separated by 10 nm or more during exfoliation. An exfoliated nanocomposite consists of nanoparticles distributed homogeneously throughout the polymer matrix (Dennis and others 2001; Zeng and others 2005).

Bio-nanocomposites can be obtained by several methods which include in-situ polymerization, solution exfoliation, and melt intercalation. In the in-situ polymerization method, monomers are intercalated into layered clays and subsequently polymerized via heat, radiation, or catalyst. In solution exfoliation, layered clays are exfoliated into single platelets using a solvent and the polymer is adsorbed onto the platelets by mixing in the clay suspension. In melt intercalation, layered clays are mixed with the polymer matrix in molten state (Zeng and others 2005).

Flexible bio-nanocomposite films with improved properties can be obtained by reinforcing SPI-plasticizer system with suitable filler materials such as MMT. Very few studies on SPI-MMT bio-nanocomposites have been reported in literature (Dean and Yu 2005; Rhim and others 2005; Chen and Zhang 2006; Yu and others 2007). These studies show that bio-nanocomposite films based on SPI and MMT could potentially achieve mechanical and barrier properties similar to those of plastics.

Melt intercalation in an extruder is one of the most promising techniques for preparing nanocomposites because of its ease and versatility. Layered clays (6-13 μm) are sheared and peeled apart into platelets (~1-10 nm) due to high shear mixing inside the extruder. These platelets are then mixed with the polymer matrix in molten state to achieve exfoliation (Dennis and others 2001). The same technique can be used to prepare

biopolymer-based nanocomposites in an extruder. Extrusion is one of the most important processing techniques to produce plastics on a commercial scale. Therefore, biopolymer-based nanocomposite films using extrusion will increase the potential for commercialization of these films. Feasibility of applying extrusion processing to produce biopolymers and biocomposites has been demonstrated (Ha and Padua 2001; Redl and others 1999; Zhang and others 2001; Mohanty and others 2005). Extrusion processing parameters such as screw speed and barrel temperature distribution have an important influence on the structure and properties of nanocomposites (Borse and Kamal 2006; Lertwimolnun and Vergnes 2007).

Exfoliation is the desirable arrangement for improving the properties of nanocomposites. However, exfoliation is harder to achieve during processing because layered clays such as MMT have a strong tendency to agglomerate because of their hydrophilic nature. Some of the approaches to break down nanoparticle agglomerates for producing exfoliated nanocomposites are – modification of the clay surface by organic modifiers, use of compatibilizers for better reinforcement between nanoparticles and polymer matrix, and optimization of processing conditions (Li and others 2006). Better exfoliation can be achieved by increasing the interlayer distance (d-spacing) between clay layers because it enables biopolymer chains to penetrate easily into the galleries of layered clays. The d-spacing of the layered silicates can be increased by ion exchange reaction of sodium ions present in natural MMT with various organic cations such as primary or quaternary amine. The influence of the type of organic modifier (primary and secondary amine) and the extent of surface coverage of clay on the structure and mechanical properties of nanocomposites has been investigated (Li and others 2006). The results showed that MMT modified with

quaternary amine had longer interlayer distances and resulted in nanocomposites with improved mechanical properties.

The above studies indicate that natural and modified MMTs show potential for development of biopolymer-based nanocomposite films with enhanced mechanical and barrier properties. However, to date, a cost-effective biopolymer-based nanocomposite film with mechanical and barrier properties similar to those of plastics has not been produced. The main reason for that is the difficulty in achieving exfoliation of nanoparticles in the biopolymer matrix. Better exfoliation could be achieved either by using high shear mixing in an extruder or by modifying the surface of MMT. Extrusion processing will also increase the potential for production of these films on a commercial scale. Thus, the current study was undertaken with the main objective of developing SPI-MMT bio-nanocomposite films with enhanced mechanical and barrier properties by melt intercalation using extrusion processing.

Chapter 2

REVIEW OF LITERATURE

2.1 Food packaging and plastics

Foods are packaged to protect them from the environment and to maintain them in proper condition during shipping, distribution, retailing, and home storage. Food packaging enables foods to be safe and wholesome from the time of production until the food is consumed. Functions of a package are to contain, carry, dispense, protect, communicate, and offer convenience. Food packaging can extend the shelf life of a product by retarding deterioration of the product and retaining the beneficial effects of processing. A package has to provide protection from chemical, biological, and physical agents. Chemical agents lead to compositional changes by factors such as exposure to gases, moisture, or light (visible, infrared, or ultraviolet). Biological agents such as microorganisms, insects, and rodents lead to spoilage of food products. Physical agents such as mechanical forces (impact, vibration, and compression) damage the product (Marsh and Bugusu 2007).

Traceability, convenience, and tamper indication are secondary functions of increasing importance. Traceability is defined as the ability to follow the movement of a food through specific stages of production, processing, and distribution. Traceability improves supply chain management and facilitates trace-back for food safety. For a package to be convenient, it should be easy to hold, open, and pour. Other features of convenience include product visibility, resealability, and adaptability to heating. The tamper indication reduces or eliminates the risk of tampering and intentional adulteration of foods after packaging. Some

of features which achieve tamper indication include banding, breakaway closures, special printing on bottle liners in the form of graphics or text that irreversibly change upon opening (Marsh and Bugusu 2007).

Materials that have been traditionally used in food packaging include glass, metal, paper and paperboard, and plastics. The use of plastics over glass and metals has continued to increase because they offer several advantages over other materials. Plastics are inexpensive, light-weight, and chemically inert. Plastics are heat-sealable, easy to print on, and offer flexibility in fabricating different shapes of containers. Plastics are organic molecules consisting of several repeating units (monomers) linked to produce a long chain molecule of high molecular weight. Plastics are made by condensation polymerization (polycondensation) or addition polymerization (polyaddition) of monomers of hydrocarbons or hydrocarbon-like materials. In polycondensation, the polymer chain grows by condensation reactions between molecules and is accompanied by formation of low molecular weight by-products such as water and methanol. In polyaddition, the polymer chain grows by addition reactions of 2 or more molecules to form a larger molecule and is not accompanied by formation of any by-products. There are two types of plastics – thermoset and thermoplastic. Thermosets solidify or set irreversibly when heated and cannot be remolded. Thermosets are used primarily in automobiles and construction applications because of their strength and durability. Thermoplastics soften upon exposure to heat and return to their original condition at ambient conditions. Thermoplastics are mainly used for food packaging because they can be easily molded in various shapes and sizes. Plastics find their origin in the petrochemical industry

making them non-biodegradable and non-renewable. The non-biodegradable and non-renewable nature of plastics overshadows its merits (Marsh and Bugusu 2007).

2.2 Biopolymer-based packaging materials

The non-biodegradable and non-renewable nature of plastic packaging has given way to packaging materials based on biopolymers derived from renewable sources. The use of biopolymer-based materials can solve the waste disposal problem to a certain extent. Such biopolymers include naturally occurring proteins, cellulose, starches, and other polysaccharides and those synthesized chemically from naturally derived monomers such as lactic acid. A detailed literature review on packaging materials based on starch, cellulose, protein, poly hydroxyalkanoate (PHA), and polylactic acid (PLA) and their bio-nanocomposites has been described in chapter 3.

2.2.1 Soy protein-based packaging films

The increased interest in bio-based packaging has resulted in the development of protein-based films from soy protein, whey protein, casein, collagen, corn zein, gelatin, and wheat gluten. Recently, soy protein has been used to develop biodegradable films because it is easily available and inexpensive. Soybeans contain approximately 42% protein, 20% lipid, 33% carbohydrate, and 5% ash on a dry basis (Zhang and others 2001). Soy protein isolate (SPI) is a commercial form of soy protein that contains more than 90% protein. Soy proteins are classified as 2S, 7S, 11S, and 15S based on their sedimentation rate in fractional ultracentrifugation. Larger Svedberg (S) number indicates a larger protein (Hernandez-Izquierdo and Krochta 2008). 7S (β-conglycinin) and 11S (glycinin) fractions of soy proteins, constituting about 90% of total protein, have the ability of polymerization, resulting in the

formation of films. β-conglycinin (molecular weight of 140-170 kDa) consists of three types of subunits with molecular weights of 58, 57, and 42 kDa. Glycinin (molecular weight of 340-375 kDa) consists of 6 acidic (35 kDa) and 6 basic (35 kDa) polypeptide chains which are linked together by disulfide bonds (Petruccelli and Anon 1995).

The quaternary structure of β-conglycinin and glycinin depends on pH and ionic strength. β-conglycinin exists as a trimeric glycoprotein (7S) at a pH range of 2 to 10 and ionic strength higher than 0.1. At an ionic strength less than 0.1, β-conglycinin exists as a hexamer (9S) at pH higher than 5 whereas it dissociates into a 2-3 S and 5-6 S fraction at pH range 2 to 5. At ambient temperature and pH of 7.6, glycinin exists in hexameric form (11S), while it exists as trimeric complexes (7S) at a pH of 3.8 (Renkema and others 2002).

Film formation from soy protein is supposed to be a two-stage process. In the first stage (heating phase), protein is denatured and some disulfide bonds are cleaved. This exposes sulfhydryl and hydrophobic groups. During the second stage (drying phase), new network is formed by disulfide linkage, hydrogen bonds, and hydrophobic interactions (Lefevre and others 2005). Denaturation of protein depends on pH and ionic strength of the film forming solution. The onset denaturation temperature of β-conglycinin is around 60-75 °C. The onset denaturation temperature of glycinin is around 80-90 °C for the 11 S form and 60-70 °C for the 7S form (Renkema and others 2002). Soy protein film formation has been achieved within pH ranges of 1 to 3 and 6 to 12. Film formation is inhibited near the isoelectric point (pH 4.5) of soy protein due to coagulation of protein (Mauri and Anon 2006).

It has been reported that soy protein films made without the use of plasticizer are extremely brittle. Brandenburg and others (1993) developed soy protein isolate (SPI) films with improved properties by adding glycerol as a plasticizer. Plasticizers are additives which improve the mechanical properties and processability of films by disrupting intermolecular associations and increasing intermolecular spacing between adjacent polymer chains (Lefevre and others 2005). Brandenburg and others (1993) also studied the effects of mild alkali treatment and pH on tensile strength (TS), percentage elongation (%E) at break, water vapor permeability (WVP), and oxygen permeability (OP) of soy protein films. Alkali treatment, used to solubilize and partially denature the soy protein, had no effect on WVP, OP, and TS, but it resulted in a higher %E. Increase in pH of the solution resulted in films with lower WVP and OP and higher TS and %E. This might have been due to better solubilization of soy protein at a higher pH resulting in improved cross-linking. Appearance of alkali-treated films was smoother and more uniform as compared to the untreated films. The maximum TS and %E achieved with soy proteins were 5.23 MPa and 115.21% respectively.

Effects of pH, moisture content, processing conditions, plasticizers (polyhydric alcohol,), cross-linking agents (formaldehyde, glyoxal, and adipic/acetic anhydride), and cellulose as a filler on mechanical and physical properties of compression molded soy-based polymers have been studied (Paetau and others 1994a; Paetau and others 1994b; Wang and others 1996). Wang and others (1996) studied the effect of polyhydric alcohols such as ethylene glycol, glycerol, propylene glycol, 1,3-propanediol and polyethylene glycol on tensile, thermal, and dynamic mechanical properties of soy-based polymers. The results

showed that glycerol, ethylene glycol, and propylene glycol were better plasticizers than 1,3-propanediol. Polyethylene glycol had an insignificant effect on the properties of soy-based polymers. Paetau and others (1994b) examined the effects of cross-linking agents and cellulose as a filler on mechanical and physical properties of soy-based polymers. The results showed significant increase in TS of films treated with formaldehyde. Treatment with glyoxal or adipic/acetic anhydride resulted in films with reduced TS. Cellulose addition increased rigidity and decreased %E. Tensile strength increased with the addition of short fiber cellulose. Addition of long fiber cellulose decreased TS whereas addition of microcrystalline cellulose had an insignificant effect on TS of the soy-based polymers.

Zhang and others (2001) produced soy protein sheets by extrusion and investigated the effects of plasticizers (water, glycerol, methyl glucoside) and cross linking agents ($ZnSO_4$ for chelating cross-links; epichlorohydrin and glutaric dialdehyde for covalent cross-links) on mechanical and dynamic mechanical properties of soy protein sheets. They found that sheets made with 5.3% glycerol had highest TS (40.6 MPa), but %E was only 3%. As glycerol content was increased to 14.3%, TS decreased to 14.0 MPa and %E increased to 133%. TS and %E further increased when glycerol was partially replaced by methyl glucoside. Addition of cross-linking agents did not change TS significantly, however %E increased significantly.

Soy protein films have been reported to have good oxygen barrier properties, but poor water vapor barrier properties due to their hydrophilic nature. Cross-linking of proteins by means of physical, chemical, and enzymatic treatments could potentially improve the barrier and mechanical properties. Park and others (2001) produced soy protein films with calcium

salts and glucono-δ-lactone (GDL) and investigated their mechanical properties (TS and %E) and WVP. The results showed that SPI films treated with $CaSO_4$ had higher TS (8.6 MPa) as compared to that (5.5 MPa) of the control whereas TS (6.4 MPa) of SPI films treated with $CaCl_2$ did not improve significantly. Addition of GDL increased TS and %E due to the increase in number of hydrogen bonds. Addition of calcium salts and GDL also resulted in improved water barrier properties of SPI films.

Another approach to improve barrier and mechanical properties is to prepare composite films by blending soy proteins with other bio-polymers. Addition of other bio-polymers in soy protein films also helps in overcoming the beany flavor associated with soy protein films. Sabato and others (2001) produced films based on SPI alone and in combination with whey protein isolate (WPI) by means of γ-radiation and thermal treatment. The combination of γ-radiation with thermal treatment improved mechanical and water vapor barrier properties by generating cross-linking in proteins.

Pol and others (2002) produced SPI-zein laminated films by a thermal compaction technique and studied the physical and mechanical properties of the formed laminates. They found that single and double coated soy protein laminates had 20% and 50% lower WVP respectively as compared to those of the unlaminated base soy film. The WVP values of the laminates were however approximately 3 orders of magnitude higher than those of LDPE (low density polyethylene) and HDPE (high density polyethylene). OP values of double coated laminates were significantly lower than those of the unlaminated base soy film. The OP values of the laminates were approximately 2 orders of magnitude lower than those of

LDPE and HDPE. Coating of zein films on soy films was also found to increase TS and decrease %E.

Cao and others (2007) prepared composite films based on SPI and gelatin and investigated the effects of SPI to gelatin ratio, type of plasticizer, pH, thermal treatment, and salt concentration on mechanical properties of SPI-gelatin composite films. Addition of gelatin increased TS of the films. However, there was no significant change in %E. The results also suggested that TS first increased and then decreased as the pH of SPI solution was increased from 6 to 10 with a maximum value at a pH of 8.5. Percentage elongation (%E) increased with an increase in the pH of solutions. Kurose and others (2007) prepared unplasticized and glycerol-plasticized SPI films by compression molding and investigated the effect of various uniaxial drawing ratios (1 - 2.5) of SPI film on mechanical properties. Tensile strength of the undrawn SPI film was approximately doubled by subjecting the film to a draw ratio of 2.5.

2.2.2 Limitations of soy protein-based packaging films

Soy protein-based packaging films cannot meet the requirements of a cost-effective film with mechanical and barrier properties similar to those of plastics. Biopolymer-based films have higher water vapor permeability as compared to plastic films due to the hydrophilic nature of most biopolymers. Therefore, research has been geared to develop techniques to improve mechanical and water vapor barrier properties of these bio-based packaging materials. Some of the techniques developed include chemical modification of biopolymers, addition of plasticizers such as glycerol to overcome brittleness, incorporation of other biodegradable polymers (with superior properties) into biopolymers to produce a

material with intermediate properties, and addition of compatibilizers to increase miscibility of incompatible polymers to decrease interfacial energy and stabilize polymer blends. However, none of the above mentioned methods can produce a cost-effective film with mechanical and barrier properties similar to those of plastics. Therefore, there is a need to explore new techniques to produce biopolymer-based films with improved mechanical and barrier properties.

2.3 Nanotechnology and bio-nanocomposites

Nanotechnology involves study and use of materials at a scale of 1 to 100 nanometers. Nanotechnology exploits the fact that material properties could be very different at a nanometer scale than at a macro level. Recently, a new class of materials represented by bio-nanocomposites has proven to be a promising option in improving mechanical and barrier properties. The bio-nanocomposites consist of a biopolymer matrix reinforced with particles (nanoparticles) having at least one dimension in the nanometer range (1-100 nm) and exhibit much improved properties due to the high aspect ratio and high surface area of nanoparticles (Ray and Bousmina 2005; Rhim and Ng 2007; Zhao and others 2008). Nanoparticles can be three-dimensional spherical and polyhedral particles such as colloidal silica, two-dimensional nanofibers such as nanotubes or nanowhiskers, or one-dimensional disc-like clay platelets. The most common class of materials used as nanoparticles are layered inorganic solids such as clay minerals, graphite, and metal phosphates. Clay minerals such as montmorillonite (MMT), hectorite, sapnotite, and laponite have been proven to be very effective due to their unique structure and properties. These clay minerals belong to the general family of 2:1 layered silicates indicating that they have 2 tetrahedral sheets

sandwiching a central octahedral sheet (Zeng and others 2005). A detailed review on the structure and properties of layered silicates, preparation, characterization, and properties (mechanical and barrier) of nanocomposites, and bio-nanocomposites based on starch, cellulose, protein, PLA, and PHB has been described in chapter 3.

2.3.1 Soy protein-based bio-nanocomposites

Biopolymers made from SPI alone possess good biodegradability, but poor flexibility. Plasticizers are used to overcome the brittleness of SPI-based biopolymer films. However, the use of plasticizers leads to significant decrease in TS of the films. Flexible nanocomposite films having high TS can be obtained by reinforcing the SPI-plasticizer system with suitable filler materials such as nanoparticles. In the recent years, montmorillonite (MMT) has been used in the formation of nanocomposites because of its high surface area and aspect ratio. MMT has a very high elastic modulus (178 GPa) as compared to most biopolymers. The high value of elastic modulus enables MMT to improve mechanical properties of biopolymers by carrying a significant portion of the applied stress (Fornes and Paul 2003). A basic understanding of the molecular interaction and structure of these bio-nanocomposites is essential for their commercialization. Very few studies on SPI-MMT bio-nanocomposites have been reported in literature. Dean and Yu (2005) developed an effective method to exfoliate MMT lamellae in water using ultrasonic and prepared MMT-reinforced soy protein films plasticized by a mixture of water and glycerol. The ultrasonic treated bio-nanocomposite material exhibited an exfoliated structure and an improvement in tensile modulus and tensile strength of 84% and 47% respectively. The glass transition temperature of ultrasonic treated bio-nanocomposite showed an increase of 9.5 °C

as compared to that of neat soy protein composite. However, water barrier properties of the bio-nanocomposites were not reported. Rhim and others (2005) prepared and studied the mechanical and water barrier properties of composite films of SPI with various clay minerals. The tensile strength of SPI-layered clay films increased by as much as 30% whereas the water vapor permeability decreased by 52%.

Chen and Zhang (2006) prepared highly exfoliated and intercalated SPI-MMT nanocomposites by using the solution exfoliation method in a neutral aqueous medium and investigated the correlation between the microstructure and mechanical properties. The results showed that the heterogeneous distribution of positive charges provided soy globulins to anchor into the negative charged MMT interlayers (distance between two MMT layers). Electrostatic attraction and hydrogen bonding at the interfaces of soy protein and MMT lead to good dispersion of MMT layers in the protein matrix. Highly exfoliated structure with 1-2 nm MMT layers dispersed in protein matrix resulted when the MMT content was less than 12% (w/w). Intercalated structure was predominant when the MMT content was more than 12%. The results also showed improvement in tensile strength (increase from 8.77 to 15.43 MPa) and thermal stability of SPI-MMT bio-nanocomposites. Yu and others (2007) prepared bio-nanocomposite sheets based on soy proteins and rectorite (REC) by compression molding. REC is a 1:1 layered silicate which is composed of a regular stacking of mica-like layers and MMT-like layers. Interlayer spacing in REC is approximately 2.4 nm as compared to 1.2 nm of MMT. Thus, REC is expected to allow better penetration of protein molecules in between interlayers. The results showed exfoliated nanocomposite structure up to REC content of 12%, and above this, intercalated structures were formed. This correlated well

with the mechanical properties results with TS of the nanocomposite sheets being maximum (12.92 MPa) at a REC content of 12%. Percentage elongation (%E) at break of the nanocomposite sheets decreased sharply with increasing REC content.

2.4 Extrusion

Extrusion is defined as a process in which a material is forced to flow, under one or more conditions of mixing, heating, and shear through a die which is designed to form and/or puff-dry the ingredients (Rossen and Miller 1973). The extrusion mechanism can be as simple as a piston contained in a cylinder with a die at one end. Material is loaded into the cylinder and emerges in its defined shape from the die due to the pressure created by the moving piston. This type of extrusion is a batch process. However, an extrusion process can be made continuous by replacing the piston with a helical screw. Material is fed continuously in an inlet hopper and transported towards the die by rotating screws. As the material reaches the die, the pressure increases to the level required to propel the extrudate through the die. The friction between the material and the screw surface results in heating of the material (Hauck and Huber 1989). Thus, extrusion combines several unit operations such as mixing, cooking, kneading, shearing, shaping, and forming to make a variety of products with high quality, high productivity, and low cost (Riaz 2000).

2.4.1 Classification of extruders

Extruders are classified by the method of operation and type of construction. Extruders are classified into four types based on the method of operation – cold, hot, isothermal, and adiabatic. The temperature of the material remains at ambient conditions in cold extruders whereas the material is heated to above 100 °C in hot extruders. The

temperature of the material is essentially constant throughout the extruder in isothermal extruders whereas there is no addition or removal of heat in adiabatic extruders (Riaz 2000).

Extruders are classified as single-screw and twin-screw extruder based on the type of construction. Single-screw extruders consist of a cylindrical screw that rotates in a grooved cylindrical barrel. Single screw extruders can further be classified based on the extent of shear as high, medium, and low shear. On the other hand, twin-screw extruders have two screws that rotate in the cylindrical barrel. Twin-screw extruders can handle viscous, oily, and sticky materials and can be easily cleaned due to its self-wiping nature. Twin-screw extruders are classified according to the direction of screw rotation as counter-rotating or co-rotating. In counter-rotating twin-screw extruders, the screws rotate in opposite directions. Counter-rotating twin-screw extruders can be further classified into intermeshing and non-intermeshing based on the manner in which the screws engage. In an intermeshing extruder, the flight of one screw engages the channels of the other screw. It provides a positive pumping action, efficient mixing and is self-cleaning. In a non-intermeshing extruder, the flight of one screw does not engage the channels of the other screw. This type of extruder depends on friction for extrusion. In co-rotating twin-screw extruders, the screws are in constant contact with each other, creating a natural wiping action. These extruders provide high degrees of heat transfer, efficient pumping, controlled residence time distribution, a self-cleaning mechanism, and a uniform process. Co-rotating twin-screw extruders can also be classified as intermeshing and non-intermeshing based on the manner in which the screws engage (Riaz 2000).

2.4.2 Elements of an extruder

The main elements of an extruder include metering or feed system, preconditioner, screw, barrel, die, and rotating knife (Figure 1). A variable speed metering and feeding screw is used for continuous and uniform discharge of materials to the extruder. There are two types of feeding systems – volumetric and gravimetric. Volumetric feeding system controls feed rate by adjusting feeder speed. Thus, the actual feed rate is affected by changes in bulk density of raw materials. It is simple in design and lower in cost. The actual feed rate in a gravimetric feeding system is not affected by bulk density of raw materials because the system controls feed rate automatically. Gravimetric feeding systems have become a standard for most extrusion processing systems because they offer constant feed rate for dry ingredients and liquid additives (Riaz 2000).

The feeding system can feed materials directly into the extruder or into a preconditioner. Preconditioning is beneficial for extrusion processes involving higher moisture content. The purpose of a preconditioner is to pre-blend steam and water with dry ingredients and to mix them long enough for temperature and moisture equilibration. The goal of preconditioning is to plasticize or soften the materials. The addition of water lowers the glass transition temperature and steam heats the materials above the glass transition temperature. This glass transition changes the materials from a glassy state to a rubbery (soft) state. Some of the advantages of preconditioning include increased throughput, decreased wear and tear of the extruder, and improved flavor and texture (Riaz 2000).

The screw is the central part of an extruder. The screw rotates inside the barrel and conveys the material from the feed end to the discharge end. The screw of the extruder is

divided into three sections – feed section, compression or melting section, and metering section. The portion of the screw which accepts food material is known as the feed section. The feed section should have sufficient material for conveying it down the screw. The compression section is the portion of the screw between the feed and metering section. In this section, material is heated, compressed, and worked into a continuous mass. The material changes from a granular state to an amorphous state. The metering section is the portion of the screw nearest to the discharge of the extruder (Riaz 2000).

Barrel is the cylindrical casing which fits tightly around the screw of the extruder. Bore (D) is the inside diameter of the barrel and it ranges from 5 cm to 25.4 cm. Length (L) of the extruder is the distance from the rear edge of the feed section to the discharge end of the metering section. Length to diameter ratio (L/D) is the ratio of the length to the diameter of the barrel and it usually ranges from 1:1 to 30:1. Screws with higher L/D ratio provide higher shear heating, better mixing, and longer residence time in the extruder. A barrel is made up of several segments that make it relatively easy to change the configuration of the barrel and to replace the discharge section which wears out the fastest. The barrel is constructed of special hard alloys such as Xaloy® 306 and stainless steel (SS 431) to withstand the pressure developed in the barrel and to resist wear (Riaz 2000).

The extruder barrel is equipped with a die with one or more openings through which the extrudate flows. The openings shape the final product and provide resistance against the flow of extrudate. Dies may be designed to be highly restrictive for increasing barrel fill, residence time, and energy input. Coextrusion dies are used to make a single product from two different products. One such example is a product with an outer shell and an inner filling

material. Sheeting dies are used to make sheets of thickness ranging from 0.8 mm to 1.5 mm. A rotating knife, installed at the exit of the die, cuts the product, giving it the final shape and length.

2.4.3 Process parameters

There are two types of process parameters in an extrusion process – independent and dependent. Independent variables are those variables which can be controlled directly. Independent variables include feed ingredients and feed rate (Q), screw speed (N) and screw configuration, and temperature distribution within the barrel. Dependent variables are those variables which are dependent upon the magnitude of the independent variables. Dependent variables include in-barrel moisture, specific mechanical energy, specific thermal energy, residence time, and pressure. In-barrel moisture is the actual moisture in an extrusion process. Moisture is added in the form of either steam or water in the extruder. Specific mechanical energy is the amount of mechanical energy per unit mass dissipated as heat inside an extruder. Specific thermal energy is the amount of thermal energy added from heat sources or sinks in the extruder per unit mass. Residence time is a measure of the time a material spends in the extruder. Residence time is used to determine optimal processing conditions for mixing, cooking, and shearing reactions during an extrusion process. The pressure at the discharge of the extruder regulates the product output of the extruder by affecting the flow through the die (Harper 1981).

2.4.4 Nanocomposite preparation using extrusion

Melt intercalation is one of the most promising techniques for preparing nanocomposites because of its ease and versatility. Melt intercalation in a twin-screw

extruder can be used to prepare exfoliated polymer nanocomposites. Layered clays (6-13 μm) are sheared and peeled apart into platelets (~1-10 nm) due to high shear mixing inside the extruder. These platelets are then mixed with the polymer matrix in molten state to achieve exfoliation. The same technique can be used to prepare biopolymer-based nanocomposites in an extruder. Extrusion is one of the most important processing techniques to produce plastics on a commercial scale. Extrusion processing involves melting, mixing, kneading, stretching, and molding of polymers. Therefore, biopolymer-based nanocomposite films using extrusion will increase the potential for commercialization of these films.

Process parameters (feed rate, screw speed and configuration, and temperature distribution within the barrel) used in an extruder have an important influence on the structure and properties of nanocomposites. Decrease in feed rate has shown to improve exfoliation in nanocomposites which can be explained by better dispersion due to increased residence time at a lower feed rate. Increase in screw speed has been shown to result in better dispersion of nanoparticles in the polymer matrix. This behavior has been observed for nanocomposites based on polyamide (PA), polyethylene (PE), and polypropylene (PP). This is explained by breaking of agglomerates into smaller aggregates at high shear rates, corresponding to higher screw speeds. There are contradictory results in literature for the effect of temperature distribution within the barrel. Better dispersion of nanoparticles in polyethylene at higher temperature has been reported. However, better dispersion in polypropylene was observed at lower temperature (Lertwimolnun and Vergnes 2007)

Ha and Padua (2001) demonstrated the feasibility of applying extrusion processing to produce zein-fatty acids sheets. Granular zein resins containing a mixture of fatty acids were

extruded into sheets using a co-rotating twin-screw extruder with 5 heating zones. Processing variables studied were barrel temperature (100, 120, and 130 °C) in zones 4 and 5, screw speed (150, 200, and 250 rpm), and amount of solvent (70% ethanol) added to the extruder (20, 30, and 40% v/w). The results showed that TS increased with an increase in barrel temperature. However, %E decreased as the barrel temperature increased. Screw speed and addition of solvent had an insignificant effect on mechanical properties.

Redl and others (1999) investigated the effect of extrusion processing parameters on flow behavior and rheological properties of wheat gluten plasticized with glycerol. The processing parameters studied were feed rate (1.9, 4.9, 8.1 kg/h), screw speed (50, 100, 200 rpm), and barrel temperature (40, 60, and 80 °C). Higher screw speeds resulted in rupturing of the extrudate because of higher viscous heat dissipation.

Zhang and others (2001) developed a multistep process to prepare soy protein isolate (SPI) sheets. The process involved mixing of SPI, water, glycerol, and others additives in a high speed mixer, compounding the mixture into pellets in a twin-screw extruder, and extruding sheets from pellets using a single-screw extruder. The compounding extruder had a diameter of 18 mm and a length to diameter ratio (L/D) of 30. Screw speed was 150 rpm and barrel temperature in the five heating zones varied from 60 to 115 °C. The single-screw extruder operated at 20 to 25 rpm and the barrel temperature varied from 120 to 160 °C. Soy protein sheets were usually in glassy state with higher tensile strength and modulus except at high moisture level or when glycerol was used as a plasticizer.

Mohanty and others (2005) prepared biocomposites from soy based biopolymer and chopped industrial hemp fiber using twin-screw extrusion and an injection molding process.

The screw speed was 100 rpm and the temperatures of the heating zones were 95, 105, 115, 125, 130, and 130 °C. The pellets from the extruder were injection molded to form biocomposites. The results showed a 9 fold increase in TS as the hemp fiber content increased from 0 to 30%. However, %E decreased with an increase in hemp fiber content. The flexural modulus increased 10 fold as the hemp fiber content increased from 0 to 30%. However, there was poor dispersion of the hemp fiber in the biocomposite indicating the need for better treatment of fiber surface and use of a compatibilizer.

Li and others (2006) developed nanocomposites based on polypropylene (PP) containing MMT modified with two different intercalants (primary and secondary amine). Intercalants have longer aliphatic tails which can increase the interlayer distance of layered silicates. This is desirable to increase the dispersion of layered clays in a polymer matrix. A primary amine intercalant is expected to provide greater reactivity with the compatibilizer. The influence of the type of intercalant and the extent of surface coverage on structure and mechanical properties were investigated. The nanocomposites were prepared in an extruder with a counter-rotating screw configuration. The results showed that MMT modified with quaternary amine intercalants had longer interlayer distances. The interlayer distance also increased with an increase in the surface coverage of clays. MMT modified with quaternary amine intercalants also resulted in nanocomposites with improved mechanical properties.

Borse and Kamal (2006) prepared polyamide-6 (PA-6) nanocomposites using a natural MMT and two modified MMTs. Two different extrusion systems with different residence times and mixing conditions were used. One system had conventional mixing and residence time whereas the other system was modified to achieve a longer residence time and

a higher mixing efficiency. The effects of extrusion processing conditions and interactions between the polymer and clay surface on the structure and mechanical properties of PA-6-clay nanocomposites were studied. The extrusion system with longer residence time and higher mixing efficiency resulted in the highest degree of exfoliation and improvement in mechanical properties.

Lertwimolnun and Vergnes (2007) characterized the influence of extrusion processing conditions (feed rate and screw speed) and screw configuration on the microstructure (intercalation and exfoliation) of PP-MMT. The results showed that the level of intercalation is independent of the processing conditions. It was shown that exfoliation is partially controlled by processing conditions and screw configuration. The level of exfoliation was found to be proportional to the ratio of screw speed to feed rate (N/Q). Increasing the total deformation (shear rate × residence time) and/or specific energy resulted in better exfoliation of MMTs in the PP matrix. A mixed intercalated-exfoliated structure of MMT in PP matrix was observed for all processing conditions.

The above studies indicate that natural and modified MMTs show potential for development of SPI-based nanocomposite films with enhanced mechanical and barrier properties. However, to date, a cost-effective SPI-based nanocomposite film with mechanical and barrier properties similar to those of plastics has not been produced. The main reason for that is the difficulty in achieving exfoliation of nanoparticles in the biopolymer matrix. Better exfoliation could be achieved by increasing the interlayer distance between the clay layers because a larger interlayer distance will enable biopolymer chains to penetrate easily into the galleries of layered clays. The interlayer distance could be increased either by using high

shear mixing in an extruder or by modifying the clay surface. Process parameters used in an extruder play an important role in the formation of nanocomposites. Process parameters such as feed rate, screw speed, and temperature distribution within the barrel can be modified to achieve longer residence time and higher shear mixing. Longer residence time and higher shear mixing is desirable for achieving better exfoliation in the nanocomposites. Extrusion processing will also increase the potential for production of these films on a commercial scale. Natural MMT is modified by quaternary or primary amine to achieve a larger interlayer distance. The longer aliphatic chains and high surface coverage of clay by these organic modifier increase the interlayer distance. Therefore, the type of organic modifier will have an important influence on the structure and properties of nanocomposites.

The main objective of this research was to develop SPI-MMT bio-nanocomposite films with enhanced mechanical and barrier properties by melt intercalation using extrusion processing. The main objective has been sub-divided into smaller specific objectives as follows:

i) To study the effect of processing parameters (screw speed and barrel temperature distribution) of a twin-screw extruder on the structure (degree of intercalation and exfoliation) and properties (mechanical, dynamic mechanical, thermal stability, and water vapor permeability) of SPI-MMT bio-nanocomposite films

ii) To study the effect of type (natural and modified) and content (0-15%) of MMT on the structure (degree of intercalation and exfoliation) and

properties (mechanical, dynamic mechanical, thermal stability, and water vapor permeability) of SPI-MMT bio-nanocomposite films

The rest of this dissertation is organized in the form of five manuscripts. Manuscript I reviews recent advances in biopolymers and biopolymer-based nanocomposites for food packaging materials. Manuscript II presents a review of analytical techniques for structural characterization of bio-nanocomposites. A review of experimental and modeling techniques to determine properties of bio-nanocomposites is presented in manuscript III. Manuscript IV investigates the effects of the pH of film forming solution, MMT content, and extrusion processing parameters on the structure and properties of bio-nanocomposites based on SPI and MMT. The effect of different types and contents of modified MMT on the structure and properties of SPI-MMT bio-nanocomposite films has been presented in Manuscript V.

SYMBOLS

%E	Percent elongation at break
D	Diameter of the barrel (m)
L	Length of the barrel (m)
N	Screw speed (rpm)
OP	Oxygen permeability
Q	Feed rate (kg/h)
TM	Tensile modulus (MPa)
TS	Tensile strength (MPa)
WVP	Water vapor permeability

Abbreviations

GDL	Glucono-δ-lactone
HDPE	High density polyethylene
LDPE	Low density polyethylene
MMT	Montmorillonite
MSW	Municipal solid waste
PA	Polyamide
PE	Polyethylene
PHA	Poly hydroxyalkanoate
PLA	Polylactic acid
PP	Polypropylene
REC	Rectorite

S	Svedberg
SPI	Soy protein isolate
WPI	Whey protein isolate

REFERENCES

Borse NK, Kamal MR. 2006. Melt processing effects on the structure and mechanical properties of PA-6/clay nanocomposites. Polymer engineering and science 46(8): 1094-1103.

Brandenburg AH, Weller CL, Testin RF. 1993. Edible films and coatings from soy protein. Journal of food science 58(5): 1086-1089.

Cao N, Fu Y, He J. 2007. Preparation and physical properties of soy protein isolate and gelatin composite films. Food hydrocolloids 21: 1153-1162.

Chen P, Zhang L. 2006. Interaction and properties of highly exfoliated soy protein/montmorillonite nanocomposites. Biomacromolecules 7: 1700-1706.

Dean K, Yu L. 2005. Biodegradable protein-nanoparticles composites. In: Smith R. editor. Biodegradable polymers for industrial applications. UK: Woodhead Publishing Ltd. p 289-312.

Dennis HR, Hunter DL, Chang D, Kim S, White JL, Cho JW, Paul DR. 2001. Effect of melt processing conditions on the extent of exfoliation in organoclay-based nanocomposites. Polymer 42: 9513-9522.

Fornes TD, Paul DR. 2003. Modeling properties of nylon 6/clay nanocomposites using composite theories. Polymer 44: 4993-5013.

Ha TT, Padua GW. 2001. Effect of extrusion processing on properties of zein-fatty acids sheets. Transactions of the ASAE 44(5): 1223-1228.

Harper JM. 1981. Extrusion of foods. Vol. 1., CRC Press, Inc., Boca Raton, FL. pp 1-212.

Hauck BW, Huber GR. 1989. Single screw vs twin screw extrusion. Cereals foods world 34(11): 930-939.

Hernandez-Izquierdo VM, Krochta JM. 2008. Thermoplastic processing of proteins for film formation – a review. Journal of food science 73(2): R30-R39.

Jahangir S, Leber MJ. 2007. Biodegradable food packaging: an environmental imperative. Industry Report. pp 1-20.

Kurose T, Urman K, Otaigbe JU, Lochhead RY, Thames SF. 2007. Effect of uniaxial drawing of soy protein isolate biopolymer films on structure and mechanical properties. Polymer engineering and science 47(4): 374-380.

Lefevre T, Subirade M, Pezolet M. 2005. Molecular description of the formation and structure of plasticized globular protein films. Biomacromolecules 6: 3209-3219.

Lertwimolnun W, Vergnes B. 2007. Influence of screw profile and extrusion conditions on the microstructure of polypropylene/organoclay nanocomposites. Polymer engineering and science 47(12): 2100-2109.

Li J, Ton-That MT, Tsai SJ. 2006. PP-based nanocomposites with various intercalant types and intercalant coverages. Polymer engineering and science 46 (8): 1060-1068.

Marsh K, Bugusu B. 2007. Food packaging – roles, materials, and environmental issues. Journal of food science 72(3): R39-R55.

Mauri AN, Anon MC. 2006. Effect of solution pH on solubility and some structural properties of soybean protein isolate films. Journal of the science of food and agriculture 86: 1064-1072.

Mohanty AK, Tummala P, Liu W, Misra M, Mulukutla PV, Drzal LT. 2005. Injection molded biocomposites from soy protein based bioplastic and short industrial hemp fiber. Journal of polymers and environment 13(3): 279-285.

Park SK, Rhee CO, Bae DH, Hettiarachchy NS. 2001. Mechanilca properties and water vapor permeability of soy protein films affected by calcium salts and glucono-δ-lactone. Journal of agricultural and food chemistry 49: 2308-2312.

Paetau I, Chen C, Jane J. 1994a. Biodegradable plastic made from soybean products. 1. Effect of preparation and processing on mechanical properties and water absorption. Industrial and engineering chemistry research 33: 1821-1827.

Paetau I, Chen C, Jane J. 1994b. Biodegradable plastic made from soybean products. II. Effects of cross-linking agents and cellulose incorporation on mechanical properties and water absorption. Journal of environmental polymer degradation 2(3): 211-217.

Petruccelli S, Anon MC. 1995. Soy protein isolate components and their interactions. Journal of agricultural and food chemistry 43: 1762-1767.

Pol H, Dawson P, Acton J, Ogale A. 2002. Sor protein isolate/corn-zein laminated films: transport and mechanical properties. Journal of food science 67(1): 212-217.

Ray SS, Bousmina M. 2005. Biodegradable polymers and their layered silicate nanocomposites: in greening the 21st century materials world. Progress in materials science 50: 962-1079.

Redl A, Morel MH, Bonicel J, Vergnes B, Guilbert S. 1999. Extrusion of wheat gluten plasticized with glycerol: influence of process conditions on flow behavior, rheological properties, and molecular size distribution. Cereal Chemistry 76(3): 361-370.

Renkema JMS, Gruppen H, Vliet TV. 2002. Influence of pH and ionic strength on heat-induced formation and rheological properties of soy protein gels in relation to denaturation and their protein compositions. Journal of agricultural and food chemistry 50: 6064-6071.

Rhim JW, Lee JH, Kwak HS. 2005. Mechanical and barrier properties of soy protein and clay mineral composite films. Food science and biotechnology 14: 112-116.

Rhim JW, Ng PKW. 2007. Natural biopolymer-based nanocomposite films for packaging applications. Critical reviews in food science and nutrition 47(4): 411-433.

Riaz MN. 2000. Introduction to extruders and their principles. In: Riaz, M.N., editor. Extruders in food applications. Technomic Publishing Company, Inc., Lancasrer, PA. pp. 1-23.

Rossen JL, Miller RC. 1973. Food extrusion. Food technology 27(8): 46-53.

Sabato SF, Ouattara B, Yu H, Aprano GD, Le Tien C, Mateescu MA, Lacroix M. 2001. Mechanical and barrier properties of cross-linked soy and whey protein based films. Journal of agricultural and food Chemistry 49: 1397-1403.

Schlechter M. 2007. Biodegradable polymers. Report code PLS025C. Available from: http://bccresearch.com/report/PLS025C.html. Accessed 2009 September 2.

Wang S, Sue HJ, Jane J. 1996. Effects of polyhydric alcohols on the mechanical properties of soy protein plastics. Journal of macromolecular science, Part A 33(5): 557-569.

Yu J, Cui G, Wei M, Huang J. 2007. Facile exfoliation of rectorite nanoplatelets in soy protein matrix and reinforced bio-nanocomposites thereof. Journal of applied polymer science 104: 3367-3377.

Zeng QH, Yu AB, Lu GQ, Paul DR 2005. Clay-based polymer nanocomposites: research and commercial development. Journal of nanoscience and nanotechnology 5: 1574-1592.

Zhang J, Mungara P, Jane J. 2001. Mechanical and thermal properties of extruded soy protein sheets. Polymers 42: 2569-2578.

Zhao R, Torley P, Halley PJ. 2008. Emerging biodegradable materials: starch- and protein-based bio-nanocomposites. Journal of materials science 43: 3058-3071.

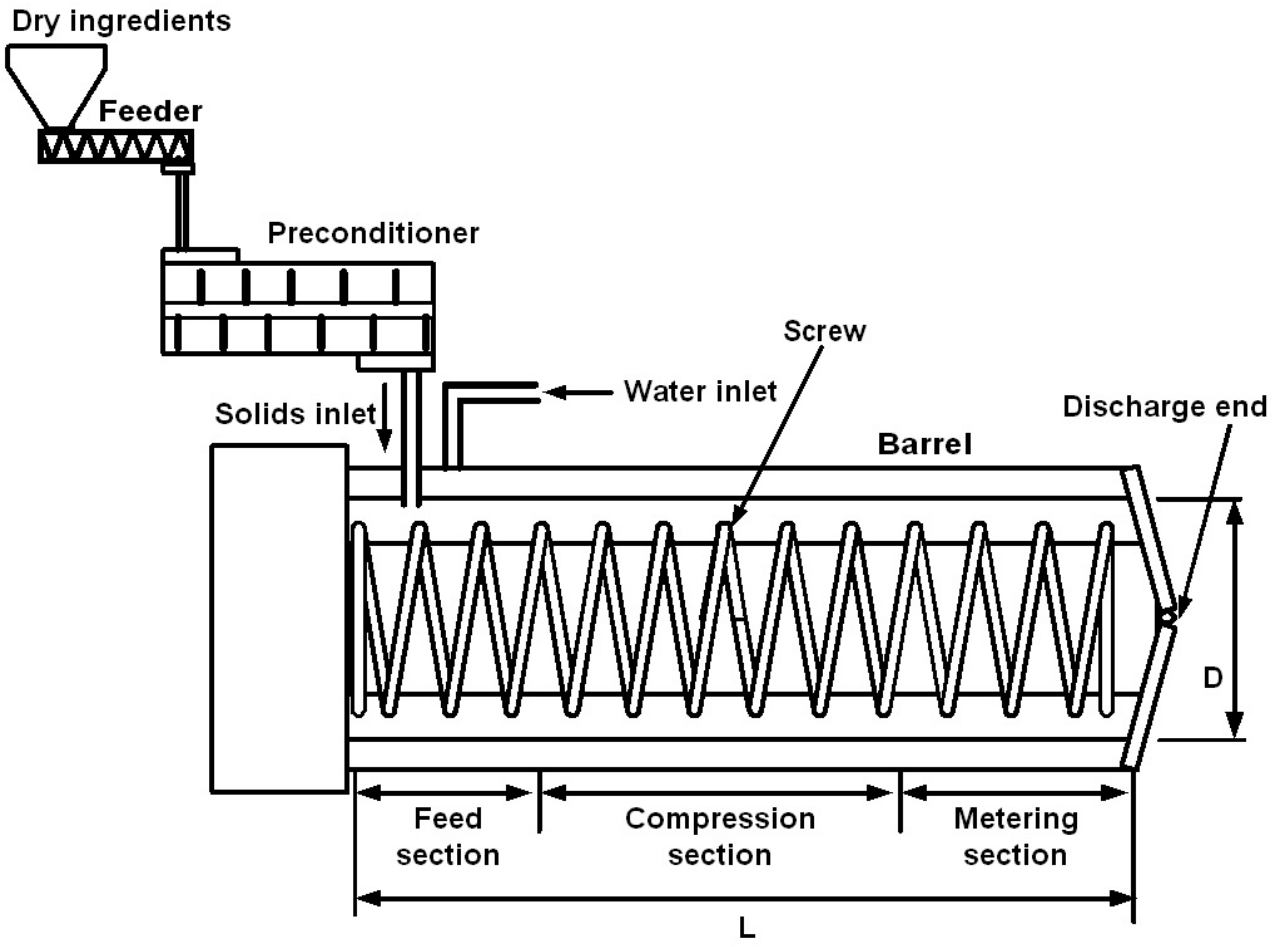

Figure 1 – Schematic of the elements of an extruder.

Chapter 3

MANUSCRIPT I

Recent Advances in Biopolymers and Biopolymer-based Nanocomposites for Food Packaging Materials

X.Z. TANG[1], P. KUMAR[2], S. ALAVI[1], AND K.P. SANDEEP[2]

(1) Department of Grain Science and Industry, Kansas State University, Manhattan, KS
(2) Department of Food, Bioprocessing, and Nutrition Sciences, North Carolina State University, Raleigh, NC

Abstract

Plastic packaging for food and non-food applications is non-biodegradable and it also uses valuable and scarce non-renewable resources like petroleum. With the current focus on exploring alternatives to petroleum and emphasis on reducing environmental impact, research is increasingly being directed at development of biodegradable food packaging from biopolymer-based materials. The proposed paper presents a review of recent developments in biopolymer-based food packaging materials including natural biopolymers (such as starches and proteins), synthetic biopolymers (such as polylactic acid), biopolymer blends, and bio-nanocomposites based on natural and synthetic biopolymers. The paper discusses various techniques that have been used for developing cost-effective biodegradable packaging materials with optimum mechanical and barrier properties. This is a timely review as there has been a recent renewed interest in research studies both in the industry and academia towards development of a new generation of biopolymer-based food packaging materials with possible applications in other areas.

Keywords: Biopolymers, Bio-nanocomposites, Biodegradable packaging

Introduction

Foods are primarily packaged to protect them from environment and to provide ingredient and nutritional information to the consumers. Traceability, convenience, and tamper identification are secondary functions of increasing importance. Materials that have been traditionally used in food packaging include glass, metal, paper and paperboard, and plastics. However, food packaging has become a central focus of waste reduction efforts because proper waste management is important to protect human health and environment. There has been a 37% increase in municipal solid waste from 179.6 million tons in 1988 to 245.7 million tons in 2005. Packaging has maximum contribution to total solid wastes at 31.2%. Food packaging alone accounts for almost two-thirds of total packaging waste by volume (Marsh and Bugusu 2007).

The use of plastics over glass and metals has continued to increase due to their better materials properties and low cost. Typically, plastics are made by condensation polymerization or addition polymerization of monomers of hydrocarbon or hydrocarbon-like raw materials. Thus, they find their origin in the petrochemical industry making them non-biodegradable and non-renewable. With the current focus on exploring alternatives to petroleum and emphasis on reducing environmental impact, research is increasingly being directed at development of biodegradable food packaging from renewable resources. The use of these biopolymer-based materials can solve the waste disposal problem to some extent. However, poor mechanical and water vapor barrier properties as compared to plastics limit their industrial use. Therefore, research has been geared to develop techniques to improve mechanical and water vapor barrier properties of these bio-based packaging materials. Some

of the techniques developed include chemical modification of biopolymers, addition of plasticizer to overcome brittleness, incorporation of other biodegradable polymers with improved properties into biopolymers to produce material with intermediate properties, and addition of compatibilizers to increase miscibility of incompatible polymers to decrease interfacial energy and stabilize polymer blends.

Recently, a new class of materials represented by nanocomposites has proven to be a promising option in order to improve barrier and mechanical properties. The nanocomposites consist of a polymer matrix reinforced with particles having at least one dimension in the nanometer range (nanoparticles) and exhibit much improved properties due to high aspect ratio and high surface area of nanoparticles. Nanoparticles can be three-dimensional spherical and polyhedral particles such as colloidal silica, two-dimensional nanofibers such as nanotube or nanowhisker, or one-dimensional disc like clay platelets. The most common class of material used as nanoparticle is layered inorganic solids such as graphite, clay minerals, and metal phosphates. Clay minerals such as montmorillonite (MMT), hectorite, sapnotite, and laponite have been proved to be very effective due to their unique structure and properties (Zeng and others 2005). Biopolymers can be reinforced with these clay minerals in order to enhance their mechanical and barrier properties while maintaining their biodegradability. The biopolymer-based nanocomposites with improved properties could potentially replace conventional packaging materials such as plastics.

This review presents recent developments in biopolymers and biopolymer-based nanocomposites for food packaging materials. The review starts with a brief introduction to definitions and categories of biopolymers, followed by detailed description of materials

based on biopolymers. Various techniques used for developing cost-effective biodegradable packaging materials with optimum mechanical and barrier properties are discussed. Polymer blends have resulted in commercialization of biopolymer-based plastics, while bio-nanocomposites are the most promising way to further improve their properties.

Definitions and categories

'Biodegradable' is defined by ASTM as: "capable of undergoing decomposition into carbon dioxide, methane, water, inorganic compounds, or biomass in which the predominant mechanism is enzymatic action of microorganisms, that can be measured by standard tests, in a specified period of time, reflecting available disposal condition (ASTM 2005)." In essence, biodegradable polymers should break down, in a defined time period, to simple molecules found in the environment such as carbon dioxide and water due to the enzyme action.

Two types of biopolymers are discussed in this article: those derived from renewable resources and those derived from living organisms. The first type of biopolymers include polysaccharide (starch, cellulose), protein (wheat gluten, soy protein, gelatin), and polylactic acid (PLA). The second type of biopolymers include polyesters like polyhydroxyalkanoates (PHAs), produced by bacteria. For the purpose of this review article, the term 'biopolymer' will refer to those polymers which are based on renewable polymers and are biodegradable.

Biopolymer materials

Starch based packaging materials

Among all natural biopolymer based food packaging materials, starch has been considered as one of the most promising one because of its easy availability, biodegradability, and lower cost. Starch is the major form of stored carbohydrate in plants

such as corn, wheat, rice, and potatoes. Starch is composed of a mixture of two polymers of α-glucose – linear amylose and a highly branched amylopectin. Amylose molecules consist of 200-20,000 glucose units which form a helix as a result of the bond angles between the glucose units. Amylopectin is a highly branched polymer containing short side chains of 30 glucose units attached to every 20-30 glucose units along the chain. Amylopectin molecules may contain up to two million glucose units (Ray and Bousmina 2005).

Starch can be used to form edible or biodegradable films. Different sources of starch, high amylose starch, modified starch (Mali and Grossmann 2003; Mali and others 2006; Roth and Mehltretter 1967; Wolff and others 1951) have been used to form self-supporting films by film casting from aqueous solution. These films appear to have moderate oxygen barrier properties but poor moisture barrier and mechanical properties, which limit their application. Starch can also be used as a filler to produce reinforced plastics (Evangelista and others 1991; Bagheri 1999). Usually, a small amount of starch (6-30%) is compounded with synthetic polymer, increasing the biodegradability of the product.

Starch exhibits thermoplastic behavior when a plasticizer such as water or glycerol is added. Thermoplastic starch (TPS) can be developed by gelatinizing granular starch in the presence of plasticizer, heat, and pressure. TPS products with different viscosity, water solubility, and water absorption have been prepared by altering the moisture/plasticizer content, amylose/amylopectin ratio of raw material, and the temperature and pressure in the extruder (Mohanty and others 2000). Studies have been reported on the plasticization of TPS using glycerol (Forssell and others 1997), sorbitol (Gaudin and others 1999), formamide (Ma and others 2004), dimethyl sulfoxide (Nakamura and Tobolsky 1967), and low molecular

weight sugars (Kalichevsky and others 1993). Plasticizers increase the flexibility and processability of TPS.

Thermoplastic starch cannot be used in many applications because of its sensitivity to humidity and inferior mechanical properties. They find use in soluble compostable foams, expanded trays, shape molded parts, and expanded layers as a replacement of polystyrene. BIOTEC (Emmerich, Germany) has three product lines of thermoplastic starch which include Bioplast® granules for injection molding, Bioflex® film, and Biopur® foamed starch (Mohanty and others 2000).

Cellulose based packaging materials

Cellulose, which is essentially a linear polymer of anhydroglucose, is the most abundant natural polymer on earth. The major source of cellulose is wood which contains 40-50% cellulose by weight. Cellulose is unsuitable for film production because it is highly crystalline, fibrous, and insoluble in water. Therefore, cellulose is dissolved in a mixture of sodium hydroxide and carbon disulphide and recast into sulphuric acid to make cellophane film. Cellophane has good mechanical properties, but it has poor water vapor barrier. It is often coated with nitrocellulose wax or polyvinylidene chloride to improve its water vapor barrier properties. Coated cellophane is used for baked gods, fresh produce, processed meat, cheese, and candy. Cellophane has good gas barrier properties at low relative humidity. However, its barrier properties are reduced at intermediate and high relative humidity. Cellophane is not heat sealable owing to its non-thermoplastic nature (Peterson and others 1999).

Alternatively, cellulose can be derivatized from the solvated state by either esterification or etherification of individual hydroxyl groups on the polysaccharide backbone. A number of derivatives such as cellulose acetate, ethyl cellulose, hydroxyl-ethyl cellulose, and hydroxyl-propyl cellulose are commercially available. Steps involved in making these thermoplastic materials include producing cellulose ester biopolymers in powder form and extruding the ester powders in the presence of different plasticizers and additives. The phthalate plasticizer, used in commercial cellulose ester plastic, is now under scrutiny because of its health implications. Recently, efforts have been geared to replace the phthalate plasticizer by eco-friendly plasticizer such as citrate and blends of citrate and derivatized oil (Ray and Bousmina 2005). The gas and water vapor barrier properties of cellulose acetate are not optimal for food packaging. However, the film is excellent for high moisture products as it allows respiration and reduces fogging (Peterson and others 1999). Cellulose acetate is biodegradable for degrees of substitution up to 2.5. Mazzucchelli (Castiglione Olona, Italy) and Planet Polymer (CA, USA) manufacture biodegradable plastics based on cellulose acetate under the trade names of BIOCETA® and EnviroPlastic® Z respectively. BIOCETA® is used for the manufacture of biodegradable packaging films, retractable films, and tubes (Mohanty and others 2000). Recently, there is an increased interest in reinforcing synthetic plastics with cellulose fibers rather than glass fibers because cellulose fibers can offer desired aspect ratio and increased biodegradability (Mwaikambo 2006; Yin and others 2007).

Other polysaccharide based packaging materials

Chitin is one of the most abundant polysaccharides in nature. It is the second most abundant organic compound on earth after cellulose. Soluble chitin, known as chitosan, is a

natural product obtained from deacetylated chitin. Chitosan possesses repeating units of 1, 4 linked 2-deoxy-2-aminoglucose. The amino group NH_2 can be protonated to NH_3^+ which can have electrostatic interactions with anionic groups in an acid environment. Clear, tough, and flexible chitosan films can be formed by film casting from aqueous solution. Systematic investigations have been reported on the effects of factors such as plasticizer concentrations, storage time (Butler and others 1996), acid types and concentrations (Caner and others 1998), molecular weights of chitosan (Park and others 2002), and the degree of deacetylation of chitosan (Wiles and others 2000) on the mechanical and barrier properties of chitosan films. Limitation of chitosan films is the lack of long term stability and higher water vapor permeability (WVP). Chitosan films can be used to protect foods from fungal decay and modify atmosphere of fresh fruits (Krochta and De Mulder-Johnston 1997).

Pectin is a family of heterogeneous branched polysaccharides consisting mostly of variably methylated galacturonan segments separated by rhamnose residues, some of which may be linked to short neutral sugar side chains. Pectin is a secondary product of fruit juice, sunflower oil, and sugar manufacture. As a food industry waste, pectin is suitable for producing eco-friendly biodegradable materials. Considerable attention has been given to pectin because it is widely available as waste material and is readily modified, through demethylation, to give preparations that can form edible films in the presence of calcium ions (Krochta and De Mulder-Johnston 1997). However, WVP of pectin films is quite high, which limits its use in food packaging. Several studies on the combination of pectin with other biodegradable materials have been reported (Hoagland and Parris 1996; Coffin and Fishman 1997; Fishman and others 2006).

Protein based packaging materials

Protein-based films have become a research focus because of their better film forming properties, low cost, and biodegradable nature. Protein films have been developed from wheat gluten, soy protein, gelatin, corn zein, casein, and whey protein. It has been demonstrated that protein films have low oxygen permeability (OP). However, protein films have higher water vapor permeability (WVP) as compared to plastic films due to the hydrophilic nature of most proteins.

Wheat gluten is an enriched protein (70-80%) complex containing water insoluble and ethanol soluble prolamins (gliadins) and water and ethanol insoluble glutelins (glutenins) in combination with small amounts of wheat oils, starch, and insoluble hemicellulose. The gliadins are mainly monomeric single chain polypeptides whereas the glutenins are polymeric and disulfide-linked polymeric chains (Pallos and others 2002). Gluten-based films have good oxygen barrier properties while remaining permeable to carbon oxide, making them suitable to modified atmosphere packaging of products such as mushrooms. One major challenge associated with processing of gluten to make packaging materials is a lack of basic understanding of the tertiary and quaternary structure of gluten (Peterson and others 1999).

Soy protein is a globulin with mainly polar amino acids including acidic and basic amino acids and nonpolar amino acids. The major components of soy proteins are β-conglycinin (7S, about 35%) and glycinin (11S, about 52%). Various chemical treatments and plasticizers have been used to improve the brittleness and water resistance of soy protein polymers. For soy proteins, glycerol, ethylene glycol, and propylene glycol have been found

to be better plasticizers than 1,3-propanediol. Glycerol and water significantly increase the flexibility of soy protein polymers, but greatly decrease the tensile strength (Mo and others 1999).

Gelatin is prepared by thermal denaturation of collagen, found in animal skins and bones, in the presence of dilute acid. Gelatin contains a large number of glycine, proline, and 4-hydroxyproline residues. Gelatin is a heterogeneous mixture of single or multi-stranded polypeptides, each with extended left-handed praline helix conformations and containing between 300 and 4,000 amino acids. Gelatin is primarily used as a gelling agent forming transparent elastic thermoreversible gels on cooling below 35 °C. Gelatin can be used as a valuable biopolymer in tissue engineering. However, its poor mechanical properties limit its application as a packaging material. Many techniques such as vapor crosslink, orientation technique, and use of fillers such as hydroxylapatite and tricalcium phosphate have been developed to reinforce gelatin-based films, but the strength is still not high enough, especially in the wet state (Ray and Bousmina 2005).

Corn zein is a group of alcohol soluble (prolamins) proteins found in the endosperm of corn. Corn zein has a molecular weight of 18 to 45 kDa and is soluble in 60% to 70% ethanol. Corn zein is produced commercially by extraction with aqueous alcohol and dried to a granular powder. Zein films are formed by dissolving zein into aqueous ethanol or isopropanol, heating to 65-85 °C, cooling down to 40-50 °C, and casting on a petri dish. Glycerol is often used to reduce brittleness of zein films. However, glycerol tends to migrate through the film matrix because of the weak interaction between protein and glycerol molecules. Migration of glycerol results in loss of flexibility in the film. A mixture of

glycerol and polyethylene glycol (PEG) has been shown to slow the migration rate in zein films. Tensile strength (TS) of zein films is similar to that of wheat gluten films. Water vapor permeability (WVP) of zein films is lower than or similar to those of other protein films. However, WVP of zein films is higher than that of low density polyethylene (LDPE). Many techniques such as addition of lipids and use of cross-linking agents have been developed to improve WVP of zein films. Oxygen permeability (OP) of zein films is higher than that of wheat gluten films. This has been attributed to easier permeation of oxygen molecules through helical conformation of zein as compared to highly cross-linked structure of wheat gluten (Padua and Wang 2002; Hernandez-Izquierdo and Krochta 2008).

Biodegradable films can be formed from total milk protein or components of milk protein. Milk proteins are classified into two types as casein and whey protein. Casein, comprising 80% of total milk protein, consists of three main components, α, β, and γ with molecular weights between 19 and 25 kDa. Casein forms colloidal micelles in milk and is stabilized by calcium-phosphate bridging. Casein precipitates when milk is acidified to the isoelectric point (pH = 4.6) of casein. Acidified casein is converted to functional soluble caseinates (sodium and calcium caseinates) by neutralization through addition of alkali. Biodegradable films based on caseinates can be obtained by solubilization in water followed by casting and drying. Films from caseinates have water vapor permeability comparable to wheat gluten and soy protein films (Krochta 1997; Hernandez-Izquierdo and Krochta 2008).

Whey protein is the milk protein which remains soluble in milk serum after casein is coagulated during cheese or casein production. Whey proteins, comprising 20% of total milk proteins, contains a mixture of proteins such as β-lactoglobulin (molecular weight of 18

kDa), α-lactalbumin (molecular weight of 14 kDa), bovine serum albumin, and immunoglobulins. β-lactoglobulin comprises approximately 57% of total whey protein and it contains 2 disulfide groups, one free sulfhydryl group, and hydrophobic groups located in the interior. α-lactalbumin comprises approximately 20% of total whey protein and in contains four disulfide bonds. Formation of whey protein films involves heat denaturation in aqueous solutions. Denaturation breaks existing disulfide bonds and forms new intermolecular disulfide and hydrophobic bonds. Water vapor permeability of whey protein films is affected by relative humidity, type and concentration of plasticizer. Whey protein isolate (WPI) films have poorer WVP than wheat gluten, soy protein, corn zein, and caseinate films (Krochta 1997; Perez-Gago and Krochta 2002).

Poly hydroxyalkanoate (PHA) based packaging materials

PHAs are the polymers of hydroxyalkanoates which are accumulated as a source of carbon or energy in various microorganisms under the condition of limiting nutritional elements. More than 300 different microorganisms are known to synthesize and accumulate PHAs (Lee and others 1999). The best known biopolymer types are the polyhydroxyalkanoates, mainly polyhydroxy-butyrate (PHB) and polyhydroxy-butyrate-valerate (PHBV). PHBV is a copolymer of hydroxyl-butyrate (HB) and hydroxyl-valerate (HV). Such copolymers, produced by Metabolix, are better known as Biopol™. Manufacture of blow-molded bottles using Biopol for packaging shampoo was started by Wella AG (Darmstadt, Germany) (Mohanty and others 2000). Other companies producing bacterial PHBV include PHB Industrial SA from Brazil and Tianan from China. Recently, Procter and

Gamble has begun to develop a large range of polyhydroxybutyrate co-hydroxyalkanoates with a trademark of Nodax.

Packaging materials made from PHA possess excellent film forming and coating properties. PHAs have properties close to that of polypropylene (PP) (Brandl and Puchner 1992). The properties of the film can be adjusted by changing the ratio of HB and HV. A high content of polyhydroxybutyrate (PHB) gives a strong and stiff material whereas polyhydroxyvalerate (PHV) improves flexibility and toughness. Properties of PHBV properties can be improved by using plasticizers (Kotnis and others 1995). The polyalkanoates are more hydrophobic than polysaccharide-based materials resulting in their better moisture barrier properties. PHAs are biodegradable in soil and have excellent processability. Higher cost of production, brittleness, and poor gas barrier properties limit the use of PHAs (Peterson and others 1999). Several processes for producing PHA from cheap carbon sources have been developed which have been reviewed by Lee and others (1999).

Polylactic acid (PLA) based packaging materials

The manufacture of PLA by ring opening polymerization of lactic acid was started by Carothers in 1932 and it was further developed by Dupont and Ethicon (Peterson and others 1999). Lactic acid can be produced by fermentation of carbohydrate by lactobacillus, therefore, PLA is considered a renewable material. Compared to the other biodegradable polyesters, PLA is a preferred product because of its availability low cost. Cargill-Dow has offered a series of PLA product (NatureWorks®) manufactured using renewable agricultural resources such as corn or sugar beets. The company has the production capacity of 400

million lb/yr. Different companies such as Mitsui Chemicals (Japan) and Shimadzu (Japan) also manufacture PLA with smaller production capacity.

PLA has good mechanical and thermal properties, however, properties of PLA are highly related to the ratio between two mesoforms (D and L). L-PLA has higher crystallinity, which can lead to higher melting temperatures and brittleness. Furthermore, PLA can be plasticized using Polyethylene glycol (PEG), triethyl citrate (TC), and partial fatty acid esters (Jacobsen and Fritz 1999; Ke and Sun 2001). PLA has moderate barrier properties (WVP and OP) as compared to those of polystyrene. However, high density, high polarity, poor heat resistance, and brittleness limit its use. PLA is currently used in packaging as films, thermoformed and blow molded containers, food service ware, and short shelf-life bottles (Gross and Kalra 2002).

Biopolymer blends

Blends of biopolymers with other biodegradable polymers have been considered a promising option for preparing polymers with "tailor-made" (functional physical properties and biodegradability) properties. Incorporating relatively low cost natural biopolymers into biodegradable synthetic polymers provides a way to reduce the overall cost of the material and offers a method of modifying both properties and degradation rates.

Starch based polymer blends

Starch and PLA blends

PLA is often blended with starch to increase biodegradability and reduce costs. Ajioka and others (1995) first reported starch and PLA blends by using a sealed mixer and hot-pressing the blends into transparent films. Jacobsen and Fritz (1996) studied the thermal

behavior of PLA filled with native corn starch in the presence of polyethylene-glycol (PEG) as a plasticizer. PEG lowered the glass transition temperature and enhanced crystallization of PLA at room temperature. The addition of native corn starch to either pure PLA or to the blend of PLA-PEG did not influence the thermal behavior of PLA. Kim and others (1998) prepared blends of poly (L-lactic acid) (PLLA) and corn starch. They found that the tensile strength (TS) and percent elongation (%E) at the break of the blends decreased as starch content increased. At the same starch content, the blend with high-amylose corn starch gave higher TS than with native corn starch. Park and others (1999) compared the blends from PLLA and S-PLLA (star-shaped PLLA) in the presence of polycaprolactone (PCL) and high-amylose corn starch. At the same starch content, blends from PLLA had better mechanical properties as compared to those from S-PLA. Toughness of the blends was improved by adding PCL. Ke and Sun (2000) characterized the properties and morphology of PLA-starch blends at large range of starch and PLA ratios. They found that the PLA phase became discontinuous and water absorption of the blends increased sharply when starch content increased to more than 60%. Park and Im (2000) melt blended PLA and gelatinized starch with various ratios of water/glycerol by using twin screw mixer. Results showed that gelatinization of starch led to destruction of hydrogen bonding in granules and a decrease in crystallinity of starch. The addition of gelatinized starch improved the interfacial adhesion between starch and PLA. Blends of linear PLA and gelatinized starch with water/glycerol ratio of 100/40 had the best mechanical properties and the toughness was improved as compared to PLA/pure starch blends.

From a thermodynamics point of view, PLA and starch are immiscible (Wool and Sun 2005). The interfacial fracture strength is low due to the poor interdiffusion of molecules necessary for creating entanglements at the interface between PLA and starch. Interfacial adhesion plays a vital role in the mechanical properties of polymer blends. In this case, reactive interfacial coupling agents (or compatibilizers) are often used to improve interfacial properties and control morphologies of polymer blends. Wang and others (2002) used methylenediphenyl diisocyanate (MDI), which is highly reactive with both hydroxyl and carboxyl groups, as a coupling agent for blends of starch and PLA. Results showed that the blend with 45% starch and 0.5 wt% MDI had a smooth microstructure and gave the highest TS (about 68 MPa) with %E of about 5.1%. However, MDI is a hazardous material, which makes it unsuitable for food packaging applications. Zhang and Sun (2004) used another coupling agent maleic anhydride (MA) to compatibilize PLA and starch blends. MA is highly reactive with PLA free radicals induced by an initiator, such as 2,5-bis (*tert*-butylperoxy)-2,5-dimethylhexane (L101) and the anhydride group can react with hydroxyls from starch to form ester linkages. Their results showed that mechanical properties of the blends with MA improved significantly as compared to blends without MA. The PLA/starch composites at a ratio of 55/45 compatibilized by 1% MA and initiated by 10% L101 (MA basis) resulted in highest TS (52.4 MPa) and %E (4.1%).

Starch and polycaprolactone (PCL) blends

Polycaprolactone (PCL) is not widely used for biodegradable packaging applications because of its higher cost. The main use of PCL is for medical applications. However, starch/PCL blends made it possible to overcome the cost barrier. Several commercial blends

of starch and PCL exist in the market: Mater-Bi from Novamont SA (Novara, Italy), Envar from Michigan State University (Lansing, MI), and Bioplast from Biotech Corp. (Emmerich, Germany).

Many studies on PCL-starch composites have been reported (Koenig and Huang 1995; Averous and others 2000; Mani and Bhattacharya 2001). Mani and Bhattacharya (2001) reported that the addition of starch to PCL caused a decrease in tensile modulus (TM) by a factor of 1.5 to 3, a decrease in TS by 50%, and a large decrease in %E by a factor of 5 to10. However, at 25% high amylose starch (70% amylose), PCL-starch composites showed only a small (20%) decrease in TS than neat PCL. When the content of high amylose starch was above 25%, the TS of the PCL-starch composites decreased rapidly. According to dynamic mechanical thermal analysis, amylose behaved as a phase-separated and low particle size filler for PCL. In addition, starch was also found to affect biodegradation kinetics by increasing the biodegradation rate over that of PCL alone (Bastioli and others 1995).

Similar to PLA-starch blends, small amounts of compatibilizers can increase the amount of starch that can be incorporated into PCL matrix without deteriorating the properties. Mani and others (1998) reported grafting of PCL onto starch as a compatibilizer by introducing urethane linkages. They found that the compatibility of the starch/PCL blend was enhanced with the compatibilizer. The study demonstrated that the compatibilized starch/PCL blend has finer phase domains and an improved interfacial adhesion. Mechanical properties of the compatibilized blend were also found to be significantly higher than those of the corresponding uncompatibilized starch/PCL blend. In another study, Choi and others (1999)

prepared starch-g-PCL (SGCL) graft copolymer and investigated the effect of SGCL as a compatibilizer on the mechanical properties of the PCL/starch blends. They found that at a PCL/starch ratio of 60:40, the TS and TM decreased with an increase in content of grafted compatibilizers. However, the percent elongation (%E) at break increased. They also found that grafted compatibilizers with short graft lengths and a high degree of graft polymerization were the most effective. All of the studies mentioned above are based on compatibilizer that has been produced by graft polymerization of a PCL monomer on the starch backbone. Studies have been done on the addition of various amounts of maleic anhydride (MA) modified polyester to produce a compatibilized blend. Mani and Bhattacharya (2001) reported a 3-fold increase in the TS of starch-PCL blends with 50% starch and 5% MA modified polyester. However, no changes in the TM or %E were observed. Similarly, Avella and others (2001) reported a 3-fold increase in the resilience of starch-PCL blends with 50% starch and 10% MA modified polyester as a compatibilizer.

Starch and PHA/PHB blends

When PHB and starch are mixed together, the resulting blends have poor mechanical properties due to the high crystallinity of both polymers (Innocentini-Mei and others 2003). Innocentini-Mei and others (2003) prepared PHB/starch blends from natural starch, starch-adipate, and grafted starch-urethane derivatives. For all blends, a significant decrease of glass transition temperature and melting point was observed. The best results were obtained with grafted starch-urethane blends using poly(propylene glycol). In another study (Parulekar and Mohanty 2007), high amylose starch was used to prepare PHA/starch blends. Starch was destructurized and plasticized followed by melt-blending with PHA. They found that aging

problem with starch and PHA blends was effectively reduced by limiting the moisture uptake of the starch component, hindering the leaching of glycerol, and inhibiting the secondary crystallization of PHA component in the films.

Starch and polybutylene succinate (PBS) blends

There are limited studies focused on the addition of low cost corn starch to polybutylene succinate (PBS) or polybutylene succinate adipate (PBSA) to reduce cost while maintaining adequate mechanical properties and processability (Ratto and others 1999). Usually, starch and PBS or PBSA blends are used to produce biodegradable plastic sheet which can be thermoformed into products such as biscuit trays or films. Ratto and others (1999) investigated the properties of PBSA and corn starch blends of varied compositions (corn starch from 5% to 30%). Results showed that the values of TS of the blends were lower than that of the polyester alone, but there was not a significant drop in TS with increasing starch content. In addition, melt temperature and processing properties were not appreciably affected by starch content. They also investigated the biodegradability properties of PBSA and starch blends by measuring CO_2 production in a soil burial test. Addition of only 5% starch showed a large reduction in half-life from that of the pure PBSA. The half-life was found to decline with increasing starch content until a minimum was reached at 20% starch content.

Starch and polyvinyl alcohol (PVOH) blends

PVOH is water soluble synthetic polymer which has excellent film forming, emulsifying, and adhesive properties. It has high TS and %E as well as better oxygen barrier properties. Starch and PVOH have been blended to yield thermoplastic material with

properties far superior to starch alone. Mao and others (2000) prepared extruded corn starch-glycerol-PVOH blends. They reported that samples of starch-glycerol without PVOH had TS and %E of 1.8 MPa and 113% respectively whereas those containing PVOH had TS and %E of 4 MPa and 150% respectively. Stenhouse and others (1993) utilized extruded blown films of starch-glycerol-PVOH to examine the effect of PVOH molecular weight on the physical properties of the film. Formulation with intermediate molecular weight of PVOH exhibited very low OP in addition to acceptable mechanical properties. Lawton and Fanta (1994) observed that the %E of starch-PVOH-glycerol films could be further improved by adding a small amount of poly (ethylene-co-acrylic acid) (EAA). Their study concluded that a small amount of EAA (3%) was optimum for obtaining films having %E of at least 100% and TS of 25 MPa, while maintaining starch content above 50%.

Chen and others (1996) found that the relative absorption rates of starch-PVOH films was similar to starch under higher relative humidity conditions, while under low humidity conditions it showed an overall trend similar to that of PVOH alone. The TS decreased with increased relative humidity. Another problem with PVOH is its slower biodegradation rate. Chiellini and others (1999) found that degradation of PVOH-based materials was rather limited under simulated composting and soil burial conditions. When 9% of PVOH was added to starch-glycerol formulations, the weight loss was only 59% within 22 days of exposure in compost. Chen and others (1996) observed that the rate of biodegradation in starch-PVOH cast films slowed down with an increase in PVOH content.

In general, PVOH is a readily available biodegradable material and blends of starch and PVOH have many advantages. They can be used in multiple applications. Starch-PVOH

blends are being explored for replacement of LDPE films in applications where mechanical properties are critical for intended use and good moisture barrier properties are not necessary.

Starch and ethylene vinyl alcohol (EVOH) blends

EVOH has been explored as an alternative to PVOH (Dell and Kohlman 1994; Simmons and Thomas 1995; Stenhouse and others 1997). EVOH is a random copolymer of PVOH and polyethylene and is, therefore, less hydrophilic than PVOH. Its properties depend on the ethylene/vinyl alcohol composition ratio. EVOH with an ethylene content of 38% exhibits good mechanical (TS of 65 MPa; %E = 280%) and oxygen barrier properties (Stenhouse and others 1997).

Dell and Kohlman (1994) investigated the effects of water content (4 to18%) on the properties of starch/EVOH blends. Results showed that the morphology, rheology, and tensile properties are highly correlated to water content. Stenhouse and others (1997) prepared blends of native corn starch and EVOH with starch:EVOH ratios of 1:1 and 2:1. Results showed that there was a strong dependence of mechanical properties on starch content, moisture content, and processing history. Percent elongation at break of 1:1 blend was only about one-third that of EVOH, while that of the 2:1 blends was even lower. EVOH has excellent oxygen barrier properties and is mainly used as an oxygen barrier layer in multilayer film packaging. However, the high cost of EVOH is a significant barrier to its widespread use in other biodegradable plastics applications.

Other biodegradable natural and synthetic polymer blends

Compared to starch-based biodegradable polymer blends, very few studies have reported on blends of other natural and synthetic biodegradable polymers. Some of the

studies done include those on cellulose/biodegradable synthetic polymer blends (Nishio and Manley 1988; Masson and Manley 1992), Chitosan/PVOH blends (Zheng and others 2001; Drambei and others 2006), Chitosan/PLA blends (Li and others 2004), Pectin/PVOH blends (Coffin and Fishman 1997; Fishman and others 2006). However, most of these polymer blends are not directly designed for food packaging applications or the cost of the polymer blends is very high.

PLA/PCL blends have been extensively studied (Kim and others 2000; Maglio and others 1999; Maglio and others 2004; Meredith and Amis 2000). Various compatibilizers such as P(LA-*co*-CL) copolymer were used to improve the miscibility between PLA and PCL. The blends displayed good dispersion of the PCL minor phase in the PLA matrix, resulting in better mechanical properties compared to those of neat PLA. Other studies on PLA/poly (butylene adipate-co-terephthalate) blends (Jiang and others 2006) and PLA/PHA blends (Noda and others 2004) show the potential for modifying the mechanical and thermal properties of PLA.

Another promising area is soy protein-based blends. Zhong and Sun (2001) prepared blends of soy protein isolate (SPI) with 10, 20, 30, 40, and 50% PCL alone or with addition of 0.5, 1.0, 2.0 and 5.0% methylene diphenyl diisocyanate (MDI). In their study, they found that compatibility between SPI and PCL improved with the addition of MDI. Mechanical properties of the 50/50 (SPI/PCL) blends increased with an increase in MDI content. TS of the SPI/PCL blends with 2% MDI decreased and %E of the blends increased with increasing PCL content. Water resistance of the blends improved significantly by incorporation of PCL and MDI. Graiver and others (2004) reported blends of soy protein concentrate and

biodegradable polyester using glycerol as a compatibilizing agent. They concluded that use of soy protein concentrate instead of the more expensive soy protein isolate will lead to new potential opportunities based on renewable resources.

Food packaging materials based on bio-nanocomposites

Recently, the use of nanoparticles as additives to enhance the polymer performance has been established. Various nanoreinforcements currently being developed are layered silicates (Pinnavaia and Beall 2001), cellulose nanowhiskers (Neus Angles and Dufresne 2000; Neus Angles and Dufresne 2001), ultra fine layered titanate (Hiroi and others 2004), and carbon nanotubes (Kumar 2004). Among these, the layered silicates such as clay have attracted great attention by the packaging industry because of their environmental friendliness, natural abundance, low cost, and improved properties.

Polymer layered silicate (PLS) nanocomposite technology was first developed for automotive applications by Toyota researchers in the late 1980s (Fukushima and Inagaki 1987; Okada and others 1987) and Toyota was the first company to commercialize these nanocomposites (nylon 6-clay nanocomposites) (Ray and others 2006). In the following years, PLS nanocomposites attracted increasing interest as a means for improving properties of synthetic polymers. These studies include nanocomposites of nylon 6-clay (Kojima and others 1993a, 1993b), polyurethane-clay (Wang and Pinnavaia 1998), polypropylene-clay (Kurokawa and others 1996; Usuki and others 1997; Kawasumi and others 1997), polyimide-clay (Yano and others 1993; Yano and others 1997), polystyrene-clay (Vaia and others 1995; Vaia and Giannelis 1997) and polysiloxane-clay (Mark 1996) etc. Nanocomposites exhibit remarkable improvement in properties with very low silicate content ($\leq 5\%$). These

improvements can include high tensile modulus, increased strength and heat resistance, and improved barrier properties. Nanocomposites also offer other benefits such low density, transparency, better surface properties, and recyclability (Giannelis 1996).

Potential applications of these nanocomposites include automobiles (gasoline tanks, bumpers, interior and exterior panels etc.), construction (building sections, structural panels), aerospace (flame retardant panels, high performance components), electronics (printed circuit boards, electric components), and pigments (Ray and others 2006). In order to take advantage of their substantially enhanced properties, polymer nanocomposites have also been studied for food packaging applications including injection molded bottles for beverage or beer, coatings for paperboard juice cartons, and cast and blown films (Ray and others 2006). Use of these nanocomposites for food packaging with oxygen scavenging, reduced flavor scalping, increased heat resistance, and better gas barrier properties has resulted in shelf-life of 3 to 5 years for packaged food (Sajilata and others 2007).

In contrast with polymer-based PLS nanocomposites, biopolymer-based PLS nanocomposites (bio-nanocomposites) have received little attention. However, several research groups have reported preparation and characterization of various kinds of bio-nanocomposites showing potential for a wide range of applications. In this part, the review is restricted to bio-nanocomposites, including a brief outline of synthesis, characterization, and recent developments in various bio-nanocomposites.

Structure and properties of layered silicates

The most commonly used silicates in PLS nanocomposites include montmorillonite (MMT), hectorite and saponite, and their various modifications. These layered silicates

belong to the general family of 2:1 layered silicates or phyllosilicates (Giannelis 1996). Their crystal lattice structure consists of a two-dimensional, 1 nm thick layers which are made up of an octahedron sheet of aluminum sandwiched in between two tetrahedral sheets of silicon (Figure 1). The lateral dimensions of these layers vary from 30 nm to several microns or larger, depending on the particular layered silicate. Stacking of the layers leads to a regular van der Waals gap between the layers called the interlayer or gallery. Isomorphic substitution within the layers (Al^{3+} replaced by Mg^{2+} or Fe^{2+} in octahedron sheet, or Si^{4+} replaced by Al^{3+} in tetrahedron sheets) results in net negative charge that are counterbalanced by alkali and alkaline earth cations such as Na^{+} residing in the galleries.

In natural layered silicates, the interlayer cations are usually hydrated Na^{+} or K^{+}, showing hydrophilic surface properties. In this natural state, layered silicates are only miscible with hydrophilic polymers. To render layered silicates miscible with hydrophobic polymers, one must convert the hydrophilic silicates surface to an organophilic one. This is done by ion-exchange reactions with various organic cations (e.g. alkylammonium cations, cationic surfactant etc.). The organic cations lower the surface energy of the silicate surface and result in a larger interlayer spacing. Additionally, the organic cations may contain various functional groups that react with the polymer to improve interaction between the silicates and the polymer matrix.

Preparation and characterization of nanocomposite

For preparation of nanocomposite, polymer chains must diffuse into the galleries between silicate layers to produce structures ranging from intercalated to exfoliated (Figure 2). Intercalation occurs when a small amount of polymer penetrates into the galleries,

resulting in finite expansion of the silicate layers. This leads to a well-ordered multilayered structure with a repeat distance of a few nanometers, and is observed in systems with limited miscibility. Extensive polymer penetration leads to exfoliation or delamination of silicate layers. An exfoliated nanocomposite consists of nanometer thick platelets distributed homogeneously throughout the polymer matrix. In contrast, when the polymer and silicate are immiscible, the layers do not separate and exist as agglomerates or tactoids.

The complete dispersion of clay platelets in a polymer optimizes the number of available reinforcing elements for carrying an applied load and deflecting cracks. The coupling between the tremendous surface area of the clay and the polymer matrix facilitates stress transfer to the reinforcement phase, allowing for such mechanical improvements. In addition, the impermeable clay layers mandate a tortuous pathway for a permeant to transverse the nanocomposites (Figure 3). The enhanced barrier properties, chemical resistance, reduced solvent uptake, and flame retardance of polymer-clay nanocomposites result from the hindered diffusion pathway through the nanocomposites.

Synthesis of PLS nanocomposites initially involved either intercalation of a suitable monomer followed by polymerization (in-situ polymerization) (Okada and others 1987; Messersmith and Giannelis 1993) or polymer intercalation from solution (Ruiz-Hitzky and Aranda 1990; Wu and Lerner 1993) i.e., intercalation of dissolved polymer from a solution. However, for most polymers, both in-situ polymerization and intercalation from solution are limited because neither a suitable monomer nor a compatible polymer-silicate solvent system is always available. Vaia and others (1993) discovered a more versatile and environmentally benign approach based on direct polymer melt intercalation. The process involved mixing the

layered silicate with the polymer and heating the mixture above the softening point of the polymer. This allowed use of processing techniques such as hot-mixing, melt-extrusion, and ultrasonication for preparing nanocomposites. Recently, a new alternative method for the preparation of nanocomposites, which involves a solid-state mixing at room temperature (ball milling) (Sorrentino and others 2005; Mangiacapra and others 2006) was proposed. In this case, solid layered dispersion is promoted by the energy transfer between milling tools (generally balls) and polymer/inorganic particles mixture, which in turn results grinded and intimately mixed.

Generally, the structure of nanocomposites is characterized by two complementary analytical techniques, namely, X-ray diffraction (XRD) and transmission electron microscopy (TEM). XRD is used to identify intercalated structures by determination of the interlayer spacing (d-spacing). Intercalation of the polymer chains increases the interlayer spacing and according to Bragg's law, it causes a shift of the diffraction peak towards lower angle. As more polymer chains enter the interlayer spacing, the clay platelets become disordered, thus causing broader peaks and a wider distribution of such peaks, which implies exfoliation of the layered silicates in the polymer matrix (McGlashan and Halley 2003). In addition, TEM images provide further evidence for the occurrence of intercalation or exfoliation. TEM allows a qualitative understanding of the internal structure, spatial distribution and dispersion of the nanoparticles within the polymer matrix through direct visualization.

Both TEM and XRD are essential tools for evaluating nanocomposite structure. However, other techniques such as DSC (Giannelis 1996), NMR (VanderHart and others

2001), and FTIR (Loo and Gleason 2003) have also been used for structural characterization of nanocomposites.

Bio-nanocomposites

The extraordinary success of the nanocomposite concept in the area of synthetic polymer has stimulated new research on nanocomposites based on biodegradable polymers as matrix. So far, the most studied bio-nanocomposites are based on starch, cellulose, pectin, proteins, polyhydroxy-butyrate (PHB) and polylactide (PLA).

Starch based bio-nanocomposites

Owing to its complete biodegradability, wide availability and low cost, starch-based bio-nanocomposites have attracted a lot of attention in recent years. De Carvalho and others (2001) provided a first insight in the preparation and characterization of thermoplasticized starch-kaolin composites by melt intercalation techniques. Several other studies have been performed on the preparation of starch-clay nanocomposites by melt intercalation (Park and others 2002 and 2003; Wilhelm and others 2003; Avella and others 2005; Chen and Evans 2005; Huang and others 2005; Pandey and Singh 2005; Chiou and others 2007). Park and others (2002 and 2003) reported an increase in TS and %E by more than 25% and 20%, respectively, and a 35% decrease in water vapor transmission rate for bio-nanocomposites based on potato starch and 5% clay. Wilhelm and others (2003) observed a 70% increase in TS of Cará root starch-hectorite nanocomposite films at 30% clay content. However, %E decreased by 50%. Avella and others (2005) reported preparation of starch-MMT bio-nanocomposite films for food packaging applications. Result showed an increase in TM and TS. Conformity of the bio-nanocomposite samples with European directives on

biodegradable materials was verified by migration tests and by putting the films into contact with vegetables and simulants. Pandey and Singh (2005) investigated different methods of preparing corn starch-MMT films and determined that the order of adding different components affected the mechanical properties. Chiou and others (2007) observed an improvement in thermal stability and water absorbance of wheat starch-MMT bio-nanocomposites.

In some other reports, starch and biodegradable polyester blends were used for synthesis of starch-polyester-clay nanocomposites (McGlashan and Halley 2003; Kalambur and Rizvi 2004 and 2005). McGlashan and Halley (2003) used melt extrusion for the preparation of starch-polyester-organically modified clay (organoclay) nanocomposites. XRD data indicated that the best results were obtained for 30% starch blends. The level of dispersion depended on the ratio of starch to polyester and amount of organoclay added. The results showed that TM and TS increased by 275% and 40% respectively whereas %E increased by 40%. Kalambur and Rizvi (2005) reported preparation of starch-PCL-organoclay nanocomposites by reactive extrusion. The results showed that %E of these nanocomposites was comparable to that of polyester.

Cellulose based bio-nanocomposites

Cellulosic derived plastics such as cellulose acetate (CA), cellulose acetate propionate (CAP), and cellulose acetate butyrate (CAB) are thermoplastic materials produced through esterification of cellulose. CA is of particular interest because it is a biodegradable polymer which has excellent optical clarity and high toughness. Park and others (2004a) reported preparation of bio-nanocomposites based on plasticized CA and clay. The results showed that

the addition of TEC plasticizer at 20% exhibited best intercalation and exfoliation of clays as well as the best properties of the resulting bio-nanocomposites. The tensile strength, tensile modulus, and heat deflection temperature improved and the water vapor permeability reduced by 50%. Park and others (2004b) investigated the effect of compatibilizer maleic anhydride grafted cellulose acetate butyrate (CAB-g-MA) on the structure of the bio-nanocomposites based on CA and organoclay. Results showed that the bio-nanocomposites with 5% compatibilizer showed greater extent of exfoliation than the ones without the compatibilizer.

Other polysaccharide based bio-nanocomposites

Mangiacapra and others (2006) reported the preparation of bio-nanocomposites based on natural pectins and MMT to improve the mechanical and barrier properties of natural pectins. They used a new alternative method for the preparation of bio-nanocomposites, which involved a solid-state mixing at room temperature (ball milling). The elastic modulus of the bio-nanocomposites increased from 1630 MPa to 2962 MPa and the oxidation was delayed by 30^{o}C. Bio-nanocomposites also resulted in reduced WVP and OP.

Protein based bio-nanocomposites

Wheat gluten is one alternative to synthetic plastics in food packaging applications due to its high gas barrier properties and relatively hydrophobic nature compared to other biopolymers. Olabarrieta and others (2006) used two types of nanoclay (Cloisite Na^{+} (MMT) and Cloisite 10A) preparing gluten-based bio-nanocomposites. The films were cast from ethanol/water solutions of pH 4 and 11. TEM and XRD results showed that the films

prepared from solution of pH 11 with natural MMT resulted in greater extent of exfoliation. These films also had the best mechanical and barrier properties of all the films tested.

Gelatin is obtained by hydrolytic cleavage of collagen chains. Edible coatings from gelatin reduce oxygen, moisture, and oil migration and can also carry an antioxidant or antimicrobial. However, poor mechanical properties are the main limitation of gelatin films. Zheng and others (2002) prepared gelatin-MMT nanocomposites. The results showed that TS and TM of the bio-nanocomposites improved significantly with increase in MMT content.

Biopolymers made from soy protein isolate (SPI) alone possess good biodegradability, but poor flexibility. Plasticizers are used to overcome the brittleness of SPI-based biopolymer films. However, the use of plasticizers leads to significant decrease in TS of the films. Flexible nanocomposite films having high TS can be obtained by reinforcing the SPI-plasticizer system with suitable filler materials such as nanoparticles. Dean and Yu (2005) developed an effective method to exfoliate MMT lamellae in water using ultrasonic and prepared MMT-reinforced soy protein films plasticized by a mixture of water and glycerol. The ultrasonic treated bio-nanocomposite material exhibited an exfoliated structure and an improvement in tensile modulus and tensile strength of 84% and 47% respectively. The glass transition temperature of ultrasonic treated bio-nanocomposite showed an increase of 9.5 °C as compared to that of neat soy protein composite. However, water barrier properties of the bio-nanocomposites were not reported. Rhim and others (2005) prepared and studied the mechanical and water barrier properties of composite films of SPI with various clay minerals. The tensile strength of SPI-layered clay films increased by as much as 30% whereas the water vapor permeability decreased by 52%.

Chen and Zhang (2006) prepared highly exfoliated and intercalated SPI-MMT nanocomposites by using the solution exfoliation method in a neutral aqueous medium and investigated the correlation between the microstructure and mechanical properties. The results showed that the heterogeneous distribution of positive charges provided soy globulins to anchor into the negative charged MMT interlayers (distance between two MMT layers). Electrostatic attraction and hydrogen bonding at the interfaces of soy protein and MMT lead to good dispersion of MMT layers in the protein matrix. Highly exfoliated structure with 1-2 nm MMT layers dispersed in protein matrix resulted when the MMT content was less than 12% (w/w). Intercalated structure was predominant when the MMT content was more than 12%. The results also showed improvement in tensile strength (increase from 8.77 to 15.43 MPa) and thermal stability of SPI-MMT bio-nanocomposites. Yu and others (2007) prepared bio-nanocomposite sheets based on soy proteins and rectorite (REC) by compression molding. REC is a 1:1 layered silicate which is composed of a regular stacking of mica-like layers and MMT-like layers. Interlayer spacing in REC is approximately 2.4 nm as compared to 1.2 nm of MMT. Thus, REC is expected to allow better penetration of protein molecules in between interlayers. The results showed exfoliated nanocomposite structure up to REC content of 12%, and above this, intercalated structures were formed. This correlated well with the mechanical properties results with TS of the nanocomposite sheets being maximum (12.92 MPa) at a REC content of 12%. Percentage elongation (%E) at break of the nanocomposite sheets decreased sharply with increasing REC content.

PHB based bio-nanocomposites

Maiti and others (2003) reported the preparation of PHB-organoclay bio-nanocomposites using melt extrusion. XRD results showed formation of well-ordered intercalated bio-nanocomposite structure. However, bio-nanocomposites based on organically modified MMT showed thermal degradation because thermoplastic PHB is very unstable and degrades at temperatures near its melting point. Maiti and others (2007) prepared bio-nanocomposites based on PHB and clay and showed significant improvement in thermal and mechanical properties of bio-nanocomposites as compared to the neat polymer. The rate of biodegradation of PHB was also enhanced significantly in the bio-nanocomposites.

PLA based bio-nanocomposites

The large-scale use of PLA is still prevented by its relatively poor performance as compared to plastics. Use of nanoclay as a reinforcement agent has the potential to expand the application of PLA. Many studies (Ogata and others 1997; Bandyopadhyay and others 1999; Maiti and others 2002; Pluta and others 2002; Ray and others 2002a, 2002b, 2002c, 2003a, 2003b; Chang and others 2003; Krikorian and others 2003; Lee and others 2003; Paul and others 2003; Cabedo and others 2006) have reported preparation and characterization of PLA-clay bio-nanocomposites. Ogata and others (1997) prepared PLA-organoclay blends by dissolving the polymer in hot chloroform in the presence of dimethyl disteary ammonium modified MMT. The results showed a strong tendency of tactoids formation by solvent-cast method. Bandyopadhyay and others (1999) reported successful preparation of PLA-organoclay nanocomposites by melt extrusion technique with much improved thermal and

mechanical properties. Ray and others (2002a, 2002b, 2002c) used melt extrusion for the preparation of PLA-organoclay bio-nanocomposites with improved properties. XRD patterns and TEM observations established that the silicate layers were intercalated and randomly distributed in the bio-nanocomposite matrix. The intercalated bio-nanocomposites exhibited significant improvement in properties in both solid and melt states as compared to those of PLA matrices without clay.

Maiti and others (2002) prepared a series of PLA-layered silicate bio-nanocomposites with three different types of natural and modified layered silicates (saponite, MMT, and synthetic mica). Layered silicates were modified with alkylphosphonium salts having different chain lengths. The study showed that miscibility of an organic modifier (phosphonium salt) and PLA is enhanced as the chain length of modifier is increased. They also studied the effects of dispersion, intercalation, and aspect ratio of the clay on the material properties. Bio-nanocomposites of blends of PLA and PCL were obtained by melt-mixing with a modified kaolinite (Cabedo and others 2006). Blending of PCL was aimed at decreasing the brittleness of PLA. Bio-nanocomposites with 4% modified kaolinite showed better processability, thermal stability, and improvement in mechanical properties as compared to the polymer and blends without clay.

Concluding remarks

Biopolymer-based biodegradable food packaging materials could potentially replace non-biodegradable plastics. However, poor mechanical and water vapor barrier properties of these biodegradable materials limit their widespread use in food packaging. Techniques developed to improve the properties of these biodegradable materials include modification of biopolymers, incorporation of other biopolymer with improved technology, and bio-nanocomposites. Table 1 summarizes the properties of biopolymers and bio-nanocomposite films. Blends of biopolymers with other biodegradable polymers are the easiest way to prepare polymers with "tailor-made" (functional physical properties and biodegradability) properties. Several companies have commercialized these types of products.

Bio-nanocomposites are another promising option to further improve material properties while maintaining their biodegradability. The major challenge with bio-nanocomposites is to reduce production and materials cost of these bio-nanocomposites to make them cost-effective against synthetic polymers. To overcome this challenge, there is a need to improve bio-nanocomposite formulation and processing methods to prepare these bio-nanocomposites at a lower cost. Melt intercalation using extrusion offers a potential alternative for industrial production of bio-nanocomposites. There is also a need for better understanding of clay modification, bio-nanocomposite structure formation (exfoliated vs. intercalated), and interaction between biopolymer and nanoparticles. More research is also needed to utilize different types of nanoparticles such as carbon nanotubes and nanocelluloses for producing new nanocomposite materials with improved properties.

References

Ajioka, M., Enomoto, K., and Yamagachi, A. (1995). Degradable polymer composition. *U.S. patent 5444107*.

ASTM. (2005). Standard terminology of packaging and distribution environments, D996-04. In *Annual Book of ASTM*; American Society for Testing and Material: Philadelphia, PA.

Avella, M., Errico, M.E., Rimedio, R., and Sadocco, P. (2001). Preparation of biodegradable polyesters/high amylose starch composites by reactive blending and their characterization. *Journal of Applied Polymer Science*. 83: 1432-1442.

Avella, M., De Vlieger, J.J., Errico, M.E., Fischer, S., Vacca, P., and Volpe, M.G. (2005). Biodegradable starch/clay nanocomposite films for food packaging applications. *Food Chemistry*. 93: 467-474.

Averous, L., Moro, L., Dole, P., and Fringant, C. (2000). Properties of thermoplastic blends: starch–polycaprolactone. *Polymer*. 41 (11): 4157-4167.

Bagheri, R. (1999). Effect of processing on the melt degradation of starch-filled polypropylene. *Polymer International*. 48: 1257-1263.

Bandyopadhyay, S., Chen, R., and Giannelis, E.P. (1999). Biodegradable organic inorganic hybrids based on poly(l-lactic acid). *Polymer Materials: Science and Engineering*. 81: 159-160.

Bastioli, C., Cerutti, A., Guanella, I., Romano, G.C., and Tosin, M. (1995). Physical state and biodegradation behavior of starch-polycaprolactone systems. *Journal of Environmental Polymer Degradation*. 3(2): 81-95.

Brandl, H., and Puchner, P. (1992). Biodegradation of plastic bottles made from 'Biopol' in an aquatic ecosystem under *in situ* conditions. *Biodegradation*. 2: 237-243.

Butler, B.L., Vergano, P.J., Testin, R.F., Bunn, J.M., and Wiles, J.L. (1996). Mechanical and barrier properties of edible chitosan films as affected by composition and storage. *Journal of Food Science*. 61: 953-955.

Cabedo, L., Feijoo, J.L., Villanueva, M.P., Lagaron, J.M., and Gimenez, E. (2006). Optimization of biodegradable Nanocomposites based on aPLA/PCL blends for food packaging applications. *Macromolecular Symposia*. 233: 191-197.

Caner, C., Vergano, P.J., and Wiles, J.L. (1998). Chitosan film mechanical and permeation properties as affected by acid, plasticizer, and storage. *Journal of Food Science*. 63: 1049-1053.

Chang, J.H., Uk-An, Y., and Sur, G.S. (2003). Poly(lactic acid) nanocomposites with various organoclays. I. thermomechanical properties, morphology, and gas permeability. *Journal of Polymer Science Part B: Polymer Physics*. 41: 94–103.

Chen, L., Iman, S.H., Stein, T.M., Gordon, S.H., Hou, C.T., and Greene, R.V. (1996). Starch-polyvinyl alcohol cast film-performance and biodegradation. *Polymer Preprints*. 37: 461-462.

Chen, B., and Evans, J.R.G. (2005). Thermplastic starch-clay nanocomposites and their characteristics. *Carbohydrate Polymers*. 61: 455-463.

Chen, P., and Zhang, L. (2006). Interaction and properties of highly exfoliated soy protein/montmorillonite nanocomposites. *Biomacromolecules*. 7: 1700-1706.

Chiellini, E., Corti, A., D'Antone, S., and Solaro, R. (1999). Biodegradation of PVA-based formulations. *Macromolecular Symposia*. 144: 127-139.

Chiou, B. S., Wood, D., Yee, E., Imam, S. H., Glenn, G. M., and Orts, W. J. (2007). Extruded starch-nanoclay nanocomposites: effects of glycerol and nanoclay concentration. *Polymer Engineering and Science*. 47: 1898-1904.

Choi, E.J., Kim, C.H., and Park, J.K. (1999). Structure-property relationship in PCL/starch blend compatibilized with starch-g-PCL copolymer. *Journal of Polymer Science Part B: Polymer Physics*. 37: 2430-2438.

Coffin, D.R., and Fishman, M.L. (1997). Films fabricated from mixtures of pectin and poly(vinyl alcohol). *U.S. patent 5646206*.

De Carvalho, A.J.F., Curvelo, A.A.S., and Agnelli, J.A.M. (2001). A first insight on composites of thermoplastic starch and Kaolin. *Carbohydrate Polymers*. 45: 189-194.

Dell, P.A., and Kohlman, W.G. (1994). Effects of water content on the properties of starch/poly(ethylene-vinyl alcohol) blends. *Journal of Applied Polymer Science*. 52: 353-363.

Drambei, P., Nakano, Y., Bin, Y.Z., Okuno, T., and Matsuo, M. (2006). Characterization of PVA and chitosan/PVA blends prepared from aqueous solutions of various Na_2SO_4 concentrations. *Macromolecular Symposia*. 242: 146-156.

Evangelista, R.L., Nikolov, Z.L., Sung, W., Jane, J., and Gelina, R.J. (1991). Effect of compounding and starch modification on properties of starch-filled low density polyethylene. *Industrial and Engineering Chemistry Research*. 30: 1841-1846.

Fishman, M.L., Coffin, D.R., Onwulata, C.I., and Willett, J.L. (2006). Two stage extrusion of plasticized pectin/poly (vinyl alcohol) blends. *Carbohydrate Polymer*. 65: 421-429.

Forssell, P.M., Mikkia, J.M., Moates, G.K., and Parker, R. (1997). Phase and glass transition behavior of concentrated barley starch-glycerol-water mixtures, a model for thermoplastic starch. *Carbohydrate Polymers*. 34: 275-282.

Fukushima, Y., and Inagaki, S. (1987). Synthesis of an intercalated compound of montmorillonite and 6-polyamide. *Journal of Inclusion Phenomena*. 5: 473-482.

Gaudin, S., Lourdin, D., Le Botlan, D., Ilari, J.L., and Colonna, P. (1999). Plasticization and mobility in starch-sorbitol film. *Journal of Cereal Science*. 29 (3): 273-284.

Giannelis, E.P. (1996). Polymer layered silicate nanocomposites. *Advanced Materials*. 8(1): 29-35.

Gross, R.A., and Kalra, B. (2002). Biodegradable polymers for the environment. *Green Chemistry*. 297: 803-807.

Hernandez-Izquierdo, V.M., and Krochta, J.M. (2008). Thermoplastic processing of proteins for film formation – a review. *Journal of Food Science*. 73(2): R30-R39.

Hiroi, R., Ray, SS., Okamoto, M., and Shiroi T. (2004). Organically modified layered titanate: a new nanofiller to improve the performance biodegradable polylactide. *Macromolecular Rapid Communications*. 25: 1359-1363.

Hoagland, P.D. and Parris, N. (1996). Chitosan/pectin laminated films. *Journal of Agricultural and Food Chemistry*. 44: 1915-1919.

Huang, M., Yu, J., and Ma, X. (2005). High mechanical performance MMT-urea and formamide-plasticized thermoplastic cornstarch biodegradable nanocomposites, *Carbohydrate Polymers*. 62: 1-7.

Innocentini-Mei, L. H., Bartoli, J. R., and Baltieri, R. C. (2003). Mechanical and thermal properties of poly(3-hydroxybutyrate) blends with starch and starch derivatives. *Macromolecular Symposia*. 197: 77-87.

Jacobsen, S., and Fritz, H.G. (1996). Filling of poly(lactic acid) with native starch. *Polymer Engineering and Science*. 36: 2799-2804.

Jacobsen, S., and Fritz, H.G. (1999). Plasticizing polylactide – the effect of different plasticizers on the mechanical properties. *Polymer Engineering and Science*. 39 (7): 1303-1310.

Jiang, L., Wolcott, M.P., and Zhang, J. (2006). Study of biodegradable polylactide/poly(butylenes adipate-co-terephthalate) blends. *Biomacromolecules*. 7: 199-207.

Kalambur, S., and Rizvi, S.S.H. (2004). Rapid report starch-based nanocomposites by reactive extrusion processing. *Polymer International*. 53: 1413-1416.

Kalambur, S., and Rizvi, S.S.H. (2005). Biodegradable and functionally superior starch-polyester nanocomposites from reactive extrusion. *Journal of Applied Polymer Science*. 96: 1072-1082.

Kalichevsky, M.T., Jaroszkiewicz, E.M., and Blanshard, J.M.V. (1993). A study of the glass transition of amylopectin-sugar mixtures. *Polymer*. 34 (2): 346-358.

Kawasumi, M., Hasegawa, N., Kato, M., Usuki, A., and Okada, A. (1997). Preparation and mechanical properties of polypropylene-clay hybrids. *Macromolecules*. 30: 6333-6338.

Ke, T.Y., and Sun, X.Z. (2000). Physical properties of poly(lactic acid) and starch composites with various blending ratios. *Cereal Chemistry*. 77(6): 761-768.

Ke, T., and Sun, X. (2001). Thermal and mechanical properties of poly(lactic acid) and starch blends with various plasticizers. *Transactions of the ASAE*. 44(4): 945-953.

Kim, C., Cho, K.Y., Choi, E., and Park, J. (2000). Effect of P(LLA-co-CL) on the compatibility and crystallization behavior of PCL/PLLA blends. *Journal of Applied Polymer Science*. 77: 226-231.

Kim, S.H., Chin, I.J., Yoon, J.S., Kim, S.H., and Jung, J.S. (1998). Mechanical properties of biodegradable blends of poly (L-lactic acid) and starch. *Korea Polymer Journal*. 6: 422-427.

Koenig, M.F., and Huang, S.T. (1995). Biodegradable blends and composites of polycaprolactone and starch derivatives. *Polymer*. 36: 1877-1882.

Kojima, Y., Usuki, A., Kawasumi, M., Okada, A., Fukushima, Y., Kurauchi, T., and Kamigaito, O. (1993a). Mechanical properties of nylon 6-clay hybrid. *Journal of Materials Research*. 8: 1185-1189.

Kojima, Y., Usuki, A., Kawasumi, M., Okada, A., Kurauchi, T., and Kamigaito, O. (1993b). Sorption of water in nylon 6-clay hybrid. *Journal of Applied Polymer Science*. 49 : 1259-1264.

Kotnis, M.A., O'Brien, G.S., and Willett, J.L. (1995). Processing and mechanical properties of biodegradable poly(hydroxybutyrate-co-valerate)/starch compositions. *Journal of Environment and Polymer Degradation*. 3 (2): 97–103.

Krikorian, V., and Pochan, D. (2003). Poly(L-lactide acid)/layered silicate nanocomposite: fabrication, characterization, and properties. *Chemistry of Materials*. 15: 4317–4324.

Krochta, J.M. (1997). Edible films and coatings. In: Food proteins and their applications, pp. 529-550. Damodaran, S., and Paraf, A. Eds., CRC Press, Boca Raton, FL.

Krochta J.M., and De Mulder-Johnston, C. (1997) Edible and biodegradable polymer films: challenges and opportunities. *Food Technology*. 51(2): 61-74.

Kumar, S. (2004). Polymer/carbon nanotube composites: challenges and opportunities. *Polymeric Materials Science and Engineering*. 90: 59-60.

Kurokawa, Y., Yasuda, H., and Oya, A. (1996). Preparation of a nanocomposite of polypropylene and smectite. *Journal of Materials Science Letters*. 15: 1481-1483.

Lawton, J.W., and Fanta, G.F. (1994). Glycerol-plasticized films prepared from starch-poly(vinyl alcohol) mixtures: effect of poly(ethylene-co-acrylic acid). *Carbohydrate Polymers*. 23(4): 275-280.

Lee, J.H., Park, T.G., Park, H.S., Lee, D.S., Lee, Y.K., and Yoon, S.C. (2003). Thermal and mechanical characteristics of poly(L-lactic acid) nanocomposite scaffold. *Biomaterials*. 24: 2773–2778.

Lee, S.Y., Choi, J., and Wong, H.H. (1999). Recent advances in polyhydrixyalkanoate production by bacterial fermentation: mini review. *International Journal of Biological Macromolecules*. 25: 31-36.

Li, L.H., Ding, S., and Zhou, C.R. (2004). Preparation and degradation of PLA/chitosan composite materials. *Journal of Applied Polymer Science*. 91: 274-277.

Loo, L.S., and Gleason, K.K. (2003). Fourier transforms infrared investigation of the deformation behavior of montmorillonite in nylon6/clay nanocomposite. *Macromolecules*. 36: 2587-2590.

Ma, X., Yu, J., and Jin, F. (2004). Urea and formamide as a mixed plasticizer for thermoplastic starch. *Polymer International*. 53: 1780-1785.

Maglio, G., Migliozzi, A., Palumbo, R., Immirzi, B., and Volpe, M.G. (1999). Compatibilized polycaprolactone/poly(L-lactide) blends for biomedical uses. *Macromolecular Rapid Communications*. 20: 236-238.

Maglio, G., Malinconico, M., Migliozzi, A., and Groeninckx, G. (2004). Immiscible poly(L-lactide)/polycaprolactone blends: influence of addition of a poly(L-lactide)-Poly (oxyethylene) block copolymer on thermal behavior and morphology. *Macromolecular Chemistry and Physics*. 205: 946-950.

Maiti, P., Yamada, K., Okamoto, M., Ueda, K., and Okamoto, K. (2002). New polylactide/layered silicate nanocomposites: role of organoclay. *Chemistry of Materials*. 14: 4654–4661.

Maiti, P., Batt, C.A., and Giannelis, E.P. (2003). Renewable plastics: synthesis and properties of PHB nanocomposites. *Polymer Materials: Science and Engineering*. 88: 58–59.

Maiti, P., Batt, C.A., and Giannelis, E.P. (2007). New biodegradable Polyhydroxybuty rate/layered silicate nanocomposites. *Biomacromolecules*. 8: 3393-3400.

Mali, S., and Grossmann, M.V.E. (2003). Effects of yam starch film on storability and quality of fresh strawberries (Fragaria ananassa). *Journal of Agricultural and Food Chemistry*. 51: 7005-7011.

Mali, S., Grossmann, M. V. E., Garcia, M. A., Martino, M. N., and Zaritzky, N. E. (2006). Effects of controlled storage on thermal, mechanical and barrier properties of plasticized films from different starch sources. *Journal of Food Engineering.* 75: 453-460.

Mangiacapra, P., Gorrasi, G., Sorrentino, A., and Vittoria, V. (2006). Biodegradable nanocomposite obtained by ball milling of pectin and montmorillonites. *Carbohydrate Polymers*. 64(4): 516-523.

Mani, R., Tang, J., and Bhattacharya, M. (1998). Synthesis and characterization of starch-graft-polycaprolactone as compatibilizer for starch/polycaprolactone blends. *Macromolecular Rapid Communications*. 19: 283-286.

Mani, R., and Bhattacharya, M. (2001). Properties of injection moulded blends of starch and modified biodegradable polyesters. *European Polymer Journal*. 37 (3): 515-526.

Mao, L.J., Imam, S., Gordon, S., Cinelli, P., and Chiellini, E. (2000). Extruded cornstarch-glycerol-polyvinyl alcohol blends: mechanical properties, morphology and biodegradability. *Journal of Polymers and the Environment*. 8(4): 205-211.

Mark, J.E. (1996). Ceramic-reinforced polymers and polymer-modified ceramics. *Polymer Engineering and Science*. 36: 2905-2920.

Marsh, K., and Bugusu, B. (2007). Food packaging – roles, materials, and environmental issues. *Journal of Food Science*. 72(3): R39-R55.

Masson, J. F., and Manley, R.St.J. (1992). Solid-state NMR of some cellulose/synthetic polymer blends. *Macromolecules*. 25: 589-592.

Messersmith, P.B., and Giannelis, E.P. (1993). Polymer-layered silicate nanocomposites: in situ intercalative polymerization of ε-caprolactone in layered silicates. *Chemistry of Materials*. 5: 1064-1066.

McGlashan, S.A., and Halley, P.J. (2003). Preparaion and characterization of biodegradable starch-based nanocomposite materials. *Polymer International*. 52: 1767-1773.

Meredith J.C., and Amis, E.J. (2000). LCST phase separation in biodegradable polymer blends: poly (D, L-lactide) and polycaprolactone. *Macromolecular Chemistry and physics*. 201: 733-739.

Mo, X., Sun, X.S., and Wang, Y. (1999). Effects of molding temperature and pressure on properties of soy protein polymers. *Journal of Applied Polymer Science*. 73: 2595-2602.

Mohanty, A.K., Misra, M., and Hinrichsen, G. (2000). Biofibres, biodegradable polymers and biocomposites: an overview. *Macromolecular Materials Engineering*. 276/277: 1-24.

Mwaikambo, L.Y. (2006). Review of the history, properties and application of plant fibers. *African Journal of Science and Technology. Science and Engineering Series*. 7 (2): 120-133.

Nakamura, S., and Tobolsky, A.V. (1967). Viscoelastic properties of plasticized amylose films. *Journal of Applied Polymer Science*. 11: 1371-1386.

Neus Angles, M., and Dufresne, A. (2000). Plasticized starch/tunicin whiskers nanocomposites. 1. Structural analysis. *Macromolecules*. 33: 8344-8353.

Neus Angles, M., and Dufresne, A. (2001). Plasticized starch/tunicin whiskers nanocomposite materials. 2. Mechanical behavior. *Macromolecules*. 34: 2921-2931.

Nishio, Y., and Manley, R.St.J. (1988). Cellulose/poly(vinyl alcohol) blends prepared from solution in N,N-Dimethylacetamide-Lithium Chloride. *Macromolecules*. 21: 1270-1277.

Noda, I., Satkowski, M.M., Dowrey, A. E., and Marcott, C. (2004). Polymer alloys of Nodax copolymers and poly (lactic acid). *Macromolecular bioscience*. 4: 269-275.

Ogata, N., Jimenez, G., Kawai, H., and Ogihara, T. (1997). Structure and thermal/mechanical properties of poly(l-lactide)-clay blend. *Journal of Polymer Science Part B: Polymer Physics*. 35: 389-396.

Okada, A., Kawasumi, M., Kurauchi, T., and Kamigaito, O. (1987). Synthesis of. nylon-6-clay hybrid. *Polymer Preparation*. 28: 447–449.

Olabarrieta, I., Gallstedt, M., Ispizua, I., Sarasua, J.R., and Hedenqvist, M.S. (2006). Properties of aged montmorillonite-wheat gluten composite films. *Journal of Agricultural and Food Chemistry*. 54: 1283-1288.

Padua, G.W., and Wang, Q. (2002). Formation and properties of corn zein films and coatings. In: Protein-based films and coatings, pp. 159-180. Gennadios, A., Ed., CRC Press, Boca Raton, FL.

Pallos, F.M., Robertson, G.H., Pavlath, A.E., and Orts, W.J. (2006). Thermoformed wheat gluten biopolymers. *Journal of Agricultural and Food Chemistry*. 54: 349-352.

Pandey, J. K., and Singh. R. P. (2005). Green nanocomposites from renewable resources: effect of plasticizer on the structure and material properties of clay-filled starch. *Starch*. 57: 8-15.

Park, H., Li, X., Jin, C., Park, C., Cho, W., and Ha, C. (2002). Preparation and properties of biodegradable thermoplastic starch/clay hybrids, *Macromolecular Materials and Engineering*. 287: 553-558.

Park, H., Lee, W., Park, C., Cho, W., and Ha, C. (2003). Enviromentally friendly polymer hybrids. part 1 Mechanical, thermal and barrier properties of thermoplastic starch/clay nanocomposites. *Journal of Materials Science*. 38: 909-915.

Park, H., Misra, M. Drzal, L.T., and Mohanty, A.K. (2004a). “Green” Nanocomposites from cellulose acetate bioplastic and clay: Effect of Eco-friendly Triethyl Citrate Plasticizer. *Biomacromolecules*. 5: 2281-2288.

Park, H., Liang, X., Mohanty, A.K., Misra, M., and Drzal, L.T. (2004b). Effect of Compatibilizer on nanostructure of the biodegradable cellulose acetate/organoclay nanocomposites. *Macromolecules*. 37: 9076-9082.

Park, J.W., Lee, D.J., Yoo, E., Im, S.S., Kim, S.H., and Kim, Y.H. 1999. Biodegradable polymer blends of poly(lactic acid) and starch. *Korea Polymer Journal*. 7: 93-101.

Park, J.W., and Im, S.S. (2000). Biodegradable polymer blends of poly(L-lactic acid) and gelatinized starch. *Polymer Engineering and Science*. 40: 2539-2550.

Park, S.Y., Marsh, K.S., and Rhim, J.W. (2002). Characteristics of different molecular weight chitosan films affected by the type of organic solvents. *Journal of Food Science*. 67: 194-197.

Parulekar Y., and Mohanty, A.K. (2007). Extruded biodegradable cast films from polyhydroxyalkanoate and thermoplastic starch blends: fabrication and characterization. *Macromolecular Materials and Engineering*. 292: 1218-1228.

Paul, M.A., Alexandre, M., Degee, P., Calberg, C., Jerome, R., and Dubois, P. (2003) Exfoliated polylactide/clay nanocomposites by in situ coordination–insertion polymerization. *Macromolecular Rapid Communications*. 24: 561–566.

Perez-Gago, M.B., and Krochta, J.M. (2002). Formation and properties of whey protein films and coatings. In: Protein-based films and coatings, pp. 43-68. Gennadios, A., Ed., CRC Press, Boca Raton, FL.

Peterson, K., Nielsen, P.V., Bertelsen, G., Lawther, M., Olsen, M.B., Nilsson, N.H., and Mortensen, G. (1999). Potential of biobased materials for food packaging. *Trends in Food Science and Technology*. 10: 52-68.

Pinnavaia, T.J., and Beall, G.W. (2001). Polymer-Clay Nanocomposites. John Wiley & Sons, Inc., NewYork, NY.

Pluta, M., Galeski, A., Alexandre, M., Paul, M.A., and Dubois, P. (2002). Polylactide/montmorillonite nanocomposites and microcomposites prepared by melt blending: structure and some physical properties. *Journal of Applied Polymer Science*. 86(6): 1497-1506.

Ratto, J.A., Stenhouse, P.J., Auerbach, M., Mitchell, J., and Farrell, R. (1999). Processing, performance, and biodegradability of a thermoplastic aliphatic polyester/starch system. *Polymer*. 40: 6777-6788.

Ray, S., Quek, S.Y., Easteal, A., and Chen, X.D. (2006). The potential use of polymer-clay nanocomposites in food packaging. *International Journal of Food Engineering*. 2 (4): 1-11.

Ray, S.S., and Bousmina, M. (2005). Biodegradable polymers and their silicate nanocomposites: In greening the 21st century materials world. *Progress in Material Science*. 50: 962-1079.

Ray, S.S., Okamoto, K., Yamada, K., and Okamoto, M. (2002a). Novel porous ceramic material via burning of polylactide/layered silicate nanocomposite. *Nano Letters*. 2: 423–426.

Ray, S.S., Yamada, K., Okamoto, M., and Ueda, K. (2002b). New polylactide/layered silicate nanocomposite: a novel biodegradable material. *Nano Letters*. 2: 1093–1096.

Ray, S.S., Maiti, P., Okamoto, M., Yamada, K., and Ueda, K. (2002c). New polylactide/layered silicate nanocomposites. 1. Preparation, characterization and properties. *Macromolecules*. 35: 3104–3110.

Ray, S.S., Yamada, K., Okamoto, M., and Ueda, K. (2003a). New polylactide/layered silicate nanocomposites. 2. Concurrent improvements of material properties, biodegradability and melt rheology. *Polymer*. 44: 857–866.

Ray, S.S., Yamada, K., Okamoto, M., Ogami, A., and Ueda, K. (2003b). New polylactide/layered silicate nanocomposites. 3. High performance biodegradable materials. *Chemistry of Materials*. 15: 1456–1465.

Roth. W.B., and Mehltretter, C.L. (1967). Some properties of hydroxypropylated amylomaize starch films. *Food Technology*. 21: 72-74.

Ruiz-Hitzky, E., and Aranda, P. (1990). Polymer-salt intercalation complexes in layer silicates. *Advanced Materials*. 2(11): 545-547.

Sajilata, M.G., Savitha, K, Singhal, R.S., and Kanetkar, V.R. (2007). Scalping of flavors in packaged foods. *Comprehensive Reviews in Food Science and Safety*. 6: 17-35.

Simmons, S., and Thomas, E. (1995). Structural characteristics of biodegradable thermoplastic starch/poly(ethylene-vinyl alcohol) blends. *Journal of Applied Polymer Science*. 58: 2259-2285.

Sorrentino, A., Gorrasi, G., Tortora, M., vittoria V., Costantino, U., and Marmottini, F. (2005). Incorporation of Mg-Al Hydrotalcite into a biodegradable Poly(ε-caprolactone) by high energy ball milling. *Polymer*. 46, 1601-1608.

Sorrentino, A., Gorrasi, G., and Vittoria, V. (2007) Potential perspectives of bio-nanocomposites for food packaging applications. *Trends in Food Science and Technology*. 18: 84-95.

Stenhouse, P.J., Ratto, J.A., and Schneider, N.S. (1997). Structure and properties of starch/poly(ethylene-co-vinyl alcohol) blown films. *Journal of Applied Polymer Science*. 64: 2613-2622.

Stenhouse, P.J., Mayer, J.M., Hepfinger, M.J., Costa, E.A., Dell, P.A., and Kaplan, D.L. (1993). Starch-based blown film. In: Biodegradable Polymer and Packaging, pp. 151-158.

Ching, C., Kaplan D.L. and Thomas E.L. (Eds.) Technical Publishing Company, Lancaster, PA.

Usuki, A., Kato, M., Okada,A., and Kurauchi, T. (1997). Synthesis of polypropylene-clay hybrid. *Journal of Applied Polymer Science*. 63: 137-139.

Vaia, R.A., Ishii, H., and Giannelis, E.P. (1993). Synthesis and properties of two dimensional nanostructures by direct intercalation of polymer melts in layered silicates. *Chemistry of Materials*. 5: 1694-1696.

Vaia, R.A., Jandt, K.D., Kramer, E.J., and Giannelis, E.P. (1995). Kinetics of polymer melt intercalation. *Macromolecules*. 28: 8080-8085.

Vaia, R.A., and Giannelis, E.P. (1997). Polymer melt intercalation in organically-modified layered silicates: model predictions and experiment. *Macromolecules*. 30: 8000-8009.

VanderHart, D.L., Asano, A., and Gilman, J.W. (2001). NMR measurements related to clay dispersion quality and organic-modifier stability in nylon6/clay nanocomposites. *Macromolecules*. 34: 3819-3822.

Wang, H., Sun, X.Z., and Seib, P. (2002). Mechanical properties of poly(lactic acid) and wheat starch blends with methylenediphenyl diisocyanate. *Journal of Applied Polymer Science*. 84: 1257-1262.

Wang, Z., and Pinnavaia, T.J. (1998). Nanolayer reinforcement of elastomeric polyurethane. *Chemistry of Materials*.10: 3769-3771.

Wiles, J.L., Vergano, P.J., Barron, F.H., Bunn, J.M., and Testin, R.F. (2000). Water Vapor transmission rates and sorption behavior of chitosan films. *Journal of Food Science*. 65: 1175-1179.

Wilhelm, H.M., Sierakowski, M.R., Souza, G.P., and Wypych, F. (2003). Starch films reinforced with mineral clay. *Carbohydrate Polymers*. 52: 101-110.

Wolff, I. A., Davis, H.A., Cluskey, J. E., Gundrum, L. J., and Rist, C.E. (1951). Preparation of films from amylose. *Industrial and Engineering Chemistry*. 43: 915-919.

Wool, R.P., and Sun, X.Z. (2005). Bio-based polymers and composites. Elsevier Inc., UK.

Wu, J.H., and Lerner, M.M. (1993). Structural, thermal, and electrical characterization of layered nanocomposites derived from sodium-montmorillonite and polyethers. *Chemistry of Materials*. 5: 835-838.

Yano, K., Usuki, A., Okada, A., Kurauchi, T., and Kamigaito, O. (1993). Synthesis and properties of polyimide-clay hybrid. *Journal of Polymer Science Part A: Polymer Chemistry*. 31: 2493-2498.

Yano, K., Usuki, A., and Okada, A. (1997). Synthesis and properties of polyimide-clay hybrid films. *Journal of Polymer Science Part A: Polymer Chemistry*. 35: 2289-2294.

Yin, S., Wang, S., Rials, T.G., Kit, K.M., and Hansen, M.G. (2007). Polypropylene composites filled with steam-exploded wood fibers from beetle-killed loblolly pine by compression-molding. *Wood and Fiber Science*. 39 (1): 95-108.

Yu, L., Dean, K., and Li, L. (2006). Polymer blends and composites from renewable resources. *Progress in Polymer Science*. 31(6): 576-602.

Yu, J., Cui, G., Wei, M., and Huang, J. (2007). Facile exfoliation of rectorite nanoplatelets in soy protein matrix and reinforced bio-nanocomposites thereof. *Journal of Applied Polymer Science*. 104: 3367-3377.

Zeng, Q.H., Yu, A.B., Lu, G.Q., and Paul, D.R. (2005). Clay-based polymer nanocomposites: research and commercial development. *Journal of Nanoscience and Nanotechnology*. 5: 1574-1592.

Zhang, J.F., and Sun, X.Z. (2004). Mechanical properties of Poly(lactic acid)/starch composites compatibilized by Maleic anhydride. *Biomacromolecules*. 5: 1446-1451.

Zheng, H., Du, Y, Yu, J., Huang, R.H. and Zhang, L. (2001). Preparation and characterization of chitosan/poly(vinyl alcohol) blend fibers. *Journal of Applied Polymer Science*. 80: 2558-2565.

Zheng, J., Li, P., Ma, Y., and Yao, K. (2002). Gelatin/Montmorillonite hybrid nanocomposite. I. preparation and properties. *Journal of Applied Polymer Science*. 86: 1189-1194.

Zhong, Z., and Sun X. S. (2001). Properties of soy protein isolate/polycaprolactone blends compatibilized by methylene diphenyl diisocyanate. *Polymer*. 42: 6961-6969.

Table 1 – Properties of typical biopolymer and bio-nanocomposite films.

Material	Film preparation	Moisture barrier[a]	Oxygen barrier[b]	Mechanical properties (TS)[c]	Mechanical properties (%E)[c]
Starch[d,e]	Aqueous	Poor	Moderate	Moderate	Poor
Cellulose Acetate[e]	Extrusion	Moderate	Poor	Moderate	Moderate
Chitosan[f,g]	Aqueous	Poor	Good	Moderate	Moderate
Gluten[e]	Aqueous-EtOH	Moderate	Good	Moderate	Moderate
Soy Protein [e,h]	Aqueous	Poor	Good	Poor	Moderate
Zein [e]	EtOH	Moderate	Moderate	Moderate	Moderate
Whey Protein [e,i]	Aqueous	Poor	Good	Poor	Poor
PHB/V[e,j,k]	Extrusion	Good	Moderate	Moderate	Moderate
PLA[e,j,k,l]	Extrusion	Moderate	Moderate	Good	Moderate
Starch/PCL[m]	Extrusion	Moderate	Moderate	Moderate	Good
Starch/PVOH[n]	Extrusion/Aqeuous	Poor	Good	Moderate	Good
Starch Nanocomposites[d]	Extrusion/Aqueous	Moderate	N/A	Moderate	Poor
Soy Protein Nanocomposites[o]	Extrusion	N/A	N/A	Moderate	Moderate
PLA Nanocomposites[l]	Solvent casting	Good	N/A	Good	Moderate

[a]Test Condition: 38°C, 90/0%RH
Poor = 10-100 g*mm/m^2*d*kPa
Moderate = 0.1-10 g*mm/m^2*d*kPa
Good = 0.01-0.1 g*mm/m^2*d*kPa
(LDPE: 0.08 g*mm/m^2*d*kPa)
d Tang and others (2008)
g Xu and others (2005)
j Van de Velde and Kiekens 2002
m Myllymaki and others 1998
TS : Tensile Strength (MPa)
N/A: not applicable

[b]Test conditions: 25°C, 0-50%RH
Poor = 100-1000cm^3*µm/m^2*d*kPa
Moderate = 10-100 cm^3*µm/m^2*d*kPa
Good = 1-10 cm^3*µm/m^2*d*kPa
(EVOH: 0.1 cm^3*µm/m^2*d*kPa)
e Krochta and De Mulder-Johnston (1997)
h Brandenburg and others (1993)
k Cava and others (2006)
n internal data, not published
%E: Percent elongation at break

[c]Test conditions: 25°C, 50%RH
Moderate TS = 10-100 MPa
Moderate E= 10-50%
(LDPE: TS=13Mpa, E=500%)

f Khan and others (2000)
i Izquierdo and Krochta (2008)
l Rhim and others (2009)
o Chen and Zhang (2006)
EtOH : Ethanol

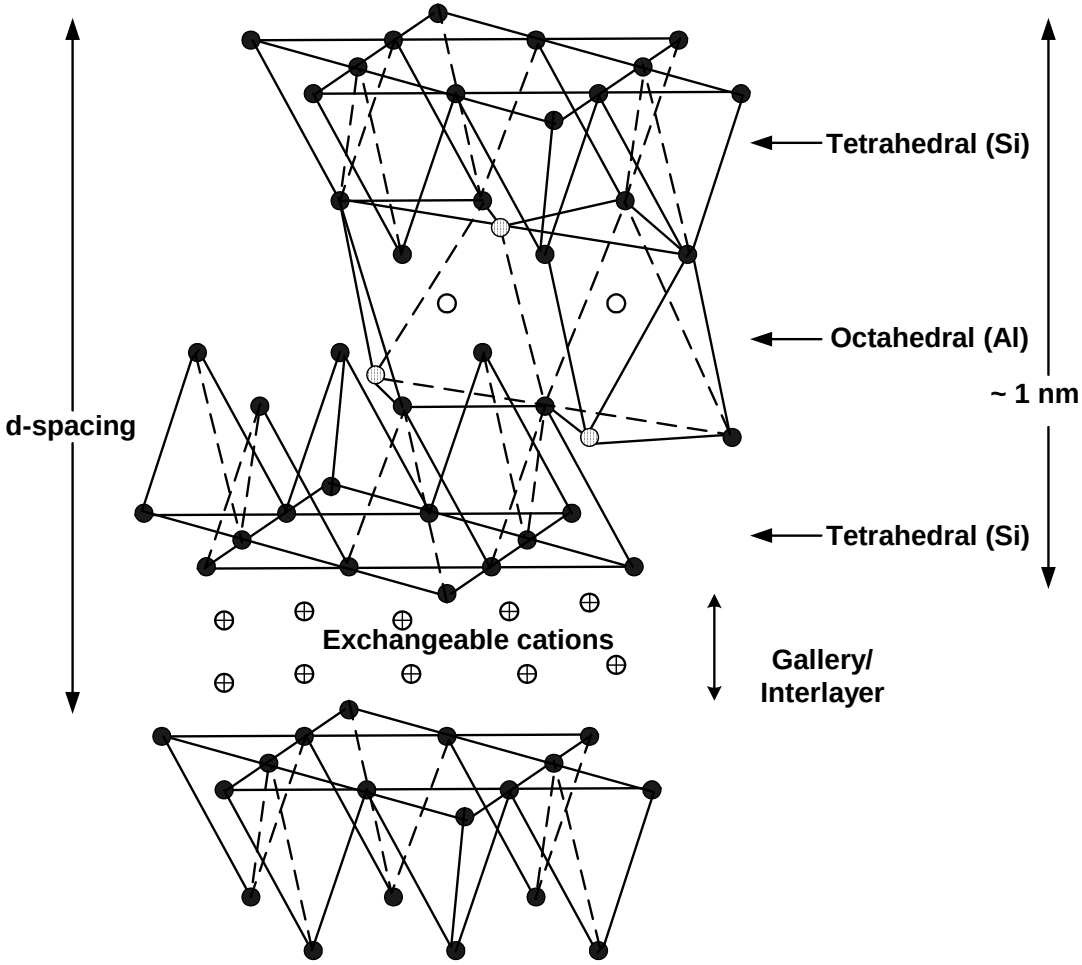

Figure 1 – Structure of 2:1 layered silicates.

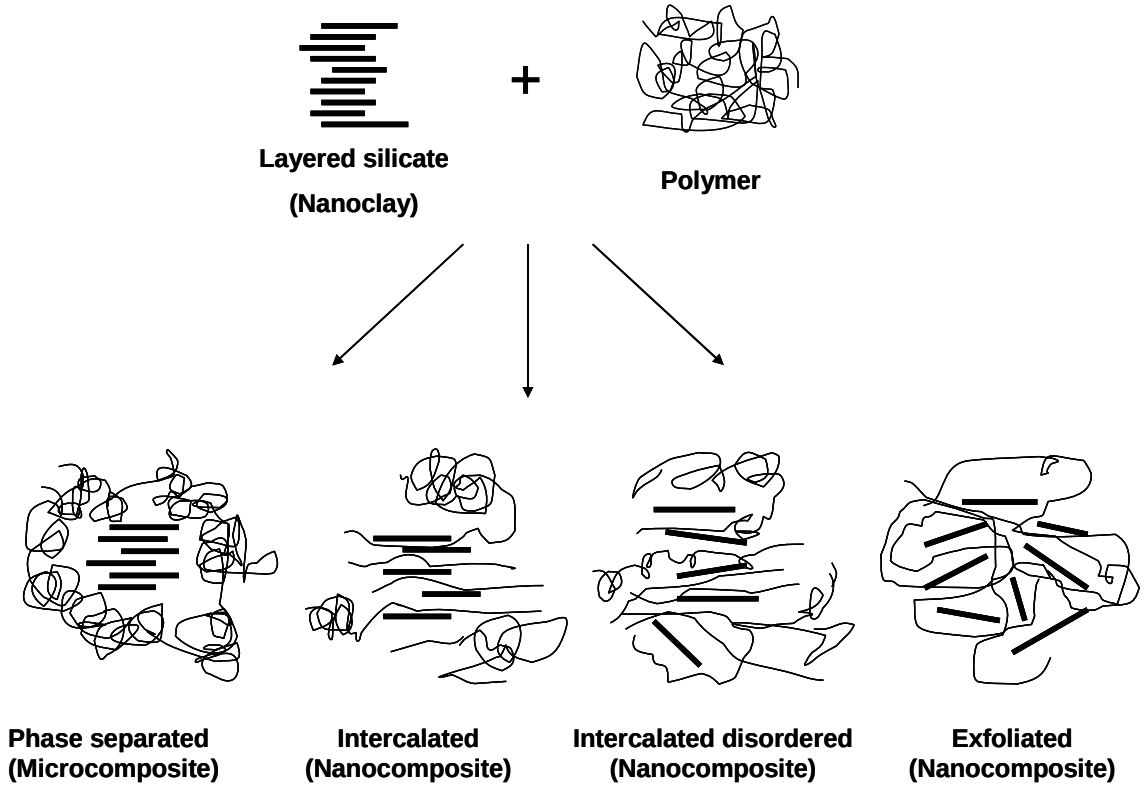

Figure 2 – Possible structures of nanocomposites.

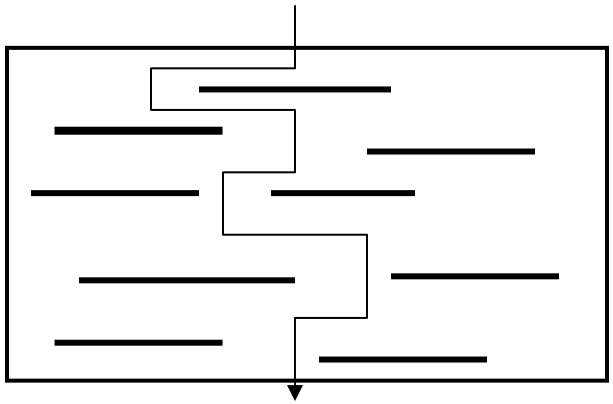

Figure 3 – Proposed model for the tortuous zigzag diffusion path in a polymer-clay nanocomposite.

Chapter 4

MANUSCRIPT II

Biopolymer-based Nanocomposites: Part I. Analytical Techniques for Structural Characterization

P. KUMAR[1], K.P. SANDEEP[1], S. ALAVI[2], AND V.D. TRUONG[3]

(1) Department of Food, Bioprocessing, and Nutrition Sciences, North Carolina State University, Raleigh, NC
(2) Department of Grain Science and Industry, Kansas State University, Manhattan, KS
(3) U.S. Dept. of Agriculture, Agricultural Research Service, South Atlantic Area, Food Science Research Unit, Raleigh, NC

Please address all correspondence to:

K.P. Sandeep
129 Schaub Hall, Box 7624
North Carolina State University
Raleigh, NC 27695
Phone: 919-515-2957
Fax: 919-515-7124
E-mail: kp_sandeep@ncsu.edu

Paper nr FSR-09-35 of the Journal Series of the Department of Food, Bioprocessing, and Nutrition Sciences, North Carolina State University, Raleigh, NC 27695-7624

Structural characterization of bio-nanocomposites…

Abstract

The non-biodegradable and non-renewable nature of plastic packaging has led to a renewed interest in packaging materials based on bio-nanocomposites (biopolymer matrix reinforced with nanoparticles such as layered silicates). Selection of proper technique for structural characterization of these bio-nanocomposites is very critical in assessing their performance. This paper presents a review of analytical techniques for the structural characterization of biopolymer-based nanocomposites. A brief introduction of different techniques for the preparation of bio-nanocomposites is given. Analytical techniques (XRD, TEM, SEM, SPM, CSLM, FTIR, and NMR) for structural characterization of these bio-nanocomposites are discussed in terms of principle of operation, technique of preparation of samples, collection and interpretation of data, and limitations.

Keywords: bio-nanocomposites, structural characterization, analytical techniques

Introduction

The non-biodegradable and non-renewable nature of plastic packaging has led to a renewed interest in packaging materials based on biopolymers derived from renewable sources. Such biopolymers include naturally occurring proteins, cellulose, starches, and other polysaccharides and those synthesized chemically from naturally derived monomers such as lactic acid. Commercialization of these bio-based polymers has already begun. Natureworks, LLC (Minnetonka, MN) manufactures polylactide from corn sugar. The polymer can be hydrolyzed back to lactic acid. Wal-Mart stores, Inc. is already using polylactide to package fresh-cut produce (Marsh and Bugusu, 2007). However, biopolymers cannot meet the requirements of a cost-effective film with mechanical and barrier properties matching those of plastics. Recently, a new class of materials represented by bio-nanocomposites has proven to be a promising option in improving the properties of these biopolymer-based packaging materials. Bio-nanocomposites consist of a biopolymer matrix reinforced with particles (nanoparticles) having at least one dimension in the nanometer range (1-100 nm). Bio-nanocomposites exhibit much improved properties as compared to biopolymers due to the high aspect ratio and high surface area of nanoparticles. Therefore, efforts have been geared towards developing bio-nanocomposites for food packaging films with improved mechanical, barrier, rheological, and thermal properties.

The most common class of materials used as nanoparticles are layered silicates such as clay minerals, graphite, and metal phosphates. Clay minerals such as montmorillonite (MMT), hectorite, sapnotite, and laponite have proven to be very effective due to their unique structure and properties. These clay minerals belong to the general family of 2:1

layered silicates indicating that they have 2 tetrahedral sheets sandwiching a central octahedral sheet (Zeng and others 2005). Paiva and others (2008) describe the properties, preparation, and applications of layered clays in detail. Biopolymers can be reinforced with these layered clays in order to enhance their properties while maintaining their biodegradability.

For preparation of a bio-nanocomposite, polymer chains must diffuse into the galleries between silicate layers to produce structures ranging from intercalated to exfoliated (Figure 1). There are four possible arrangements of layered clays dispersed in a polymer matrix – phase separated or immiscible (microcomposite), intercalated, exfoliated, and disordered intercalated (partially exfoliated). In an immiscible arrangement, platelets of layered clays exist as tactoids (stack of platelets separated by about 1 nm) and the polymer encapsulates these tactoids. Intercalation occurs when a monolayer of extended polymer chain penetrates into the galleries of the layered silicates. Intercalation results in finite expansion (2-3 nm) of the silicate layers. However, these silicate layers remain parallel to each other. Extensive penetration of polymer chains into the galleries of layered silicate leads to exfoliation or delamination of silicate layers. Clay platelets are separated by 10 nm or more during exfoliation. An exfoliated nanocomposite consists of nanoparticles distributed homogeneously throughout the polymer matrix (Dennis and others 2001; Zeng and others 2005).

Bio-nanocomposites can be prepared by several methods which include in-situ polymerization, solution exfoliation, and melt intercalation. In the in-situ polymerization method, monomers are migrated into the galleries of layered silicates and subsequently

polymerized via heat, radiation, or catalyst. In solution exfoliation, layered clays are exfoliated into single platelets. Exfoliation is achieved by dispersing the layered clays in a solvent. The polymer is adsorbed onto the platelets by mixing in the clay suspension. The solvent is removed either by evaporation or by precipitation. In melt intercalation, layered clays are mixed with the polymer matrix in molten state (Zeng and others 2005).

Several review papers discuss the preparation, characterization, properties, and applications of bio-nanocomposites (Pandey and others 2005; Ray and Bousmina 2005; Yang and others 2007; Rhim and Ng 2007; Sorrentino and others 2007; Zhao and others 2008; Bordes and others 2009). However, there is a lack of comprehensive review on various analytical techniques for the structural characterization of bio-nanocomposites. Selection of proper technique for characterization of these bio-nanocomposites is very critical in assessing their performance. A number of analytical techniques have been used to characterize the structure of bio-nanocomposites. These techniques include X-ray diffraction (XRD), microscopy {transmission electron microscope (TEM), scanning electron microscope (SEM), scanning probe microscope (SPM), and confocal scanning laser microscope (CSLM)}, Fourier transform infra-red (FTIR) spectroscopy, and nuclear magnetic resonance (NMR). Each of the above mentioned techniques has its own benefits and limitations.

This paper presents a review of analytical techniques for the structural characterization of bio-nanocomposites. A brief introduction of different techniques for the preparation of bio-nanocomposites is given. Analytical techniques for characterizing the structure of these bio-nanocomposites are discussed in terms of principle of operation, preparation of sample, interpretation of data, and limitations.

Wide angle X-ray diffraction (WA-XRD)

X-rays were discovered in 1895 by W.C. Roentgen. When incident on a crystalline material, X-rays interfere with each other. This phenomenon is known as X-ray diffraction (XRD). WA-XRD is the most commonly used method to characterize the structure of bio-nanocomposites because of its ease of use and availability. WA-XRD has been used to characterize dispersion of layered clays in nanocomposites based on protein (Chen and Zhang 2006; Shabeer and others 2007; Yu and others 2007) and starch (Dimonie and others 2008; Tang and others 2008).

Principle of operation

X-rays are part of the electromagnetic spectrum with wavelength ranging from 0.01 nm to 10 nm. A schematic of an XRD instrument is shown in Figure 2. X-rays are generated by striking a pure anode of a metal (such as copper) with high-energy electrons in a sealed vacuum tube (X-ray tube). When a parallel and monochromatic X-ray beam with a wavelength of λ is incident on a sample (single crystal or powder ground to size less than 50 μm), the beam is transmitted, absorbed, refracted, scattered, and diffracted. A detector is used to measures the intensity of the diffracted X-rays in counts per second (cps). The sample may be set at any desired angle (θ) to the incident beam. For WA-XRD, the value of 2θ is greater than 1°. A diffraction plot detects the intensity of diffracted X-rays as a function of 2θ. Sharp peaks, corresponding to the interlayer spacing, are seen on the diffraction data. These peaks are characteristic to the material and the structure of the crystal. From the diffraction data, interlayer spacing (d-spacing or d) between clay layers is estimated from Bragg's equation (Kasai and Kakudo 2005):

$$d = \frac{\lambda}{2\sin\theta} \quad (1)$$

Preparation of samples

Bio-nanocomposite samples for XRD analysis should be well ground to a particle size of less than 50 μm. Uniform particle size and random orientation of crystals are very critical for accurate XRD analysis. A sample with well-defined orientation of crystals (preferred orientation) can give a different diffraction pattern than that of a sample with randomly oriented crystals. Preferred orientation is particularly a problem with plate like crystals because they tend to lie horizontal, rather than perpendicular, on the sample holder. For a film sample, the thickness of the film should be at least 0.5 mm in order to detect the intensity of diffracted X-rays. XRD analysis should be sensitive enough to detect the crystalline structure of layered silicates present in small amounts in bio-nanocomposites (Kasai and Kakudo 2005).

Collection and interpretation of data

Diffraction pattern for a particular sample is obtained by plotting the intensity of diffracted X-rays as a function of 2θ. Bio-nanocomposites are characterized by monitoring the intensity, width, and position of the peak in the diffraction pattern. Intensity of the peak provides information about the location of atoms in the unit cell. Higher intensity corresponds to higher electron density around the atom. Peak width provides information on the size of crystal and imperfections in the crystal. Peak width increases as the size of the crystal decreases. Position of the peak is used to estimate interlayer spacing by using the Bragg's equation as mentioned above.

XRD patterns for various possible arrangements of layered silicates in biopolymers are shown in Figure 1. For an immiscible arrangement (microcomposite) of layered clays in a biopolymer matrix, the structure of the layered silicate in the composite is not affected. Thus, X-ray diffraction pattern for the microcomposite should remain same as that obtained for the pure layered silicate. Intercalation of the polymer chains increases the interlayer spacing and according to Bragg's law, it causes a shift of the diffraction peak towards lower 2θ angle. As more polymers enter the interlayer spacing, the clay platelets become disordered, thus causing broader peaks and a wider distribution of such peaks. For exfoliated nanocomposites, there is no peak in the diffraction pattern because of the much larger interlayer spacing (>8-10 nm) between the silicate layers (McGlashan and Halley 2003; Pavlidou and Papaspyrides 2008; Paul and Robeson 2008).

Limitations

XRD is a simple and convenient method to determine d-spacing for immiscible or intercalated arrangements of layered silicates in bio-nanocomposites. However, it may be insufficient to characterize exfoliated nanostructures. Absence of peak in diffraction pattern is often misinterpreted as an indication of exfoliation. Other than exfoliation, dilution and preferred orientation of clay in nanocomposites might result in a diffraction pattern with no peak. XRD cannot be used to determine the spatial distribution and dispersion of layered silicates in bio-nanocomposites (Morgan and Gilman 2003). Therefore, XRD should always be used in conjunction with some other techniques such as TEM, SEM, or AFM.

Wide-angle XRD is not useful to study intercalation once the d-spacing exceeds 6-7 nm. However, small-angle ($2\theta < 1°$) X-ray diffraction (SA-XRD) analysis in combination

with WA-XRD can be useful for characterization of such intercalated nanocomposites (Ray and Bousmina 2005).

Microscopy

Microscopy is the study of objects that are smaller than the spatial resolution (~75 μm) of human eye. Spatial resolution is the minimum possible length of an object which could be seen and separately identified from an adjacent and similar object. Light microscopes were developed in the early 17th century. The spatial resolution (δ) of a light microscope can be approximated by the classical Rayleigh criterion as (Williams and Carter 1996):

$$\delta = \frac{0.61\lambda}{\mu \sin\beta} \tag{2}$$

where λ is the wavelength of the radiation, μ is the refractive index of the viewing medium, and β is the semi-angle of collection of the magnifying lens. Wavelength for the light in the middle of the visible spectrum is ~ 550 nm. This gives light microscopes a resolution of approximately 300 nm. Early in the 20th century, the wavelike nature of electrons was discovered. The electrons have a much lower wavelength as compared to that of light. Therefore, it is possible to achieve a resolution of as low as 0.2 nm by using electrons as a radiation source.

Transmission electron microscope (TEM)

Transmission electron microscope was developed by Max Knoll and Ernst Ruska in 1931. In addition to XRD, TEM images provide further evidence for the occurrence of intercalation or exfoliation in nanocomposites. TEM allows a qualitative understanding of the

internal structure, spatial distribution, and dispersion of the nanoparticles within polymer matrices that are thin (< 100 nm) enough to transmit electrons.

Principle of operation

Transmission electron microscope operates on the same basic principles as the light microscope but uses electrons instead of light. TEM uses electrons as the radiation source and their much lower wavelength (in the order of one-tenths of a nanometer) makes it possible to achieve a resolution (0.2 nm) which is thousand times better than that of a light microscope. A schematic representation of a transmission electron microscope is shown in Figure 3. A TEM instrument can be divided into three sections: illumination system, specimen stage, and imaging system. The illumination system comprises of an electron gun, two or more condenser lens, and a condenser aperture. The specimen stage allows samples to be held for the analysis. The imaging system consists of an objective lens, an objective aperture, one or more intermediate lens, a projector lens, and a screen (Egerton 2005).

A fine beam of electrons with precisely controlled energy is produced in the electron gun. The gun consists of an electron source (filament for thermionic emission) and an accelerating chamber. The filament is made from a high melting point material such as tungsten. Once heated to a temperature above 2700 K, the tungsten filament emits electrons into the surrounding vacuum. Wehnelt cylinder is a metal electrode which surrounds the filament except for a small opening through which the electron beam emerges. Wehnelt cylinder controls the emission current of the electron gun. After emission, electrons are accelerated by applying a potential difference (accelerating voltage), V_0 (100-500 kV) between the cathode and anode. Accelerating voltage determines the velocity and wavelength

of the electron beam. Only 1% of the accelerated electrons are able to pass through the anode plate. Crossover is the effective source of illumination for the TEM. The first condenser lens (C1), which is a strong magnetic lens, creates a demagnified image of the electron beam. It also controls the minimum spot size available in the rest of the condenser system. The second condenser lens (C2), which is a weak magnetic lens, is used to vary the diameter of illuminated area of the sample. Condenser aperture controls the fraction of electron beam which illuminates the sample. Once the electron passes through the sample, the objective lens forms an inverted image. Objective aperture improves the contrast of the final image by passing only those electrons which will contribute to the final image. It also limits the blurring of image that arises from spherical and chromatic aberration. The purpose of the intermediate lens is to magnify the initial image formed by the objective lens. The intermediate lens can also be used to produce an electron diffraction pattern on the TEM screen. Projector lens produces an image or a diffraction pattern on the TEM screen. The TEM screen is used to convert the electron image to a visible form. It consists of a metal plate with a coating of $ZnSO_4$ which emits visible light under electron bombardment (Egerton 2005).

The combination of TEM with other analytical techniques such as energy dispersive X-ray spectroscopy (EDS) and electron energy loss spectroscopy (EELS) can generate information for image analysis and chemical composition of the sample. EELS can also provide information on the electronic structure of the sample (Koo 2006). Some new developments in TEM for nanotechnology have been reviewed by Wang (2003). Transmission electron microtomography (TEMT) is an emerging three-dimensional imaging

technique with a sub-nanometer resolution (~0.5 nm). Three-dimensional image obtained from TEMT can help in understanding the relationship between the structure and property of bio-nanocomposites (Jinnai and Spontak 2009).

Preparation of samples

Samples should be thin (<100 nm) enough to transmit electrons and stable to electron bombardment under high vacuum. Typically, samples are made circular with a diameter of 3 mm. The sample must be inserted into the vacuum of the TEM column without introducing air. Samples are most commonly prepared by either ultramicrotomy or focused ion beam (FIB).

TEM samples are prepared by cutting ultra thin (< 100 nm) sections from a small block of embedded material using ultramicrotomy. Ultramicrotomy is high precision cutting method using glass or diamond knife. The cut sections are floated onto a water surface. A fine-mesh copper grid (diameter of 3 mm) is then introduced below the surface of water. The grid is slowly raised and the cut section is supported by the grid. After drying in air, the ultra thin section remains attached to the grid. To produce scattering contrast, the cut section is stained by immersing in a solution of heavy metal (Egerton 2005).

Focused ion beam (FIB) milling is a technique that uses a beam of accelerated ions to modify materials with nanometer precision. A schematic representation of a focused ion beam instrument is shown in Figure 4. A FIB instrument operates similar to an SEM. FIB utilizes a liquid metal ion source (LMIS) at the top of its column to produce ions (usually Ga^{+}). The ions are focused into a beam by an electrostatic lens. After passing through the aperture and objective lens, the ion beam scans the surface of the sample. A beam diameter

of 5 nm to 0.5 μm can be achieved in a FIB. The collision of ions with the atoms of the sample can be either elastic or inelastic in nature. An elastic collision results in removal of surface atoms. Removal of atoms, which is known as sputtering, modifies the surface of the sample. During inelastic collision, ions transfer a part of their energy to either surface atoms or electrons. Inelastic collision produces secondary electrons along with X-rays. The intensity of secondary electrons at each scan position can be used to create an image of the sample. Over an extended period of time, the sputtering process leads to noticeable removal of material. This is used for milling and probing applications. The small beam size in FIB makes it ideal for preparation of samples for TEM and SEM (Giannuzzi and Stevie 1999; Yao 2005).

Samples of nanocomposite powders can be prepared by suspending the powder in a volatile solvent such as acetone. A drop of the suspension is then put on a fine-mesh copper grid. After drying in air, the nanocomposite powder remains attached to the grid and can be viewed under the TEM.

Collection and interpretation of data

An ideal TEM image should have a good resolution and contrast. For bio-nanocomposites, contrast arises from differences in the atomic number of the layered silicates and the biopolymer matrix. Layered silicates with high atomic number appear dark in TEM image. TEM results are quantified by the TEM particle density (number of platelets per unit area). The extent of exfoliation is better for samples with higher TEM particle density. Particle density per unit nanoparticles concentration is known as the specific particle density (Chavaria and Paul 2004). However, it is difficult to calculate the TEM particle

density for intercalated and partially exfoliated nanocomposites. Nam and others (2001) calculated the length, thickness, and correlation length of the dispersed clay particles from TEM images. Correlation length was defined as the inter-particle distance in the direction perpendicular to that of the length of clay layers. Vermogen and others (2005) proposed a method for quantifying TEM micrographs by measuring the length (L), thickness (t), and aspect ratio of clay layers. Inter-particle distance ($\varepsilon_{\|}$) in the direction parallel to that of the length of clay layers and inter-particle distance ($\varepsilon_{\perp}$) in the direction perpendicular to that of the length of clay layers were also measured. The number (N) of platelets in an intercalated layered silicate was calculated as:

$$N = \frac{t_p + d - t_{platelet}}{d} \quad (3)$$

where t_p is the thickness of the particle, d is the interlayer spacing, and $t_{platelet}$ is the thickness of a single platelet. Six classes of tactoids based on thickness were defined. These tactoids ranged from individual exfoliated sheet to micron size aggregate. TEM has been used to characterize dispersion of layered clays in nanocomposites based on protein (Chen and Zhang 2006; Yu and others 2007) and starch (Tang and others 2008).

Limitations

A TEM instrument is more expensive than an XRD instrument. Methods for sample preparation are tedious. Only a small portion of the sample can be viewed. Samples containing water cannot be viewed under TEM because of the high vacuum in the sample chamber. TEM results are difficult to quantify because TEM provides two-dimensional images of a three-dimensional sample. If the sample is not made very thin, electrons can be

scattered or absorbed, rather than transmitted (Williams and Carter 1996). Proper experimental conditions such as low exposure times and high accelerating voltage are necessary to prevent decomposition of the clay structure in the nanocomposites (Monticelli and others 2007).

Scanning electron microscope (SEM)

Scanning electron microscope is a type of microscope that uses high-energy beam of electrons instead of light to scan surface of a relatively thick sample. Scanning electron microscope has a resolution of 1 to10 nm.

Principle of operation

A schematic representation of a scanning electron microscope is shown in Figure 5. Similar to TEM, an SEM incorporates an electron gun to generate a beam of electrons. The maximum accelerating voltage in SEM is typically 30 kV which is lower than that in TEM (100-500 kV). The electron beam is demagnified by the first condenser lens (C1). The condenser aperture eliminates high-angle electrons by constricting the beam. The second condenser lens forms a thin and coherent beam. An objective aperture further eliminates high-angle electrons from the beam. The objective lens focuses the electron beam into a small-diameter (1-10 nm) electron probe. Electrons (primary) incident on a sample supply enough energy to the atomic electrons (secondary) present on the surface of the sample so that they can be released. A small fraction of primary electrons are elastically back-scattered (angle of deflection > 90°) with only a small loss in energy. Due to their high energy, these back-scattered electrons (BSEs) can re-enter the surrounding vacuum. However, the secondary electrons can be distinguished from the backscattered electrons because of their

much lower energy. A set of coils scans the electron beam over the sample in two perpendicular directions and covers a square or rectangular area of the sample. This procedure is known as raster scanning. An image of the raster is formed by sequential collection of secondary electrons from each scanned point. Thus, the image in SEM is generated sequentially rather than simultaneously as in TEM (Egerton 2005).

Preparation of samples

One major advantage of SEM over TEM is the ease of sample preparation. A sample does not need to be made thin. Conducting materials require no special sample preparation for SEM. Samples of insulating materials become charged when exposed to the electron probe. Negatively charged samples repel incident electrons, resulting in image distortion. Therefore, insulating materials are coated with a thin (15-40 nm) layer of metal (gold, chromium, palladium) or conducting carbon. This process of coating is known as sputter coating. In sputter coating, the specimen chamber is exposed to very low vacuum (~0.1 Pa). An inert gas such as Argon (Ar) is introduced in the chamber. Gas molecules are ionized into ions and electrons because of the high voltage applied to the chamber. When struck with ions, the target metal ejects atoms. Atoms collide with residual gas molecules and deposit on the sample. Some of the limitations of the sputter coating process are thermal damage and surface contamination of the specimen. Sputter coating also reduces the penetration depth of SEM because of the thickness of the coating (Bozzola and Russell 1999).

When coating is undesirable or difficult, low voltage should be used to avoid charging of the sample. An alternative to overcome charging of the samples is to surround the sample with a gaseous environment (low vacuum of up to 4000 Pa) rather than high

vacuum (~10^{-4} Pa). This type of SEM is known as low-vacuum SEM or environmental SEM (ESEM). However, vacuum must be maintained in environmental SEM column for the operation of electron gun, acceleration of electrons, and focusing of electrons. After being focused by the objective lens, primary electrons ionize gas molecules (usually water vapor) before reaching the sample. Ionized gas molecules neutralize the surface charge of the sample. The pressure in the sample chamber can be as high as 5000 Pa (Egerton 2005).

SEM has also been used to study the fractured surface (cross-section) of bio-nanocomposite films (Vaz and others 2002; Yu and others 2007). Sample of fractured surface is prepared by freezing the film in liquid nitrogen, followed by breaking the film to expose the fracture surface, and sputter coating the fractured surface with a conducting coating (Yu and others 2007).

Collection and interpretation of data

SEM images can be used to study the surface morphology of a material. A smooth surface can be distinguished from a rough surface by visual inspection. Comparatively larger (~1 μm) aggregates of nanoparticles at the surface can be observed in the SEM image. SEM images can be used as a quick method to study the formation of nanocomposite structure.

Limitations

An image from SEM represents only the property of a surface and not the internal structure that is visible with a TEM image. The process of generating an image in SEM is slower than that in TEM. SEM cannot be used to study detailed structure of nanocomposites because it has a poorer resolution as compared to TEM. Therefore, SEM analysis should always be used in combination with other microscopic techniques such as TEM or AFM.

Scanning probe microscope (SPM)

The use of a probe can resolve atoms as the resolution is no longer restrained by the wavelength of light or electrons. A probe can also be used to manipulate the structures along with scanning them. Some examples of SPM are scanning tunneling microscope (STM) and atomic force microscope (AFM).

Scanning tunneling microscope (STM)

Gerd Binnig and Heinrich Rohrer invented the scanning tunneling microscope in 1982 which gives three-dimensional images of conducting objects down to the atomic level. A spatial resolution of 0.01 nm can be achieved with a STM.

Principle of operation

A schematic representation of a scanning tunneling microscope is shown in Figure 6. A very sharp metallic tip (M) is fixed on top of a piezodrive (P_z) to control the height (s) of the tip above the surface of a sample. The tip is brought within about 0.3-1 nm of the sample and a small potential difference ($V_t \sim 0.01$-1 V) is applied. Electrons move between the tip and the conducting sample by the process of quantum-mechanical tunneling. Quantum-mechanical tunneling is an effect of the wavelike nature of electrons which allows them to pass through small barriers such as the vacuum barrier between the tip and the sample. The amount of electrical current (tunneling current, J_t) flowing between the tip and the sample is measured. The tunneling current is very sensitive to the distance between the tip and the surface. A feedback control unit (CU) is used to adjust the height of the tip so that the tunneling current (J_t) remains constant. Two other piezodrives (P_x and P_y) are used to scan the tip in the lateral dimensions. During scanning of the surface, voltage (V_p) supplied to P_z

is recorded as an image. This mode of operation is known as constant current mode and is mostly used to scan rough surfaces. In the constant height mode, the tip height (s) above the surface is kept constant and the variation of tunneling current reflects the corrugation of the surface (Bhushan 2004; Jia and others 2005; Egerton 2005).

Preparation of samples

Samples must be conductive enough to allow sufficient tunneling current (0.2-10 nA) which can be measured. Insulating samples can be coated with a thin layer of a conducting material and visualized with an STM (Bhushan 2004).

Collection and interpretation of data

STM images can be interpreted in a manner similar to that for AFM, as discussed in the section under atomic force microscope.

Limitations

The main limitation of STM is that it can only take images of conducting or semi-conducting surfaces under ultra high vacuum. It requires great mechanical precision to maintain a tip within 1 nm of a surface. An STM can provide structural information of only the surface of a sample. Therefore, it should be combined with some other technique such as TEM.

Atomic force microscope (AFM)

Gerd Binnig, Calvin Quate, and Christoph Gerber invented the atomic force microscope in 1985. Similar to an SEM, AFM can produce very high resolution three-dimensional images of the surface of a sample. The advantages of AFM include low cost, ease of use, and ease of sample preparation. AFM does not require the sample to be

conducting. Therefore, AFM can be used to take images of any type of surfaces including polymers, ceramics, composites, glass, and biological samples.

Principle of operation

A schematic representative of an atomic force microscope is shown in Figure 7. A probe (cantilever with a sharp tip) is brought very close to the surface of a sample and the interatomic force between the probe tip and the sample is monitored. The interatomic force is repulsive if the tip is in direct contact with the sample. At a small distance above the sample, the tip senses an attractive van der Waals force. The interatomic force is determined by precisely measuring the displacement of the cantilever. A laser beam, which is deflected from the back of the cantilever, is directed to a photodetector. The photodetector measures the normal and lateral deflections of the cantilever. The deflections of the cantilever are converted into an image. A feedback control unit (CU) is used to adjust the height of the tip so that the interatomic force remains constant. A scanner is used for three-dimensional movement of the probe or sample in AFM. The scanners are made of piezoelectric materials to provide precise positioning in the nanometer range. There are two main modes of operation in AFM: contact mode and tapping or intermittent contact mode. The tip remains in permanent contact with the sample in contact mode. The force between the tip of the cantilever and the sample is measured at each point on the surface. A feedback loop keeps the force at a constant value by adjusting the height of the surface relative to the cantilever. The change in height is used to determine the topography of the surface. In tapping mode, the cantilever tip is oscillated above the surface of the sample at its resonant frequency. Oscillation of the cantilever is reduced because contact between tip and the surface results in

loss of energy. The reduction in amplitude of oscillation is used to determine the topography of the surface. The tapping mode works well with soft materials that might be damaged in contact mode (Bhushan 2004; Magonov and Yerina 2005).

Preparation of samples

Unlike other microscopy techniques, preparation of sample is quite simple in AFM. Samples do not require staining as in TEM or conductive coating as in SEM. Surface of the sample should be free of any scratches and foreign particles. Flat surfaces of samples can be prepared by ultramicrotoming (Yalcin and Cakman 2004).

AFM is typically conducted at ambient conditions. However, AFM can also operate with its tip and sample immersed in a liquid such as water. This makes AFM very useful in taking images of biological samples (Egerton 2005). AFM measurements at elevated temperatures of 150-300 °C are now possible and AFM analysis can also be performed below 0 °C. AFM imaging at elevated temperatures can be used to study structural changes in materials related to different thermal transitioning such as melting, crystallization, recrystallization, and glass transition (Ivanov and others 2001; Magonov and Yerina 2005).

Collection and interpretation of data

AFM images can be used to study detailed structure of the surface of a sample. The basic measurement in AFM is deflection of the cantilever over each x and y coordinate of the surface. This data can be used to define an average roughness (R_a) of the surface as (Ghanbarzadeha and Oromiehib 2008):

$$R_a = \frac{\sum_{i=1}^{N}\left(Z_i - \overline{Z}\right)}{N} \qquad (4)$$

where Z_i is the deflection value, $\overline{Z}$ is the arithmetic mean of deflection values, and N is the number of x and y coordinates of the surface.

AFM can also be used to determine adhesive and mechanical properties of a surface on nano-scale. The force required to pull the tip from the surface can be used as a quantitative measure of the adhesion between tip and surface. The mechanical response of the surface can be determined by using AFM in the contact mode at different force levels (Magonov and Renekar 1997).

Limitations

AFM can be used to study only the surface of a sample. Mechanical scanning of a large area of a sample in AFM is very time consuming. The probing of materials with AFM is based on mechanical interactions. This prevents AFM from being used for studying the chemical nature of materials. Another limitation of AFM is due to the finite size and shape of the probe. AFM cannot be used to analyze a surface which has nanoparticles with dimensions smaller than the probe itself.

Confocal scanning laser microscope (CSLM)

CSLM is a non-destructive optical microscopic technique for the study of a material surface or internal structure of semi-transparent samples. CSLM can be used to form a three-dimensional image of any sample.

Principle of operation

A schematic representation of a confocal scanning laser microscope is shown in Figure 8. A beam of laser light is reflected by a dichroic mirror and focused onto a spot within the sample by the objective lens. Dichroic mirrors reflect light of one wavelength and

transmit that of another wavelength. A laser beam illuminates the sample at the focus of the objective lens and excites fluorescence in the focused spot. The sample then emits light at a lower wavelength, which goes through the objective, passes through the dichroic mirror, and is focused down to another diffraction-limited spot, which is surrounded by a narrow pinhole. The pinhole is said to be confocal to the focal point of the objective lens on the sample because it is positioned at a point conjugate to the focal point of objective lens. The pinhole spatially filters out light originating from parts of the sample not focused by the laser beam. Light from the focused spot of the sample is then passed to the detector. The laser beam is focused at different portions of the sample to cover a range of depths. This allows point-by-point construction of the three-dimensional image of the sample (Lu 2005).

Preparation of samples

Preparation of samples for CSLM requires use of a staining agent for differentiating different phases and ingredients. Staining agent can be applied by either covalent or non-covalent labeling. Covalent labeling involves covalent linking of a fluorescent dye to the desired sample. Non-covalent labeling involves addition of fluorescent dye to the sample. For non-covalent labeling, fluorescent dye with affinity for either hydrophilic or hydrophobic regions can be used. Rhodamine B, a dye with affinity for hydrophilic region, is used to stain aqueous solution of proteins. Dyes with affinity for hydrophobic regions include Nile red and Nile blue A (Tromp and others 2004).

Bio-nanocomposites based on layered clay can be stained with Safranine O by ion-exchange. Safranine O, a fluorescent dye, contains aluminum ion. Aluminum ion enables this dye to intercalate in clay galleries during ion-exchange. Confocal microscopy can then be

used to determine the extent of dispersion of clay during mixing or sonication (Yoonessi and others 2004).

Collection and interpretation of data

CSLM image can be used to evaluate the extent of mixing on micrometer scale. The CSLM image can be reconstructed to yield an image giving a three-dimensional impression of the sample. The three-dimensional image provides better insight into the extent of mixing on micrometer scale in the sample.

Limitations

One of the main limitations of CSLM is the requirement for a florescent dye which can bind to the region of interest. The resolution (~130 nm) of CSLM is poorer than that of TEM (Yoonessi and others 2004). Therefore, CSLM analysis should always be used in combination with other microscopic techniques such as TEM or AFM.

Spectroscopy

Spectroscopy is the study of the interaction between electromagnetic radiation and a material as a function of wavelength. Spectroscopy is used to determine functional groups, structural conformation, and concentration of different components in a material. The main spectroscopy techniques used for structural characterization of bio-nanocomposites are Fourier transform infra-red (FTIR), Raman, and nuclear magnetic resonance (NMR) spectroscopy.

Fourier transform infra-red (FTIR) spectroscopy

Infra-red (IR) radiation is a part of the electromagnetic spectrum with wavelength ranging from 0.8 to 100 μm. The region of infra-red radiation is further sub-divided into near

infra-red (0.8-2.5 μm), mid infra-red (2.5-15 μm), and far infra-red (15-100 μm). Typical wavenumber (1/wavelength) for mid infra-red spectroscopy ranges from 400-4000 cm^{-1}. The energy associated with absorption of IR radiation promotes rotation and vibration of chemical bonds. This vibrational energy is related to the strength of the bond and the molecular mass. IR spectroscopy measures the absorption of specific frequencies of IR radiation by a sample. The measured absorption can be used to identify chemical bonds or functional groups in a particular sample. IR spectroscopy uses high resolution diffraction monochromator for generating the absorption spectrum. This results in long measurement time because the absorption at each wavelength is measured sequentially. Another alternative form of IR analysis is Fourier transform infra-red spectroscopy. FTIR spectroscopy uses an interferometer instead of a monochromator to measure absorption at all wavelengths simultaneously. FTIR spectrometer is also fast and more sensitive as compared to a conventional IR spectrometer (Reh 2001).

Principle of operation

A schematic representation of an FTIR spectroscope is shown in Figure 9. IR radiation is produced by heating an inert solid such as silicon carbide to 1,000 to 1,800 °C. An interferometer consists of a beam splitter and two mirrors (fixed mirror and moving mirror). The beam splitter, which is a semi-reflecting device, is made by depositing a thin film of germanium onto a flat potassium bromide (KBr) substrate. The beam splitter divides the IR radiation in two beams: one beam is transmitted to the fixed mirror and the other beam is reflected to the moving mirror. When the two beams recombine after being reflected from the two mirrors, they undergo constructive and destructive interference due to the optical

path difference between them. The optical path difference is created by varying the relative position of the moving mirror with respect to the fixed mirror. This recombined IR radiation is passed through the sample. Fluctuation in the intensity of energy at the detector is digitized into an interferogram. An interferogram contains time-domain spectrum (intensity vs. time) over the entire IR region. The interferogram is converted into a conventional frequency domain spectrum (intensity vs. frequency) using Fourier transform (Sherman-Hsu 1997).

Preparation of samples

Any solid, liquid, or gas sample can be analyzed using FTIR spectroscopy. The most common method to prepare solid samples involves use of a matrix to disperse the ground sample. The matrix can be a liquid (mineral oil) or solid (potassium bromide). For a liquid matrix, the paste of the ground sample and the liquid is spread between two IR transparent windows. For a solid matrix, a mixture of ground sample and potassium bromide (KBr) is pressed under high pressure (~80 MPa) for a few minutes. Recrystallization of KBr results in a clear disk which can be inserted into the optical beam with a special sample holder. Liquids are analyzed as thin films in a cell with two IR transparent windows. A Teflon spacer is generally used to produce a film of the desired thickness (Reh 2001).

Another method to prepare samples is based on attenuated total reflectance (ATR). ATR device measures the total reflected energy from the surface of a sample in contact with an IR transmitting crystal. The refractive index of the crystal is significantly higher than that of the sample. This ensures total internal reflection of the radiation in the crystal. Infra-red radiation penetrates a small distance into the sample before reflecting back to the crystal. Therefore, there should be good optical contact between the sample and the crystal. Many

solid samples give very weak spectra because the contact is confined to small areas (Reh 2001).

Collection and interpretation of data

The spectrum for a particular sample is obtained by plotting the intensity of % transmitted radiation as a function of wavenumber. Many functional groups absorb IR radiation in a very narrow range of wavenumber. The spectrum obtained from an FTIR analysis can be used to either determine the presence of a functional group in a sample or compare the spectrum of unknown material to that of known reference material (ASTM Standards 1998).

Strong absorption bands appear in the region of 4000 to 2500 cm^{-1} because of the stretching vibrations between hydrogen and atoms with molecular weight (M) less than 19. Absorption bands in the region of 2700 to 1850 cm^{-1} usually appear because of triple bonds (C≡N) and other functional groups such as S-H, P-H, and Si-H. Many double bonded functional groups show absorption bands in the region of 1950 to 1450 cm^{-1}. Some of those double bonded functional groups include carbonyl groups, ketones, aldehydes, carboxylic acids, amides, and esters (Sherman-Hsu 1997). Absorption bands corresponding to C=O stretching (amide I), N-H bending (amide II), and C-N stretching (amide III) occur at 1630 cm^{-1}, 1530 cm^{-1} and 1230 cm^{-1} respectively (Schmidt and others 2005).

Absorption bands from stretching of silicon oxygen bonds (Si-O) occur in the region of 950 to 1100 cm^{-1}. This is particularly important for layered clay-based bio-nanocomposites because Si-O bonds are present in clay. The absorption band for agglomerated clay layers (tactoids) is broad. The absorption band becomes narrower as the

degree of exfoliation increases. Thus, FTIR spectroscopy can be used to determine the extent of exfoliation in bio-nanocomposites (Klein and others 2005). Absorption bands associated with different bonds of montmorillonite are shown in Table 1.

Limitations

FTIR spectroscopy can only be used to analyze samples which are transparent to IR radiation. Multiple functional groups can absorb IR radiation in the same range of wavenumber. Therefore, this technique should be complemented with other analytical techniques such as Raman or nuclear magnetic resonance (NMR) spectroscopy (Sherman-Hsu 1997).

Raman spectroscopy involves radiating a sample with monochromatic visible of near infra-red light from a laser. While IR spectroscopy detects the change in dipole moment, Raman spectroscopy detects change in polarizability of a sample. Some of the advantages of Raman spectroscopy over IR spectroscopy include ease of sample preparation, faster analysis, and better spatial resolution. However, heat generated by the laser in Raman spectroscopy may change the characteristics of the sample during measurement (Thygesen and others 2003).

Nuclear magnetic resonance (NMR) spectroscopy

Nuclear magnetic resonance (NMR) is a phenomenon which occurs when the nuclei of certain atoms, under a static magnetic field (B_0), are exposed to a second oscillating magnetic field (B_1). NMR spectroscopy can be performed on materials which have a net nuclear spin due to unpaired protons or neutrons. The unpaired proton or neutron with a spin generates a tiny magnetic field with a magnetic moment, μ. The alignment of the spin with

the external magnetic field can result in either a low energy or a high energy configuration. There can be a transition between the two energy configurations by absorption (low to high energy configuration) or emission (high to low energy configuration) of a photon. The energy of the photon is equal to the difference between the two energy levels. The signal in NMR spectroscopy is obtained from the difference in energy absorbed and emitted. Thus, the NMR signal is proportional to the population difference between the two energy states. At room temperature, the number of spins in low energy level is slightly greater than those in high energy level. NMR spectroscopy is sensitive enough to detect this small difference between the number of spins in low and high energy levels (Keeler 2006).

Principle of operation

A schematic representation of an NMR spectroscope is shown in Figure 10. A superconducting magnet (superconducting solenoid immersed in liquid helium) generates a static magnetic field (B_0) within the sample in the z-direction. Shim coils are used to maintain the homogeneity of the magnetic field. The sample tube is a cylindrical metal tube inserted into the bore of the magnet. The magnetic moments ($\boldsymbol{\mu}$) of all the spins in a sample can be represented by a net magnetization vector ($\mathbf{M} = \sum\boldsymbol{\mu} = M_x\mathbf{i} + M_y\mathbf{j} + M_z\mathbf{k}$). At equilibrium, the net magnetization vector ($M_z = M_0$, $M_x = M_y = 0$) lies along the direction of B_0 (z-direction). The value of B_0 is much greater than M_0. Therefore, it is not possible to detect the net magnetization vector of the sample. If the magnetization vector is tilted away from the z-axis by an angle β, it precesses around the z-axis and sweeps out a cone with an angle β. The frequency (ν in rad s^{-1}) of precession is given by (Keeler 2006):

$$\nu = \gamma B_0 \qquad (5)$$

where γ, unique to each isotope, is the gyromagnetic ratio. The values of γ for proton (^{1}H) and Carbon-13 (^{13}C) are 42.58 and 10.71 MHz/Tesla respectively. The frequency ν is also known as the resonance or Larmor frequency. Tilting of the magnetization vector is achieved by applying a very small oscillating magnetic field (B_1) along the x-axis. This oscillating secondary magnetic field is generated by transmitting radio frequency (RF) waves through a radio frequency (RF) coil. The response of the magnetization vector to this alternating field is used to receive signals in NMR spectroscopy. Resonance is achieved when the frequency of B_1 is equal to the Larmor frequency. Once resonance is achieved, the magnetization vector will precess about the x-axis with a frequency (ν_1) given by (Keeler 2006):

$$\nu_1 = \gamma B_1 \tag{6}$$

For a typical NMR experiment, B_1 is much smaller than B_0. Therefore, ν_1 is smaller than the Larmor frequency (ν). A pulsed magnetic field along the x-axis is produced by switching on and off the RF field in the coil. Pulse time (τ) is the duration of time the field is on. The pulse field rotates the magnetization vector about the x-axis by a certain angle, known as the flip angle (β). Flip angle is given by (Keeler 2006):

$$\beta = 2\pi\nu_1\tau \tag{7}$$

A pulse field giving a flip angle of β is known as a β pulse. The most common flip angles are 90° and 180°. A 90° pulse rotates the magnetization vector from its equilibrium position to the negative y-axis. A 180° pulse, known as the inversion pulse, rotates net magnetization vector from positive z-axis to negative z-axis (Keeler 2006). Rotation axis of the pulse can be changed by changing the phase offset (φ) of the RF field.

After the magnetization vector has been flipped by the RF pulse, transverse magnetization (M_{xy}) relaxes back to zero and longitudinal magnetization (M_z) relaxes back to its equilibrium value (M_0). Longitudinal or spin-lattice relaxation constant (T_1) is the time required for the longitudinal magnetization vector (M_z) to return to 63% of its equilibrium value (M_0). T_1 is also the time required by the spins to exchange energy with the surrounding lattice. The longitudinal relaxation time is most commonly measured by using an inversion recovery pulse sequence. In an inversion recovery pulse sequence, a 180° pulse is followed by a delay (τ) and a 90° pulse. Duration of the delay is longer than the duration of either the 180° pulse or 90° pulse. If the magnetization vector is placed in x-y plane, it will precess about the z-axis at the Larmor frequency. Along with precession, M_{xy} also starts to decay to its equilibrium value of zero because of the heterogeneity of magnetic field and molecular interactions. Transverse or spin-spin relaxation time (T_2) is the time required to reduce M_{xy} by a factor of e (2.718). In the absence of a heterogeneous magnetic field, T_2 can be estimated by a spin echo pulse sequence. In a spin echo pulse sequence, a 90° pulse is followed by a delay (τ), a 180° pulse, and another delay (τ). The signal is acquired after the second delay. T_2 is always less than T_1 (Keeler 2006).

The NMR signal is detected as an induced oscillating voltage (μV) in the RF coil by the RF receiver. The same RF coil is used for both exciting the spins and detecting the signal. The RF transmitter and receiver are separated by a device, known as diplexer. A diplexer is a fast acting switch which connects the receiver to the coil only when the transmitter is disconnected. The NMR signal is detectable only for a short duration because it decays due to the above mentioned relaxation processes. The decaying time-domain signal is known as

the free induction decay (FID) signal. An analog to digital convertor (ADC) converts the signal from a voltage to a binary number. Fourier transform of the FID signal produces a spectrum with intensity as a function of frequency (Keeler 2006).

Preparation of samples

During sample preparation for NMR spectroscopy, the sample tubes should be clean and free of any contaminants. The sample should be dry and free of any solvent. The NMR samples are prepared by dissolving the sample in a solvent containing deuterium. The most common solvent is deuterated chloroform. The sample should be completely dissolved in the solvent because undissolved particles can distort the homogeneity of the magnetic field.

Collection and interpretation of data

NMR spectrum is a plot of intensity as function of frequency. A typical range for frequency is from 10 to 800 MHz. NMR results are also expressed on a chemical shift scale. The chemical shift scale is set up by defining the peak frequency (ν_{ref}) from tetramethylsilane (TMS) as zero. The chemical shift (δ) is defined as (Keeler 2006):

$$\delta = 10^6 \times \frac{\left(\nu_p - \nu_{ref}\right)}{\nu_{ref}} \qquad (8)$$

Where ν_p is the frequency of the peak intensity for a sample. The chemical shift is often expressed in parts per million (ppm).

The FID signal decays quicker in solids as compared to liquids. Thus, the shape of the FID signal can be used to distinguish between solid and liquid components of a sample. The relaxation times T_1 and T_2 provide information about the molecular structures of compounds (Choi and others 2003). The values of T_1 and T_2 depend on the magnetic field, type of

nucleus, temperature, and presence of other larger molecules. The value of T_1 for nuclei bound to larger molecules such as proteins is much lower than that for nuclei bound to pure water.

Some studies on the use of NMR for structural characterization of bio-nanocomposites have been reported (Avella and others 2005; Bruno and others 2008). Bruno and others (2008) investigated the molecular structure and intermolecular interaction between the components of bio-nanocomposites based on poly(3-hydroxybutyrate) (PHB) and modified MMT using NMR. Values of T_1 were determined for the bio-nanocomposites at different MMT content. Results showed that NMR can be used as an efficient and rapid method to characterize the structures of bio-nanocomposites.

Limitations

The main limitation of NMR spectroscopy is its sensitivity. Atomic nuclei which have high sensitivity to NMR can only be analyzed by NMR spectroscopy. NMR spectroscopy can only be used for a non-paramagnetic sample.

Conclusions

This paper reviews analytical techniques for the structural characterization of biopolymer-based nanocomposites. Selection of proper technique for characterization of these bio-nanocomposites is very critical in assessing their performance. XRD is generally used as the preferred technique to determine immiscible or intercalated arrangements of nanoparticles in bio-nanocomposites. SEM can be used as a quick method to study the dispersion of larger aggregates (~ 1 μm) of nanoparticles at the surface of a bio-nanocomposite. TEM images can provide a qualitative understanding of the internal structure, spatial distribution, and dispersion of nanoparticles in bio-nanocomposites. TEM in conjunction with XRD can provide information on the occurrence and degree of intercalation or exfoliation in bio-nanocomposites. AFM can be used to study the structure as well as mechanical properties of a surface at the nano-scale. Spectroscopy techniques (FTIR and NMR) can be used in conjunction with microscopy techniques to obtain information on the interaction between nanoparticles and the biopolymer matrix.

Future studies on the characterization techniques need to focus on development of 1) microscopy techniques capable of obtaining three-dimensional images, 2) better and faster methods of sample preparation, 3) better image analysis techniques for better interpretation of results, and 4) microscopy at elevated temperature. These future developments will help in better understanding of the interaction between nanoparticles and biopolymer matrix. This will aid in the synthesis of bio-nanocomposites with improved properties.

Acknowledgments

Support for the research study undertaken here, resulting in the publication of paper nr FSR-09-35 of the Journal Series of the Dept. of Food, Bioprocessing, and Nutrition Sciences, NCSU, Raleigh, NC 27695-7624 from USDA-NRICGP Grant nr 2008-01503, titled: Development of cross-linked bio-nanocomposite packaging films with enhanced barrier and mechanical properties, is gratefully acknowledged.

The use of trade names in this publication does not imply endorsement by the North Carolina Agricultural Research Service of the products named nor criticism of similar ones not mentioned.

References

ASTM Standards. 1998. E1252-98. General techniques for obtaining infrared spectra for qualitative analysis. Philadelphia, PA.

Avella M, Vlieger JJD, Errico ME, Fischer S, Vacca P, Volpe MG. 2005. Biodegradable starch/clay nanocomposite films for food packaging applications. Food chemistry 93: 467-474.

Bhushan B. 2004. Scanning probe microscopy – principle of operation, instrumentation, and probes. In: Bhushan B, editor. Springer Handbook of Nanotechnology. New York: Springer. p 325-369.

Bordes P, Pollet E, Averous L. 2009. Nano-biocomposites: biodegradable polyester/nanoclay systems. Progress in polymer science 34(2): 125-155.

Bozzola JJ, Russell LD. 1999. Electron microscopy: principles and techniques for biologists. Boston: Jones & Bartlett Publishers. 670 p.

Bruno M, Tavares MIB, Motta LM, Miguez E, Preto M, Fernandez AOR. 2008. Evaluation of PHB/clay nanocomposites by spin-lattice relaxation time. Materials research 11(4): 483-485.

Chavaria F, Paul DR. 2004. Comparison of nanocomposites based on nylon 6 and nylon 66. Polymer 45(25): 8501-8515.

Chen G, Liu S, Chen S, Qi Z. 2001. FTIR spectra, thermal properties, and dispersibility of a polystyrene/montmorillonite nanocomposite. Macromolecular chemistry and physics 202: 1189-1193.

Chen P, Zhang L. 2006. Interaction and properties of highly exfoliated soy protein/montmorillonite nanocomposites. Biomacromolecules 7: 1700-1706.

Choi SG, Kim KM, Hanna MA, Weller CL, Kerr WL. 2003. Molecular dynamics of soy-protein isolate films plasticized by water and glycerol. Journal of food science 68(8): 2516-2522.

Dennis HR, Hunter DL, Chang D, Kim S, White JL, Cho JW, Paul DR. 2001. Effect of melt processing conditions on the extent of exfoliation in organoclay-based nanocomposites. Polymer 42: 9513-9522.

Dimonie D, Constantin R, Vasilievici G, Popescu MC, Garea S. 2008. The dependence of the XRD morphology of some bio-nanocomposites on the silicate treatment. Journal of nanomaterials doi:10.1155/2008/538421.

Egerton RF. 2005. Physical principles of electron microscopy: an introduction to TEM, SEM, and AEM. New York: Springer. 202 p.

Guiannuzzi LA, Stevie FA. 1999. A review of focused ion beam milling techniques for TEM specimen preparation. Micron 30(3): 197-204.

Jia JF, Yang WS, Xue QK. 2005. Scanning tunneling microscopy. In: Yao N, Wang ZL, editors. Handbook of Microscopy for Nanotechnology. New York: Springer. p 55-112.

Jinnai H, Spontak RJ. 2009. Transmission electron microtomography in polymer research. Polymer 50: 1067-1087.

Ivanov DA, Amalou Z, Magonov SN. 2001. Real-Time evolution of the lamellar organization of poly(ethylene terephthalate) during crystallization from the melt: high-temperature atomic force microscopy study. Macromolecules 34: 8944-8955.

Kasai K, Kakudo M. 2005. X-ray diffraction by macromolecules. New York: Springer. 504 p.

Keeler J. 2006. Understanding NMR spectroscopy. New Jersey: John Wiley & Sons Inc. 459 p.

Klein RJ, Benderly D, Kemnetz A, Ijdo WL. 2005. A new methods to determining the quality of smectite clay/plastic nanocomposites: degree of nanodispersion and clay layer alignment. Nanocomposites 2005 fifth world congress. Aug 22-24. San Franciscso, CA, USA.

Koo JH. 2006. Polymer nanocomposites: processing, characterization, and applications. New York: McGraw-Hill. 272 p.

Lu PJ. 2005. Confocal scanning optical microscopy and nanotechnology. In: Yao N, Wang ZL, editors. Handbook of Microscopy for Nanotechnology. New York: Springer. p 3-24.

Magonov SN, Yerina NA. 2005. Visualization of nanostructures with atomic force microscopy. In: Yao N, Wang ZL, editors. Handbook of Microscopy for Nanotechnology. New York: Springer. p 113-155.

Magonov SN, Reneker DH. 1997. Characterization of polymer surfaces with atomic force microscopy. Annual review of materials science 27: 175-222.

Marsh K, Bugusu B. 2007. Food packaging – roles, materials, and environmental issues. Journal of food science 72(3): R39-R55.

McGlashan SA, Halley PJ. 2003. Preparaion and characterization of biodegradable starch-based nanocomposite materials. Polymer international 52: 1767-1773.

Monticelli O, Musina Z, Russo S, Bals S. 2007. On the use of TEM in the characterization of nanocomposites. Materials letters 61: 3446-3450.

Morgan AB, Gilman JW. 2003. Characterization of polymer-layered silicate (clay) nanocomposites by transmission electron microscopy and X-ray diffraction: a comparative study. Journal of applied polymer science 87: 1329-1338.

Nam PH, Maiti P, Okamoto M, Kotaka T, Hasegawa N, Usuki A. 2001. A hierarchical structure and properties of intercalated polypropylene/clay nanocomposites. Polymer 42(23): 9633-9640.

Pandey JK, Kumar AP, Misra M, Mohanty AK, Drzal LT, Singh RP. 2005. Recent advances in biodegradable nanocomposites. Journal of nanoscience and nanotechnology 5: 497-526.

Paul DR, Robeson LM. 2008. Polymer nanotechnology: nanocomposites. Polymer 49: 3187-3204.

Pavlidou S, Papaspyrides CD. 2008. A review on polymer-layered silicate nanocomposites. Progress in polymer science 33: 1119-1198.

Ray SS, Bousmina M. 2005. Biodegradable polymers and their layered silicate nanocomposites: In greening the 21st century materials world. Progress in materials science 50: 962-1079.

Reh C. 2001. In-line and off-line FTIR measurements. In: Kress-Rogers E, Brimelow CJB, editors. Instrumentation and Sensors for the Food Industry. Boca Raton: CRC Press. p 213-232.

Rhim JW, Ng PKW. 2007. Natural biopolymer-based nanocomposite films for packaging applications. Critical reviews in food science and nutrition 47(4): 411-433.

Schmidt V, Giacomelli C, Soldi V. 2005. Thermal stability of films formed by soy protein isolate-sodium dodecyl sulfate. Polymer degradation and stability 87: 25-31.

Shabeer A, Chandrashekhara K, Schuman T. 2007. Synthesis and characterization of soy-based nanocomposites. Journal of composite materials 41(15): 1825-1849.

Sherman-Hsu CP. 1997. Infrared spectroscopy. In: Settle F, editor. Handbook of Instrumental Techniques for Analytical Chemistry. New Jersey: Prentice Hall PTR. p 247-283.

Sorrentino A, Gorrasi G, Vittoria V. 2007. Potential perspectives of bio-nanocomposites for food packaging applications. Trends in food science and technology 18: 84-95.

Tang X, Alavi S, Herald TJ. 2008. Effects of plasticizers on the structure and properties of starch–clay nanocomposite films. Carbohydrate polymers 74: 552-558.

Thygesen LG, Lokke MM, Micklander E, Engelsen SB. 2003. Vibrational microspectroscopy of food. Raman vs. FTIR. Trends in food science and technology 14: 50-57.

Tromp RH, Nicolas Y, van de Velde F, Paques M. 2003. Confocal scanning laser microscopy (CSLM) for monitoring food composition. In: Tothill IE, editor. Rapid and On-line Instrumentation for Food Quality Assurance. Boca Raton: CRC Press. p 306-323.

Vaz CM, Mano JF, Fossen M, van Tuil RF, de Graaf LA, Reis RL, Cunh AM. 2002. Mechanical, dynamic-mechanical, and thermal properties of soy protein-based thermoplastic with potential biomedical applications. Journal of macromolecular science – physics B41(1): 33-46.

Vermogen A, Masenelli-Varlot K, Sgula R, Duchet-Rumeau J, Boucard S, Prele P. 2005. Evaluation of the structure and dispersion in polymer-layered silicate nanocomposites. Macromolecules 38 (23): 9661-9669.

Wang ZL. 2003. New developments in transmission electron microscopy for nanotechnology. Advanced materials 15(18): 1497-1514.

Williams DB, Carter CB. 1996. Transmission electron microscopy: a textbook for materials science. New York: Springer. 721 p.

Yalcin B, Cakmak M. 2004. The role of plasticizer on the exfoliation and dispersion and fracture behavior of clay particles in PVC matrix: a comprehensive morphological study. Polymer 45: 6623-6638.

Yang KK, Wang XL, Wang YZ. 2007. Progress in nanocomposite of biodegradable polymer. Journal of industrial and engineering chemistry 13(4): 485-500.

Yao N. 2005. Focused ion beam systems – a multifunctional tool for nanotechnology. In: Yao N, Wang ZL, editors. Handbook of Microscopy for Nanotechnology. New York: Springer. p 247-286.

Yoonessi M, Toghiani H, Kingery WL, Pittman CU 2004. Preparation, characterization, and properties of exfoliated/delaminated organically modified clay/dicyclopentadiene resin nanocomposites. Macromolecules 37 (7): 2511-2518.

Yu J, Cui G, Wei M, Huang J. 2007. Facile exfoliation of rectorite nanoplatelets in soy protein matrix and reinforced bio-nanocomposites thereof. Journal of applied polymer science 104: 3367-3377.

Zeng QH, Yu AB, Lu GQ, Paul DR. (2005). Clay-based polymer nanocomposites: research and commercial development. Journal of nanoscience and nanotechnology 5: 1574-1592.

Zhao R, Torley P, Halley PJ. 2008. Emerging biodegradable materials: starch- and protein-based bio-nanocomposites. Journal of materials science 43: 3058-3071.

Table 1 – Absorption spectra associated with montmorillonite (Chen and others 2001).

Wavenumber (cm^{-1})	Functional groups
3627	Stretching vibration of –OH bond
3429	Stretching of interlayer H_2O
1635	Deformation of interlayer H_2O
1091, 1039	Stretching of Si-O
519, 466	Stretching of Al-O and bending of Si-O

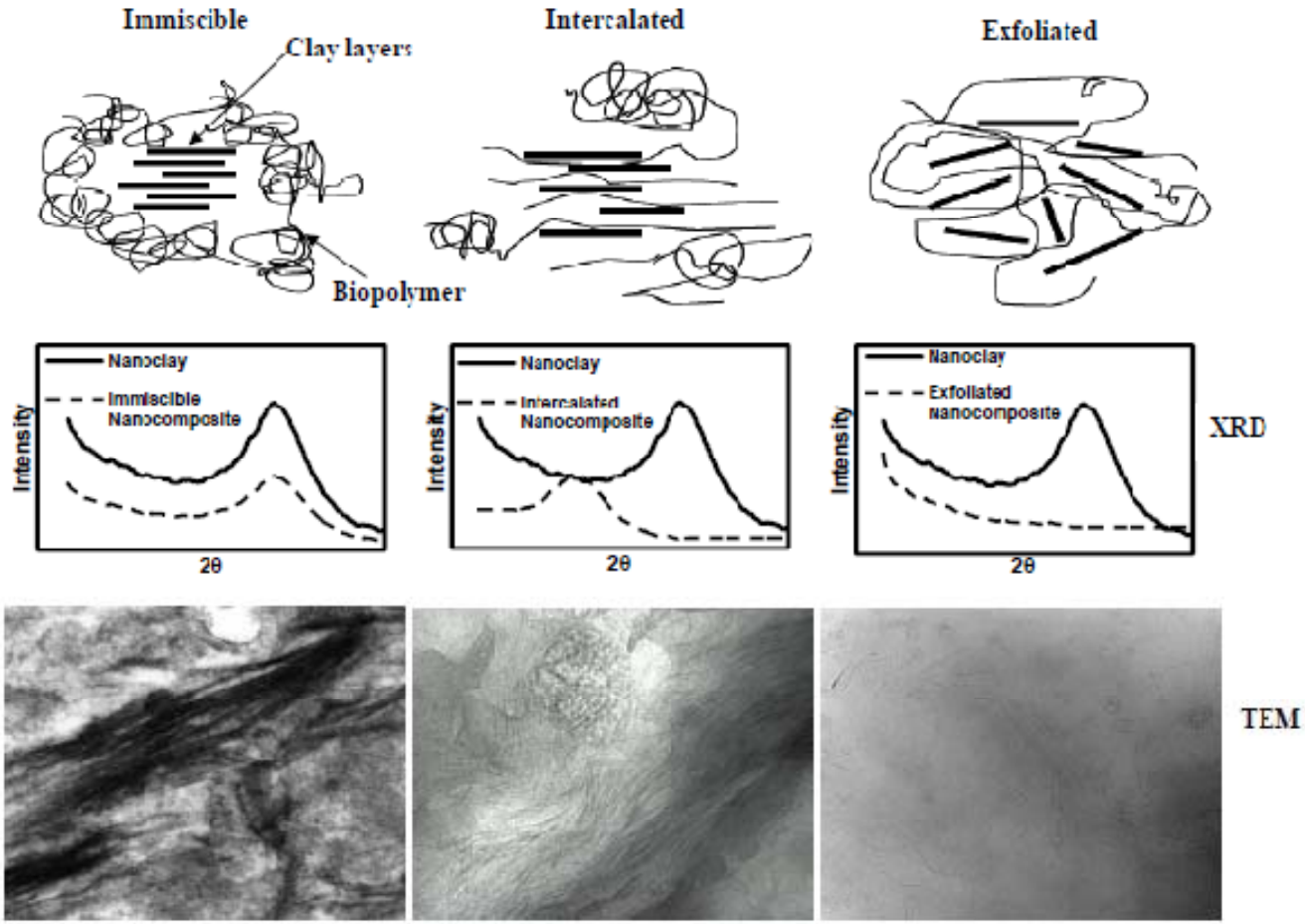

Figure 1 – Possible arrangements of layered silicates in biopolymers with corresponding XRD and TEM results.

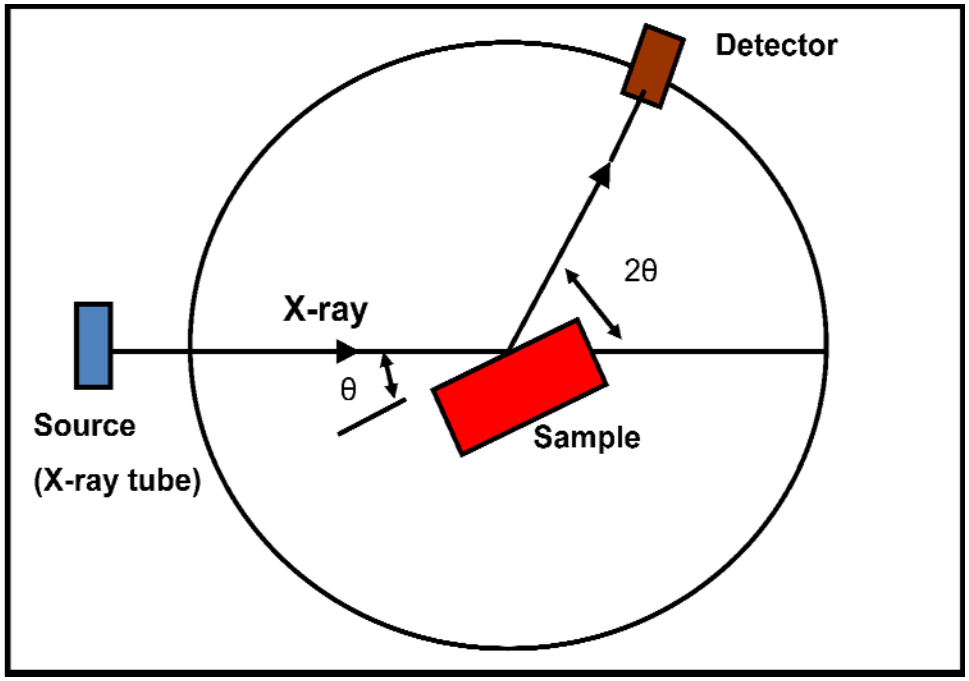

Figure 2 – A schematic of an X-ray diffraction (XRD) instrument.

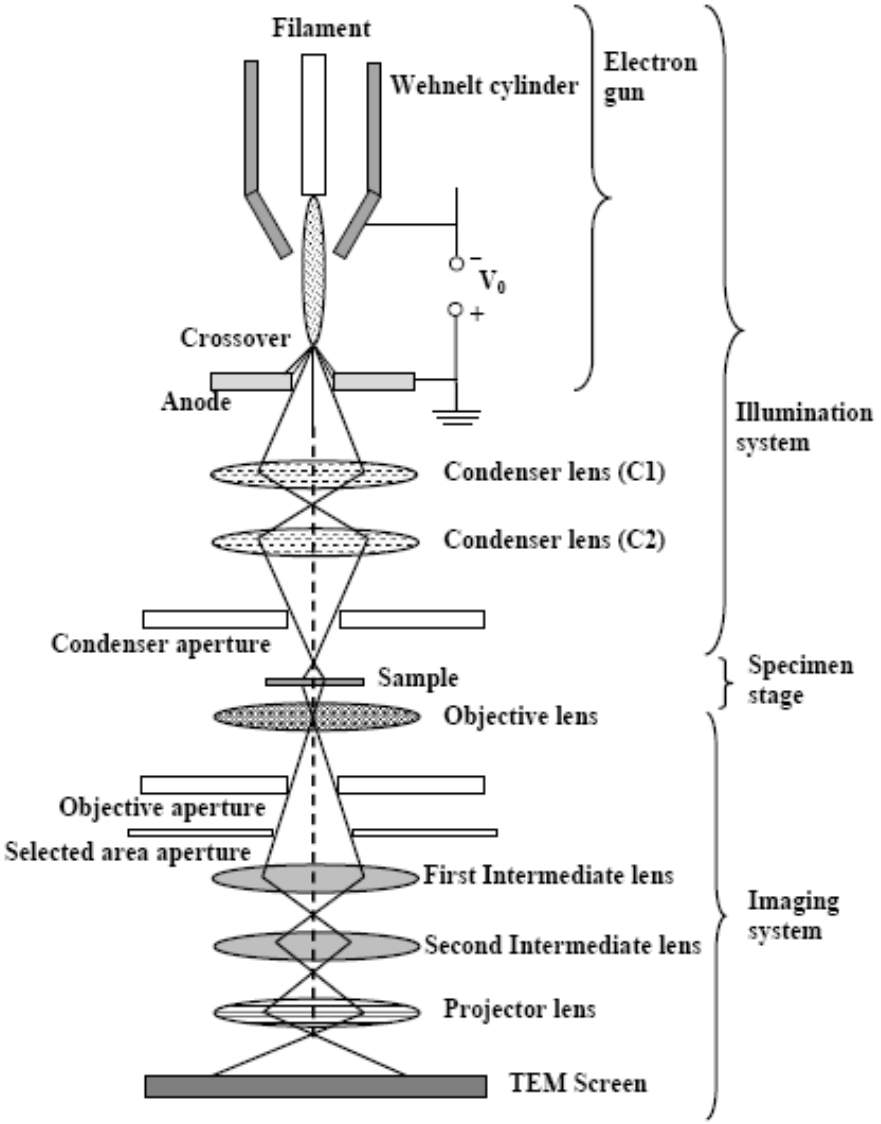

Figure 3 – A schematic representation of a transmission electron microscope (adapted from Egerton 2005).

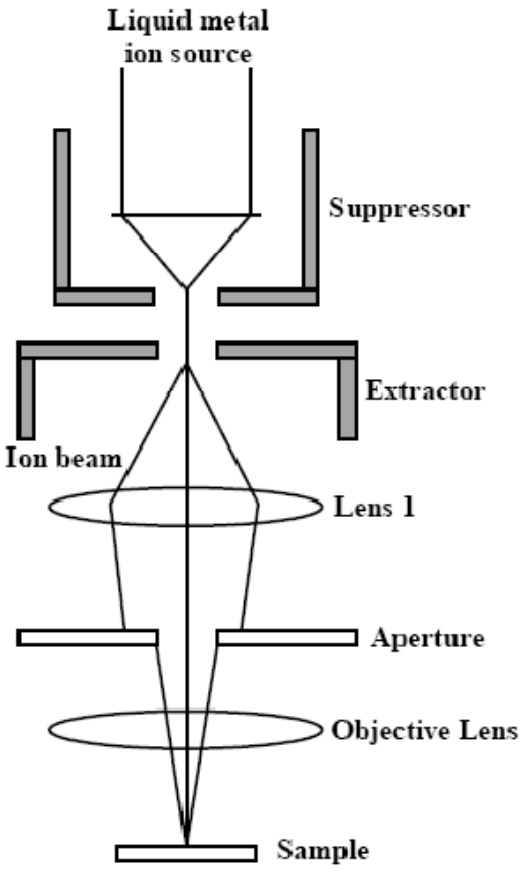

Figure 4 – A schematic representation of a focused ion beam instrument (adapted from Guiannuzzi and Stevie 1999).

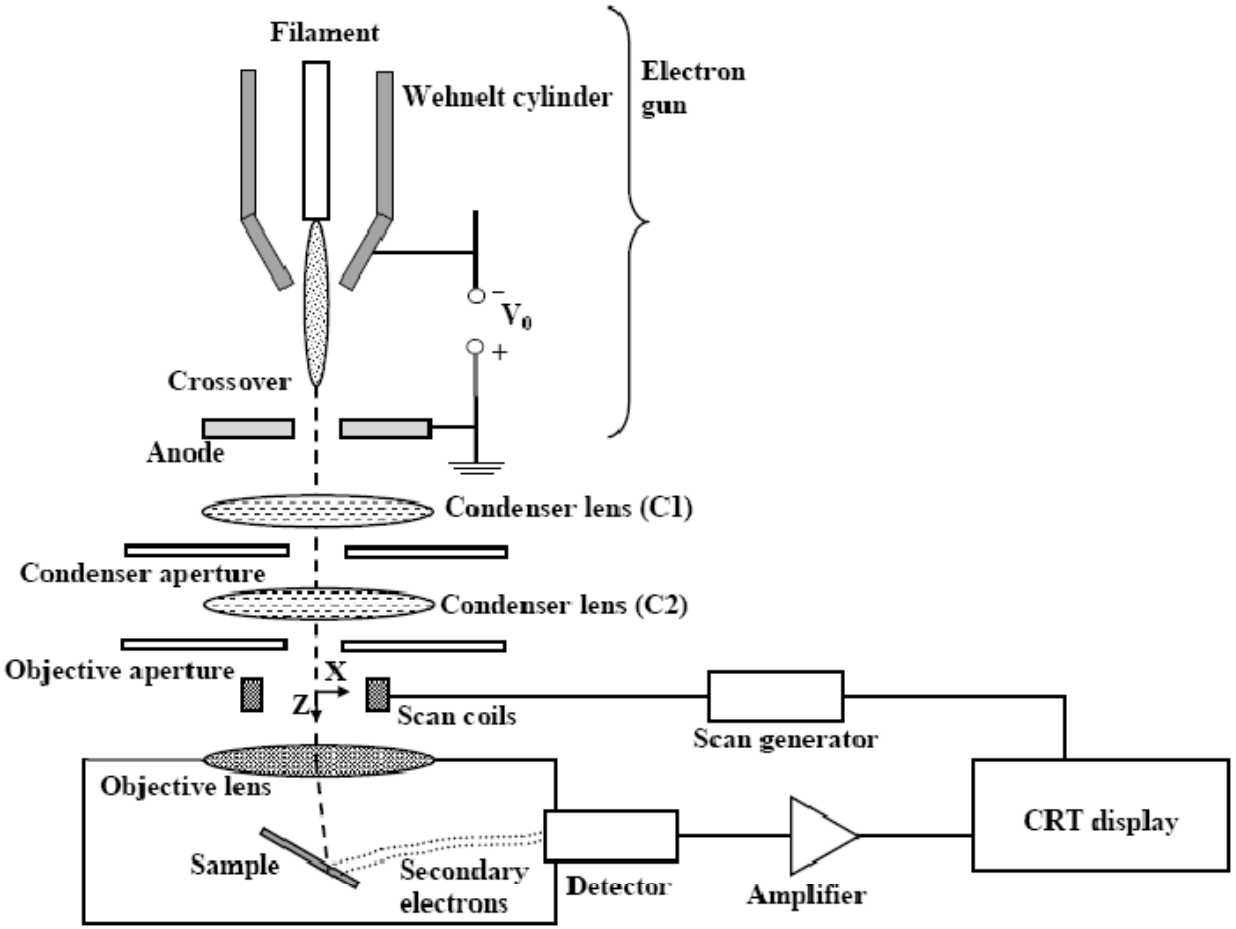

Figure 5 – A schematic representation of a scanning electron microscope (adapted from Egerton 2005).

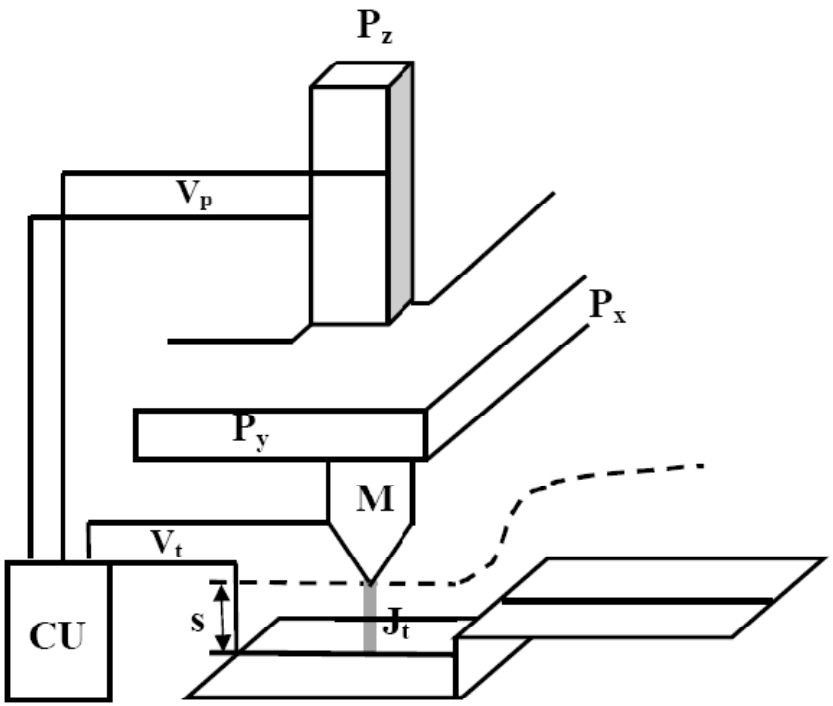

Figure 6 – A schematic representation of a scanning tunneling microscope (adapted from Jia and others 2005).

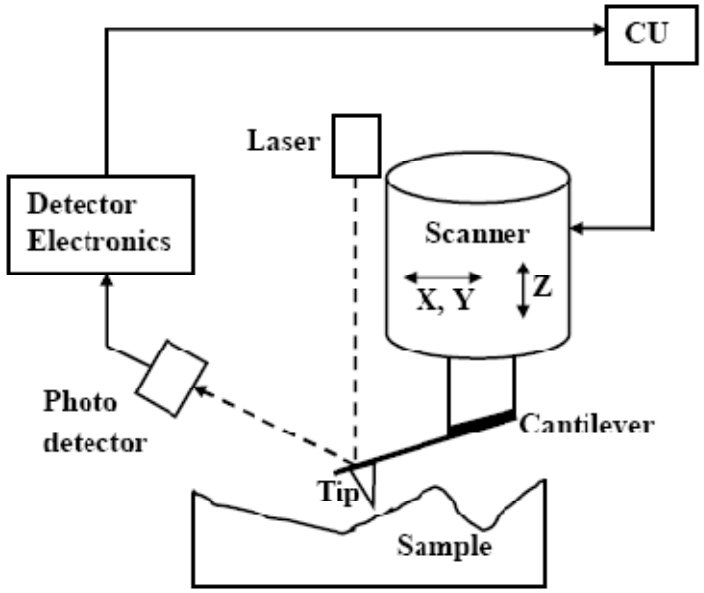

Figure 7 – A schematic representation of an atomic force microscope (adapted from Magonov and Yerina 2005).

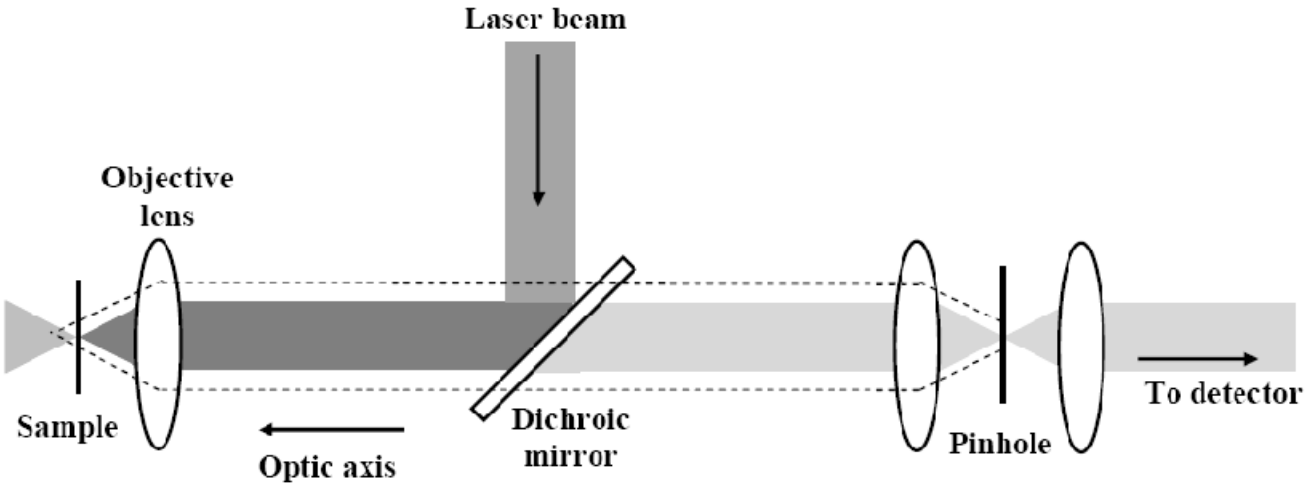

Figure 8 – A schematic representation of a confocal scanning laser microscope (adapted from Lu 2005).

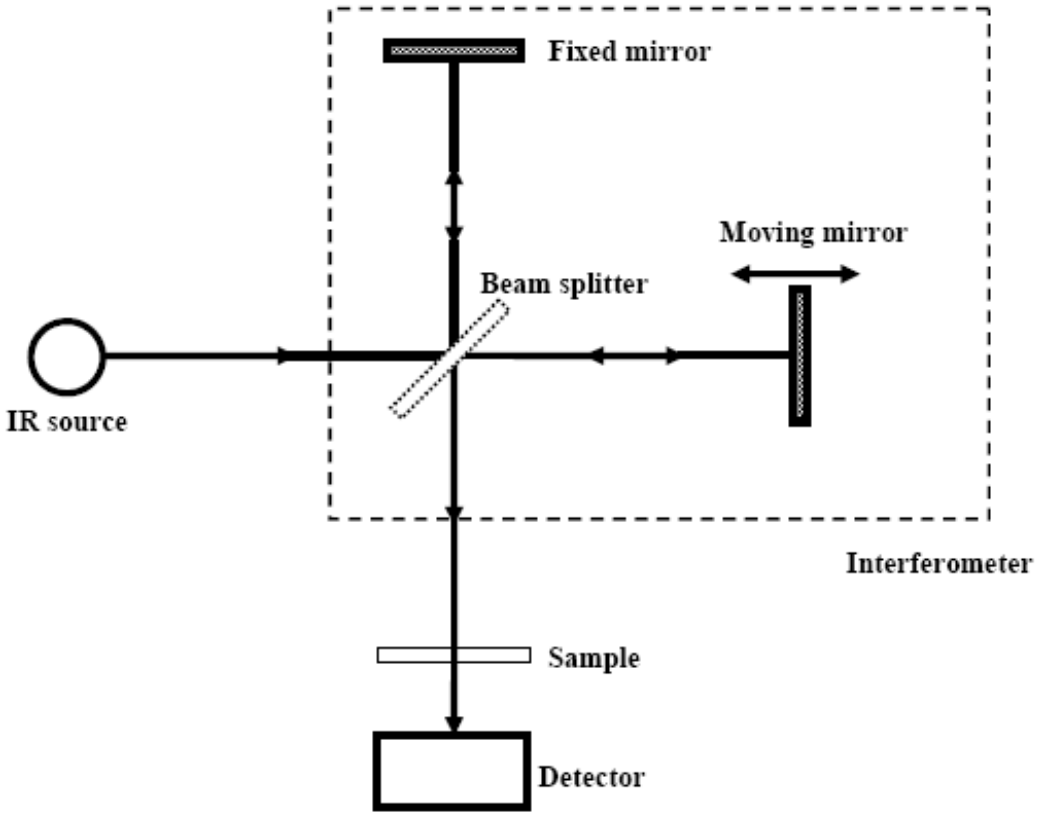

Figure 9 – A schematic representation of an FTIR spectroscope (adapted from Sherman-Hsu 1997).

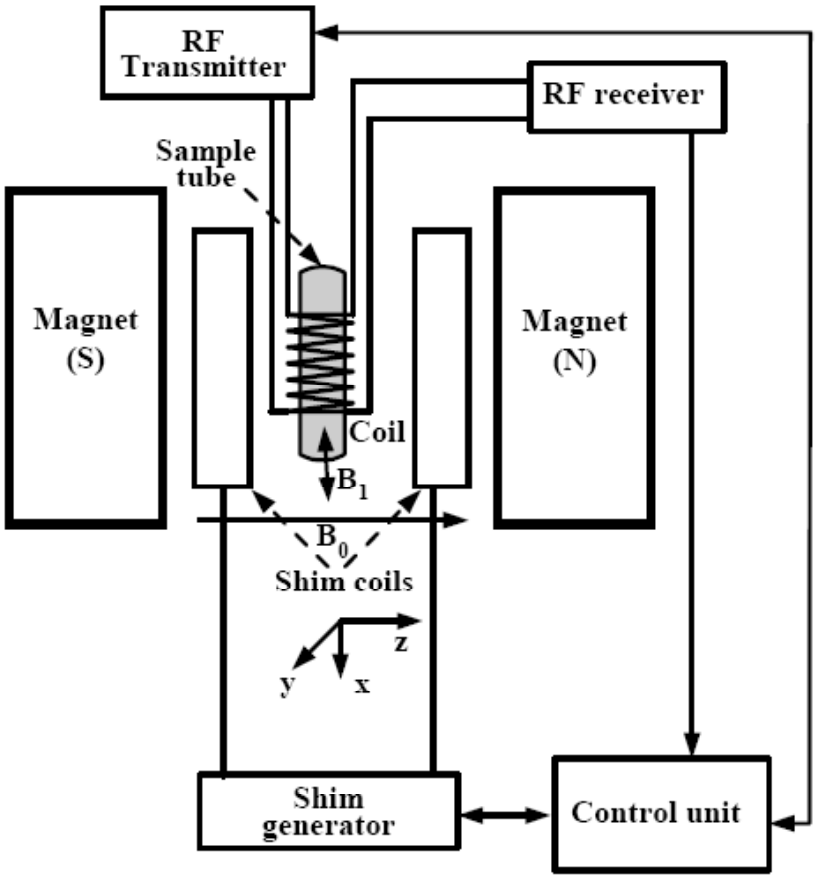

Figure 10 – A schematic representation of an NMR spectroscope (adapted from Keeler 2006).

Chapter 5

MANUSCRIPT III

Biopolymer-based Nanocomposites: Part II. Experimental and Modeling Techniques to Determine Properties

P. KUMAR[1], K.P. SANDEEP[1], S. ALAVI[2], AND V.D. TRUONG[3]

(1) Department of Food, Bioprocessing, and Nutrition Sciences, North Carolina State University, Raleigh, NC
(2) Department of Grain Science and Industry, Kansas State University, Manhattan, KS
(3) U.S. Dept. of Agriculture, Agricultural Research Service, South Atlantic Area, Food Science Research Unit, Raleigh, NC

Please address all correspondence to:

K.P. Sandeep
129 Schaub Hall, Box 7624
North Carolina State University
Raleigh, NC 27695
Phone: 919-515-2957
Fax: 919-515-7124
E-mail: kp_sandeep@ncsu.edu

Paper nr FSR-09-36 of the Journal Series of the Department of Food, Bioprocessing, and Nutrition Sciences, North Carolina State University, Raleigh, NC 27695-7624

Properties of bio-nanocomposites…

Abstract

The non-biodegradable and non-renewable nature of plastic packaging has led to a renewed interest in packaging materials based on bio-nanocomposites (biopolymer matrix reinforced with nanoparticles such as layered silicates). Properties of bio-nanocomposites are governed by the extent of dispersion of nanoparticles in the biopolymer matrix and interaction between nanoparticles and the biopolymer. Selection of proper technique to determine properties of these bio-nanocomposites is very critical in assessing their performance. This paper presents a review of experimental and modeling techniques to determine properties of bio-nanocomposites. Effect of nano-scale on the properties of bio-nanocomposites is discussed. Experimental techniques (tensile testing, barrier property measurement, dynamic mechanical analysis, differential scanning calorimetry, thermogravimetric analysis, rheological measurement) to determine the mechanical, barrier, thermal, and rheological properties of bio-nanocomposites are discussed. Lastly, the paper describes mathematical modeling of mechanical and barrier properties of bio-nanocomposites using analytical micromechanics.

Keywords: bio-nanocomposites, characterization of properties, experimental techniques, mathematical modeling

Introduction

The non-biodegradable and non-renewable nature of plastic packaging has led to a renewed interest in packaging materials based on biopolymers derived from renewable sources. Such biopolymers include naturally occurring proteins, cellulose, starches, and other polysaccharides and those synthesized chemically from naturally derived monomers such as lactic acid. Commercialization of bio-based polymers has already begun. Natureworks, LLC (Minnetonka, MN) manufactures polylactide from corn sugar. The polymer can be hydrolyzed back to lactic acid. Wal-Mart stores, Inc. is already using polylactide to package fresh-cut produce (Marsh and Bugusu, 2007). However, biopolymers cannot meet the requirements of a cost-effective film with mechanical and barrier properties matching those of plastics. Recently, a new class of materials represented by bio-nanocomposites (biopolymer matrix reinforced with nanoparticles such as layered silicates) has proven to be a promising option in improving the properties of these biopolymer-based packaging materials. Therefore, efforts have been geared towards developing bio-nanocomposites for food packaging films with improved mechanical, barrier, rheological, and thermal properties.

Several review papers discuss the preparation, characterization, properties, and applications of bio-nanocomposites (Pandey and others 2005; Ray and Bousmina 2005; Yang and others 2007; Rhim and Ng 2007; Sorrentino and others 2007; Zhao and others 2008; Bordes and others 2009). However, there is a lack of comprehensive review on various analytical techniques for the characterization of structure and properties of bio-nanocomposites. Part I of this series of two articles presented a review of different techniques for characterizing the structure of bio-nanocomposites in terms of principle of operation,

preparation of sample, interpretation of data, and limitations. A brief introduction of different techniques for the preparation of bio-nanocomposites was also given (Kumar and others 2009).

There is a lack of comprehensive review on various analytical and modeling techniques to determine properties of bio-nanocomposites. Properties of interest for bio-nanocomposites are mechanical, barrier, thermal, and rheological properties. Mechanical properties of interest are tensile modulus (TM), tensile strength (TS), and percent elongation (%E) at break. Tensile modulus is a measure of the resistance of a material to deformation. Tensile strength is the maximum tensile stress a film can sustain whereas %E is an indication of flexibility of a bio-nanocomposite film. Barrier properties of a packaging material play an important role in determining the shelf life of a food product. Barrier properties of a material indicate their resistance to sorption and diffusion of moisture and gases across the packaging material. Bio-nanocomposite films show improved barrier properties because nanoparticles dispersed in the biopolymer matrix provide a tortuous path for water and gas molecules to pass through. This increases the effective path length for diffusion, thereby improving the barrier properties (Rhim and Ng 2007). Barrier properties of interest in food packaging are water vapor permeability (WVP) and oxygen permeability (OP). Thermal properties of interest for bio-nanocomposites are glass transition temperature (T_g), thermal stability, and heat deflection temperature (HDT). Glass transition temperature defines one end of the operating range over which a polymer can be used. Thermal stability provides information on thermal behavior of a material over specific temperature ranges and environments. HDT is the temperature at which a polymer deforms under a specified load. Rheological properties of

a material are important to understand the processability of the material. Rheological measurements indicate melt processing behavior of bio-nanocomposites during unit operations such as injection molding and blown film process. These properties of bio-nanocomposites are governed by the extent of dispersion of nanoparticles in the biopolymer matrix and interaction between nanoparticles and the biopolymer. Selection of proper technique to determine properties of these bio-nanocomposites is very critical in assessing their performance.

Mathematical modeling plays an important role in predicting the properties of bio-nanocomposites and comparing them to the measured properties. This comparison helps in better understanding the mechanism for much improved properties of bio-nanocomposites. Mathematical modeling is also helpful in understanding the effects of different parameters on the properties of bio-nanocomposites. This parametric study is used to optimize processing parameters to prepare bio-nanocomposites with improved properties.

Mathematical modeling methods to predict properties of nanocomposites include the techniques of computational chemistry and computational mechanics. Computational chemistry makes use of modeling tools such as quantum mechanics and nanomechanics. Nanomechanics assumes a non-continuous composition of material and studies atomic interactions at the nano-scale. Nanomechanics includes techniques such as molecular dynamics, Monte Carlo, and ab initio simulations. Molecular dynamics predicts interaction between constituent phases of a composite at the atomic scale. Monte Carlo simulation is a probabilistic model for the prediction of properties of a system. It involves a multidimensional integration over the space of the sample. Ab initio simulation, which is

based on first principles, involves the solution of Schrondinger's wave equation for each electron (Valavala and Odegard 2005). Nanomechanics techniques can predict properties of a wide range of nanocomposite systems. However, these techniques are computationally very exhaustive. Further details on these nanomechanics techniques can be found in a review paper by Valavala and Odegard (2005).

The computational mechanics makes use of modeling tools such as micromechanics and structural mechanics. Micromechanics assumes the presence of a continuous structure of materials and does not include chemical interactions between different phases of a composite material. Micromechanics includes techniques such as computational micromechanics (finite element method, boundary element method) and analytical micromechanics (Rule of mixtures, Halpin-Tsai method, Mori-Tanaka theory) (Valavala and Odegard 2005). Most of this review focuses on mathematical modeling using analytical micromechanics, which has been widely used to model the properties of nanocomposites (Fornes and Paul 2003; Luo and Daniel 2003; Wu and others 2004; Sheng and others 2004; Weon and Sue 2005; Yung and others 2006; Rao 2007). The same modeling concepts can be applied for modeling the properties of bio-nanocomposites.

This paper presents a review of experimental and modeling techniques to determine properties of bio-nanocomposites. Effect of nano-scale on the properties of bio-nanocomposites is discussed. Experimental techniques to determine the mechanical, barrier, thermal, and rheological properties of bio-nanocomposites are also discussed. Lastly, the paper describes mathematical modeling of mechanical and barrier properties of bio-nanocomposites.

Effect of nano-scale on properties

Physics at nano-scale

One of the reasons for unique properties of materials at nano-scale is the difference in physics at nano-scale as compared to that at macro-scale. The fundamental laws of physics remain same. However, their relative importance changes at the nano-scale. Gravitational and inertial forces are volume forces (force is directly proportional to volume). Volume forces are dominant only at the macro-scale and they become almost negligible at the nano-scale. Frictional force is a volume force at macro-scale. However, frictional force becomes surface force (force is directly proportional to surface area) at nano-scale because adhesive forces between atoms and molecules become considerable at nano-scale (Rogers and others 2008). It has also been reported that water exhibits much higher viscosity at nano-scale as compared to that of bulk water (Li and others 2007).

Electrostatic and van der Waals forces are two major forces which become dominant at nano-scale. Electrostatic forces, which can be either repulsive or attractive, are very strong and act at a length scale of 1 to 100 nm. van der Waals forces are attractive and act at distances less than 2 nm. There are three types of van der Waals forces: (i) dipole-dipole force (orientation or Keesom force) occurs between polar molecules such as water, (ii) dipole-induced dipole force (induction of Debye force) arises when a polar molecule polarizes a nearby non-polar molecule, and (iii) induced dipole-induced dipole force (dispersion of London force) acts on all atoms and molecules and is the most important van der Waals force (Rogers and others 2008; Eijkel and van den Berg 2005).

Another difference between macro-scale and nano-scale is the quantum mechanics. Quantum mechanics, instead of classical mechanics, describes the motion and energy at the nano-scale. Quantum mechanics considers the wave-particle duality of electrons. A material can exhibit totally new properties with only a reduction in size because of the wave-particle duality of electrons. For example, gold at macro-scale is yellow, inert, and non-magnetic metal at macro-scale. However, 10 nm particles of gold appear red, exhibit catalytic activity, and are magnetic (Roduner 2006).

Another distinctive effect which becomes dominant at the nano-scale is the Brownian motion. Nano-scale materials undergo a random type of motion, known as the Brownian motion. Brownian motion arises because atoms are in a state of constant motion (Jones 2004).

Higher surface area to volume ratio

Surface area to volume ratio is an indication of the quantity of interfacial region as compared to the bulk region in a composite. The interfacial region controls formation of new structural arrangements on the molecular scale. The surface area (A_s) to volume (V_s) ratio for a spherical particle with radius r is given as (Crosby and Lee 2007):

$$\frac{A_s}{V_s} = \frac{4\pi r^2}{\frac{4}{3}\pi r^3} = \frac{3}{r} \tag{9}$$

Nanoparticles have higher surface area to volume ratio because of their very small size (1-100 nm). Higher surface area to volume ratio results in greater interfacial region, resulting in increased interaction between the polymer chain and the nanoparticles. This increased interaction improves the properties of the bio-nanocomposites. Other than size,

shape is an important factor in determining surface area to volume ratio (Crosby and Lee 2007). The high surface area to volume ratio also makes nanoparticles more reactive as catalysts in chemical reactions.

Confinement effect

For nano-scale particles, a very small volume fraction is sufficient to achieve average distances between particles of the same order of magnitude as the radius of gyration of the macromolecules. Thus, the polymer molecule can be confined between two nano-scale particles. This is known as the confinement effect. Confinement effect reduces the number of conformations of the polymer molecules. Confinement effect is also responsible for reducing gas permeability value by providing tortuous paths for a gas molecule to diffuse through the nanocomposite (Damme 2008).

Experimental techniques to determine properties

Mechanical properties

Tensile testing: Tensile testing is done to measure the mechanical properties of materials. Tensile testing of a bio-nanocomposite film can be done according to ASTM D882-02 or ASTM D638-03. ASTM D638-03 can be used to test materials of thickness up to 14 mm. ASTM D882-02 is the preferred method to do tensile testing of materials in the form of thin sheets of less than 1 mm in thickness. During tensile testing, a rectangular specimen is placed in the grips of movable and stationary fixtures in a testing machine capable of moving the movable fixture at a constant velocity away from the stationary fixture. One such testing machine commonly used for tensile testing of bio-nanocomposite films is Universal Testing

Machine. The sample is pulled apart until it breaks. The applied load (force) and the resulting elongation of the specimen are measured (ASTM Standards 2002; ASTM Standards 2003).

Mechanical properties of a sample are determined from the force-elongation curve (Figure 1). Tensile modulus is the slope of the initial linear portion of stress-strain curve. Tensile modulus (TM), also known as the Young's modulus or the modulus of elasticity, is calculated as:

$$TM = \frac{\frac{\Delta F}{A_i}}{\frac{\Delta L}{L_i}} \tag{10}$$

where ΔF and ΔL are the corresponding changes in force and length during the initial linear deformation. A_i is the initial minimum cross-sectional area of the specimen and L_i is the initial gauge length of the specimen in between the grips of the instrument.

Tensile strength (TS) is a measure of the strength of a material under tensile loading and is calculated as:

$$TS = \frac{F_B}{A_i} \tag{11}$$

where F_B is the force at break point. Percent elongation (%E) at break is the extent to which a material can be stretched before it breaks. It is calculated as:

$$\%E = \frac{L_B}{L_i} \times 100 \tag{12}$$

where L_B is the elongation at break point. Toughness (tensile energy to break) of a sample is the energy required to break the sample and is calculated from the area under the force-

elongation curve. It is a measure of the energy a sample can absorb before it breaks (Bhattacharya and others 2007; ASTM Standards 2002).

Most studies on tensile testing of bio-nanocomposites report TS and %E as a function of the nanoparticle content. Chen and Zhang (2006) reported an increase in tensile strength of soy protein-montmorillonite nanocomposite sheets from 8.77 MPa to 15.43 MPa as the montmorillonite content was increased to 16%. Percent elongation (%E) at break of bio-nanocomposite sheets decreased with increasing montmorillonite (MMT) content. Yu and others (2007) reported similar results for soy protein-rectorite nanocomposite sheets. The tensile strength reached a maximum of 12.92 MPa at rectorite content of 12%. Percent elongation (%E) at break of soy protein-rectorite nanocomposite sheets decreased with increasing rectorite content. Similar results on the tensile testing of bio-nanocomposites based on other biopolymers have been reported (Chang and others 2003; Wang and others 2005; Huang and Netravali 2006; Rao 2007; Zheng and others 2007; Chivrac and others 2008; Tang and others 2008; Rimdusit and others 2008; Roohani and others 2008).

Barrier properties

Water vapor permeability (WVP): WVP is the rate of water vapor transmission through unit area of a flat material of unit thickness induced by unit vapor pressure difference across the material. WVP of a bio-nanocomposite film can be determined according to ASTM E96-05. There are two basic methods: desiccant method and water method. In the desiccant method, test specimen is sealed to the top of a test dish containing a desiccant such as calcium chloride. The desiccant maintains 0% relative humidity inside the test dish. The test assembly is placed in an atmosphere of known relative humidity and temperature.

Periodic weighing of the test dish determines the rate of water vapor transmitted through the specimen into the dish. In the water method, test dish contains distilled water which maintains a relative humidity of 100% inside the dish. Periodic weighing determines the amount of water vapor lost from the test dish to the controlled atmosphere (ASTM Standards 2005a). Water vapor transmission rate (WVTR) is calculated as (ASTM standards 2005a):

$$WVTR = \frac{Q}{t\,A} \tag{13}$$

where Q is the change in weight, t is the time, and A is the area of the mouth of the cup. Water vapor permeability (WVP) is calculated as (ASTM standards 2005a):

$$WVP = \frac{WVTR \times \Delta x}{\Delta p} \tag{14}$$

Where Δx is the thickness of the test specimen and Δp is the vapor pressure difference across the test specimen.

Tang and others (2008) reported WVP of starch-clay bio-nanocomposite films with three different kinds of starches (corn, wheat, and potato starch) and two different types of clay (natural MMT and modified MMT). At the same clay content, WVP of starch-natural MMT films was significantly lower than that of starch-modified MMT films. The results showed that WVP of bio-nanocomposite films decreased significantly with an increase in natural MMT content. WVP of wheat starch film with MMT content of 21% was 70% lower than that of wheat starch film with no MMT (Tang and others 2008). Similar results on the WVP of bio-nanocomposite films based on other biopolymers have been reported (Rhim and others 2006; Tunc and others 2007).

Oxygen permeability (OP): OP is the rate of oxygen transmission through unit area of a flat material of unit thickness induced by unit vapor pressure difference across the material. OP of a bio-nanocomposite film can be determined according to ASTM E3985-05. The specimen is mounted between two chambers under ambient conditions. One chamber is slowly purged by a stream of nitrogen while the other chamber contains oxygen. Oxygen from the other chamber permeates through the test specimen into the chamber with nitrogen. Oxygen is transported by the carrier nitrogen gas to the coulometric detector where it produces an electrical current. The magnitude of electric current is proportional to the amount of oxygen flowing into the detector per unit time (ASTM standards 2005b).

Oxygen transmission rate (OTR) is calculated as (ASTM standards 2005b):

$$OTR = \frac{(V_e - V_0) \times Q_c}{A R_L} \tag{15}$$

where V_e is the steady state voltage level, V_0 is zero voltage level, Q_c is the calibration constant, A is the exposed area of the test specimen, and R_L is the value of load resistance.

Oxygen permeability (OP) is calculated as (ASTM standards 2005b):

$$OP = \frac{OTR \times \Delta x}{p} \tag{16}$$

where Δx is the thickness of the test specimen and p is the partial pressure of oxygen in the oxygen chamber.

Ray and others (2003a) determined OP of bio-nanocomposites based on polylactide and modified MMT. The results showed a 19% decrease in OP as the MMT content increased to 7%.

Thermal properties

The techniques for characterization of thermal properties of bio-nanocomposites include dynamic mechanical analysis (DMA), differential scanning calorimetry (DSC), and thermogravimetric analysis (TGA).

Glass transition temperature: Thermal transitions such as glass transition in a polymer can be described by either free volume (volume available to a molecule for internal movement) theory or relaxation time. As the temperature increases, free volume increases. This enables movements of bonds (bending and stretching) and side chains. This transition, corresponding to bending and stretching of bonds, is known as the γ-transition. β-transition is associated with the movement of side chains and is related to the toughness of the material. With further increase in temperature, free volume further increases and there is a large scale movement of polymer chains. This thermal transition is known as the α-transition or glass transition and the associated temperature is known as the glass transition temperature (T_g). Glass transition temperature is the temperature at which an amorphous solid changes from a relatively brittle (glassy) to a softer (rubbery) material. At the glass transition temperature, there is an abrupt change in properties such as storage modulus, specific heat, and coefficient of expansion (Menard 1999).

Dynamic mechanical analysis (DMA) and differential scanning calorimetry (DSC) are the two main techniques used to determine the glass transition temperature. DMA is a sensitive technique that can be used to detect β and γ-transitions which cannot be detected by methods such as DSC (Menard 1999).

Dynamic mechanical analysis (DMA): Dynamic mechanical analysis (DMA) or dynamic mechanical thermal analysis (DMTA) is method to characterize viscoelastic behavior of a material. This is done by measuring the response of a material to an oscillating force as a function of temperature. The oscillating force applies a sinusoidal stress ($\sigma = \sigma_0 \sin\omega t$) to the sample. This generates a sinusoidal strain. The amplitudes of deformation at the peak of sine wave and lag between stress and strain sine waves are measured. From these measurements, a complex modulus ($E^* = E' + iE''$) is calculated. Storage modulus (E') is defined as the stress in phase with the strain divided by the strain under a sinusoidal deformation. It is a measure of the ability of a material to store energy. Loss modulus (E") is defined as the stress out of phase with the strain divided by strain. It is a measure of the ability of a material to dissipate energy. Ratio of storage modulus and loss modulus is known as the loss tangent ($\tan\delta = E''/E'$). Complex modulus can be used to calculate complex shear modulus (G^*) and complex viscosity (η^*) of a material as (Menard 1999):

$$G^* = \frac{E^*}{2(1+\nu)}$$
$$\eta^* = \frac{G^*}{\omega} \qquad (17)$$

where ν is Poisson's ratio and ω is the frequency of oscillation.

Dynamic mechanical analysis should be conducted in the linear viscoelastic region because the viscoelastic behavior of a material is independent of deformation in this region. This region can be determined by either creep recovery or dynamic strain sweep test. Creep recovery test applies a constant stress to a material and monitors resulting strain with time. Linear viscoelastic region is determined by running a series of creep recovery tests on a

material at different stress values and plotting creep compliance as a function of time. Compliance is the ability of a material to deform and is the inverse of the complex modulus. The compliance curves should overlap in the linear viscoelastic region (Menard 1999). Dynamic strain sweep test applies increasing stress and strain at a constant frequency. The range of strain or stress in which complex modulus or complex viscosity remains constant is the linear viscoelastic region for the material at the given frequency (Bhattacharya and others 2007).

Glass transition temperature (T_g) can be determined by performing a DMA experiment as the temperature is increased at a constant heating rate according to ASTM E1640-04 (ASTM standards 2004) and ASTM D4065-06 (ASTM standards 2006). Samples can be tested under different configurations such as tension, compression, three point bending, single cantilever, dual cantilever, and torsion. The choice of configuration depends on the type of material, modulus of material, and the type of stress the material is exposed to. Flexible materials such as thin films are often tested under tension mode whereas stiff materials such as composites are tested under three point bending mode (Menard 1999).

A typical temperature scan during a DMA experiment is shown in Figure 2. Glass transition temperature can be determined from changes in one of the three parameters: the peak of tan δ curve, peak of E" curve, or onset point for abrupt decrease in E' value. The parameter used to detect the glass transition should always be reported. The part of the region above glass transition and below melting temperature is known as the rubbery plateau region. The storage modulus in the plateau region is proportional to either the number of cross-links or the chain length between entanglements of polymer chains. The length of the plateau

region increases as the molecular weight (M_e) of the entanglement of polymer chains increases. The rubbery plateau is also related to the crystallinity of a material. On further heating, melting point is reached. At the melting point, the polymer chains start sliding past each other and the material flows (Menard 1999).

Glass transition temperature is significantly affected by testing parameters such as frequency of oscillation and heating rate. The most commonly used frequency for a DMA experiment is 1 Hz. However, frequency for performing a DMA experiment should be chosen properly. Frequency scan determines the response of a material over various shear rates. At very low frequencies, materials exhibit Newtonian behavior. Viscosity in this region is dependent on the molecular weight (M_v) as (Menard 1999):

$$\eta = c\left(M_V\right)^a \qquad a = 1 \text{ for } M_V < M_e \quad \text{and} \quad 3.4 \text{ for } M_V < M_e \tag{18}$$

where c is a material constant. As the frequency increases, materials exhibit non-Newtonian behavior. Viscosity in this region can be determined by the power-law model as (Menard 1999):

$$\sigma = K\left(\dot{\gamma}\right)^n \tag{19}$$

where σ is the shear stress, $\dot{\gamma}$ is the shear rate, K is the consistency coefficient, and n is the flow behavior index. As the frequency increases further, materials exhibit Newtonian behavior once again. This region is known as the infinite shear plateau region. The material is not able to show a response to increase in shear rate in this region. This region is usually avoided in DMA because there is no entanglement of the polymer chains. Temperature of

thermal transition shifts to a higher temperature as the test frequency is increased. Ideally, the frequency should be the one that the material is exposed to during the processing under consideration. Another approach is to scan across the frequency range of interest by holding the temperature constant (Menard 1999). Heating rate of a DMA test should be slow enough to allow the entire specimen to reach equilibrium. The most commonly used heating rate for a DMA experiment ranges from 3 to 5 °C/min. Temperature of thermal transition shifts to a higher temperature as the heating rate is increased (ASTM standards 2004).

Most studies on DMA of bio-nanocomposites report temperature dependence of E', E", and tan δ as a function of the nanoparticle content. Shih and others (2007) reported higher E' of bio-nanocomposites based on poly(butylenes succinate) and modified MMTs than that of neat poly(butylenes succinate). Rimdusit and others (2008) reported an increase in glass transition temperature (T_g), corresponding to the peak of tan δ curve, for bio-nanocomposites based on methyl cellulose and MMT. This increase was attributed to restricted segmental motion of biopolymer chains in bio-nanocomposites. Similar results on increase in E' and T_g of bio-nanocomposites based on other biopolymers have been reported (Ray and others 2002; Huang and Netravali 2006; Sasmal and others 2008; Romero and others 2009).

Differential scanning calorimetry (DSC): DSC can also be used to determine glass transition temperature because it can measure the heat capacity of a material. A small quantity (5-20 mg) of sample is placed in a container (sample pan) and an inert material of known heat capacity ($C = mc_p$) is placed in another similar container (reference pan). Both pans are placed inside a calorimeter receptor. A heating element is used to heat the sample pan at a constant rate of temperature increase, set to match the temperature of the reference

pan. The result is a thermogram which gives the rate of heat input versus temperature. There is a sudden increase in the heat input corresponding to the glass transition temperature (ASTM standards 2008a; ASTM standards 2008b). Apart from determining glass transition temperature, DSC can also be used to investigate the melting point and degree of crystallization of bio-nanocomposites.

Most studies on DSC of bio-nanocomposites report temperature dependent heat flow as a function of the nanoparticle content. Rao (2007) reported a slight increase in melting point of bio-nanocomposites based on gelatin and MMT with an increase in MMT content. Hedenavist and others (2006) reported a 5 to 10 °C increase in glass transition temperature of bio-nanocomposite films based on whey protein and MMT with the addition of MMT.

Thermal stability

Thermogravimetric analysis (TGA): Thermal stability of polymeric materials is usually studied by thermogravimetric analysis according to ASTM E1131-08 (ASTM standards 2008c). TGA involves continuous monitoring of weight of a sample (10-20 mg) in a controlled environment of air or nitrogen as a function of temperature and/or time. A heating element provides controlled heating to the sample and an electrobalance continuously measures the weight. During TGA, the weight loss due to the formation of volatile products is plotted against temperature in a thermogram. Weight loss over specific temperature ranges and environments provides a mechanism for compositional analysis of the material. TGA is also used to determine the clay content of a bio-nanocomposite because clay minerals such as MMT are thermally stable up to a temperature of 900 °C.

Chen and Zhang (2006) reported improved thermal stability of bio-nanocomposites based on soy protein isolate and MMT. With an increase in MMT content, weight loss of the bio-nanocomposites was delayed at temperatures higher than 300 °C. The residual weight at 800 °C was also higher for bio-nanocomposites. Similar results on TGA of bio-nanocomposites based on other biopolymers have been reported (Paul and others 2003; Huang and Netravali 2006; Wang and others 2006; Chiou and others 2007; Shih and others 2007; Tunc and others 2007; Rimdusit and others 2008).

Heat deflection temperature (HDT)

Heat deflection temperature (HDT) is the temperature at which a polymer sample deforms under a specified load. It is an indication of heat resistance of a material to an applied load. HDT of a bio-nanocomposite can be determined according to ASTM D648-07. This test method applies to rigid or semi-rigid materials with a thickness of 3 mm or higher. According to ASTM method, a rectangular cross-section specimen is tested in three-point bending by applying a load at its center that provides a maximum stress of 0.455 MPa or 1.82 MPa. The temperature is raised at 2 ± 0.2 °C/min. The temperature at which the test specimen deflects by 0.25 mm is recorded as the HDT (ASTM standards 2007).

Ray and others (2003a) reported HDT of bio-nanocomposites based on polylactide and modified MMT. HDT of the bio-nanocomposites increased from 76 °C to 111 °C as the MMT content increased to 7%. Shelley and others (2001) estimated HDT from the storage modulus curve of DMA. HDT was defined as the temperature at which the storage modulus drops to 25% of its value at room temperature.

Rheological properties

Steady shear measurement: Steady shear measurements for bio-nanocomposites are carried out using either the rotational or capillary rheometers. Rotational rheometers with parallel plate or cone and plate geometry are suitable for low to medium range shear rate (< 10 s^{-1}) measurement whereas capillary rheometers are suitable for high shear rate measurement. Measurements at high shear rate are necessary to describe flow behavior in processes such as injection molding (Bhattacharya and others 2007).

Dynamic shear measurement: Steady shear measurements can change the microstructure and morphology of bio-nanocomposites. Therefore, dynamic shear measurement is used to study the microstructure of bio-nanocomposites by subjecting them to small deformation. Dynamic shear measurements should be conducted in the linear viscoelastic region because the viscoelastic behavior of a material is independent of deformation in this region. Dynamic shear measurements can be performed by creep recovery, stress relaxation, or dynamic oscillatory deformation (Bhattacharya and others 2007).

In the creep tests, a small stress is applied and the increase in strain is measured whereas in stress relaxation, a small strain is applied and the decay of stress is measured. During dynamic oscillatory deformation, a small amplitude sinusoidal strain is applied on a sample and the resulting sinusoidal stress is measured. Parameters obtained by dynamic oscillatory deformation include complex shear modulus ($G^* = G' + iG''$) and complex viscosity (η^*) (Bhattacharya and others 2007).

Extensional measurement: Apart from shear, a polymer is also associated with extensional flow in processes such as film blowing, blow molding, and injection molding. Extensional viscosity is a measure of the resistance of a material subjected to stretching. The two most common methods for measuring extensional properties are the Meissner-type rheometer and continuous drawing of a monofilament. The main parameter obtained by Meissner-type rheometer is the transient extensional viscosity. Continuous drawing method gives a qualitative measure of the extensional rheology (Bhattacharya and others 2007).

Rheological studies of bio-nanocomposites have focused on steady and dynamic shear measurements as a function of nanoparticle concentration. Apparent viscosity and shear thinning properties of bio-nanocomposites are obtained from steady shear measurements. The steady shear measurements also provide information on the effect of shear on the orientation of nanoparticles in bio-nanocomposites. The dynamic shear measurements on polymer-based nanocomposites have shown a transition from liquid-like to solid-like rheological behavior at relatively low loading of nanoparticles. This has been attributed to the formation of a percolated network of the exfoliated layers of nanoparticles within the nanocomposite matrix (Krishnamoorti and Yurekli 2001).

Ray and others (2003b) reported steady shear and dynamic oscillatory shear measurements for suspensions of bio-nanocomposites based on poly(butylenes succinate) and modified MMT. At 120 °C, the steady shear measurements showed that the neat poly(butylenes succinate) exhibited Newtonian behavior whereas bio-nanocomposites exhibited non-Newtonian behavior. High viscosity of bio-nanocomposites at low shear rates was explained by the flow restrictions of biopolymer chains in molten state due to the

presence of nanoparticles. At very high shear rate, the viscosities of the bio-nanocomposites were comparable to that of neat poly(butylenes succinate). This was attributed to strong orientation of clay layers along the direction of flow. A similar result was reported for dynamic oscillatory measurements of these bio-nanocomposites. Similar results on shear thinning behavior of bio-nanocomposites based on other biopolymers have also been reported (Tunc and others 2007).

Chiou and others (2005) studied dynamic rheological behavior of starch-clay suspensions containing different types of starches and MMTs. Samples of natural MMT had the highest G'. There was a two order of magnitude increase in G' with an increase in natural MMT content from 2.5 to 10%. The corresponding increase for other modified MMTs was only one order. This was attributed to the hydrophilic nature of natural MMT as compared to the modified MMTs used in the study. As compared to samples of modified MMTs, samples of natural MMT also had a larger value of G' at temperatures as high as 95 °C. Chivrac and others (2008) reported increased melt viscosity of intercalated bio-nanocomposites based on starch and MMT. This was attributed to the inability of large stacks of MMT layers to orient by shear stress. On the contrary, well exfoliated bio-nanocomposites based on starch and modified MMT did not show increase in melt viscosity.

Mathematical modeling of properties

Modeling of mechanical properties

One of the earliest theories for the determination of modulus of a composite system is based on Einstein's equation for the viscosity of a suspension of rigid spheres at very low concentration and is given as (Ahmed and Jones 1990):

$$E_c = E_m(1 + K_E \phi_f) \tag{20}$$

where E_c is the tensile or elastic modulus of the composite, E_m is the tensile or elastic modulus of the matrix, K_E is Einstein's coefficient, and ϕ_f is the volume fraction of the filler. Value of K_E for spherical filler particles is 2.5. Guth generalized Einstein's equation to account for interaction between fillers and obtained the following equation for spherical fillers (Ahmed and Jones 1990):

$$E_c = E_m\left[1 + K_E \phi_f + 14.1(\phi_f)^2\right] \tag{21}$$

Guth also developed the following equation for non-spherical fillers (Ahmed and Jones 1990):

$$E_c = E_m\left[1 + 0.67\alpha\phi_f + 1.62(\alpha\phi_f)^2\right] \tag{22}$$

where α is the shape factor or the aspect ratio and is given as the ratio of length to thickness of the filler. However, these equations were only valid for low filler concentration. Mooney further modified Einstein's equation for spherical fillers at higher concentration. Mooney's equation for determining the elastic modulus of a composite system can be generalized as (Rao 2007):

$$\ln\frac{E_c}{E_m} = \frac{K_E \phi_f}{1 - \frac{\phi_f}{\phi_m}} \tag{23}$$

where ϕ_m is the maximum packaging efficiency of the filler which is the ratio of the true volume of the filler to the apparent volume occupied by the filler. Value of ϕ_m for close

packed spheres is 0.74. The value of K_E depends on the interaction between filler and the matrix and is related to the aspect ratio ($\alpha = L/t$) through the following equation (Rao 2007):

$$K_E = 2.5\left(\frac{L}{t}\right)^{0.645} \tag{24}$$

where L and t are the length and thickness of the filler particles respectively.

Elastic modulus of a composite can also be predicted by the rule of mixtures (Fornes and Paul 2003):

$$E_c = (1-\phi_f)E_m + \phi_f E_f \tag{25}$$

where E_f is the elastic modulus of the filler. Cox modified the rule of mixtures by introducing a length dependent efficiency factor (η_l) as (Tucker and Liang 1999):

$$E_c = (1-\phi_f)E_m + \eta_l \phi_f E_f \tag{26}$$

where

$$\eta_l = \left[1 - \frac{\tanh\left(\frac{\beta L}{2}\right)}{\left(\frac{\beta L}{2}\right)}\right] \tag{27}$$

and

$$\beta^2 = \frac{H}{\pi r_f^2 E_f}, \quad H = \frac{2\pi G_m}{\ln\left(\frac{R}{r_f}\right)} \tag{28}$$

where r_f is the radius of the filler, R is the radius of the matrix, and G_m is the shear modulus of the matrix. R can be calculated as (Tucker and Liang 1999):

$$\frac{R}{r_f} = \sqrt{\frac{K_R}{\phi_f}} \tag{29}$$

where the value of K_R is 3.628. Verbeek (2003) further modified Cox's model by assuming perfect adhesion between individual components of the composite. Transfer of stress was explained by a shear mechanism. Similar to efficiency factor (η_l), a modulus reduction factor (MRF) was introduced in the equation for modulus as (Verbeek 2003):

$$E_c = (1-\phi_f)E_m + (MRF)\phi_f E_f \tag{30}$$

where

$$MRF = \left[1 - \frac{\tanh(\kappa)}{(\kappa)}\right] \tag{31}$$

and

$$\begin{aligned} \kappa &= \alpha\sqrt{\frac{(1-\chi)^3 G_m}{E_f}\left(\frac{\phi_f}{1-\phi_f}\right)} \\ \chi &= \frac{\phi}{(1-\phi_f)(1-\phi)+\phi} \\ \phi &= \frac{{\phi_f}^2\phi_m}{1-(1-\phi_f)\phi_m} \end{aligned} \tag{32}$$

where ϕ is the porosity of the composite and χ is the modified porosity (porosity relative to polymer phase).

Nielson (1977) proposed a power law equation to predict properties of composites with one continuous phase and one dispersed phase. The power law equation can be given as (Nielson 1977):

$$E_c = (1-\phi_f){E_m}^n + \phi_f {E_f}^n \qquad -1 \le n \le +1 \tag{33}$$

where n is a function of the morphology of the system.

The most commonly used composite theory model for predicting the stiffness of a composite as a function of aspect ratio was given by Halpin-Tsai. The Halpin-Tsai model is expressed as (Fornes and Paul 2003):

$$\frac{E_c}{E_m} = \frac{1 + \xi \eta \phi_f}{1 - \eta \phi_f} \tag{34}$$

where η is given as (Fornes and Paul 2003):

$$\eta = \frac{\frac{E_f}{E_m} - 1}{\frac{E_f}{E_m} + \xi} \tag{35}$$

ξ is a shape parameter and it depends on the shape and aspect ratio of the filler. ξ is given as (Fornes and Paul 2003):

$$\begin{aligned} \xi &= 2\left(\frac{L}{t}\right) \quad \text{for longitudinal modulus} \\ \xi &= 2 \quad \text{for transverse modulus} \end{aligned} \tag{36}$$

When the value of ξ becomes very small ($\xi \rightarrow 0$), the Halpin-Tsai model reduces to the inverse of the rule of mixtures (series model):

$$\frac{1}{E_c} = \frac{\phi_f}{E_f} + \frac{1 - \phi_f}{E_m} \tag{37}$$

When the value of ξ becomes very large ($\xi \rightarrow \infty$), the Halpin-Tsai model reduces to the rule of mixtures (parallel model):

$$E_c = (1 - \phi_f) E_m + \phi_f E_f \tag{38}$$

The series model underestimates (lower bound) the value of modulus whereas the parallel model overestimates (upper bound) the value of modulus. The Halpin-Tsai model leads to results that lie in between these two extreme. The Halpin-Tsai model has been shown to predict the values very well at lower filler concentrations. However, it underestimates the values at higher filler concentrations. Therefore, Lewis and Nielson modified the Halpin-Tsai model to include the maximum volumetric packaging efficiency of the filler. The Modified Halpin-Tsai model is given as (Tucker and Liang 1999):

$$\frac{E_c}{E_m} = \frac{1 + \xi \eta \phi_f}{1 - \varphi \eta \phi_f} \tag{39}$$

where φ can be estimated as (Tucker and Liang 1999):

$$\varphi = 1 + \left(\frac{1 - \phi_m}{\phi_m{}^2} \right) \phi_f$$

$$\varphi = \frac{1}{\phi_f} \left[1 - \exp\left(\frac{-\phi_f}{1 - \frac{\phi_f}{\phi_m}} \right) \right] \tag{40}$$

Another composite theory which has received considerable attention is the Mori-Tanaka average stress theory. Tandon and Weng (1999) derived complete analytical solutions for the elastic moduli of an isotropic matrix filled with aligned spherical inclusions as:

$$\frac{E_l}{E_m} = \frac{A}{A + \phi_f \left(A_1 + 2 \nu_m A_2 \right)} \tag{41}$$

$$\frac{E_t}{E_m} = \frac{2A}{2A + \phi_f \left[-2 \nu_m A_3 + \left(1 - \nu_m \right) A_4 + \left(1 + \nu_m \right) A_5 A \right]} \tag{42}$$

where the subscripts l and t denote longitudinal and transverse elastic moduli respectively, ν_m is the poisson's ratio of the matrix, A, A_1, A_2, A_3, A_4, and A_5 are parameters which depend on the properties of the filler and the matrix. Complete details of these parameters can be found in Tandon and Weng (1999).

Nielson (1966) derived an approximate equation for tensile strength (TS_c) of composites for the cases of no adhesion between the components. The equation was given as (Nielson 1966):

$$TS_c = TS_m\left(1-\phi_f^{2/3}\right)S, \quad S \le 1 \tag{43}$$

where TS_m is the tensile strength of the matrix and S is the stress concentration factor. Verbeek developed a model to predict tensile strength (TS_c) of a composite which was based on the average value of tensile strength of individual components. The model was given as (Verbeek 2003):

$$TS_c = (1-\phi_f)TS_m + K_3\,\tau_f\left(MPF\right) \tag{44}$$

where K_3 is a correction factor, τ_f is the shear strength of the filler, MPF is the matrix performance factor and is given as (Verbeek 2003):

$$\begin{aligned} MPF &= \phi_f\left(\frac{\alpha}{u}\right)\left(\frac{1}{\tanh(u)}-\frac{1}{u}\right) \\ u &= \alpha\left(\frac{G_m\phi_f}{E_f\left(1-\phi_f\right)}\right)^{0.5} \end{aligned} \tag{45}$$

Ray and others (2003b) predicted the storage modulus of bio-nanocomposite films based on poly(butylenes succinate) and modified MMT using the Halpin-Tsai model. There was a good agreement between the predicted values and the experimental values for most of

the bio-nanocomposites. Rao (2007) predicted Young's modulus of bio-nanocomposite films based on gelatin and MMT using the rule of mixtures and Halpin-Tsai model. Predicted values of Young's modulus using the Halpin-Tsai model was in agreement with the experimental data, while the rule of mixtures overestimated the values of Young's modulus.

Modeling of barrier properties

Barrier properties of a packaging material are often described by three common coefficients -- diffusion coefficient, solubility coefficient, and permeability coefficient. The diffusion coefficient (D) describes the movement of permeant molecules through a polymer and is a kinetic property of the polymer-permeant system. The solubility coefficient (S) describes the dissolution of a permeant in a polymer and is a thermodynamic property of the polymer-permeant system. At low concentrations of sorbate, the solubility coefficient is given by Henry's law of solubility as (Hernandez and others 2000):

$$c = Sp \tag{46}$$

where c is the concentration of the sorbate (mol/m^3) and p is the equilibrium vapor pressure of the permeant. The permeability coefficient (P) combines the effects of diffusion and solubility together by incorporating both kinetic and thermodynamic properties of the polymer-permeant system. The permeability coefficient (P) is related to D and S as (Hernandez and others 2000):

$$P = DS \tag{47}$$

This relation holds true when D is independent of concentration and S follows Henry's law. A polymer with good barrier properties has low values of both diffusion and solubility

coefficients. For steady state diffusion across a single sheet of a packaging material, P is given as (Hernandez and others 2000):

$$P = \left(\frac{Q}{At}\right)\frac{\Delta x}{\Delta p} = \frac{F\,\Delta x}{\Delta p} \tag{48}$$

where Q is the total amount of gas that has passed through the material in moles, A is the cross-sectional area in m^2, t is time in s, Δx is the thickness of the material in m, Δp is the pressure difference across the polymer in Pa, and F is the transmission rate. A related term to describe barrier properties of a polymer is permeance (R) which is defined as (Hernandez and others 2000):

$$R = \frac{P}{\Delta x} = \frac{F}{\Delta p} \tag{49}$$

The effective value of P in polymers is affected by the chemical composition of the polymer and permeant, morphology of the polymer, temperature, glass transition temperature of the polymer, and presence of plasticizers and fillers. Change in P with temperature follows an Arrhenius kinetics and the corresponding equation is given as (Hernandez and others 2000):

$$P = P_0 e^{E_p/RT} \tag{50}$$

where E_p is the activation energy (J/mol), R is the gas constant (8.314 J/mol-K), P_0 is a pre-exponential term, and T is temperature in Kelvin.

Bio-nanocomposite polymer films have better barrier properties as compared to homogeneous films even at low solid loadings. Solubility (S_c) of a gas in a bio-nanocomposite can be expressed as (Picard and others 2007):

$$S_c = (1-\phi_f)S_m \tag{51}$$

where S_m is the solubility of the gas in the matrix. Nanoparticles create a tortuous pathway for the diffusion of gas out of the bio-nanocomposite matrix. This increases the effective path length for diffusion of the gas, thus reducing the diffusion coefficient (D_c). The reduced D_c of a gas in the composite can be expressed as (Picard and others 2007):

$$D_c = \frac{D_m}{\tau} \tag{52}$$

where D_m is the diffusion coefficient in the matrix and τ is the tortuosity factor. Thus, P_c of a bio-nanocomposite can be expressed as:

$$\frac{P_c}{P_m} = \frac{(1-\phi_f)}{\tau} \tag{53}$$

where P_m is the permeability of the gas in the matrix.

Tortuosity factor for a membrane containing low solid loadings of spheres is given as (Yang and others 2004):

$$\tau = 1 + \frac{\phi_f}{2} \tag{54}$$

Similarly, for a membrane containing periodically arrayed infinite cylinders oriented perpendicular to the direction of diffusion, τ is given as (Yang and others 2004):

$$\tau = 1 + \phi_f \tag{55}$$

Nielson (1967) considered two-dimensional diffusion through a polymer containing infinitely long plates of rectangular cross-section. The tortuosity factor was given as (Nielson 1967):

$$\tau = 1 + \frac{\alpha \phi_f}{2} \tag{56}$$

where α is the aspect ratio (L/t) and ϕ_f is the volume fraction of the filler. This model assumed that the platelets were fully exfoliated and dispersed along an orientation perpendicular to direction of diffusion.

Bharadwaj (2001) modified the model of Nielson to include the effect of platelet orientation on the tortuosity factor. The tortuosity factor was given as:

$$\tau = 1 + \frac{\alpha \phi_f}{2}\left(\frac{2}{3}\right)\left(S + \frac{1}{2}\right) \tag{57}$$

where S is an order parameter, given by:

$$S = \frac{1}{2}\left\langle 3\cos^2\theta - 1\right\rangle, \quad -0.5 \le S \le 1 \tag{58}$$

Cussler and others (1988) considered rectangular flakes of uniform size dispersed at regular intervals in a composite and proposed the following equation for the tortuosity factor:

$$\tau = 1 + \frac{\alpha^2 \phi_f^{\,2}}{4\left(1-\phi_f\right)} + \frac{\sigma \alpha \phi_f}{2} \tag{59}$$

where

$$\alpha = \frac{L}{t}, \quad \sigma = \frac{s}{t}, \quad \phi_f = \frac{L\,t}{\left(\frac{L}{2} + s\right)\left(t + b\right)} \tag{60}$$

where L is the length of the platelets, t is the thickness of the platelets, s is the spacing between the platelets in the direction perpendicular to diffusion, and b is the spacing between the platelets in the direction of diffusion. The parameters α, σ, and ϕ_f are referred to as the aspect ratio, slit shape, and platelet volume fraction respectively. Cussler and others (1988)

also developed a model for tortuosity factor by assuming that flakes were randomly dispersed. The tortuosity factor was given as:

$$\tau = 1 + \frac{\mu \alpha^2 \phi_f^{\,2}}{4(1-\phi_f)} \tag{61}$$

where μ is a combined geometric factor. The values of μ for randomly dispersed flakes of rectangular and hexagonal cross-sections are 0.5 and 0.075.

Another model for tortuosity factor for a composite containing a random array of impermeable barriers was given by Aris as (Falla and others 1996):

$$\tau = 1 + \frac{\alpha^2 \phi_f^{\,2}}{4(1-\phi_f)} + \frac{\alpha \phi_f}{2\sigma} + \frac{2\alpha\phi_f}{\pi(1-\phi_f)} \ln\left[\frac{\pi\alpha^2\phi_f}{4\sigma(1-\phi_f)}\right] \tag{62}$$

The second term on the right hand side of this equation accounts for the tortuous path which a diffusing molecule must follow. The third term on the right hand side accounts for the constriction of slits between platelets, and the fourth term on the right hand side accounts for the resistance of a diffusing species to pass into and out of the narrow slits.

Falla and others (1996) studied diffusion across membranes containing impermeable flakes using Monte Carlo simulation. They showed the effects of tortuous paths around the flakes, diffusion through slits between the flakes, and reduced transport from entering these slits on the diffusion coefficient. They compared the results with the analytical equation developed by Aris. They found that the increase in tortuosity factor was greater for larger aspect ratio (α) and smaller slit shape (σ).

Most of the above mentioned models for barrier properties have been developed for dilute or semi-dilute and monodispersed systems. These equations are valid for

nanocomposites containing exfoliated structures and become less accurate when different types of structures from exfoliated to intercalated exist together (Picard and others 2007). Lape and others (2004) developed a model to predict the tortuosity factor of a polydispersed system. The tortuosity factor was given as (Lape and others 2004):

$$\tau = \left[1 + \left(\frac{1}{3} \frac{\phi_t}{t \sum_i n_i L_i} \right) \sum_i n_i L_i^2 \right]^2 \tag{63}$$

where ϕ_t is the total volume fraction of fillers and n_i is the number of flakes in the size category i.

Gusev and Lusti (2001) developed a finite element model to determine barrier properties of a nanocomposite in which platelets of nanoparticles were randomly dispersed. Permeability coefficients were calculated on the basis of a linear-response relation between the overall flux and the applied external chemical potential gradient. Numerical results showed that the reduction in permeability was governed by the product of aspect ratio (α) and the volume fraction (ϕ_f) of the platelets. Tortuosity factor was approximated as:

$$\tau = \exp\left[\left(\frac{\alpha \phi_f}{3.47} \right)^{0.71} \right] \tag{64}$$

The results showed that the platelets with aspect ratios greater than 1000 were much more efficient in improving barrier properties of nanocomposites. Their model can be used to identify the role of various morphological imperfections such as incomplete exfoliation, platelet misorientation, and agglomeration in nanocomposites.

Swannack and others (2005) presented two-dimensional (2D) and three-dimensional (3D) Monte Carlo simulation of a polymer-clay nanocomposite system to compute the diffusion coefficients of gas molecules permeating through a nanocomposite film containing oriented platelets. The Monte Carlo method simulated Brownian motion of a small molecule diffusing through a nanocomposite film. 2D and 3D results at low platelet loadings were compared. There were significant differences between the simulation results in 2D and 3D. The 2D simulation predicted a lower value of effective diffusion coefficient than the 3D simulation in most cases. This result is reasonable because 2D simulation is similar to 3D simulation for one infinite platelet dimension. In 3D geometry, platelets are of finite length in both directions perpendicular to the direction of solute transport, thus allowing for more permeation. This resulted in a higher value of effective diffusion coefficient in 3D simulations.

Picard and others (2007) studied polyamide 6-montmorillonite films for a wide range of clay content ranging from 0 to 18% and determined barrier properties for these nanocomposites. Nanocomposites exhibited superior barrier properties to helium, hydrogen, oxygen, and water vapor as compared to that by polyamide film. Different models of monodispersed systems were used to describe the decrease in the permeability value. The model developed by Lape and others (2004), which is based on random distribution of flakes, was found to be the most appropriate model to describe the barrier properties of nanocomposites. All the monodispersed models overestimated the value of the aspect ratio necessary to fit the experimental curves. The model for a polydispersed system given by Lape and others (2004) was also applied to the nanocomposite systems, but the properties of

the nanocomposites were not accurately predicted for high concentrations of montmorillonite. The model developed by Lape and others (2004) was modified to account for the distribution of the platelet thickness and contribution of the surfactant layer to the impermeable phase volume fraction for larger agglomerates. The modified tortuosity factor was given as (Picard and others 2007):

$$\tau = \left[1 + \left(\frac{1}{3} \frac{\phi_t}{\sum_i \left(\frac{n_i L_i}{t_i} \right)} \right) \sum_i n_i \left(\frac{L_i}{t_i} \right)^2 \right]^2 \tag{65}$$

The modified model accurately predicted the measured values of permeability in the range of 0 to 18% montmorillonite content.

Several other studies on the modeling of barrier properties of nanocomposites have been reported (Patel and others 2004; Lu and Mai 2005; Sridhar and others 2006; Xu and others 2006). A few studies on the modeling of barrier properties of bio-nanocomposites using the models discussed above have also been reported (Ray and others 2003a; Ray and others 2003b; Hedenavist and others 2006).

Conclusions

This paper reviews experimental and modeling techniques to determine properties of bio-nanocomposites. Selection of proper technique to determine properties of these bio-nanocomposites is very critical in assessing their performance. Some of the reasons for unique properties of materials at nano-scale include dominance of electrostatic and van der Waals forces over gravitational and frictional forces, wave-particle duality of electrons, dominance of Brownian motion, higher surface area to volume ratio, and confinement effect. Tensile testing is used to measure mechanical properties (tensile modulus, tensile strength, percent elongation of break) of bio-nanocomposites. Water vapor permeability and oxygen permeability are measured to study the effect of nanoparticles on the barrier properties of bio-nanocomposites. Dynamic mechanical analysis, differential scanning calorimetry, and thermogravimetric analysis are used to determine the thermal properties of bio-nanocomposites. Rheological properties are determined by performing steady shear, dynamic shear, or extensional measurement. Mathematical modeling of mechanical and barrier properties of bio-nanocomposites can help in better understanding the mechanism for much improved properties of bio-nanocomposites.

Acknowledgments

Support for the research study undertaken here, resulting in the publication of paper nr FSR-09-36 of the Journal Series of the Dept. of Food, Bioprocessing, and Nutrition Sciences, NCSU, Raleigh, NC 27695-7624 from USDA-NRICGP Grant nr 2008-01503, titled: Development of cross-linked bio-nanocomposite packaging films with enhanced barrier and mechanical properties, is gratefully acknowledged.

The use of trade names in this publication does not imply endorsement by the North Carolina Agricultural Research Service of the products named nor criticism of similar ones not mentioned.

References

Ahmed S, Jones FR. 1990. A review of particulate reinforcement theories for polymer composites. Journal of materials science 25: 4933-4942.

ASTM Standards. 2002. D882-02. Standard test method for tensile properties of thin plastic sheeting. Philadelphia, PA.

ASTM Standards. 2003. D638-03. Standard test method for tensile properties of thin plastics. Philadelphia, PA.

ASTM Standards. 2004. E1640-04. Standard test method for assignment of the glass transition temperature by dynamic mechanical analysis. Philadelphia, PA.

ASTM Standards. 2005a. E96-05. Standard test methods for water vapor transmission of materials. Philadelphia, PA.

ASTM Standards. 2005b. D3985-05. Standard test method for oxygen gas transmission rate through plastic film and sheeting using a coulometric sensor. Philadelphia, PA.

ASTM Standards. 2006. D4065-06. Standard practice for plastics: dynamic mechanical properties: determination and report of procedures. Philadelphia, PA.

ASTM Standards. 2007. D648-07. Standard test method for deflection temperature of plastics under flexural load in the edgewise position. Philadelphia, PA.

ASTM Standards. 2008a. E1356-08. Standard test method for assignment of the glass transition temperatures by differential scanning calorimetry. Philadelphia, PA.

ASTM Standards. 2008b. E3418-08. Standard test method for transition temperatures and enthalpies of fusion and crystallization of polymers by differential scanning calorimetry. Philadelphia, PA.

ASTM Standards. 2008c. E1131-08. Standard test method for compositional analysis by thermogravimetry. Philadelphia, PA.

Bharadwaj RK. 2001. Modeling the barrier properties of polymer-layered silicate nanocomposites. Macromolecules 34: 9189-9192.

Bhattacharya SN, Gupta RK, Kamal MR. 2007. Polymeric nanocomposites: theory and practice. Cincinnati: Hanser Gardner Publications, Inc. 383 p.

Bordes P, Pollet E, Averous L. 2009. Nano-biocomposites: biodegradable polyester/nanoclay systems. Progress in polymer science 34(2): 125-155.

Chang JH, An YU, Sur GS. 2003. Poly(lactic acid) nanocomposites with various organoclays. I. thermomechanical properties, morphology, and gas permeability. Journal of polymer science: part B: polymer physics 41: 94-103.

Chen P, Zhang L. 2006. Interaction and properties of highly exfoliated soy protein/montmorillonite nanocomposites. Biomacromolecules 7: 1700-1706.

Chiou BS, Yee E, Glenn GM, Orts WJ. 2005. Rheology of starch-clay nanocomposites. Carbohydrate polymers 59: 467-475.

Chiou BS, Wood D, Yee E, Imam SH, Glenn GM, Orts WJ. 2007. Extruded starch-nanoclay nanocomposites: effects of glycerol and nanoclay concentration. Polymer engineering and science 47(11): 1898-1904.

Chivrac F, Pollet E, Schmutz M, Averous L. 2008. New approach to elaborate exfoliated starch-based nanobiocomposites. Biomacromolecules 9: 896-900.

Crosby AJ, Lee JY. 2007. Polymer nanocomposites: the “nano” effect on mechanical properties. Polymer reviews 47: 217-229.

Cussler E, Hughes SE, Ward WJ, Aris R. 1988. Barrier membranes. Journal of membrane science 38(2): 161-174.

Damme HV. 2008. Nanocomposites: the end of compromise. In: Brechignac C, Houdy P, Lahmani M, editors. Nanomaterials and Nanochemistry. New York: Springer. p 348-380.

Eijkel JCT, van den Berg A. 2005. Nanofluidics: what is it and what can we expect from it. Microfluidics and nanofluidics 1: 249-267.

Falla WR, Mulski M, Cussler EL. 1996. Estimating diffusion through flake-filled membranes. Journal of membrane science 119 (1): 129-138.

Fornes TD, Paul DR. 2003. Modeling properties of nylon 6/clay nanocomposites using composite theories. Polymer 44(17): 4993-5013.

Gusev AA, Lusti HR. 2001. Rational design of nanocomposites for barrier applications. Advanced materials 13(21): 1641-1643.

Hedenavist MS, Backman A, Gallstedt M, Boyd RH, Gedde UW. 2006. Morphology and diffusion properties of whey/montmorillonite nanocomposites. Composite science and technology 66: 2350-2359.

Hernandez RJ, Selke SEM, Culter JD. 2000. Plastic packaging: properties, processing, applications, and regulations. Cincinnati: Hanser Gardner Publications, Inc. 425 p.

Huang X, Netravali AN. 2006. Characterization of nano-clay reinforced phytagel-modified soy protein concentrate resin. Biomacromolecules 7: 2783-2789.

Jones RAL. 2004. Soft machines: nanotechnology and life. Oxford: Oxford University Press. 229 p.

Krishnamoorti R, Yurekli K. 2001. Rheology of layered silicate nanocomposites. Current opinion in colloid and interface science 6: 464-470.

Kumar P, Sandeep KP, Alavi S, Truong VD. 2009. Biopolymer-based nanocomposites: part I. analytical techniques for structural characterization. Journal of food science (submitted).

Lape NK, Nuxoll EE, Cussler EL. 2004. Polydisperse flakes in barrier films. Journal of membrane science 236(1-2): 29-37.

Li TD, Gao J, Szoszkiewicz R, Landman U, Riedo E. 2007. Structured and viscous water in subnanometer gaps. Physical review B 75(11): 115415.

Lu C, Mai YW. 2005. Influence of aspect ratio on barrier properties of polymer-clay nanocomposites. Physical review letters 95(8): 1-4.

Luo JJ, Daniel IM. 2003. Characterization and modeling of mechanical behavior of polymer/clay nanocomposites. Composite science and technology 63: 1607-1616.

Marsh K, Bugusu B. 2007. Food packaging – roles, materials, and environmental issues. Journal of food science 72(3): R39-R55.

Menard KP. 1999. Dynamic mechanical analysis a practical introduction. Boca Raton: CRC Press. 208 p.

Nicolais L, Narkis M. 1971. Stress-strain behavior of styrene-acrylonitrile/glass bead composites in the glassy region. Polymer engineering and science 11(3): 194-199.

Nielson LE. 1966. Simple theory of stress-strain properties of filler polymers. Journal of applied polymer science 10: 97-103.

Nielson LE. 1967. Models for permeability of filled polymer systems. Journal of macromolecular science, part A 1: 929-942.

Pandey JK, Kumar AP, Misra M, Mohanty AK, Drzal LT, Singh RP. 2005. Recent advances in biodegradable nanocomposites. Journal of nanoscience and nanotechnology 5: 497-526.

Patel NP, Aberg CM, Sanchez AM, Capracotta MD, Martin JD, Spontak RJ. 2004. Morphological, mechanical, and gas-transport characteristics of crosslinked poly(propylene glycol): homopolymers, nanocomposites and blends. Polymer 2004: 5941-5950.

Paul MA, Alexandre M, Degee P, Henrist C, Rulmont A, Dubois P. 2003. New nanocomposite materials based on plasticized poly(L-lactide) and organo-modified montmorillonites: thermal and morphological study. Polymer: 443-450.

Picard E, Vermogen A, Gerard JF, Espuche E. 2007. Barrier properties of nylon6-montmorillonite nanocomposite membranes prepared by melt blending: Influence of the clay content and dispersion rate consequences on modeling. Journal of membrane science 292(1-2): 133-144.

Rao YQ. 2007. Gelatin-clay nanocomposites of improved properties. Polymer 48(18): 5369-5375.

Ray SS, Maiti P, Okamoto M, Yamada K, Ueda K. 2002. New polylactide/layered silicate nanocomposites. 1. Preparation, characterization, and properties. Macromolecules 35: 3104-3110.

Ray SS, Yamada K, Okamoto M, Ueda K. 2003a. New polylactide-layered silicate nanocomposites. 2. Concurrent improvements of materials properties, biodegradability and melt rheology. Polymer 44: 857-866.

Ray SS, Okamoto K, Okamoto M. 2003b. Structure-property relationship in biodegradable poly(butylenes succinate)/layered silicate nanocomposites. Macromolecules 36: 2355-2367.

Ray SS, Bousmina M. 2005. Biodegradable polymers and their layered silicate nanocomposites: In greening the 21st century materials world. Progress in materials science 50: 962-1079.

Rhim JW, Hong SI, Park HM, Ng PKW. 2006. Preparation and characterization of chitosan-based nanocomposite films with antimicrobial activity. Journal of agricultural and food chemistry 54: 5814-5822.

Rhim JW, Ng PKW. 2007. Natural biopolymer-based nanocomposite films for packaging applications. Critical reviews in food science and nutrition 47(4): 411-433.

Rimdusit S, Jingjid S, Damrongsakkul S, Tiptipakorn S, Takeichi T. 2008. Biodegradibility and property characterization of methyl cellulose: effect of nanocompositing and chemical crosslinking. Carbohydrate polymers 72: 444-455.

Roduner E. 2006. Size matters: why nanomaterials are different. Chemical society reviews 35: 583-592.

Rogers B, Pennathur S, Adams J. 2008. Nanotechnology understanding small systems. Boca Raton: CRC Press. 398 p.

Romero RB, Leite CAP, Goncalves MC. 2009. The effect of the solvent on the morphology of cellulose acetate/montmorillonite nanocomposites. Polymer 50: 161-170.

Roohani M, Habibi Y, Belgacem NM, Ebrahim G, Karimi AN, Dufresne A. 2008. Cellulose whiskers reinforced polyvinyl alcohol copolymers nanocomposites. European polymer journal 44: 2489-2498.

Sasmal A, Sahoo D, Nanda R, Nayak P, Nayak P, Nayak PL, Mishra JK, Chang YW, Yoon JY. 2008. Biodegradable nanocomposites from maleated polycaprolactone/soy protein isolate blend with organoclay: preparation, characterization, and properties. Polymer composites 30(6): 708-714.

Shelley JS, Mather PT, DeVries KL. 2001. Reinforcement and environmental degradation of nylon-6/clay nanocomposites. Polymer 42: 5849-5858.

Sheng N, Boyce MC, Parks DM, Rutledge GC, Abes JI, Cohen RE. 2004. Multiscale micromechanical modeling of polymer/clay nanocomposites and the effective clay particle. Polymer 45: 487-506.

Shih YF, Wang TY, Jeng RJ, Wu JY, Teng CC. 2007. Biodegradable nanocomposites based on poly(butylenes succinate)/organoclay Journal of polymers and the environment 15: 151-158.

Sorrentino A, Gorrasi G, Vittoria V. 2007. Potential perspectives of bio-nanocomposites for food packaging applications. Trends in food science and technology 18: 84-95.

Sridhar LN, Gupta RK, Bhardwaj M. 2006. Barrier properties of polymer nanocomposites. Industrial and engineering chemical research 45: 8282-8289.

Swannack C, Cox C, Liakos A, Hirt D. 2005. A three-dimensional simulation of barrier properties of nanocomposite films. Journal of membrane science 263(1-2): 47-56.

Tandon GP, Weng GJ. 1984. Effect of aspect ratio of inclusions on the elastic properties of unidirectional aligned composites. Polymer composites 5(4): 327-333.

Tang X, Alavi S, Herald TJ. 2008. Barrier and mechanical properties of starch-clay nanocomposite films. Cereal chemistry 85(3): 433-439.

Tucker CL, Liang E. 1999. Stiffness predictions for unidirectional short-fiber composites: review and evaluation. Composite science and technology 59: 655-671.

Tunc S, Angellier H, Cahyana Y, Chalier P, Gontard N, Gastaldi E. 2007. Functional properties of wheat gluten/montmorillonite nanocomposite films processed by casting. Journal of membrane science 289: 159-168.

Valavala PK, Odegard GM. 2005. Modeling techniques for determination of mechanical properties of nanocomposites. Reviews on advanced materials science 9: 34-44.

Verbeek CJR. 2003. The influence of interfacial adhesion, particle size and size distribution on the predicted mechanical properties of particulate thermoplastic composites. Materials letters 57: 1919-1924.

Wang SF, Shen L, Zhang WD, Tong YJ. 2005. Preparation and mechanical properties of chitosan/carbon nanotubes composites. Biomacromolecules 6: 3067-3072.

Wang S, Chen L, Tong Y. 2006. Structure-property relationship in chitosan-bsed biopolymer/montmorillonite nanocomposites. Journal of polymer science: part A: polymer chemistry 44: 686-696.

Weon JI, Sue HJ. 2005. Effects of clay orientation and aspect ratio on mechanical behavior of nylon-6 nanocomposite. Polymer 46: 6325-6334.

Wu YP, Jia QX, Yu DS, Zhang LQ. 2004. Modeling young's modulus of rubber-clay nanocomposites using composite theories. Polymer testing 23: 903-909.

Xu B, Zheng Q, Song Y, Shangguan Y. 2006. Calculating barrier properties of polymer/clay nanocomposites: effects of clay layers. Polymer 47: 2904-2910.

Yang C, Smyrl WH, Cussler EL. 2004. Flake alignment in composite coatings. Journal of membrane science 231: 1-12.

Yang KK, Wang XL, Wang YZ. 2007. Progress in nanocomposite of biodegradable polymer. Journal of industrial and engineering chemistry 13(4): 485-500.

Yu J, Cui G, Wei M, Huan J. 2007. Facile exfoliation of rectorite nanoplatelets in soy protein matrix and reinforced bio-nanocomposites thereof. Journal of applied polymer science 104: 3367-3377.

Yung KC, Wang J, Yue TM. 2006. Modeling Young's modulus of a polymer –layered silicate nanocomposites using a modified Halpin-Tsai micromechanical model. Journal of reinforced plastics and composites 25(8): 847-861.

Zhao R, Torley P, Halley PJ. 2008. Emerging biodegradable materials: starch- and protein-based bio-nanocomposites. Journal of materials science 43: 3058-3071.

Zheng H, Ai F, Wei M, Huang J, Chang PR. 2007. Thermoplastic soy protein nanocomposites reinforced by carbon nanotubes. Macromolecular materials and engineering 292: 780-788.

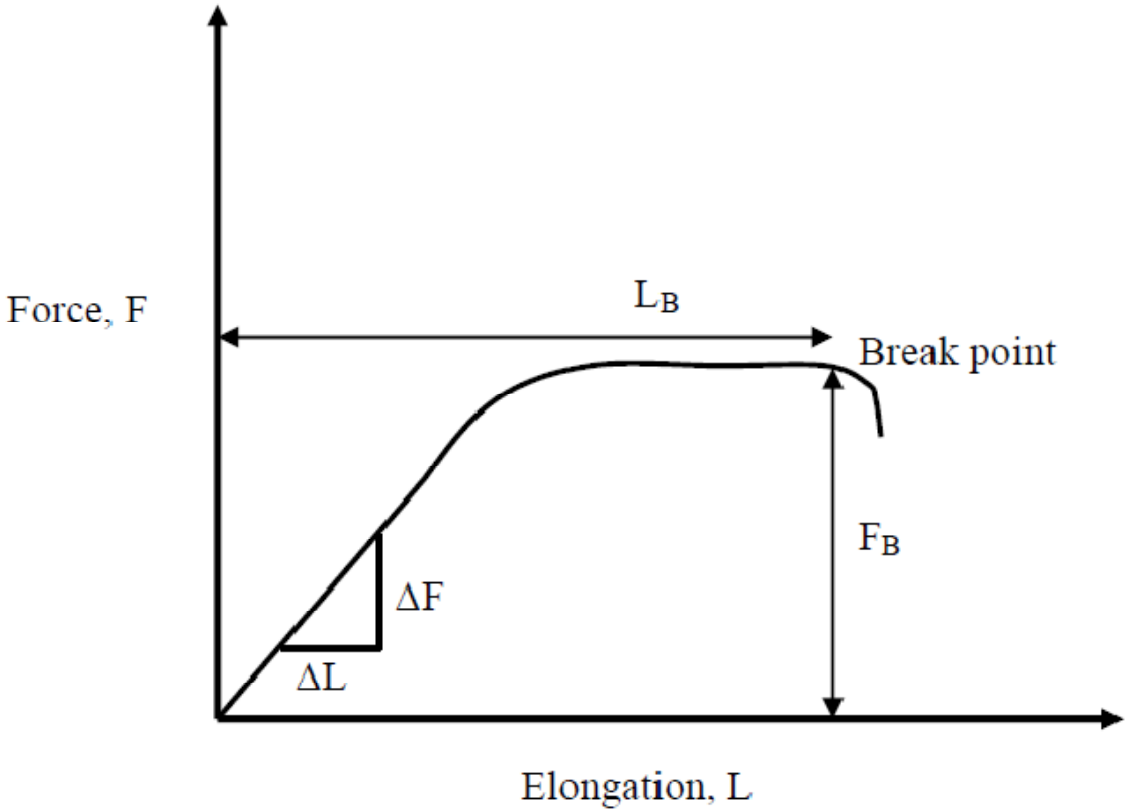

Figure 1 – A typical force-elongation curve during a tensile testing experiment.

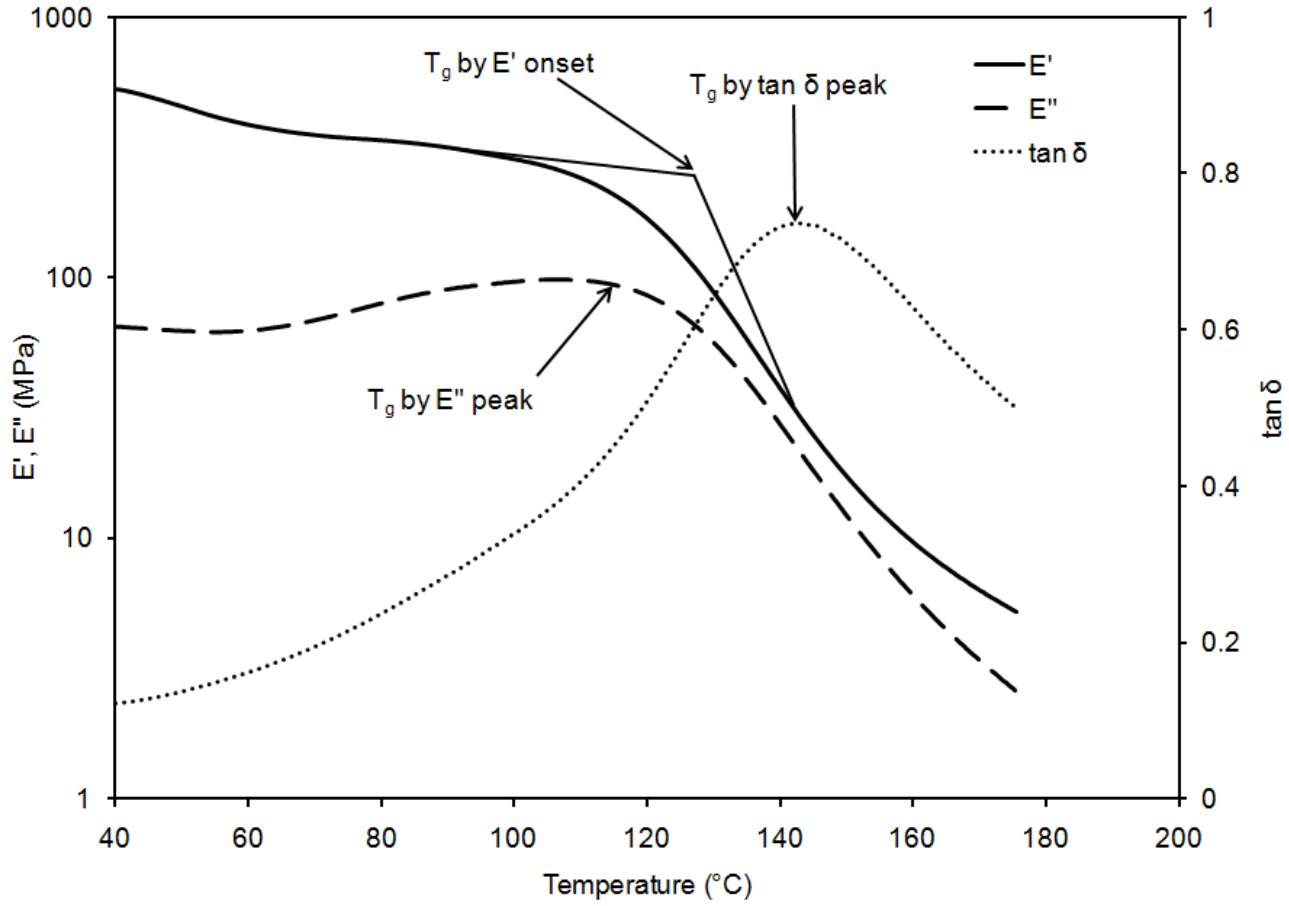

Figure 2 – A typical temperature scan from a DMA experiment.

Chapter 6

MANUSCRIPT IV

Preparation and Characterization of Bio-nanocomposite Films Based on Soy Protein Isolate and Montmorillonite Using Melt Extrusion

P. KUMAR[1], K.P. SANDEEP[1], S. ALAVI[2], V.D. TRUONG[3], AND R.E. GORGA[4]

(1) Department of Food, Bioprocessing, and Nutrition Sciences, North Carolina State University, Raleigh, NC
(2) Department of Grain Science and Industry, Kansas State University, Manhattan, KS
(3) U.S. Dept. of Agriculture, Agricultural Research Service, South Atlantic Area, Food Science Research Unit, Raleigh, NC
(4) Department of Textile Engineering, Chemistry and Science, North Carolina State University, Raleigh, NC

Please address all correspondence to:

K.P. Sandeep
129 Schaub Hall, Box 7624
North Carolina State University
Raleigh, NC 27695
Phone: 919-515-2957
Fax: 919-515-7124
E-mail: kp_sandeep@ncsu.edu

Paper nr FSR-09-37 of the Journal Series of the Department of Food, Bioprocessing, and Nutrition Sciences, North Carolina State University, Raleigh, NC 27695-7624

Abstract

The non-biodegradable and non-renewable nature of plastic packaging has led to a renewed interest in packaging materials based on bio-nanocomposites (biopolymer matrix reinforced with nanoparticles such as layered silicates). Bio-nanocomposite films based on soy protein isolate (SPI) and montmorillonite (MMT) were prepared using melt extrusion. Effects of the pH of film forming solution, MMT content, and extrusion processing parameters (screw speed and barrel temperature distribution) on the structure and properties of SPI-MMT bio-nanocomposite films were investigated. X-ray diffraction (XRD), transmission electron microscopy (TEM), and scanning electron microscopy (SEM) were used for structural characterization of the films. Properties of the films were determined by tensile testing, dynamic mechanical analysis (DMA), thermogravimetric analysis (TGA), and water vapor barrier measurement. The arrangement of MMT in the soy protein matrix ranged from exfoliated at lower MMT content (5%) to intercalated at higher MMT content (15%). There was a significant improvement in mechanical (tensile strength and percent elongation at break) and dynamic mechanical properties (glass transition temperature and storage modulus), thermal stability, and water vapor permeability of the films with the addition of MMT. The results presented in this study show the feasibility of using bio-nanocomposite technology to improve the properties of biopolymer films based on SPI.

Keywords: bio-nanocomposite films, soy protein isolate, montmorillonite, extrusion, structural characterization, mechanical properties, water vapor permeability

Introduction

The non-degradable and non-renewable nature of plastic packaging has led to a renewed interest in packaging materials based on biopolymers derived from renewable sources. The use of biopolymer-based packaging materials can solve the waste disposal problem to a certain extent. Such biopolymers include those derived from naturally occurring proteins, cellulose, starches, and other polysaccharides and those synthesized chemically from naturally derived monomers such as lactic acid. Commercialization of biopolymer-based packaging materials has already started. Natureworks, LLC (Minnetonka, MN) manufactures polylactide from corn sugar. The polymer can be hydrolyzed back to lactic acid. Wal-Mart stores, Inc. is already using polylactide to package fresh-cut produce (Marsh and Bugusu 2007). Currently, bio-based packaging materials constitutes about 1-2% of the food packaging market even though food packaging accounts for about 40 percent of the $460 billion global packaging industry (Jahangir and Leber 2007). According to a report, bio-based packaging materials will grow at an annual rate of 17.3% between 2007 and 2012. The report predicts that the current capacity of bio-based packaging materials will increase from about 0.185 million tons annually to 0.545 million tons by 2012 (Schlechter 2007).

The increased interest in bio-based packaging has resulted in the development of protein-based films from soy protein, whey protein, casein, collagen, corn zein, gelatin, and wheat gluten (Cuq and others 1998). Among all the protein sources, soy proteins have attracted attention as a potential source for bio-based packaging materials because it has excellent film forming properties (Brandenburg and others 1993; Gennadios and others 1993;

Zhang and others 2001; Park and others 2001; Mauri and Anon 2006; Kurose and others 2007). Soy protein isolate (SPI) is a commercial form of soy protein that contains more than 90% protein. Soy proteins are classified as 2S, 7S, 11S, and 15S based on their sedimentation rate in fractional ultracentrifugation. Larger Svedberg (S) number indicates a larger protein (Hernandez-Izquierdo and Krochta 2008). 7S (β-conglycinin) and 11S (glycinin) fractions of soy proteins, constituting about 90% of total protein, have the ability of polymerization, resulting in the formation of films. β-conglycinin (molecular weight of 140-170 kDa) consists of three types of subunits with molecular weights of 58, 57, and 42 kDa. Glycinin (molecular weight of 340-375 kDa) consists of 6 acidic (35 kDa) and 6 basic (35 kDa) polypeptide chains which are linked together by disulfide bonds (Petruccelli and Anon 1995).

Film formation from globular proteins such as soy protein is a two-stage process. In the first stage (heating phase), protein is denatured and a few disulfide bonds are cleaved. This exposes the sulfhydryl and hydrophobic groups. During the second stage (drying phase), a new network is formed by disulfide linkage, hydrogen bonds, and hydrophobic interactions (Lefevre and others 2005). pH of the film forming solution is one of the important variables in film formation because it influences the denaturation of proteins. Film formation from SPI has been achieved within pH ranges of 1 to 3 and 6 to 12. Film formation is inhibited near the isoelectric point (pH 4.5) of soy protein due to coagulation of protein (Mauri and Anon 2006).

SPI-based packaging films cannot meet the requirements of a cost-effective film with mechanical and barrier properties similar to those of plastics. Mechanical properties of interest in food packaging are tensile modulus (TM), tensile strength (TS), and percent

elongation (%E) at break. Tensile modulus is a measure of stiffness of a material. Tensile strength is the maximum tensile stress a film can sustain whereas %E is an indication of flexibility of a film. Barrier properties of interest are water vapor permeability (WVP) and oxygen permeability (OP). Biopolymers made from SPI alone are extremely brittle. Plasticizers such as glycerol and polyethylene glycol impart flexibility to SPI-based biopolymer films. However, the use of plasticizers leads to significant decrease in tensile strength (TS) of the films (Wang and others 1996). Soy protein-based films have been reported to have oxygen permeability (OP) similar to that of plastic films (Brandenburg and others 1993). However, they have higher water vapor permeability (WVP) as compared to plastic films due to the hydrophilic nature of proteins. Therefore, research has been geared to develop techniques to improve mechanical and water vapor barrier properties of soy protein-based packaging materials.

Recently, a new class of materials represented by bio-nanocomposites (biopolymer matrix including proteins reinforced with nanoparticles such as montmorillonite) has proven to be a promising option in improving mechanical and barrier properties of biopolymers. The bio-nanocomposites consist of a biopolymer matrix reinforced with particles (nanoparticles) having at least one dimension in the nanometer range (1-100 nm) and exhibit much improved properties due to high aspect ratio and high surface area of nanoparticles (Ray and Bousmina 2005; Rhim and Ng 2007; Zhao and others 2008). The most common class of materials used as nanoparticles are layered clay minerals such as montmorillonite (MMT), hectorite, sapnotite, and laponite. These clay minerals have been proven to be very effective due to their unique structure and properties. These clay minerals belong to the general family of 2:1

layered silicates indicating that they have 2 tetrahedral sheets sandwiching a central octahedral sheet (Zeng and others 2005). MMT has a very high elastic modulus (178 GPa) as compared to most biopolymers. The high value of elastic modulus enables MMT to improve mechanical properties of biopolymers by carrying a significant portion of the applied stress (Fornes and Paul 2003).

There are four possible arrangements of layered clays dispersed in a polymer matrix – phase separated or immiscible (microcomposite), intercalated, exfoliated, and disordered intercalated (partially exfoliated). In an immiscible arrangement, platelets of layered clays exist as tactoids (stack of platelets) and the polymer encapsulates these tactoids. Intercalation occurs when a monolayer of extended polymer chains penetrates into the galleries (gap between layers of clay) of the layered silicates. Intercalation results in finite expansion (2-3 nm) of the silicate layers. However, these silicate layers remain parallel to each other. Extensive penetration of polymer chains into the galleries of layered silicate leads to exfoliation or delamination of silicate layers. Clay platelets are separated by 10 nm or more during exfoliation. An exfoliated nanocomposite consists of nanoparticles distributed homogeneously throughout the polymer matrix (Dennis and others 2001; Zeng and others 2005).

Bio-nanocomposites can be obtained by several methods which include in-situ polymerization, solution exfoliation, and melt intercalation. In the in-situ polymerization method, monomers are intercalated into layered clays and subsequently polymerized via heat, radiation, or catalyst. In solution exfoliation, layered clays are exfoliated into single platelets using a solvent and the polymer is adsorbed onto the platelets by mixing in the clay

suspension. In melt intercalation, layered clays are mixed with the polymer matrix in molten state (Zeng and others 2005).

Flexible bio-nanocomposites with improved properties can be obtained by reinforcing the SPI-plasticizer system with suitable filler materials such as MMT. Very few studies on SPI-MMT bio-nanocomposites have been reported in literature. Dean and Yu (2005) developed an effective method to exfoliate MMT lamellae in water using ultrasonic and prepared MMT-reinforced soy protein films plasticized by a mixture of water and glycerol. The ultrasonic treated bio-nanocomposite material exhibited an exfoliated structure and an improvement in tensile modulus and tensile strength of 84% and 47% respectively. However, water barrier properties of the bio-nanocomposites were not reported. Rhim and others (2005) prepared and studied the mechanical and water barrier properties of composite films of SPI with various clay minerals. The tensile strength of SPI-layered clay films increased by as much as 30% whereas the water vapor permeability decreased by 52%. Chen and Zhang (2006) prepared highly exfoliated and intercalated SPI-MMT nanocomposites by using the solution exfoliation method in a neutral aqueous medium and investigated the correlation between the microstructure and mechanical properties. Electrostatic attraction and hydrogen bonding at the interfaces of soy protein and MMT lead to good dispersion of MMT layers in the protein matrix. Highly exfoliated structure with 1-2 nm MMT layers dispersed in protein matrix resulted when the MMT content was less than 12% (w/w). Intercalated structure was predominant when the MMT content was more than 12%. The results also showed improvement in tensile strength (increase from 8.77 to 15.43 MPa) and thermal stability of SPI-MMT bio-nanocomposites.

Melt intercalation in an extruder is one of the most promising techniques for preparing bio-nanocomposites because of its ease and versatility. Layered clays (6-13 μm) are sheared and peeled apart into platelets (~1-10 nm) due to high shear mixing inside the extruder. These platelets are then mixed with the biopolymer matrix in molten state to achieve exfoliation (Dennis and others 2001). Extrusion is one of the most important processing techniques to produce plastics on a commercial scale. Therefore, bio-nanocomposite films using extrusion will increase the potential for commercialization of these films. Extrusion processing parameters such as screw speed and barrel temperature distribution have an important influence on the structure and properties of nanocomposites. Increase in screw speed has been shown to result in better dispersion of nanoparticles in the polymer matrix. This behavior, observed for nanocomposites based on polyethylene (PE) and polypropylene (PP), is explained by breaking of agglomerates into smaller aggregates at high shear rates, corresponding to higher screw speeds. There are contradictory results in literature for the effect of barrel temperature distribution. Better dispersion of nanoparticles in PE at higher temperature has been reported. However, better dispersion in PP was observed at lower temperature (Lertwimolnun and Vergnes 2007).

The objective of this study was to prepare and characterize bio-nanocomposite films based on SPI and MMT using melt extrusion. Effects of the pH of film forming solution, MMT content, and extrusion processing parameters (screw speed and barrel temperature distribution) on the structure and properties (mechanical, dynamic mechanical, thermal stability, and water vapor permeability) of SPI-MMT bio-nanocomposite films were investigated.

Materials and Methods

Materials

Soy protein isolate (Supro 760) with a protein content of 92.5 % (dry basis) was obtained from Protein Technologies International (St. Louis, MO). Natural montmorillonite (Cloisite Na^+) was obtained from Southern Clay Products (Austin, TX). Cloisite Na^+ has a moisture content of 4-9% and a density of 2.86 g/cm^3. Glycerol, used as a plasticizer, was obtained from Fisher Scientific (Pittsburg, PA). Glycerol was chosen as the plasticizer because it is nontoxic whereas other potential polyhydric alcohols such as propylene glycol and ethylene glycol are toxic and hazardous (Wang and others 1996).

Preparation of SPI-MMT nanocomposites

Process flow diagram for the preparation and characterization of soy protein isolate (SPI)-montmorillonite (MMT) bio-nanocomposite films is shown in Figure 1. The formulation consisted of SPI (70-85%, dry basis), glycerol (15%, dry basis), and MMT (0-15%, dry basis). The ingredients were mixed and left at room temperature for 2 hours for hydration. The mixture was subsequently extruded in a twin-screw co-rotating extruder (ZSK 26, Coperion Corp., Ramsey, NJ). The extruder had a 5 head barrel configuration with a screw diameter of 25 mm and length to diameter ratio (L/D) of 20. The extrudate was dried in an oven at 50 °C for 48 hrs. The dried extrudate was ground in a grinder (MicroMill, Bel-Art Products, Pequannock, NJ) for further testing and film casting.

Film casting

Bio-nanocomposite powders (4% w/v) and deionized water were mixed for 30 min at room temperature. pH of the suspension was adjusted to the desired value by adding either 1

M NaOH or 1 M HCL solution. The suspension was heated to 95 °C and held at that temperature for 20 min with continuous stirring. Subsequently, the solution was cooled to 65 °C and 25 ml of the suspension was poured in 10 cm diameter petri dishes for casting nanocomposite films. The cast petri dishes were dried at ambient conditions for 48 hours. The dried films were peeled off the petri dish and pre-conditioned before further testing.

Structural characterization of SPI-MMT films

X-ray diffraction (XRD)

X-ray diffraction studies of bio-nanocomposite powders were performed with a diffraction unit (MS Philips XLF ATPS XRD 100, Omni Scientific Instruments, Biloxi, MS) operating at 35 kV and 25 mA. The radiation was generated from a Cu-Kα ($\lambda = 0.154$ nm) source. The diffraction data was collected from 2θ values of 2.5 to 10° with a step size of 0.01°, where θ is the angle of incidence of the X-ray beam on the sample.

Transmission electron microscopy (TEM)

The structure and morphology of bio-nanocomposite powders were visualized by a transmission electron microscope (Hitachi HF2000, Hitachi High-Technologies Europe GmbH, Krefeld, Germany) operating at 200 kV. Samples of bio-nanocomposite powders were prepared by suspending the powders in methanol. The suspension was sonicated for 5 min in an ultrasonic bath (Branson 1510, Branson Ultrasonics Co., Danbury, CT). A drop of the suspension was put on a fine-mesh carbon-coated TEM support grid (C-flat™, Protochips Inc., Raleigh, NC). After drying in air, the nanocomposite powder remained attached to the grid and was viewed under the transmission electron microscope.

Scanning electron microscopy (SEM)

The morphology of the fracture surface (cross-sectional surface) of the bio-nanocomposite films were visualized using a field emission scanning electron microscope (JEOL 6400F, Japan Electron Optics Ltd., Tokyo, Japan) operating at 5 kV. Small pieces (0.5 × 0.5 cm) of bio-nanocomposite films were frozen in liquid nitrogen, cut using a sharp razor blade, and mounted on specimen stubs with 2 sided carbon tape. The fracture surfaces of the films were sputter-coated with a thin layer (~8-10 nm) of gold-palladium (Au-Pd) using a sputter-coater (Hummer II, Anatech Ltd., Union City, CA). After coating, the samples were viewed under the scanning electron microscope.

Measurement of properties of SPI-MMT films

Film thickness

Thickness of the films was measured at five different randomly selected locations using a digital micrometer (CO 030025, Marathon Watch Company Ltd., Ontario, Canada). The average value of the film thickness was used in determining mechanical properties, dynamic mechanical properties, and water vapor permeability.

Mechanical properties

Tensile strength (TS) and percent elongation (%E) at break of the bio-nanocomposite films were determined by tensile testing using a Universal Testing Machine (model 5565, Instron, Corp., Canton, MA) equipped with a 5 kN static load cell according to the ASTM standard D882-02 (ASTM Standards 2002). The length and width of the film samples were 5 cm and 2.5 cm respectively. The initial grid separation was set at 2.5 cm and the cross-head speed was 50 cm/min. Stress vs. strain curves were plotted. Tensile strength was calculated

by dividing peak load by initial specimen cross-sectional area. Percent elongation at break was calculated as the percentage change in length of the specimen between the grips. Three specimens of each sample were evaluated.

Dynamic mechanical properties

The dynamic mechanical properties of bio-nanocomposite films were determined using a dynamic mechanical analyzer (Q800, TA Instruments, New Castle, DE). Dynamic mechanical analysis (DMA) was performed in tension mode at a frequency of 1 Hz and an amplitude of 15 μm. The length and width of the film samples were 4 cm and 0.6 cm respectively. The samples were heated from 40 °C to 200 °C at a heating rate of 5 °C/min. The storage modulus (E'), loss modulus (E''), and loss tangent (tan δ = E''/ E') were recorded as a function of temperature. Glass transition temperature (T_g) was determined as the temperature at which tan δ attained its peak value.

Thermal stability

The thermal stability of bio-nanocomposite films were investigated using a thermogravimetric analyzer (Pyris 1 TGA, Perkin Elmer, Shelton, CT). The mass of the sample used varied from 10 to 12 mg. Thermogravimetric analysis (TGA) was carried out separately under nitrogen and air flow. The temperature of the sample was increased from room temperature to 900 °C at a heating rate of 20 °C/min. Weight loss of the sample was measured as a function of temperature. Three parameters were determined from the TGA data: the temperature at 10% weight loss, the temperature at 50% weight loss, and the yield of charred residue at 850 °C.

Water vapor permeability

Water vapor permeability (WVP) of the bio-nanocomposite films was determined according to ASTM E96-05 (ASTM Standards 2005). The sample film was cut into a circle of 8.75 cm diameter. The sample was placed on a test dish (8.2 cm in diameter and 1.9 cm in depth) filled with 50 ml deionized water to expose the films to 100% relative humidity. The test dishes were sealed and a turntable carrying 8 test dishes was rotated uniformly to ensure that all dishes were exposed to the same average ambient conditions during the test. The setup was subjected to a temperature and relative humidity of 22 °C and 65% respectively. The test dishes were allowed to equilibrate for two hours before taking the initial weight. The final weight was taken after a 24 hour interval. Water vapor transmission rate (WVTR) was calculated as (ASTM Standards 2005):

$$\mathrm{WVTR} = \frac{\mathrm{G}}{\mathrm{t\,A}} \tag{66}$$

where G is the change in weight (g), t is the time (hr), and A is the area of the mouth of the test dish (m^2). Water vapor permeability (WVP) was calculated as (ASTM standards 2005):

$$\mathrm{WVP} = \frac{\mathrm{WVTR} \times \mathrm{L}}{\Delta \mathrm{P}} \tag{67}$$

where L is the thickness of the test specimen (mm) and ΔP is the partial pressure difference of water vapor across the film. WVP of two specimens for each sample was calculated and reported.

Design of experiments and statistical analysis

Five different levels (3.0, 6.0, 7.5, 9.0, and 10.5) of pH at MMT contents of 0 and 5% were tested to optimize the pH of film forming solution. Screw speed and barrel temperature

distribution used for these experiments were 100 rpm and T_1 (70, 90, 100, 110, and 90 °C) respectively. Subsequent experiments were carried out with the optimized pH value. Four different levels (0, 5, 10, and 15%) of MMT content were used to study the effect of MMT content on the properties of bio-nanocomposite films. Screw speed and barrel temperature distribution used to study the effect of MMT content were 100 rpm and T_1 (70, 90, 100, 110, and 90 °C) respectively. Two levels of screw speed (N_1: 50 rpm and N_2: 100 rpm) and three levels of barrel temperature distribution [T_1: (70, 90, 100, 110, and 90 °C); T_2: (80, 100, 110, 120, and 110 °C); T_3: (90, 110, 120, 130, and 120 °C)] were tested to study the effect of extrusion processing parameters on the properties of bio-nanocomposite films. A sample associated with a screw speed of N_x and barrel temperature distribution of T_y was coded as N_xT_y.

All experiments were performed in duplicate. Statistical analysis was performed using Minitab statistical software (Minitab Inc., State College, PA). Data were analyzed by either general linear model (GLM) or one-way analysis of variance (ANOVA). Differences at $P < 0.05$ were considered to be significant. Pair-wise comparison of all means was performed using the Fisher's least significant difference (LSD) method.

Results and Discussion

Effect of pH of film forming solutions on the properties of films

In the preliminary study, the effect of pH of film forming solutions on the mechanical and dynamic mechanical properties was investigated. There was no film formation at a pH value of 6.0. This pH was near the isoelectric point of soy protein isolate. It has been reported earlier that film formation does not take place near the isoelectric point of proteins (Brandenburg and others 1993, Gennadios and others 1993). Films formed at pH values of 3.0 and 10.5 were too brittle to be tested. Effect of pH and MMT content on mechanical properties (TS and %E) of SPI-MMT films is shown in Table 1. Effect of MMT content on TS was significant ($P = 0.001$) whereas the effect of pH on TS was not significant ($P = 0.061$). Films with MMT content of 5% had significantly higher TS than those with MMT content of 0%. Effect of MMT content and pH on %E was significant ($P < 0.05$). Analysis of variance using the general linear model showed that there was also a significant ($P < 0.05$) interaction effect of MMT content and pH on %E. At MMT content of 5%, films with higher %E were obtained at pH 9.0 as compared to those at pH 7.5.

Effect of temperature on tan δ of SPI-MMT films at pH values of 7.5 and 9.0 is shown in Figure 2. Glass transition temperature (T_g), corresponding to the peak of the tan δ curve, was significantly ($P < 0.05$) affected by MMT content and pH. At a MMT content of 0%, T_g increased from to 112.1 ± 2.3 °C to 119.7 ± 1.9 °C as the pH increased from 7.5 to 9.0. This might be attributed to increase in cross-linking of the films at pH 9 than those at pH 7.5. At a pH value of 9, T_g increased from to 119.7 ± 1.9 °C to 142.8 ± 2.0 °C as the MMT content increased from 0% to 5%. This is attributed to a reduction in the mobility of

biopolymer chains of SPI in bio-nanocomposite films due to the interaction of SPI with MMT.

Effect of temperature on storage modulus (E') of SPI-MMT films at pH values of 7.5 and 9.0 is shown in Figure 3. Over the entire temperature range, E' of the films at pH 9.0 was higher than those at pH 7.5. There was an increase of 175.3% in E' of the films at 40 °C as the MMT content increased to 5% and pH changed from 7.5 to 9.0. This significant increase in E' of films is attributed to the reduced mobility of biopolymer chains of SPI in bio-nanocomposite films. The increase in E' is also in agreement with the results of TS where TS increased with an increase in pH and MMT content. The films with MMT content of 5% had higher onset temperature of E' decay and E' reached a plateau at higher temperatures.

Based on the preliminary results, pH value of 9.0 was chosen as the optimum pH to obtain SPI-MMT films with desired mechanical and dynamic mechanical properties. pH value of 9.0 was used for the remaining part of the study.

Effect of MMT content on the structure of powders/films

XRD patterns of MMT and SPI-MMT bio-nanocomposite powders with 0%, 5%, 10%, and 15% MMT contents are shown in Figure 4. Powders of MMT showed a diffraction peak at a 2θ angle of 7.3°. Interlayer distance (d or d-spacing) between clay layers can be estimated from Bragg's equation (Kasai and Kakudo 2005):

$$d = \frac{\lambda}{2\sin\left(\frac{\pi\theta}{180}\right)} \tag{68}$$

where λ is the wavelength of X-ray beam. The d-spacing of MMT corresponding to the diffraction peak was calculated to be 1.20 nm using Bragg's equation. This is in close

agreement with the d-spacing value of 1.17 nm provided by the supplier. There was no diffraction peak in the 2θ range of 2.5° to 10° for the bio-nanocomposites at all MMT contents. Due to the limitation of the XRD instrument, diffraction patterns below a 2θ value of 2.5° could not be observed. Absence of diffraction peaks for SPI-MMT bio-nanocomposites suggests that MMT layers have a d-spacing of at least 3.53 nm (corresponding to a 2θ value of 2.5°) in SPI-MMT bio-nanocomposites with MMT content of up to 15%. Chen and Zhang (2006) reported a d-spacing value of 3 nm for SPI-MMT bio-nanocomposite powder prepared by a solution intercalation method at a MMT content of 16%. Higher d-spacing value reported in this study might have been achieved because of high shear mixing inside the twin-screw extruder. Morgan and Gilman (2003) showed that XRD by itself is insufficient to characterize the structure of nanocomposites for exfoliated and disordered intercalated arrangements. Therefore, XRD studies should always be complemented with microscopy techniques such as TEM or SEM.

TEM images of SPI-MMT bio-nanocomposite powders with 0%, 5%, 10%, and 15% MMT contents are shown in Figure 5. The dark lines in the TEM images correspond to MMT platelets and the gap between two adjacent lines is the d-spacing. It can be seen from Figure 5b that the MMT layers are exfoliated in bio-nanocomposites with MMT content of 5%. As MMT content increased to 10%, the arrangement of MMT changed from exfoliated to disordered intercalated (partially exfoliated). At MMT content of 15%, MMT layers are intercalated in bio-nanocomposites (Figure 5d). However, d-spacing values, which ranged from 5 to 10 nm, were higher than the detection limit of XRD analysis (3.53 nm). This explains the absence of diffraction peaks for these bio-nanocomposites in the XRD analysis.

SEM images of the fracture surface (cross-sectional surface) of SPI-MMT bio-nanocomposite films with 0%, 5%, 10%, and 15% MMT contents are shown in Figure 6. The white strands in the SEM images correspond to MMT platelets. At a MMT content of 5%, MMT platelets were well dispersed in the bio-nanocomposite film (Figure 6b). This suggests exfoliation of MMT in the bio-nanocomposite film at a MMT content of 5%. The fracture surface of the films became rougher as the MMT content increased. Some aggregates of MMT were found at a MMT content of 15% (Figure 6d).

Based on the XRD, TEM, and SEM results, it can be concluded that extrusion of SPI and MMT resulted in bio-nanocomposites with exfoliated structures at lower MMT content (5%) and intercalated structures at higher MMT content (15%).

Effect of MMT content on the properties of films

Mechanical properties (TS and %E) of SPI-MMT films with 0%, 5%, 10%, and 15% MMT contents were compared with those of other biopolymers, bionanocomposites, and plastic films (Table 2). SPI films had a TS of 2.26 ± 0.41 MPa and %E of 11.85 ± 0.41. These values of TS and %E are comparable to those for films based on soy protein and whey protein as reported in literature (Table 2). Films containing MMT had significantly higher TS as compared to that of SPI film. The value of TS increased from 2.26 ± 0.41 MPa to 15.60 ± 0.41 MPa as the MMT content increased from 0 to 15%. This is attributed to the high rigidity and aspect ratio of MMT and interaction of SPI with MMT. Films containing 5% MMT had significantly higher %E as compared to that of SPI film. However, %E decreased as the MMT content increased from 5% to 15%. This is attributed to the restricted motion of soy protein molecules in bio-nanocomposite films due to incorporation of MMT and interaction

of SPI with MMT. TS values of films containing 10% and 15% MMT are comparable to those of low density polyethylene (LDPE) and polyvinylidene chloride (PVDC) which are currently used in food packaging applications. However, %E values for these plastic films range from 100%-900% which is much higher than those for SPI-MMT films (11.85%-64.60%). The lower value of %E might limit the application of these SPI-MMT films as food packaging materials. Mechanical properties of SPI-MMT films could further be improved by changing the type and content of plasticizer and incorporating other synthetic biodegradable polymers with improved properties. One such biodegradable polymer is polyvinyl alcohol (PVOH) which has higher TS (44-64 MPa) and %E (150-400%). Su and others (2007) reported that %E of films based on blends of SPI and PVOH increased from 2.7% to 102% as the PVOH content increased from 0% to 40%.

Effect of temperature on tan δ of SPI-MMT films with 0%, 5%, 10%, and 15% MMT contents is shown in Figure 7. There was a significant ($P < 0.05$) increase in glass transition temperature (T_g), depicted by the peak in the tan δ curve, with an increase in MMT content. SPI films had a T_g of 119.7 ± 1.9 °C which is in the range of T_g (111.9-150 °C) of SPI films as reported by Ogale and others (2000). Glass transition temperature increased from 142.8 ± 2.1 °C to 199.5 ± 3.0 °C as the MMT content increased from 5 to 15%. This is attributed to reduced mobility of biopolymer chains of SPI in the bio-nanocomposite matrix. It can also be seen from Figure 7 that the magnitude of tan δ peak value increases as MMT content increases to 5% and then decreases with further increase in MMT content. The area and magnitude of tan δ peak is an indication of the motion of polymer chains in amorphous phase (Yu and others 2004). The broad peak with reduced magnitude at higher MMT contents can

be attributed to restricted motion of biopolymer chains of SPI due to the interaction of SPI with MMT. It was also observed that there was a linear dependence of TS on T_g, given as:

$$TS = 0.1727 \times T_g - 18.17 \qquad (r^2 = 0.98) \qquad (69)$$

Similar linear dependence of TS on T_g of biopolymer films based on blends of PVOH and gelatin has been reported by Maria and others (2008).

Effect of temperature on storage modulus (E') of SPI-MMT films with 0%, 5%, 10%, and 15% MMT contents is shown in Figure 8. Over the entire temperature range, E' of SPI-MMT films was significantly ($P < 0.05$) higher than that of SPI films. Storage modulus of the films at 40 °C increased from 337 ± 31 MPa to 529 ± 24 MPa as the MMT content increased from 0% to 5%. Storage modulus of the films at 40 °C further increased to 2064 ± 54 MPa as the MMT content increased to 15%. This significant increase in E' of films is attributed to the reduced mobility of biopolymer chains of SPI in bio-nanocomposite films. The increase in E' is also in agreement with the results of tensile testing where TS increased with an increase in MMT content.

The thermal stability of SPI-MMT films was investigated using TGA separately under nitrogen and air flow (Figures 9 and 10). It can be seen from Figure 9 that there are 2 to 3 steps of thermal degradation of the films in the temperature range of 100 to 900 °C. The temperature range for the first step of thermal degradation is 100 to 150 °C. This corresponds to the loss of water from the films. The temperature range for the second step of thermal degradation is 300 to 400 °C. This corresponds to the decomposition of soy protein and loss of glycerol from the films. Under air flow, there is an additional third step of thermal degradation in the temperature range of 500 to 800 °C. This might be due to oxidation of

partially decomposed soy protein under air flow. Similar results for different types of bio-nanocomposite films have been reported (Wang and others 2006; Tunc and others 2007).

TGA curves of SPI-MMT bio-nanocomposite films with different MMT contents under air flow are shown in Figure 10. As the MMT content increased, the bio-nanocomposite films exhibited a significant delay in weight loss at temperatures greater than 400 °C. The temperature at 50% weight loss (during TGA) increased from 355.5 ± 2.2 °C to 377.3 ± 2.6 °C with an increase in MMT content from 0 to 5%. The temperature at 50% weight loss further increased to 395.4 ± 3.2 °C as the MMT content increased to 15%. This can be attributed to the fact that MMT platelets reduce the rate of diffusion of volatile decomposition products out of the bio-nanocomposite bulk. MMT platelets create a tortuous pathway for volatile decomposition products to diffuse out of the bio-nanocomposite matrix. This increases the effective path length for diffusion, thus reducing the rate of diffusion (Chen and others 2001). The mechanism for improved thermal stability has also been attributed to the thermal insulation behavior of MMT and changes in the dynamics of molecular motion in bio-nanocomposites (Leszczynska and Pielichowski 2008). After decomposition at 850 °C, the films yielded charred residue proportional to their clay content. The yield of charred residue at 850 °C increased from 4.2 ± 0.3% to 7.8 ± 0.4% with an increase in MMT content from 0 to 5%. The yield of charred residue at 850 °C further increased to 20.5 ± 0.4% as MMT content increased to 15%. This increased yield of charred residue can be attributed to the addition of MMT which is thermally stable up to a temperature of 900 °C. Kim and White (2005) reported that MMT (Cloisite Na^{+}) yields more than 85% solid residue at 800 °C.

Water vapor permeability (WVP) of SPI-MMT films with 0%, 5%, 10%, and 15% MMT contents was compared with that of other biopolymers, bionanocomposites, and plastic films (Table 3). Higher WVP is one of the major limitations in using protein based films as food packaging materials. Therefore, reduction in WVP is desirable for potential applications in food packaging. SPI films had a WVP of 3.80 ± 0.11 g-mm/(m^2-hr-kPa) which is comparable to the WVP of other biopolymer films based on protein, chitosan, and starch as reported in literature (Table 3). Films containing MMT had significantly ($P < 0.05$) lower WVP as compared to that of SPI film. WVP for films with 5% MMT reduced by 22.1%. This reduction is comparable to the results with chitosan-MMT (25.4% reduction) and starch-MMT (34.2% reduction) reported in literature (Table 3). The reduction in WVP by MMT has been attributed to the creation of a tortuous pathway for water vapor to diffuse out of the bio-nanocomposite matrix. This increases the effective path length for diffusion of water vapor molecules, thus reducing WVP (Zeng and others 2005). WVP reduced by as much as 42.9% as the MMT content increased from 0% to 15%. However, the WVP values for SPI-MMT films are still much higher as compared to those for plastics such as low density polyethylene (LDPE), polypropylene (PP), polyvinylidene chloride (PVDC). This might limit the application of these bio-nanocomposite films to packaging of high moisture foods such as fresh fruits and vegetables.

Effect of extrusion parameters on the properties of films

Effect of extrusion processing parameters (screw speed and barrel temperature distribution) on mechanical properties (TS and %E) of SPI-MMT films with MMT content of 5% is shown in Table 4. There was a significant ($P < 0.05$) increase in TS of the films with

an increase in screw speed and barrel temperature. Improved TS at higher screw speed can be attributed to better dispersion of MMT. Higher shear rate, corresponding to higher screw speed, can break bigger agglomerates of MMT into smaller aggregates. Improved TS at higher barrel temperature can be attributed to a decrease in viscosity with increase in temperature. The stress required to break MMT aggregates is reduced as the viscosity decreases (Lertwimolnun and Vergnes 2007). An increase in barrel temperature can also increase the extent of protein denaturation. Denatured proteins will have more biopolymer chains available for network formation, resulting in films with improved TS. Analysis of variance using the general linear model showed that the interaction effect of screw speed and barrel temperature distribution on TS was insignificant ($P > 0.05$). There was a significant ($P < 0.05$) increase in %E of the films with an increase in screw speed. Effect of barrel temperature distribution and interaction effect of barrel temperature distribution and screw speed on %E were insignificant ($P > 0.05$). It can be concluded that higher screw speed and barrel temperature are desirable to prepare films with higher TS and %E.

Effect of temperature on tan δ of SPI-MMT films with MMT content of 5% at different extrusion processing parameters is shown in Figure 11. There was a significant ($P < 0.05$) increase in glass transition temperature with an increase in screw speed and barrel temperature. At a barrel temperature distribution of T_1, T_g increased from 134.3 ± 1.1 °C to 142.8 ± 2.0 °C as the screw speed increased from N_1 (50 rpm) to N_2 (100 rpm). At a screw speed of N_2, T_g increased from 142.8 ± 2.0 °C to 158.6 ± 0.8 °C as the barrel temperature distribution changed from T_1 (70, 90, 100, 110, and 90 °C) to T_3 (90, 110, 120, 130, and 120 °C). This can be attributed to better dispersion of MMT and network formation at higher

screw speed and barrel temperature. It can also be seen from Figure 11 that the magnitude of tan δ peak decreases with an increase in barrel temperature. This result supports the fact that more biopolymer chains of soy protein were involved in network formation with MMT at higher barrel temperature.

Effect of temperature on storage modulus (E') of SPI-MMT films with MMT content of 5% at different extrusion processing parameters is shown in Figure 12. Over the entire temperature range, E' of films at higher screw speed and higher barrel temperature was higher than that of films at lower screw speed and lower barrel temperature. There was an increase of 51.2% in E' of the films at 40 °C as the screw speed increased from 50 to 100 rpm. The corresponding increase was 139.3% as the barrel temperature distribution changed from T_1 to T_3. The increase in E' is also in agreement with the results of tensile testing where TS increased with an increase in screw speed and barrel temperature.

Effect of extrusion processing parameters (screw speed and barrel temperature distribution) on water vapor permeability (WVP) of SPI-MMT films with MMT content of 5% is shown in Table 5. Analysis of variance using the general linear model showed that the effect of screw speed on WVP was significant ($P < 0.05$). The effect of barrel temperature distribution and interaction effect of barrel temperature distribution and screw speed on WVP were insignificant ($P > 0.05$).

Conclusions

Bio-nanocomposite films based on soy protein isolate (SPI) and montmorillonite (MMT) with improved properties were prepared using melt extrusion. The arrangement of MMT in the bio-nanocomposite matrix ranged from exfoliated at lower MMT content (5%) to intercalated at higher MMT content (15%). There was a significant improvement in mechanical (tensile strength and percent elongation at break) and dynamic mechanical properties (glass transition temperature and storage modulus), thermal stability, and water vapor permeability of the films with the addition of MMT. Properties of the SPI-MMT films were significantly affected by the pH of film forming solutions, MMT content, and extrusion processing parameters (screw speed and barrel temperature distribution). The results presented in this study show the feasibility of using bio-nanocomposite technology to improve the properties of biopolymer films based on SPI. The same technology can also be applied to biopolymers based on starch and other proteins. These bio-nanocomposite films could potentially be used in food packaging to replace some of the existing plastics such as low density polyethylene (LDPE) and polyvinylidene chloride (PVDC). However, there is a need to further improve the properties of these SPI-MMT films for commercial application.

Acknowledgments

Support for the research study undertaken here, resulting in the publication of paper nr FSR-09-37 of the Journal Series of the Dept. of Food, Bioprocessing, and Nutrition Sciences, NCSU, Raleigh, NC 27695-7624 from USDA-NRICGP Grant nr 2008-01503, titled: Development of cross-linked bio-nanocomposite packaging films with enhanced barrier and mechanical properties, is gratefully acknowledged. We would also like to thank Birgit Anderson, Gail Liston, Roberto Garcia, Chuck Mooney, Jonathan Pierce, and Sharon Ramsey for their assistance in conducting the experiments.

The use of trade names in this publication does not imply endorsement by the North Carolina Agricultural Research Service of the products named nor criticism of similar ones not mentioned.

References

ASTM Standards. 2002. D882-02. Standard test method for tensile properties of thin plastic sheeting. Philadelphia, PA.

ASTM Standards. 2005. E96-05. Standard test methods for water vapor transmission of materials. Philadelphia, PA.

Bohlmann GM. 2005. General characteristics, processability, industrial applications and market evolution of biodegradable polymers. In: Bastioli C, editor. Handbook of Biodegradable Polymers. Shropshire, UK: Rapra Technology Ltd. p 183-218.

Brandenburg AH, Weller CL, Testin RF. 1993. Edible films and coatings from soy protein. Journal of food science 58: 1086-1089.

Chen G, Liu S, Chen S, Qi Z. 2001. FTIR spectra, thermal properties, and dispersibility of a polystyrene/montmorillonite nanocomposite. Macromolecular chemistry and physics 202: 1189-1193.

Chen P, Zhang L. 2006. Interaction and properties of highly exfoliated soy protein/montmorillonite nanocomposites. Biomacromolecules 7: 1700-1706.

Cuq B, Gontard N, Guilbert S. 1998. Proteins as agricultural polymers for packaging production. Cereal chemistry 75(1): 1-9.

Dean K, Yu L. 2005. Biodegradable protein-nanoparticles composites. In: Smith R, editor. Biodegradable Polymers for Industrial Applications. UK: Woodhead Publishing Ltd. p 289-312.

Dennis HR, Hunter DL, Chang D, Kim S, White JL, Cho JW, Paul DR. 2001. Effect of melt processing conditions on the extent of exfoliation in organoclay-based nanocomposites. Polymer 42: 9513-9522.

Fornes TD, Paul DR. 2003. Modeling properties of nylon 6/clay nanocomposites using composite theories. Polymer 44: 4993-5013.

Gennadios A, Brandenburg AH, Weller CL, Testin RF. 1993. Effect of pH on properties of wheat gluten and soy protein isolate films. Journal of agricultural and food chemistry 41: 1835-1839.

Jahangir, S., and Leber, M.J. 2007. Biodegradable food packaging: an environmental imperative. Industry Report. p 1-20.

Hernandez-Izquierdo VM, Krochta JM. 2008. Thermoplastic processing of proteins for film formation – a review. Journal of food science 73(2): R30-R39.

Kamper SL, Fennema O. 1984. Water vapor permeability of edible bilayer films. Journal of food science 49: 1478-1481.

Kasai K, Kakudo M. 2005. X-ray diffraction by macromolecules. New York: Springer. 504 p.

Kim Y, White JL. 2005. Formation of polymer nanocomposites with various organoclays. Journal of applied polymer science 96: 1888-1896.

Krochta JM. 2002. Proteins as raw materials for films and coatings: definitions, current status, and opportunities. In: Gennadios A, Editor. Protein-based Films and Coatings. Boca Raton, FL: CRC press. p 1-41.

Krochta JM. 2003. Package permeability In: Heldman DR, editor. Encyclopedia of Agricultural, Food, and Biological engineering. NY: Marcel Dekker, Inc. p 720-726.

Kurose T, Urman K, Otaigbe JU, Lochhead RY, Thames SF. 2007. Effect of uniaxial drawing of soy protein isolate biopolymer films on structure and mechanical properties. Polymer engineering and science 47(4): 374-380.

Lange Y, Wyser Y. 2003. Recent innovations in barrier technologies for plastic ackaging – a review. Packaging technology and science 16: 149-158.

Lefevre T, Subirade M, Pezolet M. 2005. Molecular description of the formation and structure of plasticized globular protein films. Biomacromolecules 6: 3209-3219.

Lertwimolnun W, Vergnes B. 2007. Influence of screw profile and extrusion conditions on the microstructure of polypropylene/organoclay nanocomposites. Polymer engineering and science 47(12): 2100-2109.

Leszczynska A, Pielichowski K. 2008. Application of thermal analysis methods for characterization of polymer/montmorillonite nanocomposites. Journal of thermal analysis and calorimetry 93(3): 677-687.

Maria TMC, de Carvalho RA, Sobral PJA, Habitante AMBQ, Feria JS. 2008. The effect of the degree of hydrolysis of the PVA and the plasticizer concentration on the color, opacity, and thermal and mechanical properties of films based on PVA and gelatin blends. Journal of food engineering 87: 191-199.

Marsh K, Bugusu B. 2007. Food packaging – roles, materials, and environmental issues. Journal of food science 72(3): R39-R55.

Mauri AN, Anon MC. 2006. Effect of solution pH on solubility and some structural properties of soybean protein isolate films. Journal of the science of food and agriculture 86: 1064-1072.

Morgan AB, Gilman JW. 2003. Characterization of polymer-layered silicate (clay) nanocomposites by transmission electron microscopy and X-ray diffraction: a comparative study. Journal of applied polymer science 87: 1329-1338.

Ogale AA, Cunningham P, Dawson PL, Acton JC. 2000. Viscoelastic, thermal, microstructural characterization of soy protein isolate films. Journal of food science 65(4): 672-679.

Park SK, Rhee CO, Bae DH, Hettiarachchy NS. 2001. Mechanical properties and water vapor permeability of soy protein films affected by calcium salts and glucono-δ-lactone. Journal of agricultural and food chemistry 49: 2308-2312.

Petruccelli S, Anon MC. 1995. Soy protein isolate components and their interactions. Journal of agricultural and food chemistry 43: 1762-1767.

Ray SS, Bousmina M. 2005. Biodegradable polymers and their layered silicate nanocomposites: in greening the 21st century materials world. Progress in materials science 50: 962-1079.

Rhim JW, Lee JH, Kwak HS. 2005. Mechanical and barrier properties of soy protein and clay mineral composite films. Food science and biotechnology 14: 112-116.

Rhim JW, Hong SI, Park HM, Ng PKW. 2006. Preparation and characterization of chitosan-based nanocomposite films with antimicrobial activity. Journal of agricultural and food chemistry 54: 5814-5822.

Rhim JW, Ng PKW. 2007. Natural biopolymer-based nanocomposite films for packaging applications. Critical reviews in food science and nutrition 47(4): 411-433.

Rhim JW, Hong, SK, Ha CS. 2009. Tensile, water vapor barrier and antimicrobial properties of PLA/nanoclay composite films. LWT food science and technology 42: 612-617.

Schlechter M. 2007. Biodegradable polymers. Report code PLS025C. Available from : http://bccresearch.com/report/PLS025C.html. Accessed 2009 September 2.

Selke SEM. 1997. Understanding Plastics Packaging Technology. New York: Hanser Publication. 206 p.

Su JF, Huang Z, Liu K, Fu LL, Liu HR. 2007. Mechanical properties, biodegradation, water vapor permeability of blend films of soy protein isolates and poly(vinyl alcohol) compatibilized by glycerol. Polymer bulletin 58: 913-921.

Tang X, Alavi S, Herald HJ. 2008. Barrier and mechanical properties of starch-clay nanocomposite films. Cereal chemistry 85(3): 433-439.

Tunc S, Angellier H, Cahyana Y, Chalier P, Gontard N, Gastaldi E. 2007. Functional properties of wheat gluten/montmorillonite nanocomposite films processed by casting. Journal of membrane science 289: 159-168.

Wang S, Sue HJ, Jane J. 1996. Effects of polyhydric alcohols on the mechanical properties of soy protein plastics. Journal of macromolecular science, Part A 33(5): 557-569.

Wang S, Chen L, Tong Y. 2006. Structure-property relationship in chitosan-based biopolymer/montmorillonite nanocomposites. Journal of polymer science: Part A: polymer chemistry 44: 686-696.

Yu ZZ, Yan C, Yang M, Mai, YW. 2004. Mechanical and dynamic mechanical properties of nylon 66/montmorillonite nanocomposites fabricated by melt compounding. Polymer international 53: 1093-1098.

Zeng QH, Yu AB, Lu GQ, Paul DR 2005. Clay-based polymer nanocomposites: research and commercial development. Journal of nanoscience and nanotechnology 5: 1574-1592.

Zhang J, Mungara P, Jane J. 2001. Mechanical and thermal properties of extruded soy protein sheets. Polymers 42: 2569-2578.

Zhao R, Torley P, Halley PJ. 2008. Emerging biodegradable materials: starch- and protein-based bio-nanocomposites. Journal of materials science 43: 3058-3071.

Table 1 – Effect of pH on mechanical properties (TS and %E) of SPI-MMT films.[A]

	TS (MPa)	%E
SPI film (pH 7.5)	1.86 ± 0.17 [a]	14.29 ± 1.17[a]
SPI film (pH 9.0)	2.26 ± 0.48 [a]	11.85 ± 0.39[a]
SPI-5% MMT film (pH 7.5)	4.79 ± 0.23[b]	47.34 ± 3.56[b]
SPI-5% MMT film (pH 9.0)	6.28 ± 0.88[b]	64.60 ± 4.69[c]

[A] Values are mean of two replicates ± standard deviation. Means in the same column followed by the same letter are not significantly different ($P > 0.05$).

Table 2 – Comparison of mechanical properties (TS and %E) of SPI-MMT films[A] with other biopolymer, bio-nanocomposite, and plastic films.

Films	TS (MPa)	%E
SPI	2.26 ± 0.48[a]	11.85 ± 0.39[a]
SPI-5% MMT	6.28 ± 0.88[b]	64.60 ± 4.69[b]
SPI-10% MMT	12.62 ± 0.54[c]	23.98 ± 5.02[c]
SPI-15% MMT	15.60 ± 1.69[d]	17.80 ± 2.27[ac]
Soy protein (Krochta 2002)	3-14	10-172
Whey protein (Krochta 2002)	1-29	4-41
Chitosan (Rhim and others 2006)	32.9	54.6
Chitosan-5% MMT (Rhim and others 2006)	35.1	50.3
Starch (Tang and others 2008)	14.22	5.26
Starch-6% MMT (Tang and others 2008)	18.60	4.44
Cellophane (Krochta 2002)	55-124	16-604
Polylactic acid (PLA) (Rhim and others 2009)	50.5	3
Polyvinyl alcohol (PVOH) (Bohlmann 2005)	44-64	150-400
Low density polyethylene (LDPE) (Selke 1997)	8.2-31.4	100-965
Polypropylene (PP) (Selke 1997)	31-41.3	100-600
Polyvinylidene chloride (PVDC) (Selke 1997)	19.3-34.5	160-400

[A] Values are mean of two replicates ± standard deviation. Means in the same column followed by the same letter are not significantly different ($P > 0.05$).

Table 3 – Comparison of water vapor permeability (WVP) of SPI-MMT films[A] with other biopolymer, bio-nanocomposite, and plastic films.

Films	WVP (g-mm/(m^2-hr-kPa))
SPI	3.80 ± 0.11^{a}
SPI-5% MMT	2.96 ± 0.10^{b}
SPI-10% MMT	2.49 ± 0.08^{c}
SPI-15% MMT	2.17 ± 0.06^{d}
Soy protein	1.62-6.42 (Krochta 2002)
Whey protein	1.58-12.12 (Krochta 2002)
Chitosan	4.72 (Rhim and others 2006)
Chitosan-5% MMT	3.52 (Rhim and others 2006)
Starch	1.61 (Tang and others 2008)
Starch-6% MMT	1.06 (Tang and others 2008)
Cellophane	0.05-0.25 (Kamper and Fennema 1984)
Polylactic acid (PLA)	0.06 (Rhim and others 2009)
Polyvinyl alcohol (PVOH)	3.15 (Lange and Wyser 2003)
Low density polyethylene (LDPE)	0.001 (Krochta 2003)
Polypropylene (PP)	0.02-0.04 (Lange and Wyser 2003)
Polyvinylidene chloride (PVDC)	0.01 (Lange and Wyser 2003)

[A] Values are mean of two replicates ± standard deviation. Means in the same column followed by the same letter are not significantly different ($P > 0.05$).

Table 4 – Effect of extrusion processing parameters on mechanical properties (TS and %E) of SPI-MMT films with MMT content of 5%.[A]

Extrusion processing parameters	TS (MPa)	%E
N_1T_1	4.63 ± 0.46^a	$11.24 \pm 1.08\%^a$
N_1T_2	5.24 ± 0.14^b	$20.43 \pm 2.18\%^a$
N_1T_3	6.49 ± 0.12^b	$25.20 \pm 3.67\%^a$
N_2T_1	6.28 ± 0.88^b	$64.60 \pm 4.69\%^b$
N_2T_2	8.29 ± 0.71^c	$38.00 \pm 6.07\%^b$
N_2T_3	9.25 ± 0.34^c	$41.00 \pm 5.00\%^b$

[A] Values are mean of two replicates ± standard deviation. Means in the same column followed by the same letter are not significantly different ($P > 0.05$).

N_1 = 50 rpm, N_2 = 100 rpm

T_1: (70, 90, 100, 110, and 90 °C)

T_2: (80, 100, 110, 120, and 110 °C)

T_3: (90, 110, 120, 130, and 120 °C)

Table 5 – Effect of extrusion processing parameters on WVP of SPI-MMT films with MMT content of 5%.[A]

Extrusion processing parameters	WVP (g-mm/(m^2-hr-kPa))
N_1T_1	3.19 ± 0.11^a
N_1T_2	3.09 ± 0.10^a
N_1T_3	3.13 ± 0.08^a
N_2T_1	2.96 ± 0.10^b
N_2T_2	2.91 ± 0.11^b
N_2T_3	2.76 ± 0.07^b

[A] Values are mean of two replicates ± standard deviation. Means in the same column followed by the same letter are not significantly different ($P > 0.05$).

N_1 = 50 rpm, N_2 = 100 rpm

T_1: (70, 90, 100, 110, and 90 °C)

T_2: (80, 100, 110, 120, and 110 °C)

T_3: (90, 110, 120, 130, and 120 °C)

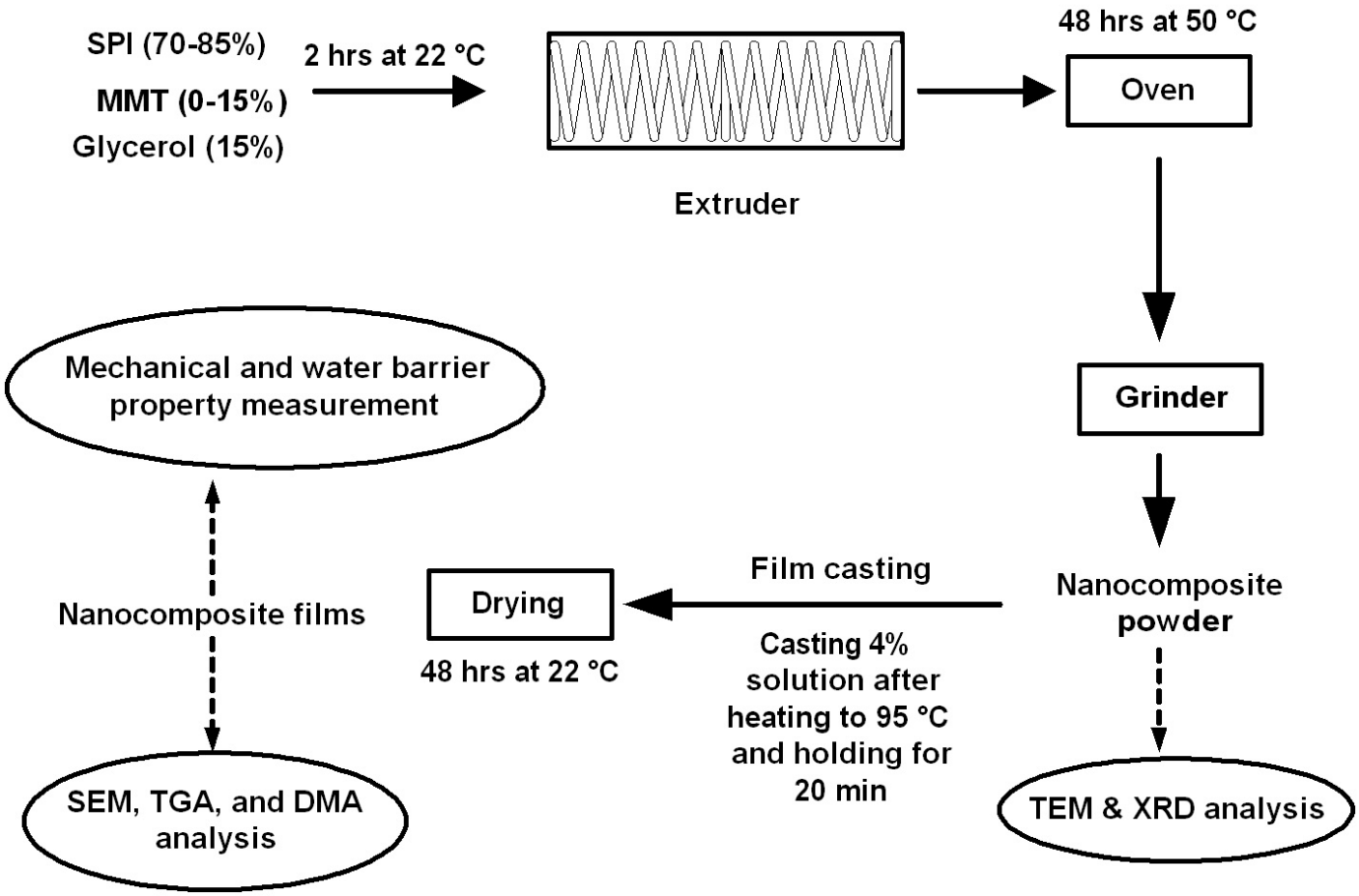

Figure 1 – Process flow diagram for the preparation and characterization of SPI-MMT bio-nanocomposite films.

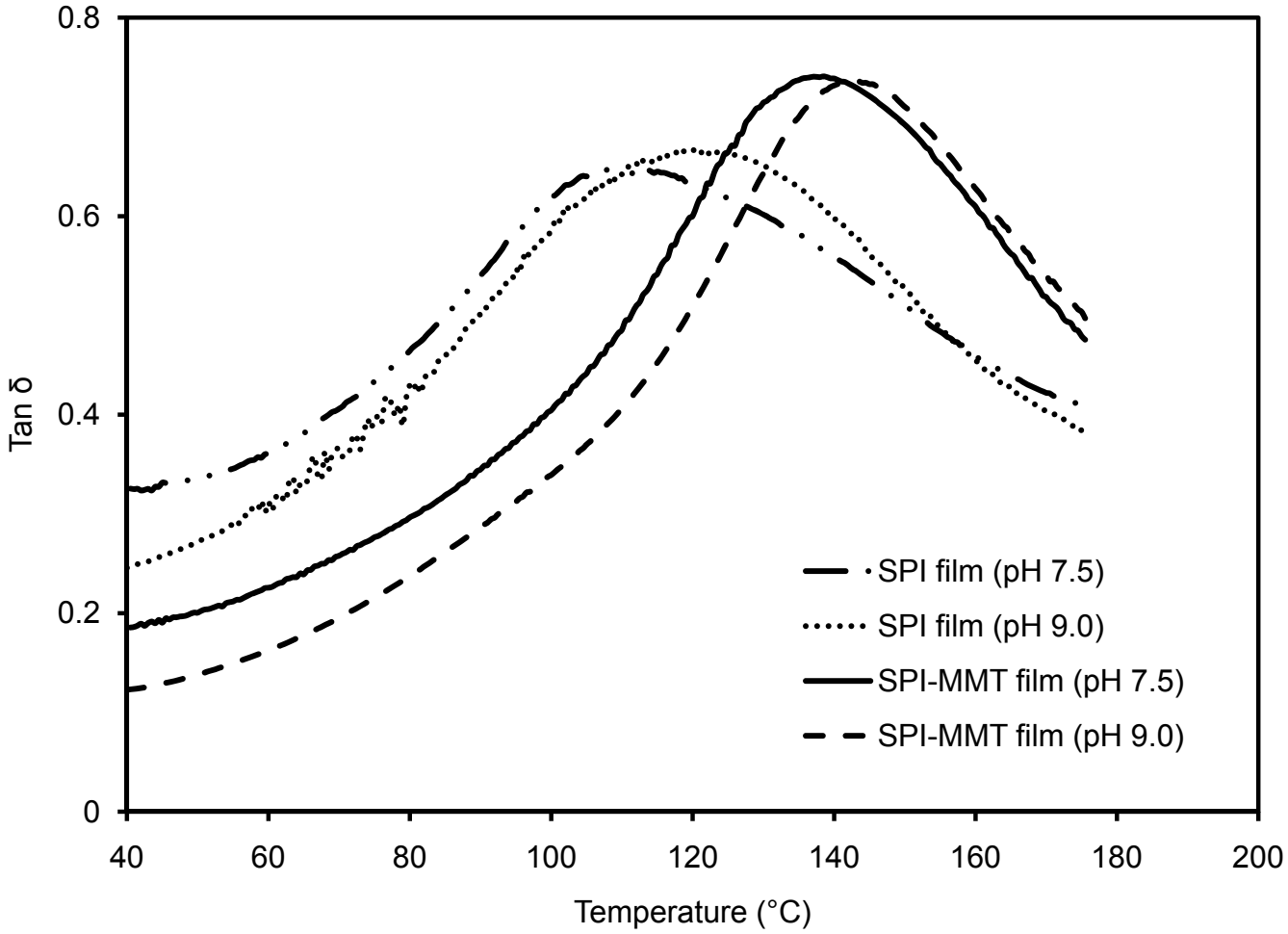

Figure 2 – Effect of temperature on tan δ of SPI-MMT films at different pH values.

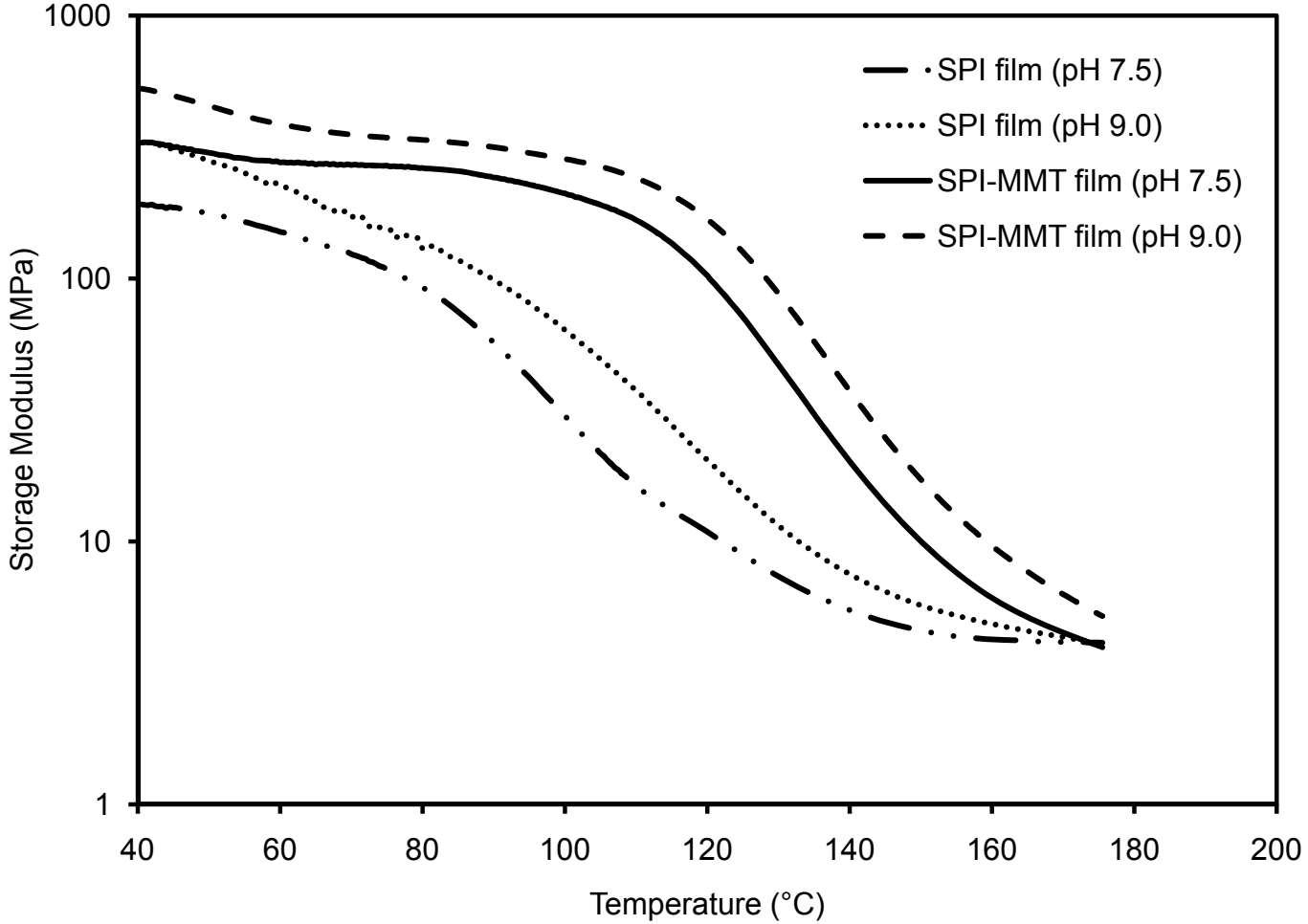

Figure 3 – Effect of temperature on storage modulus of SPI-MMT films at different pH values.

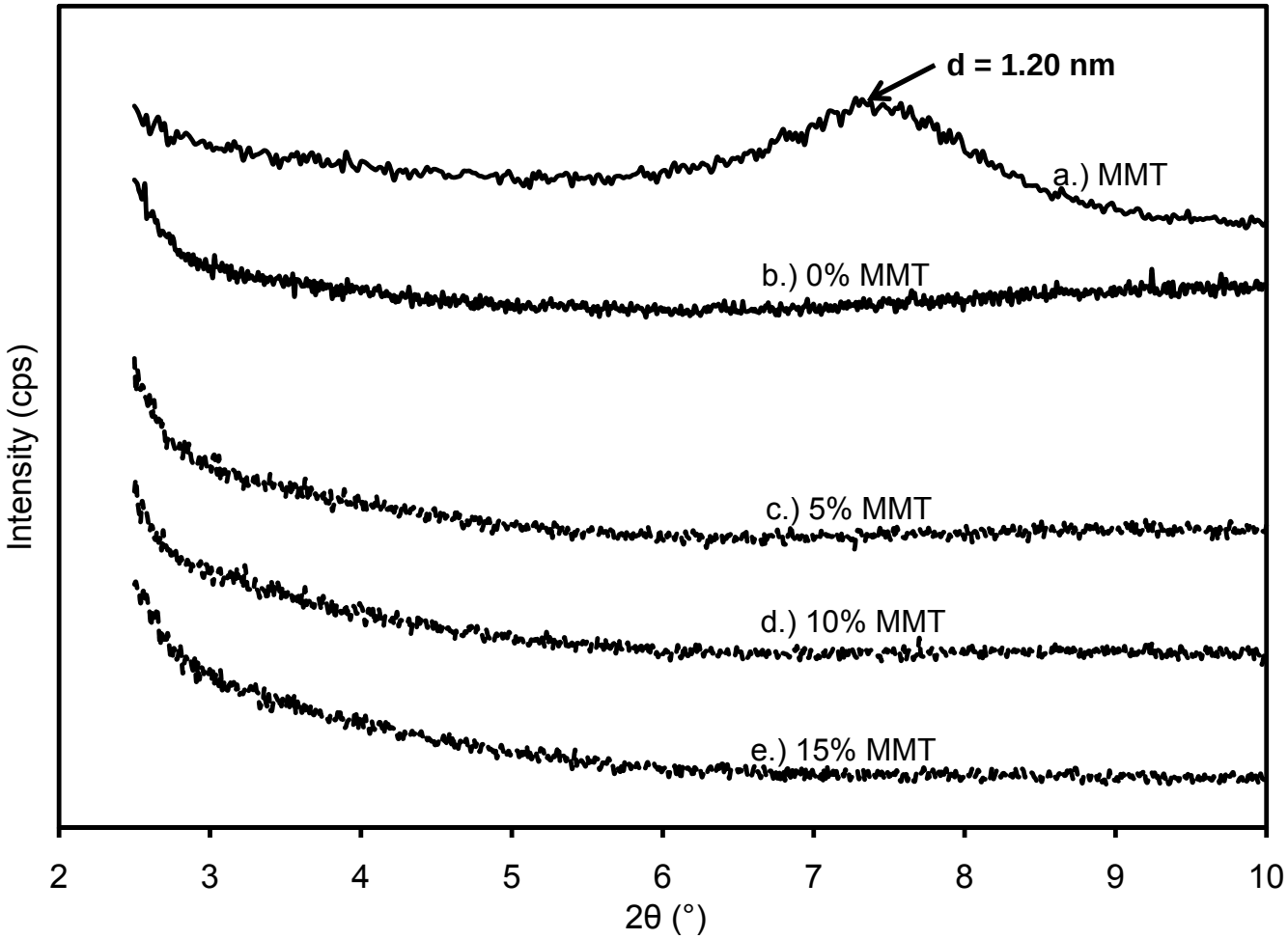

Figure 4 – XRD patterns of MMT and SPI-MMT bio-nanocomposites with different MMT contents.

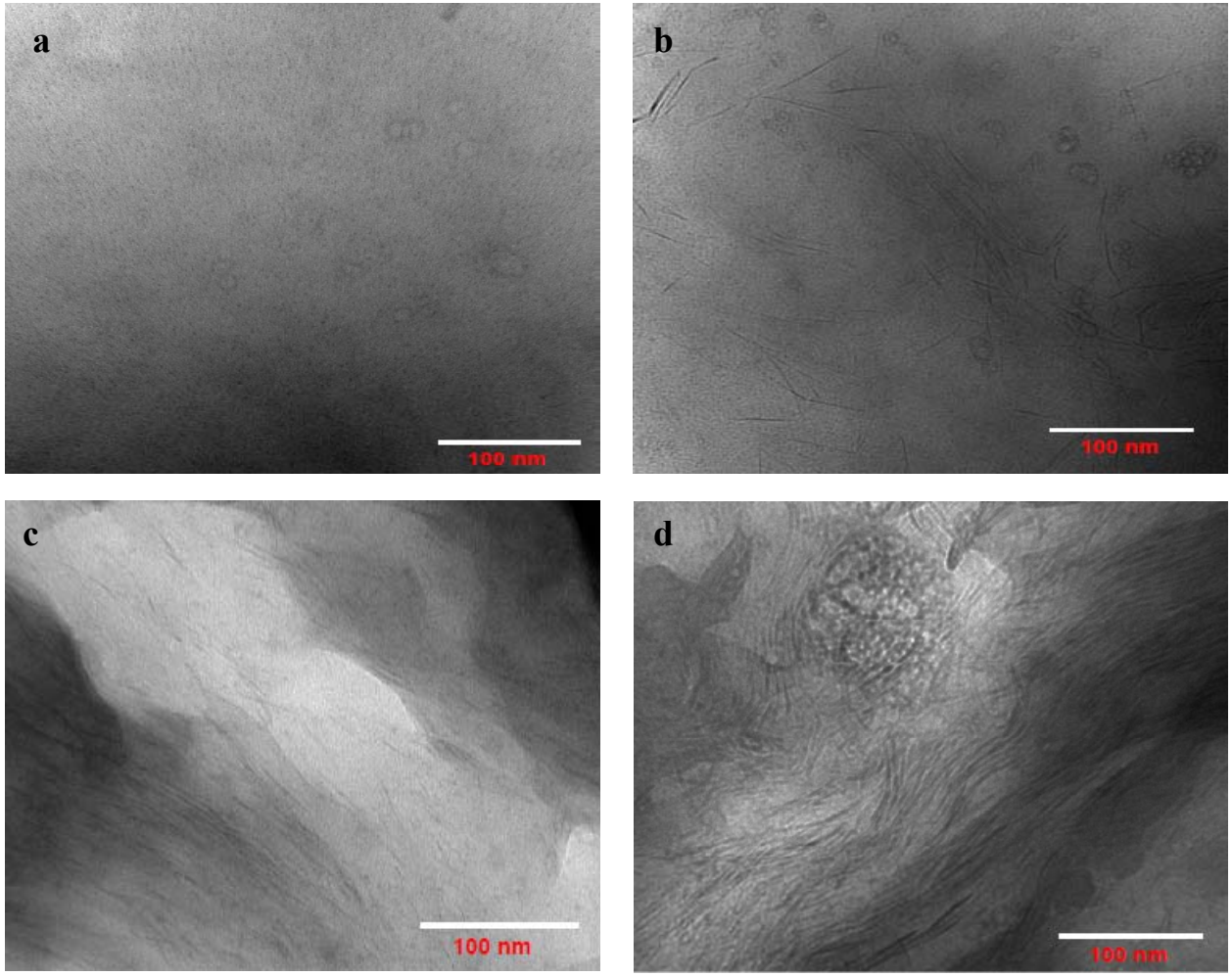

Figure 5 – TEM images of SPI-MMT bio-nanocomposites with (a) 0%, (b) 5%, (c) 10%, and (d) 15% MMT contents.

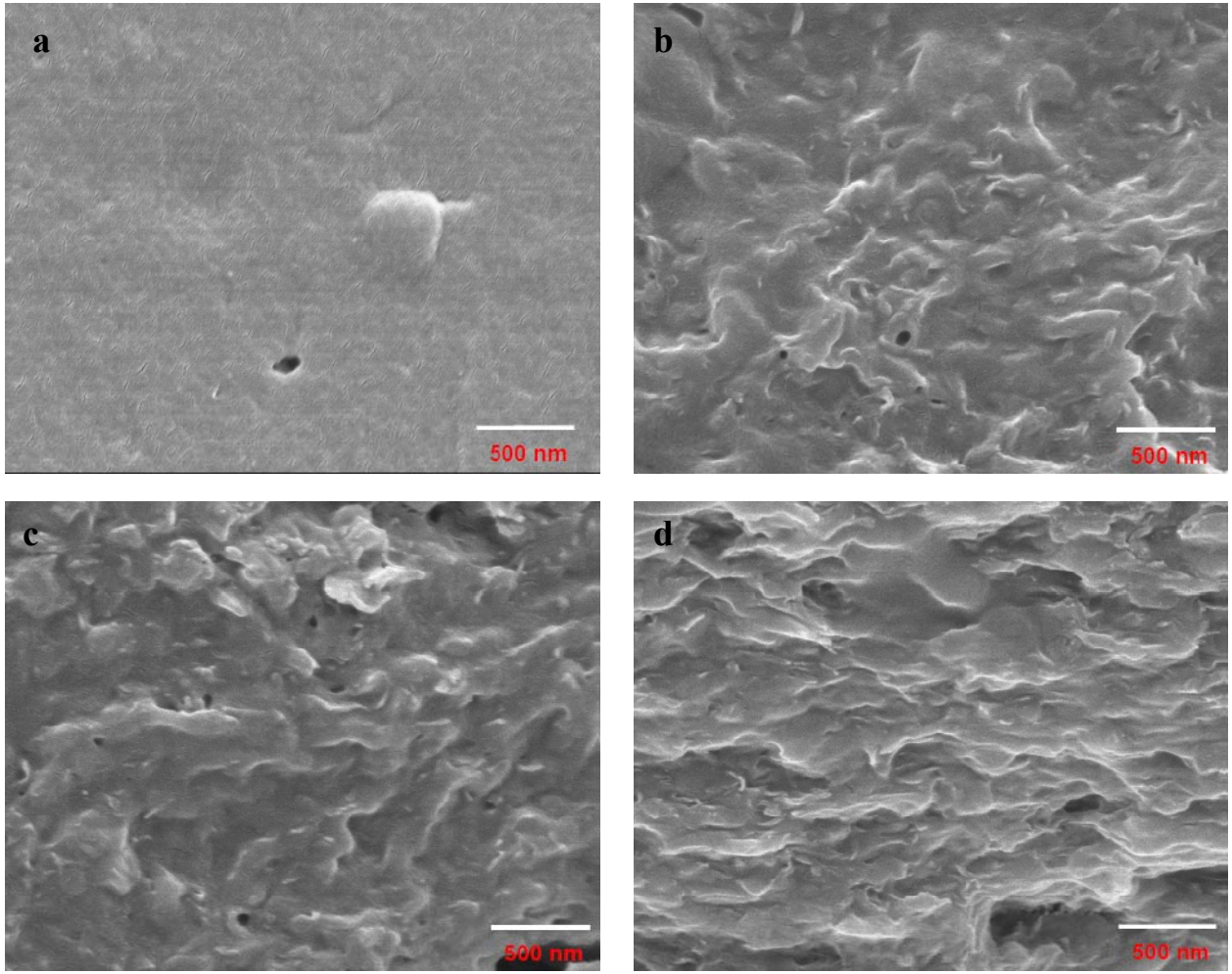

Figure 6 – SEM images of SPI-MMT bio-nanocomposite films with (a) 0%, (b) 5%, (c) 10%, and (d) 15% MMT contents.

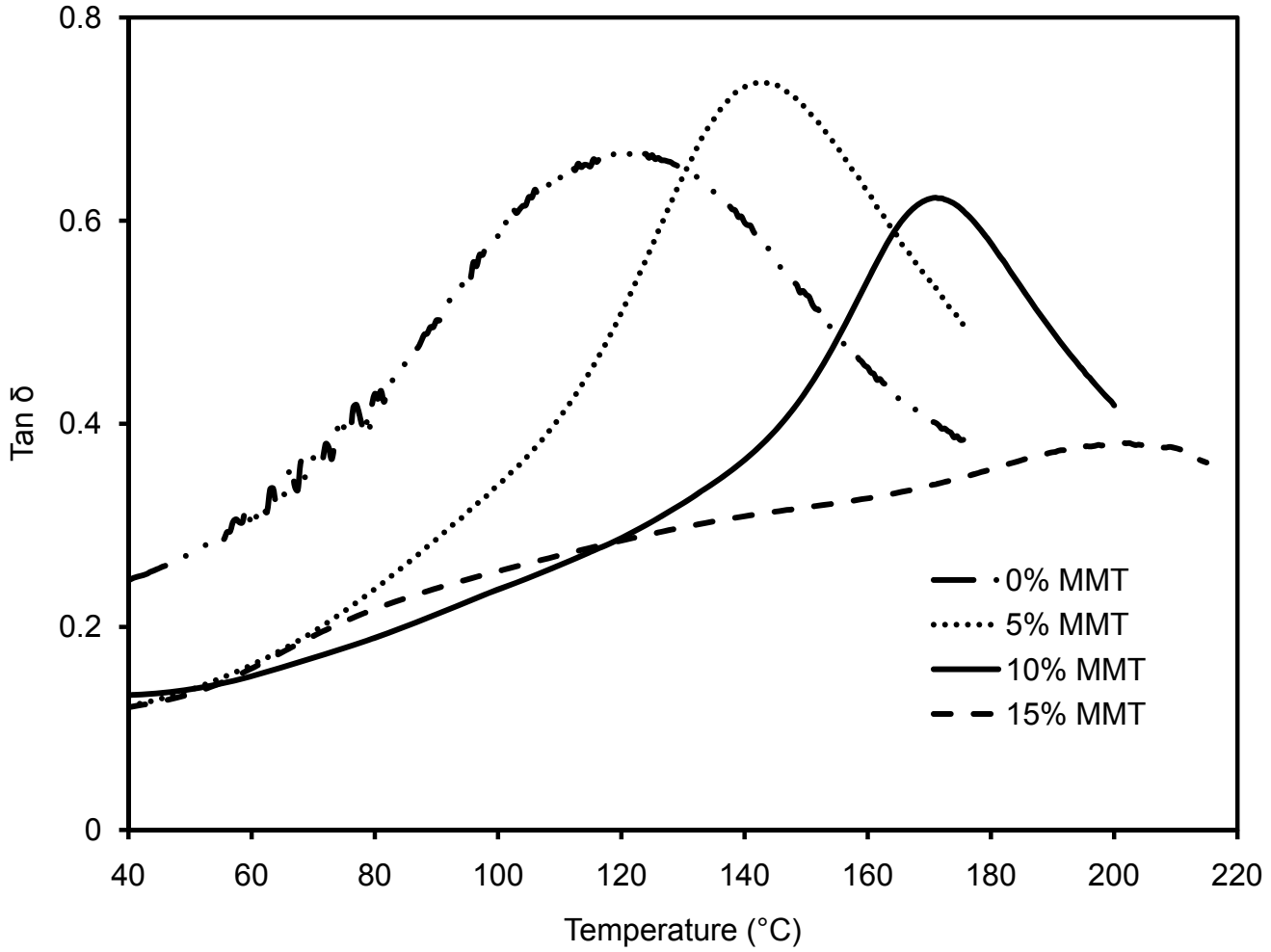

Figure 7 – Effect of temperature on tan δ of SPI-MMT films with different MMT contents.

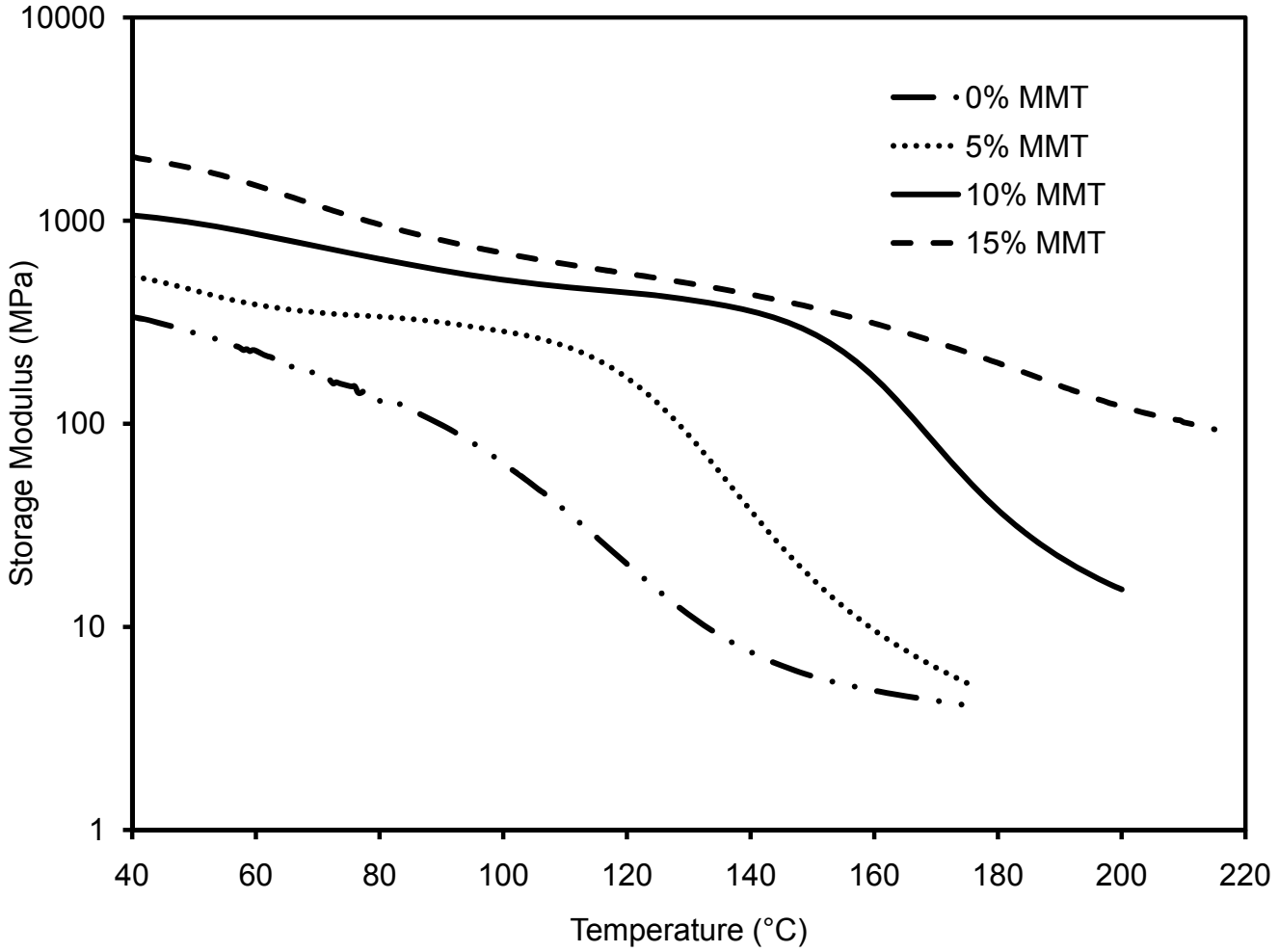

Figure 8 – Effect of temperature on storage modulus of SPI-MMT films with different MMT contents.

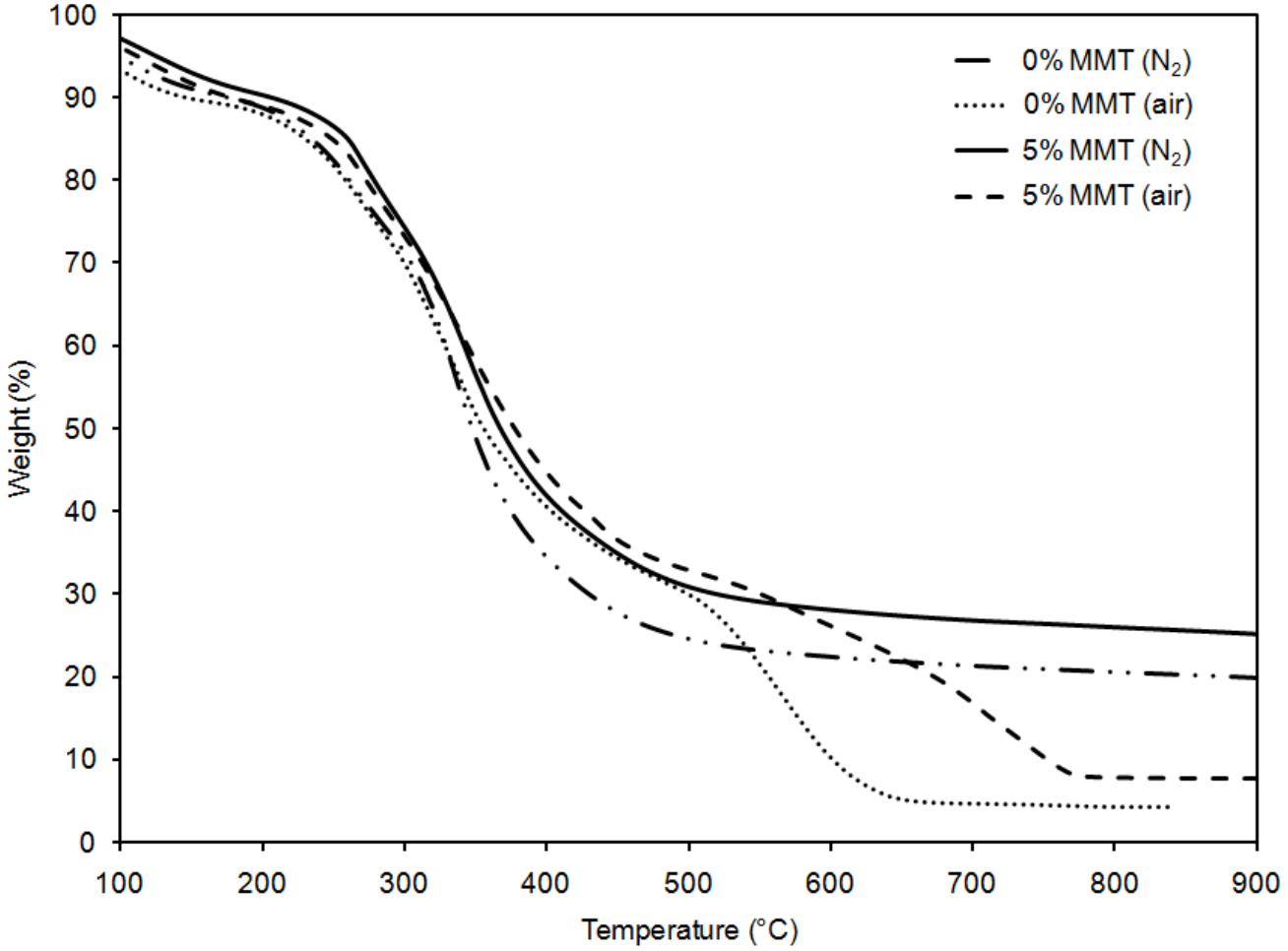

Figure 9 – TGA curves of SPI-MMT bio-nanocomposite films under N_2 and air flow.

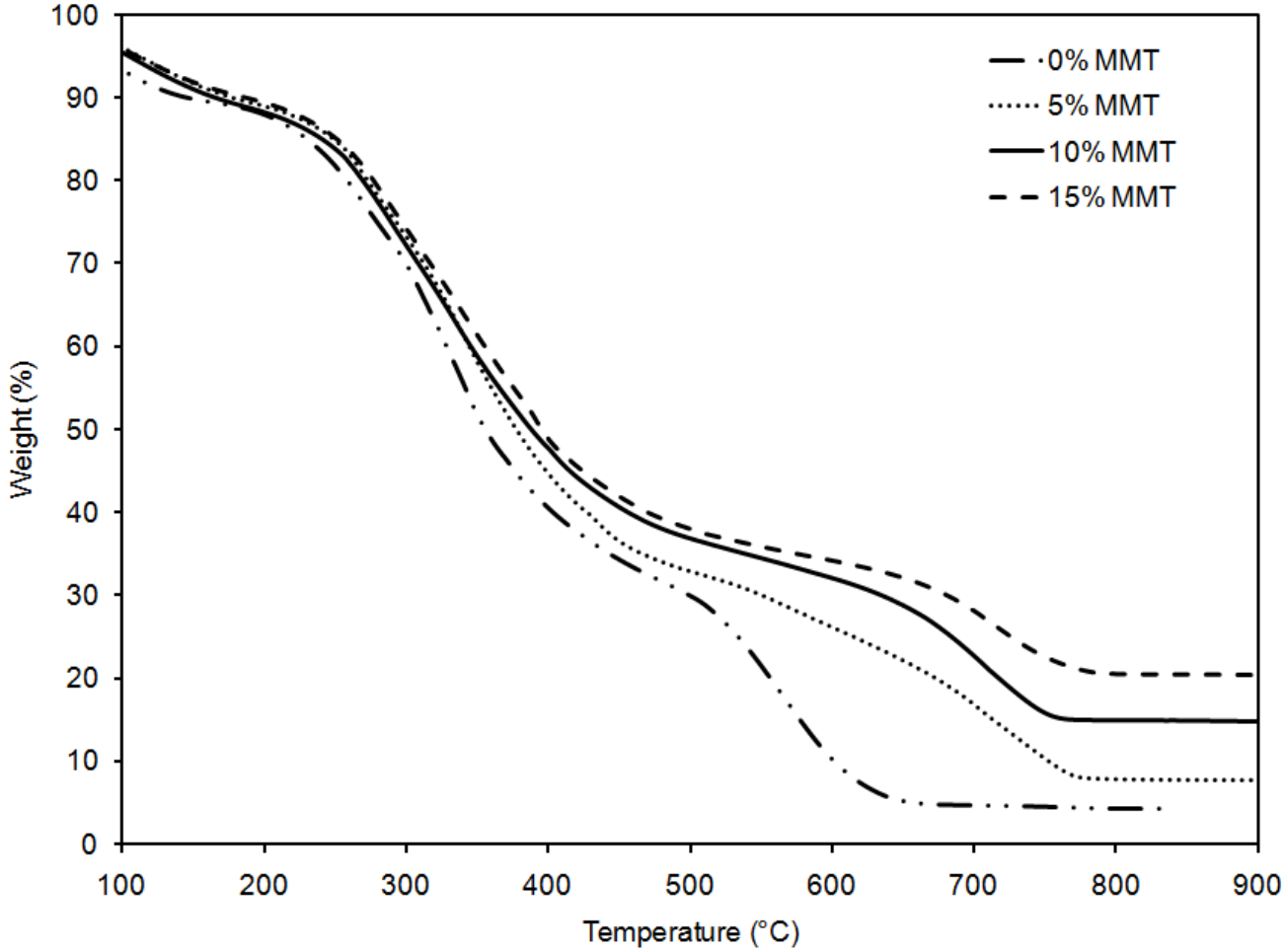

Figure 10 – TGA curves of SPI-MMT bio-nanocomposite films with different MMT contents under air flow.

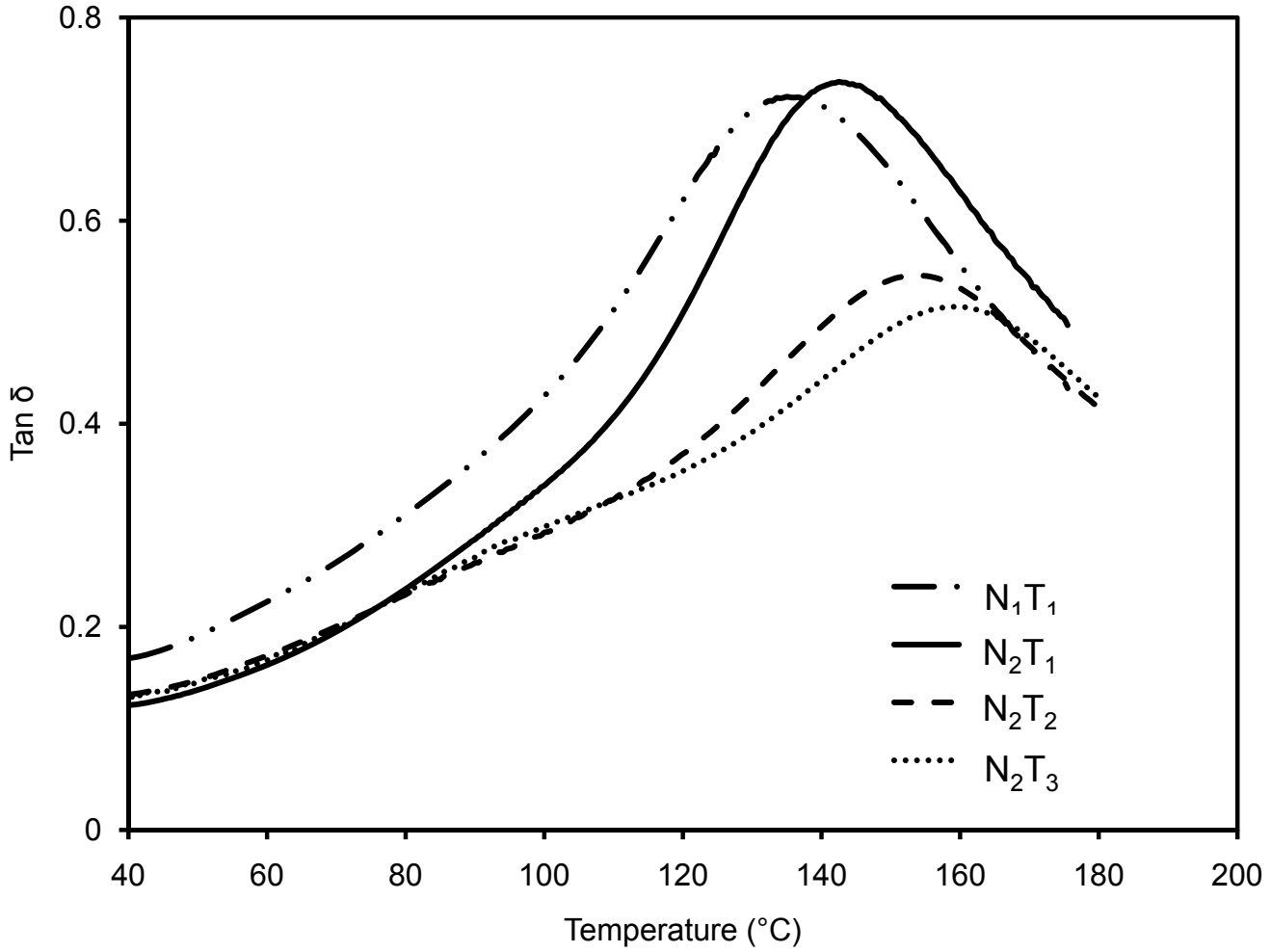

Figure 11 – Effect of temperature on tan δ of SPI-MMT films at different extrusion processing parameters.

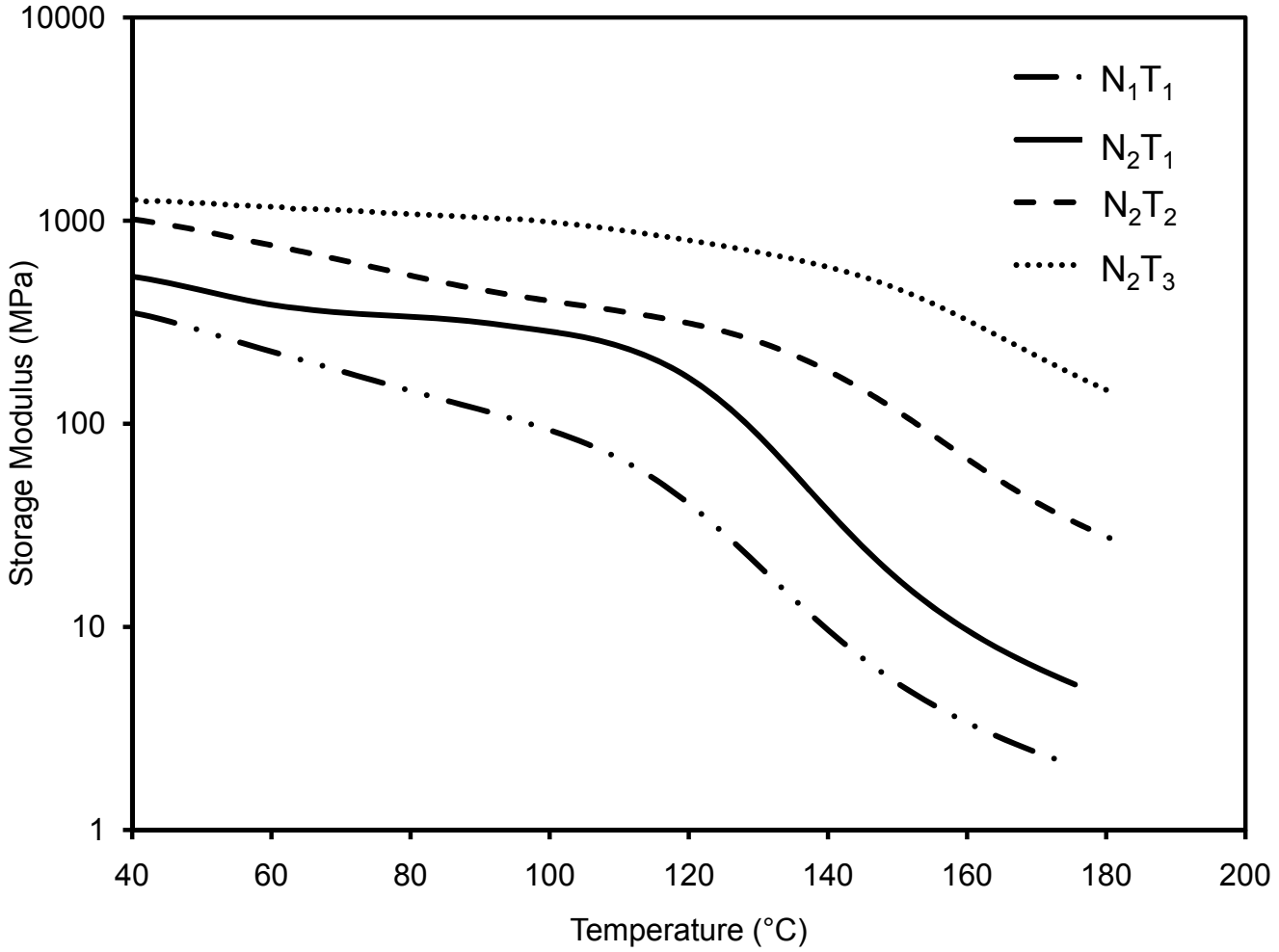

Figure 12 – Effect of temperature on storage modulus of SPI-MMT films at different extrusion processing parameters.

Chapter 7

MANUSCRIPT V

Effect of the Type and Content of Montmorillonite on the Structure and Properties of Soy Protein Isolate-Montmorillonite Bio-nanocomposite Films

P. KUMAR[1], K.P. SANDEEP[1], S. ALAVI[2], V.D. TRUONG[3], AND R.E. GORGA[4]

(1) Department of Food, Bioprocessing, and Nutrition Sciences, North Carolina State University, Raleigh, NC
(2) Department of Grain Science and Industry, Kansas State University, Manhattan, KS
(3) U.S. Dept. of Agriculture, Agricultural Research Service, South Atlantic Area, Food Science Research Unit, Raleigh, NC
(4) Department of Textile Engineering, Chemistry and Science, North Carolina State University, Raleigh, NC

Please address all correspondence to:

K.P. Sandeep
129 Schaub Hall, Box 7624
North Carolina State University
Raleigh, NC 27695
Phone: 919-515-2957
Fax: 919-515-7124
E-mail: kp_sandeep@ncsu.edu

Paper nr FSR-09-38 of the Journal Series of the Department of Food, Bioprocessing, and Nutrition Sciences, North Carolina State University, Raleigh, NC 27695-7624

Bio-nanocomposite films based on soy protein isolate and modified montmorillonite…

Abstract

The non-biodegradable and non-renewable nature of plastic packaging has led to a renewed interest in packaging materials based on bio-nanocomposites (biopolymer matrix reinforced with nanoparticles such as layered silicates). Bio-nanocomposite films based on soy protein isolate (SPI) and modified montmorillonite (MMT) were prepared using melt extrusion. Effect of different types (Cloisite 20A and Cloisite 30B) and contents (0-15%) of modified MMT on the structure and properties of SPI-MMT nanocomposite films were investigated. X-ray diffraction (XRD), transmission electron microscopy (TEM), and scanning electron microscopy (SEM) were used for structural characterization of the films. Properties of the films determined included color, mechanical and dynamic mechanical properties, thermal stability, and water vapor permeability (WVP). The arrangement of MMT in the bio-nanocomposite matrix ranged from exfoliated to intercalated depending on the type and content of modified MMT. At a MMT content of 5%, bio-nanocomposite films based on modified MMTs (Cloisite 20A and Cloisite 30B) had better mechanical, dynamic mechanical, and water barrier properties as compared to those based on natural MMT (Cloisite Na^+). Bio-nanocomposite films based on 10% Cloisite 30B had mechanical properties comparable to those of some of the plastics which are currently used in food packaging applications. However, much higher WVP values of these films as compared to those of existing plastics might limit the application of these films to packaging of high moisture foods such as fresh fruits and vegetables.

Keywords: bio-nanocomposite films, soy protein isolate, modified montmorillonite, structural characterization, mechanical properties, water barrier properties

Introduction

The non-degradable and non-renewable nature of plastic packaging has led to a renewed interest in packaging materials based on biopolymers derived from renewable sources. The use of biopolymer-based packaging materials can solve the waste disposal problem to a certain extent. The increased interest in biopolymer-based packaging has resulted in the development of protein-based films from soy protein, whey protein, casein, collagen, corn zein, gelatin, and wheat gluten (Cuq and others 1998). Among all the protein sources, soy proteins have attracted attention as a potential source for bio-based packaging materials because it has excellent film forming properties (Brandenburg and others 1993; Gennadios and others 1993; Zhang and others 2001; Park and others 2001; Mauri and Anon 2006; Kurose and others 2007). Soy protein isolate (SPI) is a commercial form of soy protein that contains more than 90% protein. Soy proteins are classified as 2S, 7S, 11S, and 15S based on their sedimentation rate in fractional ultracentrifugation. Larger Svedberg (S) number indicates a larger protein (Hernandez-Izquierdo and Krochta 2008). 7S (β-conglycinin) and 11S (glycinin) fractions of soy proteins, constituting about 90% of total protein, have the ability of polymerization, resulting in the formation of films. β-conglycinin (molecular weight of 140-170 kDa) consists of three types of subunits with molecular weights of 58, 57, and 42 kDa. Glycinin (molecular weight of 340-375 kDa) consists of 6 acidic (35 kDa) and 6 basic (35 kDa) polypeptide chains which are linked together by disulfide bonds (Petruccelli and Anon 1995).

SPI-based packaging films cannot meet the requirements of a cost-effective film with mechanical and barrier properties similar to those of plastics. Mechanical properties of

interest in food packaging are tensile modulus (TM), tensile strength (TS), and percent elongation (%E) at break. Tensile modulus is a measure of stiffness of a material. Tensile strength is the maximum tensile stress a film can sustain whereas %E is an indication of flexibility of a film. Barrier properties of interest are water vapor permeability (WVP) and oxygen permeability (OP). Biopolymers made from SPI alone are extremely brittle. Plasticizers such as glycerol and polyethylene glycol impart flexibility to SPI-based biopolymer films. However, the use of plasticizers leads to significant decrease in tensile strength (TS) of the films (Wang and others 1996). Soy protein-based films have been reported to have oxygen permeability (OP) similar to that of plastic films (Brandenburg and others 1993). However, they have higher water vapor permeability (WVP) as compared to plastic films due to the hydrophilic nature of proteins. Therefore, research has been geared to develop techniques to improve mechanical and water vapor barrier properties of soy protein-based packaging materials.

Recently, a new class of materials represented by bio-nanocomposites (biopolymer matrix including proteins reinforced with nanoparticles such as montmorillonite) has proven to be a promising option in improving mechanical and barrier properties of biopolymers. The bio-nanocomposites consist of a biopolymer matrix reinforced with particles (nanoparticles) having at least one dimension in the nanometer range (1-100 nm) and exhibit much improved properties due to high aspect ratio and high surface area of nanoparticles (Ray and Bousmina 2005; Rhim and Ng 2007; Zhao and others 2008). The most common class of materials used as nanoparticles are layered clay minerals such as montmorillonite (MMT), hectorite, sapnotite, and laponite. These clay minerals have been proven to be very effective due to

their unique structure and properties. These clay minerals belong to the general family of 2:1 layered silicates indicating that they have 2 tetrahedral sheets sandwiching a central octahedral sheet (Zeng and others 2005). MMT has very high elastic modulus (178 GPa) as compared to most biopolymers. The high value of elastic modulus enables MMT to improve the mechanical properties of biopolymers by carrying a significant portion of the applied stress (Fornes and Paul 2003).

There are four possible arrangements of layered clays dispersed in a polymer matrix – phase separated or immiscible (microcomposite), intercalated, exfoliated, and disordered intercalated (partially exfoliated). In an immiscible arrangement, platelets of layered clays exist as tactoids (stack of platelets) and the polymer encapsulates these tactoids. Intercalation occurs when a monolayer of extended polymer chains penetrates into the galleries (gaps between layers of clay) of the layered silicates. Intercalation results in finite expansion (2-3 nm) of the silicate layers. However, these silicate layers remain parallel to each other. Extensive penetration of polymer chains into the galleries of layered silicate leads to exfoliation or delamination of silicate layers. Clay platelets are separated by 10 nm or more during exfoliation. An exfoliated nanocomposite consists of nanoparticles distributed homogeneously throughout the polymer matrix (Dennis and others 2001; Zeng and others 2005).

Bio-nanocomposites can be obtained by several methods which include in-situ polymerization, solution exfoliation, and melt intercalation. In the in-situ polymerization method, monomers are intercalated into layered clays and subsequently polymerized via heat, radiation, or catalyst. In solution exfoliation, layered clays are exfoliated into single platelets

using a solvent and the polymer is adsorbed onto the platelets by mixing in the clay suspension. In melt intercalation, layered clays are mixed with the polymer matrix in molten state (Zeng and others 2005). A few studies on the preparation of SPI-MMT bio-nanocomposites by solution exfoliation method have been reported (Dean and Yu 2005; Rhim and others 2005; Chen and Zhang 2006). In our recent work, bio-nanocomposite films based on SPI and MMT with improved properties were prepared using melt extrusion (Kumar and others 2009). There was a significant improvement in mechanical (tensile strength and percent elongation at break) and dynamic mechanical properties (glass transition temperature and storage modulus), thermal stability, and water vapor permeability of the films with the addition of MMT. However, the results showed that there is a need to further improve the properties of SPI-MMT films for commercial application.

Exfoliation is the desirable arrangement for improving the properties of nanocomposites. However, exfoliation is harder to achieve during processing because layered clays such as MMT have a strong tendency to agglomerate because of their hydrophilic nature. Better exfoliation can be achieved by increasing the interlayer distance (d-spacing) between clay layers because it enables biopolymer chains to penetrate easily into the galleries of layered clays. The d-spacing of the layered silicates can be increased by ion exchange reaction of sodium ions present in natural MMT with various organic cations such as primary or quaternary amine (Li and others 2006). The influence of the type of organic modifier (primary and secondary amine) and the extent of surface coverage of clay on the structure and mechanical properties of nanocomposites based on polypropylene and MMT has been investigated by Li and others (2006). The results showed that MMT modified with

quaternary amine had longer interlayer distances and resulted in nanocomposites with improved mechanical properties. The interlayer distance also increased with an increase in the surface coverage of clays with organic modifiers. Borse and Kamal (2006) prepared polyamide-6 (PA-6) nanocomposites using a natural MMT (Cloisite Na^+) and two modified MMTs (Cloisite 30B and Cloisite 15A). The results showed that Cloisite 30B produced exfoliated structures, Cloisite 15A produced partially exfoliated structures, and Cloisite Na^+ produced phase separated structures.

Very few studies on the properties of bio-nanocomposites based on modified MMT have been reported in literature. Lee and others (2002) prepared bio-nanocomposites based on aliphatic polyester and two different types of MMT (Cloisite 30B and Cloisite 10A). Bio-nanocomposites based on Cloisite 30B showed higher degree of intercalation as compared to those based on Cloisite 10A. This was attributed to strong hydrogen bonding between aliphatic polyester and hydroxyl group in the organic modifier of Cloisite 30B. Paul and others (2003) prepared bio-nanocomposites based on polylactic acid (PLA) and different types of MMT (Cloisite Na^+, Cloisite 20A, Cloisite 25A, and Cloisite 30B) using melt blending and studied the effect of MMT type and content on the structure and thermal properties of bio-nanocomposites. The results showed that improvement in thermal stability was more pronounced for Cloisite 30B as compared to other MMT types. Magalhaes and Andrade (2009) prepared bio-nanocomposites based on thermoplastic corn starch and two different types of MMT (natural MMT and Cloisite 30B) using melt extrusion. Scanning electron microscopy (SEM) results showed that bio-nanocomposites based on Cloisite 30B showed a higher degree of exfoliation.

The above mentioned studies show that the type of organic modifier has an important influence on the structure and properties of bio-nanocomposites based on modified MMT. Therefore, the objective of this study was to study the effect of different types (Cloisite 20A and Cloisite 30B) and contents (0-15%) of modified MMT on the structure (degree of intercalation and exfoliation) and properties (color, mechanical, dynamic mechanical, thermal stability, and water vapor permeability) of SPI-MMT bio-nanocomposite films.

Materials and Methods

Materials

Soy protein isolate (Supro 760) with a protein content of 92.5 % (dry basis) was obtained from Protein Technologies International (St. Louis, MO). Two types of modified montmorillonites (Cloisite 20A and Cloisite 30B) were obtained from Southern Clay Products (Austin, TX). Cloisite 20A and Cloisite 30B are MMTs modified by the addition of quaternary ammonium salts. Cloisite 20A contains dimethyl dihydrogenated tallow ammonium chloride whereas Cloisite 30B contains methyl tallow bis-2-hydroxyethyl ammonium chloride. Tallow is derived from beef and is predominantly composed of chains with 18 carbons (~65% C18; ~30% C16; ~5% C14). Hydrogenated tallow is derived from tallow by hydrogenation of the double bonds (Cui and others 2008). Cloisite 20A, containing two tallow groups, is more hydrophobic than Cloisite 30B. The properties of modified MMTs used this in study are given in Table 1. Glycerol, used as a plasticizer, was obtained from Fisher Scientific (Pittsburg, PA). Glycerol was chosen as the plasticizer because it is nontoxic whereas other potential polyhydric alcohols such as propylene glycol and ethylene glycol are toxic and hazardous (Wang and others 1996).

Preparation of SPI-MMT nanocomposites

Process flow diagram for the preparation and characterization of soy protein isolate (SPI)-montmorillonite (MMT) bio-nanocomposite films is shown in Figure 1. The formulation consisted of SPI (70-85%, dry basis), glycerol (15%, dry basis), and MMT (0-15%, dry basis). All three types of clays (Cloisite Na^+, Cloisite 20A, and Cloisite 30B) were used at four different levels (0, 5, 10, and 15%). The ingredients were mixed and left at room

temperature for 2 hours for hydration. The mixture was subsequently extruded in a twin-screw co-rotating extruder (ZSK 26, Coperion Corp., Ramsey, NJ). The extruder had screw diameter of 25 mm and length to diameter ratio (L/D) of 20. The extruder was operated at a screw speed of 100 rpm. The extruder had a 5 head barrel configuration. Temperatures in the 5 head barrel were maintained at 70, 90, 100, 110, and 90 °C respectively. The extrudate was dried in an oven at 50 °C for 48 hrs. The dried extrudate was ground in a grinder (MicroMill, Bel-Art Products, Pequannock, NJ) for further testing and film casting.

Film casting

Bio-nanocomposite powders (4% w/v) and deionized water were mixed for 30 min at room temperature. pH of the suspension was adjusted to 9 by adding 1 M NaOH. The suspension was heated to 95 °C and held at that temperature for 20 min with continuous stirring. Subsequently, the solution was cooled to 65 °C and 25 ml of the suspension was poured in 10 cm diameter petri dishes for casting nanocomposite films. The cast petri dishes were dried at ambient conditions for 48 hours. The dried films were peeled off the petri dish and pre-conditioned before further testing.

Structural characterization of SPI-MMT films

X-ray diffraction (XRD)

X-ray diffraction studies of bio-nanocomposite powders were performed with a diffraction unit (MS Philips XLF ATPS XRD 100, Omni Scientific Instruments, Biloxi, MS) operating at 35 kV and 25 mA. The radiation was generated from a Cu-Kα source with a wavelength (λ) of 0.154 nm. The diffraction data was collected from 2θ values of 2.5 to 10° with a step size of 0.01°, where θ is the angle of incidence of the X-ray beam on the sample.

Transmission electron microscopy (TEM)

The structure and morphology of bio-nanocomposite powders were visualized by a transmission electron microscope (Hitachi HF2000, Hitachi High-Technologies Europe GmbH, Krefeld, Germany) operating at 200 kV. Samples of bio-nanocomposite powders were prepared by suspending the powders in methanol. The suspension was sonicated for 5 min in an ultrasonic bath (Branson 1510, Branson Ultrasonics Co., Danbury, CT). A drop of the suspension was put on a fine-mesh carbon-coated TEM support grid (C-flat^{TM}, Protochips Inc., Raleigh, NC). After drying in air, the nanocomposite powder remained attached to the grid and was viewed under the transmission electron microscope.

Scanning electron microscopy (SEM)

The morphology of the fracture surface (cross-sectional surface) of the bio-nanocomposite films were visualized using a field emission scanning electron microscope (JEOL 6400F, Japan Electron Optics Ltd., Tokyo, Japan) operating at 5 kV. Small pieces (0.5 × 0.5 cm) of bio-nanocomposite films were frozen in liquid nitrogen, cut using a sharp razor blade, and mounted on specimen stubs with 2 sided carbon tape. The fracture surfaces of the films were sputter-coated with a thin layer (~8-10 nm) of gold-palladium (Au-Pd) using a sputter-coater (Hummer II, Anatech Ltd., Union City, CA). After coating, the samples were viewed under the scanning electron microscope.

Measurement of properties of SPI-MMT films

Film thickness

Thickness of the films was measured at five different randomly selected locations using a digital micrometer (CO 030025, Marathon Watch Company Ltd., Ontario, Canada).

The average value of the film thickness was used in determining mechanical properties, dynamic mechanical properties, and water vapor permeability.

Color

Color values of the films were measured with a Chroma Meter (CR-300, Minolta Camera Co., Osaka, Japan). Films were placed on the surface of a white standard plate (calibration plate CR-200) and the Hunter-Lab color scale {L: 0 (black) to 100 (white); a: -80 (green) to 100 (red); b: -80 (blue) to 70 (yellow)} was used to measure color. D_{65}, which represents daylight at noon, was used as the light source. Total color difference (ΔE), yellowness index (YI), and whiteness index (WI) were calculated as (Rhim and others 1999):

$$\Delta E = \left(\Delta L^2 + \Delta a^2 + \Delta b^2\right)^{0.5}$$
$$YI = \frac{142.86\,b}{L} \qquad (1)$$
$$WI = 100 - \left((100 - L)^2 + \Delta a^2 + \Delta b^2\right)^{0.5}$$

where $\Delta L = L_{standard} - L_{sample}$; $\Delta a = a_{standard} - a_{sample}$; $\Delta b = b_{standard} - b_{sample}$. Values of L, a, and b for the standard white plate were 96.87, 0.19, and 2.00 respectively. ΔE indicates the color difference from the standard plate whereas YI and WI indicate the degree of yellowness and whiteness respectively. Three specimens of each film sample were evaluated.

Mechanical properties

Tensile strength (TS) and percent elongation (%E) at break of the bio-nanocomposite films were determined by tensile testing using a Universal Testing Machine (model 5565, Instron, Corp., Canton, MA) equipped with a 5 kN static load cell according to the ASTM standard D882-02 (ASTM Standards 2002). The length and width of the film samples were 5

cm and 2.5 cm respectively. The initial grid separation was set at 2.5 cm and the cross-head speed was 50 cm/min. Stress vs. strain curves were plotted. Tensile strength was calculated by dividing peak load by initial specimen cross-sectional area. Percent elongation at break was calculated as the percentage change in length of the specimen between the grips. Three specimens of each sample were evaluated.

Dynamic mechanical properties

The dynamic mechanical properties of bio-nanocomposite films were determined using a dynamic mechanical analyzer (Q800, TA Instruments, New Castle, DE). Dynamic mechanical analysis (DMA) was performed in tension mode at a frequency of 1 Hz and an amplitude of 15 μm. The length and width of the film samples were 4 cm and 0.6 cm respectively. The samples were heated from 40 °C to 200 °C at a heating rate of 5 °C/min. The storage modulus (E'), loss modulus (E''), and loss tangent (tan δ = E''/ E') were recorded as a function of temperature. Glass transition temperature (T_g) was determined as the temperature at which tan δ attained its peak value.

Thermal stability

The thermal stability of bio-nanocomposite films were investigated using a thermogravimetric analyzer (Pyris 1 TGA, Perkin Elmer, Shelton, CT). The mass of the sample used varied from 10 to 12 mg. Thermogravimetric analysis (TGA) was carried out under air flow. The temperature of the sample was increased from room temperature to 900 °C at a heating rate of 20 °C/min. Weight loss of the sample was measured as a function of temperature. Three parameters were determined from the TGA data: the temperature at 10% weight loss, the temperature at 50% weight loss, and the yield of charred residue at 850 °C.

Water vapor permeability

Water vapor permeability (WVP) of the bio-nanocomposite films was determined according to ASTM E96-05 (ASTM Standards 2005). The sample film was cut into a circle of 8.75 cm diameter. The sample was placed on a test dish (8.2 cm in diameter and 1.9 cm in depth) filled with 50 ml deionized water to expose the films to 100% relative humidity. The test dishes were sealed and a turntable carrying 8 test dishes was rotated uniformly to ensure that all dishes were exposed to the same average ambient conditions during the test. The setup was subjected to a temperature and relative humidity of 22 °C and 65% respectively. The test dishes were allowed to equilibrate for two hours before taking the initial weight. The final weight was taken after a 24 hour interval. Water vapor transmission rate (WVTR) was calculated as (ASTM Standards 2005):

$$\mathrm{WVTR} = \frac{\mathrm{G}}{\mathrm{t\,A}} \tag{2}$$

where G is the change in weight (g), t is the time (hr), and A is the area of the mouth of the test dish (m^2). Water vapor permeability (WVP) was calculated as (ASTM standards 2005):

$$\mathrm{WVP} = \frac{\mathrm{WVTR} \times \mathrm{L}}{\Delta \mathrm{P}} \tag{3}$$

where L is the thickness of the test specimen (mm) and ΔP is the partial pressure difference of water vapor across the film. WVP of two specimens for each sample was calculated and reported.

Statistical analysis

All experiments were performed in duplicate. Statistical analysis was performed using Minitab statistical software (Minitab Inc., State College, PA). Data were analyzed by

general linear model (GLM). Differences at $P < 0.05$ were considered to be significant. Pair-wise comparison of all means was performed using Tukey's multiple comparison procedure.

Results and Discussion

Effect of modified MMTs on the structure of powders/films

XRD patterns of Cloisite 20A and SPI-Cloisite 20A (0%, 5%, 10%, and 15%) bio-nanocomposite powders are shown in Figure 2. Powders of Cloisite 20A showed a diffraction peak at a 2θ angle of 3.56°. Interlayer distance (d or d-spacing) between clay layers can be estimated from Bragg's equation (Kasai and Kakudo 2005):

$$d = \frac{\lambda}{2\sin\left(\frac{\pi\theta}{180}\right)} \quad (4)$$

where λ is the wavelength of X-ray beam. The d-spacing of Cloisite 20A corresponding to the diffraction peak was calculated to be 2.48 nm. This is in close agreement with the d-spacing value of 2.42 nm provided by the supplier (Table 1). XRD patterns of Cloisite 30B and SPI-Cloisite 30B (0%, 5%, 10%, and 15%) bio-nanocomposite powders are shown in Figure 3. The d-spacing of Cloisite 30B corresponding to the diffraction peak at a 2θ angle of 5.0° was calculated to be 1.77 nm. This is in close agreement with the d-spacing value of 1.85 nm provided by the supplier (Table 1). There was no diffraction peak in the 2θ range of 2.5° to 10° for the bio-nanocomposites at all MMT contents of Cloisite 20A and Cloisite 30B. Due to the limitation of the XRD instrument, diffraction patterns below a 2θ value of 2.5° could not be observed. Absence of diffraction peaks for SPI-MMT bio-nanocomposites suggests that the layers of MMTs have a d-spacing of at least 3.53 nm (corresponding to a 2θ value of 2.5°) in all the bio-nanocomposites.

TEM images of SPI-MMT bio-nanocomposite powders with 5% and 15% contents of Cloisite 20A and Cloisite 30B are shown in Figure 4. The dark lines in the TEM images

correspond to MMT platelets and the gap between two adjacent lines is the d-spacing. It can be seen from Figures 4a and 4c that the MMT layers are exfoliated in bio-nanocomposites with MMT content of 5%. At MMT content of 15%, MMT layers are intercalated in bio-nanocomposites with Cloisite 20A (Figure 4b) whereas the arrangement of MMT changed from exfoliated to disordered intercalated (Figure 4d) for bio-nanocomposites with Cloisite 30B. However, d-spacing values, which ranged from 4 to 10 nm, were higher than the detection limit of XRD analysis (3.53 nm). This explains the absence of diffraction peaks for these bio-nanocomposites in the XRD analysis. It can also be concluded that XRD by itself is insufficient to characterize the structure of nanocomposites for intercalated and disordered intercalated arrangements. Therefore, XRD studies should always be complemented with microscopy techniques such as TEM or SEM.

SEM images of the fracture surface (cross-sectional surface) of SPI-MMT bio-nanocomposite films with 5% and 15% contents of Cloisite 20A and Cloisite 30B are shown in Figure 5. The white strands in the SEM images correspond to MMT platelets. At a MMT content of 5%, MMT platelets were well dispersed in the bio-nanocomposite films (Figures 5a and 5c). This suggests exfoliation of MMT in the bio-nanocomposite film with MMT content of 5%. The fracture surface of the films with both Cloisite 20A and Cloisite 30B became rougher as the MMT content increased to 15% (Figures 5b and 5d). In agreement with the TEM results of intercalated structures, larger aggregates of Cloisite 20A were found in bio-nanocomposite films with MMT content of 15% (Figure 5d).

Based on the XRD, TEM, and SEM results, it can be concluded that extrusion of SPI and modified MMTs resulted in bio-nanocomposites with exfoliated structures at lower

MMT content (5%). At higher MMT content (15%), the structure of bio-nanocomposites ranged from intercalated for Cloisite 20A to disordered intercalated for Cloisite 30B.

Effect of modified MMTs on the properties of films

Hunter color values (L, a, and b) of films based on SPI and modified MMTs are shown in Table 2. SPI films without modified MMTs were translucent and yellow with L, a, and b values of 81.42, 3.61, and 44.14 respectively. Changes in color can be better described using color functions such as total color difference (ΔE), whiteness index (WI), and yellowness index (YI). There was a significant ($P < 0.05$) increase in WI of the films with the addition of 5% of modified MMTs. Further addition of modified MMTs had insignificant effect on WI. In contrast, there was a significant ($P < 0.05$) decrease in YI of the films with the addition of 5% of modified MMTs. Further addition of modified MMTs had insignificant effect on YI. It can be concluded from these results that the SPI-MMT films were lighter (higher WI) and less yellow (lower YI) as compared to those of SPI films.

Effect of type and content of modified MMTs on tensile strength of SPI-MMT films is shown in Table 3. Analysis of variance using the general linear model showed that the effects of clay type, clay content, and interaction between clay type and content on TS were significant ($P < 0.05$). Tensile strength of SPI films was 2.26 ± 0.41 MPa. The values of TS for bio-nanocomposite films with 5% of Cloisite 20A and Cloisite 30B were 12.40 ± 0.65 MPa and 15.11 ± 0.86 MPa respectively. Kumar and others (2009) reported a TS value of 6.28 ± 0.88 MPa for bio-nanocomposite films based on SPI and 5% natural MMT (Cloisite Na^+). The density of natural MMT is 2.86 g/cm^3 whereas the density values of Cloisite 20A and Cloisite 30B are 1.77 and 1.98 g/cm^3. At the same MMT content, Cloisite 20A and

Cloisite 30B have higher volume fractions in the bio-nanocomposites as compared to that of natural MMT. It has been reported that the improvement in properties of nanocomposites is proportional to the volume fraction of nanoparticles (Fornes and Paul 2003). Modified MMTs also have longer d-spacing values as compared to that of natural MMT. This enables better interaction of SPI with modified MMT because biopolymer chains of soy proteins can penetrate easily into the galleries of modified MMTs. Thus, the higher TS values for modified MMTs might be attributed to higher volume fraction at the same MMT content and better interaction of SPI with modified MMTs.

As MMT content increased to 10%, TS of Cloisite 20A films increased and then TS of the films decreased above 10%. Fornes and Paul (2003) reported that intercalation of layered clays in nanocomposites reduces their reinforcing efficiency due to decrease in aspect ratio and effective modulus of clays. Bio-nanocomposites with Cloisite 20A had intercalated structures at 15%. This can explain the decrease in TS of films of Cloisite 20A at a content of 15%. TS of Cloisite 30B films increased continuously as MMT content increased. However, there was only a slight increase in TS above 5% which is due to disordered intercalated structures in bio-nanocomposites with Cloisite 30B at higher MMT contents.

Effect of type and content of modified MMTs on percent elongation (%E) at break of SPI-MMT films is shown in Table 4. Analysis of variance using the general linear model showed that the effects of clay type, clay content, and interaction between clay type and content on %E were significant ($P < 0.05$). Percent elongation at break of SPI films was 11.85 ± 0.39. The values of %E for bio-nanocomposite films with 5% of Cloisite 20A and Cloisite 30B were 42.80 ± 0.57 and 81.60 ± 2.83 respectively. As MMT content increased to

10%, %E of Cloisite 20A and Cloisite 30B films increased and then %E of the films decreased above 10%. This is attributed to the restricted motion of soy protein molecules in bio-nanocomposite films due to incorporation of MMT and interaction of SPI with MMT.

TS values of films containing 10% of both modified MMTs are comparable to those of low density polyethylene (LDPE) and polyvinylidene chloride (PVDC) which are currently used in food packaging applications (8.2-31.4 MPa for LDPE and 19.3-34.5 MPa for PVDC). However, %E values for these plastic films range from 100%-900% (Selke 1997). Maximum %E value obtained for SPI-MMT films was 103.6% which was obtained with Cloisite 10% 30B. This shows the potential of films based on SPI and Cloisite 30B to be used in flexible food packaging to replace some of the existing plastics such as LDPE and PVDC.

Effect of temperature on tan δ of bio-nanocomposite films based on SPI and modified MMTs at MMT contents of 0%, 5%, and 15% is shown in Figure 6. Glass transition temperature (T_g) was determined from the peak in tan δ curve. Analysis of variance using the general linear model showed that the effects of clay type, clay content, and interaction between clay type and content on T_g were significant ($P < 0.05$). SPI films had a T_g of 119.7 ± 1.9 °C which is in the range of T_g (111.9-150 °C) of SPI films as reported by Ogale and others (2000). The values of T_g for bio-nanocomposite films with 5% of Cloisite 20A and Cloisite 30B were 154.7 ± 0.8 °C and 148.1 ± 0.8 °C respectively. Kumar and others (2009) reported a T_g value of 142.8 ± 2.1 °C for bio-nanocomposite films based on SPI and 5% natural MMT (Cloisite Na^+). It can be seen from Figure 6 that there was a slight increase in T_g as MMT content increased from 5% to 15%. However, the magnitude of the peak value of

tan δ decreased as MMT content increased from 5% to 15%. The magnitude of tan δ peak is an indication of the motion of polymer chains in amorphous phase (Yu and others 2004). The reduced magnitude of tan δ peak at higher MMT contents can be attributed to restricted motion of biopolymer chains of SPI due to the interaction of SPI with MMT.

Effect of temperature on storage modulus (E') of bio-nanocomposite films based on SPI and modified MMTs at MMT contents of 0%, 5%, and 15% is shown in Figure 7. Over the entire temperature range, E' of SPI-MMT films was significantly ($P < 0.05$) higher than that of SPI films. Storage modulus of SPI films at 40 °C was 337 ± 31 MPa. The values of storage modulus for bio-nanocomposite films with 5% Cloisite 20A and Cloisite 30B were 1164 ± 37 MPa and 870 ± 53 MPa respectively. Kumar and others (2009) reported a storage modulus value of 529 ± 24 MPa for bio-nanocomposite films based on SPI and 5% natural MMT (Cloisite Na^+). In agreement with the tensile strength results, the higher E' values for modified MMTs is attributed to higher volume fraction at the same MMT content and better interaction of SPI with modified MMTs.

TGA curves of bio-nanocomposite films based on SPI and modified MMTs at MMT contents of 0%, 5%, and 15% are shown in Figure 8. It can be seen from Figure 8 that there are 3 steps of thermal degradation of the films in the temperature range of 100 to 900 °C. The temperature range for the first step of thermal degradation is 100 to 150 °C. This corresponds to the loss of water from the films. The temperature range for the second step of thermal degradation is 300 to 400 °C. This corresponds to the decomposition of soy protein, decomposition of organic modifiers of modified MMT, and loss of glycerol from the films. The third step of thermal degradation is in the temperature range of 500 to 750 °C. This

might be due to oxidation of partially decomposed soy protein and organic modifiers under air flow. Similar results for different types of bio-nanocomposite films have been reported (Tunc and others 2007).

The temperature at 50% weight loss (during TGA) for SPI films was 355.5 ± 2.2 °C. The temperatures at 50% weight loss for bio-nanocomposite films with 5% of Cloisite 20A and Cloisite 30B were 367.7 ± 1.7 °C and 378.6 ± 2.3 °C respectively. These temperatures are comparable to the temperature at 50% weight loss of 377.3 ± 2.6 °C for bio-nanocomposite films based on SPI and 5% natural MMT (Cloisite Na^+) as reported by Kumar and others (2009). As the MMT content increased, the bio-nanocomposite films exhibited a significant delay in weight loss at temperatures greater than 500 °C. The yield of charred residue at 850 °C for SPI films was 4.2 ± 0.3%. The yields of charred residue at 850 °C for bio-nanocomposite films with 15% of Cloisite 20A and Cloisite 30B were 10.9 ± 0.6% and 11.2 ± 0.4% respectively. These yields of charred residue for modified MMTs are much lower than that (20.5 ± 0.4%) of bio-nanocomposite films based on SPI and 15% natural MMT (Cloisite Na^+) as reported by Kumar and others (2009). This reduction in yields of charred residue is attributed to the thermal decomposition of organic modifier of modified MMTs. Cloisite 20A and Cloisite 30B contain 36.4% and 52.4% of organic modifiers respectively (Table 1). Cervantes-Uc and others (2007) reported that the onset temperatures of thermal degradation for Cloisite 20A and Cloisite 30B are198 °C and 174 °C respectively. This was attributed to the thermal decomposition of organic modifiers of the modified MMTs. In another study, Kim and White (2005) reported that Cloisite 20A and Cloisite 30B

yield 68% and 72% of solid residues at 800 °C whereas the solid residue at 800 °C corresponding to natural MMT (Cloisite Na^+) was 88%.

Effect of type and content of modified MMTs on water vapor permeability (WVP) of SPI-MMT films is shown in Table 5. Higher WVP is one of the major limitations in using protein based films as food packaging materials. Therefore, reduction in WVP is desirable for potential applications in food packaging. Analysis of variance using the general linear model showed that the effects of clay type, clay content, and interaction between clay type and content on WVP were significant ($P < 0.05$). SPI films had a WVP of 3.80 ± 0.11 g-mm/(m^2-hr-kPa) which is comparable to the WVP (1.62-6.42 g-mm/(m^2-hr-kPa)) of soy protein-based films as reported in literature (Krochta 2002). The values of WVP for films with 5% Cloisite 20A and Cloisite 30B reduced by 30.8% and 18.7% respectively. Kumar and others (2009) reported a reduction of 22.1% for bio-nanocomposite films based on SPI and 5% natural MMT (Cloisite Na^+). The reduction in WVP by MMT has been attributed to the creation of a tortuous pathway for water vapor to diffuse out of the bio-nanocomposite matrix. This increases the effective path length for diffusion of water vapor molecules, thus reducing WVP (Zeng and others 2005). At 5% MMT content, greater reduction in WVP associated with Cloisite 20A is attributed to the hydrophobic nature of Cloisite 20A. For Cloisite 20A, there was a slight decrease in WVP as the MMT content increased from 10% to 15%. This can be explained by the formation of intercalated structures in bio-nanocomposites based on Cloisite 20A at higher MMT content (15%) as observed in TEM and SEM results. As the MMT content increased from 0% to 15%, WVP for films containing Cloisite 20A and Cloisite 30B reduced by 46.1% and 38.7% respectively. However, the WVP values for SPI-

MMT films are still much higher as compared to those {0.001 g-mm/(m^2-hr-kPa) for LDPE and 0.01 g-mm/(m^2-hr-kPa) for PVDC} of LDPE and PVDC which are currently used in food packaging applications (Krochta 2003; Lange and Wyser 2003). This might limit the application of these bio-nanocomposite films to packaging of high moisture foods such as fresh fruits and vegetables.

Conclusions

Bio-nanocomposite films based on soy protein isolate (SPI) and modified montmorillonite (MMT) with improved properties were prepared using melt extrusion. The arrangement of MMT in the bio-nanocomposite matrix ranged from exfoliated to intercalated depending on the type and content of modified MMT. Bio-nanocomposite films based on modified MMTs were lighter (higher WI) and less yellow (lower YI) as compared to those of SPI films. At a MMT content of 5%, bio-nanocomposite films based on modified MMTs (Cloisite 20A and Cloisite 30B) had better mechanical (tensile strength and percent elongation at break), dynamic mechanical (glass transition temperature and storage modulus), and water barrier properties as compared to those based on natural MMT (Cloisite Na^+). However, films based on modified MMTs were thermally less stable at temperatures higher than 500 °C as compared to films based on natural MMT. Bio-nanocomposite films based on 10% Cloisite 30B had mechanical properties comparable to those of LDPE and PVDC which are currently used in food packaging applications. Thus, this study shows the potential of films based on SPI and Cloisite 30B to be used in flexible food packaging to replace some of the existing plastics such as LDPE and PVDC. However, much higher WVP values of these films as compared to those of LDPE and PVDC might limit the application of these bio-nanocomposite films to packaging of high moisture foods such as fresh fruits and vegetables. Some of the other challenges associated with commercial application of these bio-nanocomposite films include higher cost of ingredients and complexity associated with the approval of these bio-nanocomposite films as food contact materials.

Acknowledgments

Support for the research study undertaken here, resulting in the publication of paper nr FSR-09-38 of the Journal Series of the Dept. of Food, Bioprocessing, and Nutrition Sciences, NCSU, Raleigh, NC 27695-7624 from USDA-NRICGP Grant nr 2008-01503, titled: Development of cross-linked bio-nanocomposite packaging films with enhanced barrier and mechanical properties, is gratefully acknowledged. We would also like to thank Birgit Anderson, Gail Liston, Roberto Garcia, Chuck Mooney, Jonathan Pierce, and Sharon Ramsey for their assistance in conducting the experiments.

The use of trade names in this publication does not imply endorsement by the North Carolina Agricultural Research Service of the products named nor criticism of similar ones not mentioned.

References

ASTM Standards. 2002. D882-02. Standard test method for tensile properties of thin plastic sheeting. Philadelphia, PA.

ASTM Standards. 2005. E96-05. Standard test methods for water vapor transmission of materials. Philadelphia, PA.

Borse NK, Kamal MR. 2006. Melt processing effects on the structure and mechanical properties of PA-6/clay nanocomposites. Polymer engineering and science 46(8): 1094-1103.

Brandenburg AH, Weller CL, Testin RF. 1993. Edible films and coatings from soy protein. Journal of food science 58: 1086-1089.

Cervantes-Uc JM, Cauich-Rodriguez JV, Vazquez-Torres H, Garfias-Mesias LF, Paul DR. 2007. Thermal degradation of commercially available organoclays studied by TGA-FTIR. Thermochimica acta 457: 92-102.

Chen P, Zhang L. 2006. Interaction and properties of highly exfoliated soy protein/montmorillonite nanocomposites. Biomacromolecules 7: 1700-1706.

Cui L, Khramov DM, Bielawski CW, Hunter DL, Yoon PJ, Paul DR. 2008. Effect of organoclay purity and degradation on nanocomposite performance, part 1: surfactant degradation. Polymer 49: 3751-3761.

Cuq B, Gontard N, Guilbert S. 1998. Proteins as agricultural polymers for packaging production. Cereal chemistry 75(1): 1-9.

Dean K, Yu L. 2005. Biodegradable protein-nanoparticles composites. In: Smith R, editor. Biodegradable Polymers for Industrial Applications. UK: Woodhead Publishing Ltd. p 289-312.

Dennis HR, Hunter DL, Chang D, Kim S, White JL, Cho JW, Paul DR. 2001. Effect of melt processing conditions on the extent of exfoliation in organoclay-based nanocomposites. Polymer 42: 9513-9522.

Fornes TD, Paul DR. 2003. Modeling properties of nylon 6/clay nanocomposites using composite theories. Polymer 44: 4993-5013.

Gennadios A, Brandenburg AH, Weller CL, Testin RF. 1993. Effect of pH on properties of wheat gluten and soy protein isolate films. Journal of agricultural and food chemistry 41: 1835-1839.

Hernandez-Izquierdo VM, Krochta JM. 2008. Thermoplastic processing of proteins for film formation – a review. Journal of food science 73(2): R30-R39.

Kasai K, Kakudo M. 2005. X-ray diffraction by macromolecules. New York: Springer. 504 p.

Kim Y, White JL. 2005. Formation of polymer nanocomposites with various organoclays. Journal of applied polymer science 96: 1888-1896.

Krochta JM. 2002. Proteins as raw materials for films and coatings: definitions, current status, and opportunities. In: Gennadios A, Editor. Protein-based Films and Coatings. Boca Raton, FL: CRC press. p 1-41.

Krochta JM. 2003. Package permeability In: Heldman DR, editor. Encyclopedia of Agricultural, Food, and Biological engineering. NY: Marcel Dekker, Inc. p 720-726.

Kumar P, Sandeep KP, Alavi S, Truong VD, Gorga RE. 2009. Preparation and characterization of bio-nanocomposite films based on soy protein isolate and montmorillonite using melt extrusion. Journal of food science (submitted).

Kurose T, Urman K, Otaigbe JU, Lochhead RY, Thames SF. 2007. Effect of uniaxial drawing of soy protein isolate biopolymer films on structure and mechanical properties. Polymer engineering and science 47(4): 374-380.

Lange Y, Wyser Y. 2003. Recent innovations in barrier technologies for plastic ackaging – a review. Packaging technology and science 16: 149-158.

Lee SR, Park HM, Lim H, Kang T, Li X, Cho WJ, Ha CS. 2002. Microstructure, tensile properties, and biodegradability of aliphatic polyester/clay nanocomposites. Polymer 43: 2495-2500.

Li J, Ton-That MT, Tsai SJ. 2006. PP-based nanocomposites with various intercalant types and intercalant coverages. Polymer engineering and science 46 (8): 1060-1068.

Magalhaes NF, Andrade CT. 2009. Thermoplastic corn starch/clay hybrids: effects of clay type and content on physical properties. Carbohydrate polymers 75: 712-718.

Mauri AN, Anon MC. 2006. Effect of solution pH on solubility and some structural properties of soybean protein isolate films. Journal of the science of food and agriculture 86: 1064-1072.

Ogale AA, Cunningham P, Dawson PL, Acton JC. 2000. Viscoelastic, thermal, microstructural characterization of soy protein isolate films. Journal of food science 65(4): 672-679.

Park SK, Rhee CO, Bae DH, Hettiarachchy NS. 2001. Mechanical properties and water vapor permeability of soy protein films affected by calcium salts and glucono-δ-lactone. Journal of agricultural and food chemistry 49: 2308-2312.

Paul MA, Alexandre M, Degee P, Henrist C, Rulmont A, Dubois P. 2003. New nanocomposite materials based on plasticized poly(L-lactide) and organo-modified montmorillonites: thermal and morphological study. Polymer: 443-450.

Petruccelli S, Anon MC. 1995. Soy protein isolate components and their interactions. Journal of agricultural and food chemistry 43: 1762-1767.

Ray SS, Bousmina M. 2005. Biodegradable polymers and their layered silicate nanocomposites: in greening the 21st century materials world. Progress in materials science 50: 962-1079.

Rhim JW, Wu Y, Weller CL, Schnepf M. 1999. Physical characteristics of a composite films of soy protein isolate and propyleneglycol alginate. Journal of food science 64(1): 149-152.

Rhim JW, Lee JH, Kwak HS. 2005. Mechanical and barrier properties of soy protein and clay mineral composite films. Food science and biotechnology 14: 112-116.

Rhim JW, Ng PKW. 2007. Natural biopolymer-based nanocomposite films for packaging applications. Critical reviews in food science and nutrition 47(4): 411-433.

Selke SEM. 1997. Understanding Plastics Packaging Technology. New York: Hanser Publication. 206 p.

Tunc S, Angellier H, Cahyana Y, Chalier P, Gontard N, Gastaldi E. 2007. Functional properties of wheat gluten/montmorillonite nanocomposite films processed by casting. Journal of membrane science 289: 159-168.

Wang S, Sue HJ, Jane J. 1996. Effects of polyhydric alcohols on the mechanical properties of soy protein plastics. Journal of macromolecular science, Part A 33(5): 557-569.

Yu ZZ, Yan C, Yang M, Mai, YW. 2004. Mechanical and dynamic mechanical properties of nylon 66/montmorillonite nanocomposites fabricated by melt compounding. Polymer international 53: 1093-1098.

Zeng QH, Yu AB, Lu GQ, Paul DR 2005. Clay-based polymer nanocomposites: research and commercial development. Journal of nanoscience and nanotechnology 5: 1574-1592.

Zhang J, Mungara P, Jane J. 2001. Mechanical and thermal properties of extruded soy protein sheets. Polymers 42: 2569-2578.

Zhao R, Torley P, Halley PJ. 2008. Emerging biodegradable materials: starch- and protein-based bio-nanocomposites. Journal of materials science 43: 3058-3071.

Table 1 – Properties of modified MMTs used in this study.[A]

Commercial designation	Organic modifier	Molecular weight of organic modifier (g/mol)[B]	Modifier concentration (meq/100 g of clay)	Organic content (%)[B]	Density (g/cm^3)	d-spacing (nm)
Cloisite 20A	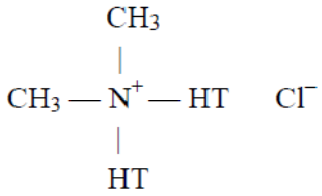	551.6	95	36.4	1.77	2.42
Cloisite 30B	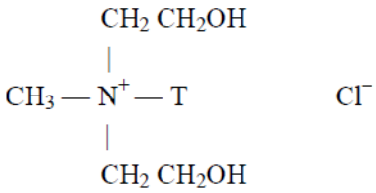	404.8	90	52.4	1.98	1.85

[A] As provided by the supplier

[B] Kim and White (2005)

HT is hydrogenated tallow and T is tallow

Table 2 – Effect of type and content of modified MMTs on Hunter color values (L, a, and b) of SPI-MMT films.[A]

Films	L	a	b
SPI	81.42 ± 0.99[a]	3.61 ± 0.83[a]	44.14 ± 2.22[a]
SPI-5% Cloisite 20A	90.83 ± 0.04[b]	-0.09 ± 0.02[b]	16.42 ± 0.14[b]
SPI-10% Cloisite 20A	88.90 ± 0.49[b]	0.11 ± 0.02[b]	18.07 ± 0.09[b]
SPI-15% Cloisite 20A	88.29 ± 0.76[b]	0.42 ± 0.05[b]	17.29 ± 0.44[b]
SPI-5% Cloisite 30B	86.44 ± 0.40[c]	1.16 ± 0.05[b]	23.77 ± 0.50[c]
SPI-10% Cloisite 30B	87.23 ± 0.28[c]	0.56 ± 0.06[b]	21.99 ± 0.42[c]
SPI-15% Cloisite 30B	88.43 ± 0.34[c]	0.57 ± 0.11[b]	19.89 ± 0.15[c]

[A] Values are mean of two replicates ± standard deviation. Means in the same column followed by the same letter are not significantly different ($P > 0.05$).

Table 3 – Effect of type and content of modified MMTs on tensile strength (TS) of SPI-MMT films.[A]

	TS (MPa)	
MMT content	**Cloisite 20A**	**Cloisite 30B**
0% MMT	2.26 ± 0.48^{a}	2.26 ± 0.48^{a}
5% MMT	12.40 ± 0.65^{b}	15.11 ± 0.86^{d}
10% MMT	14.15 ± 0.33^{c}	16.19 ± 0.75^{e}
15% MMT	13.66 ± 0.28^{c}	18.64 ± 0.23^{e}

[A] Values are mean of two replicates ± standard deviation. Means in the same row and column followed by the same letter are not significantly different ($P > 0.05$).

Table 4 – Effect of type and content of modified MMTs on percent elongation of break (%E) of SPI-MMT films.[A]

	%E	
MMT content	**Cloisite 20A**	**Cloisite 30B**
0% MMT	11.85 ± 0.39[a]	11.85 ± 0.39[a]
5% MMT	42.80 ± 0.57[b]	81.60 ± 2.83[e]
10% MMT	71.00 ± 3.68[c]	103.60 ± 4.53[f]
15% MMT	22.80 ± 1.70[d]	54.80 ± 2.26[g]

[A] Values are mean of two replicates ± standard deviation. Means in the same row and column followed by the same letter are not significantly different ($P > 0.05$).

Table 5 – Effect of type and content of modified MMTs on water vapor permeability (WVP) of SPI-MMT films.[A]

	WVP (g-mm/(m^2-hr-kPa))	
MMT content	**Cloisite 20A**	**Cloisite 30B**
0% MMT	3.80 ± 0.11^{a}	3.80 ± 0.11^{a}
5% MMT	2.63 ± 0.03^{b}	3.09 ± 0.05^{e}
10% MMT	2.16 ± 0.10^{c}	2.67 ± 0.08^{f}
15% MMT	2.05 ± 0.11^{d}	2.33 ± 0.09^{g}

[A] Values are mean of two replicates ± standard deviation. Means in the same row and column followed by the same letter are not significantly different ($P > 0.05$).

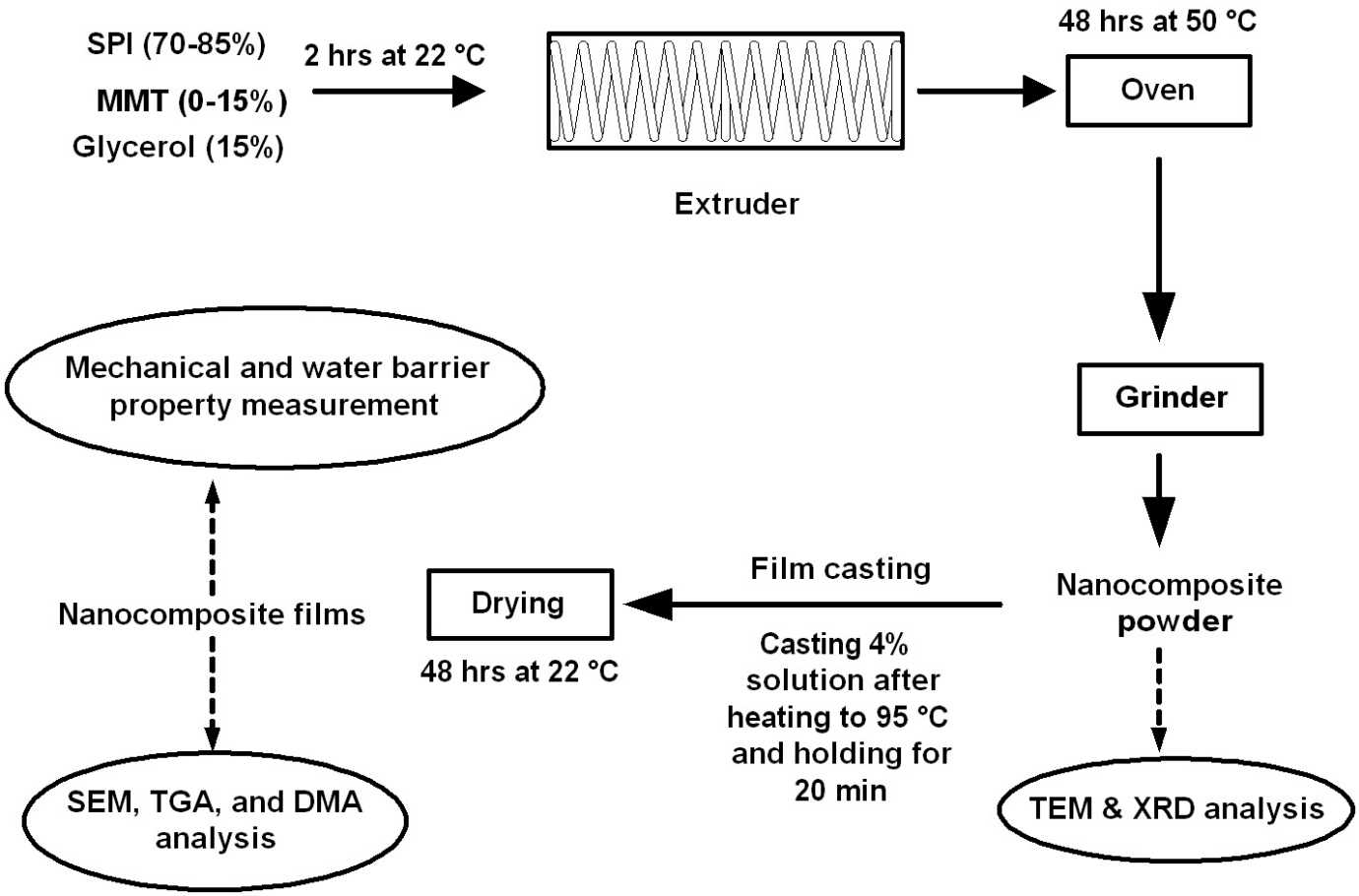

Figure 1 – Process flow diagram for the preparation and characterization of SPI-MMT bio-nanocomposite films.

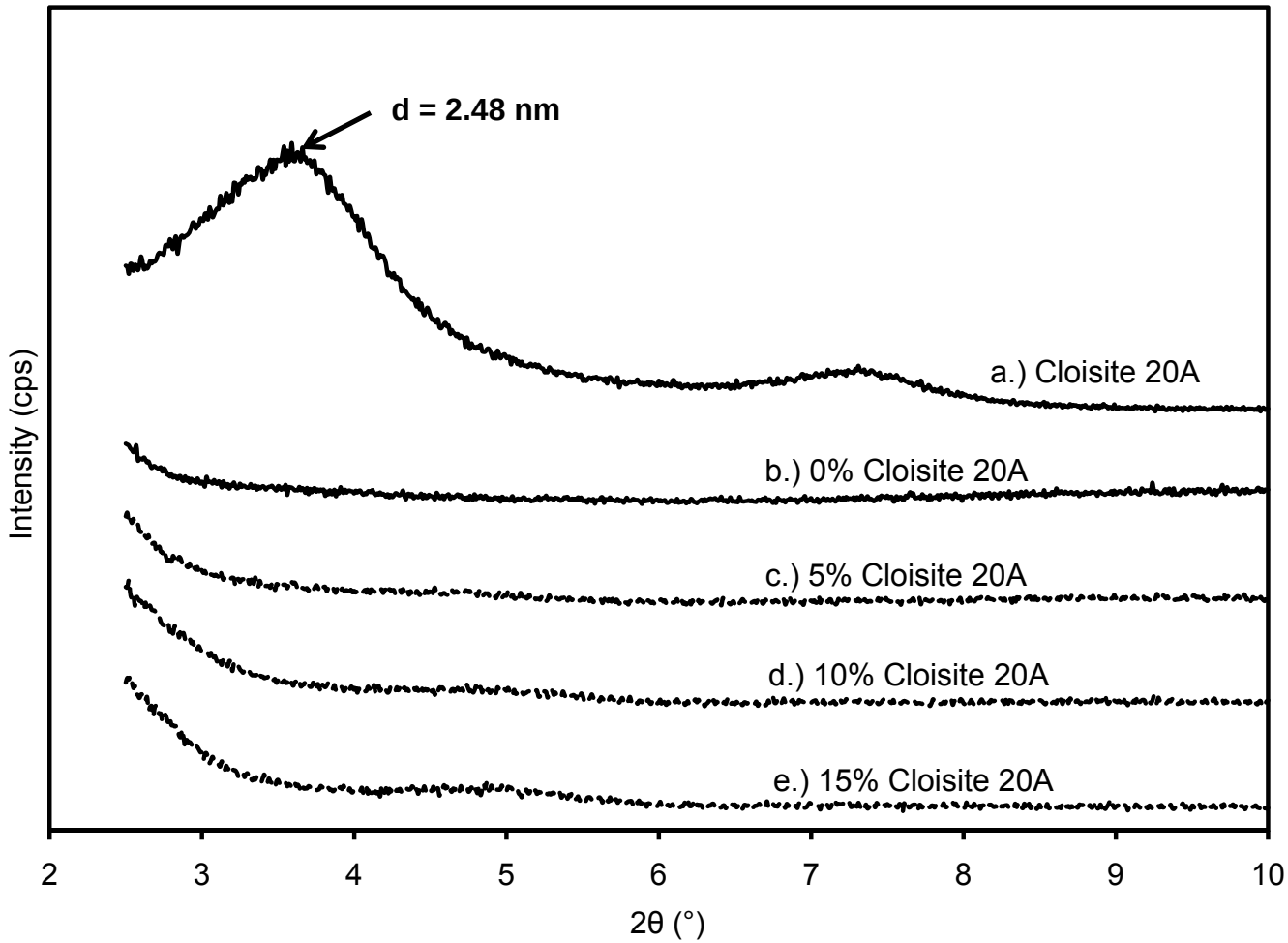

Figure 2 – XRD patterns of Cloisite 20A and SPI-Cloisite 20A bio-nanocomposites with different Cloisite 20A contents.

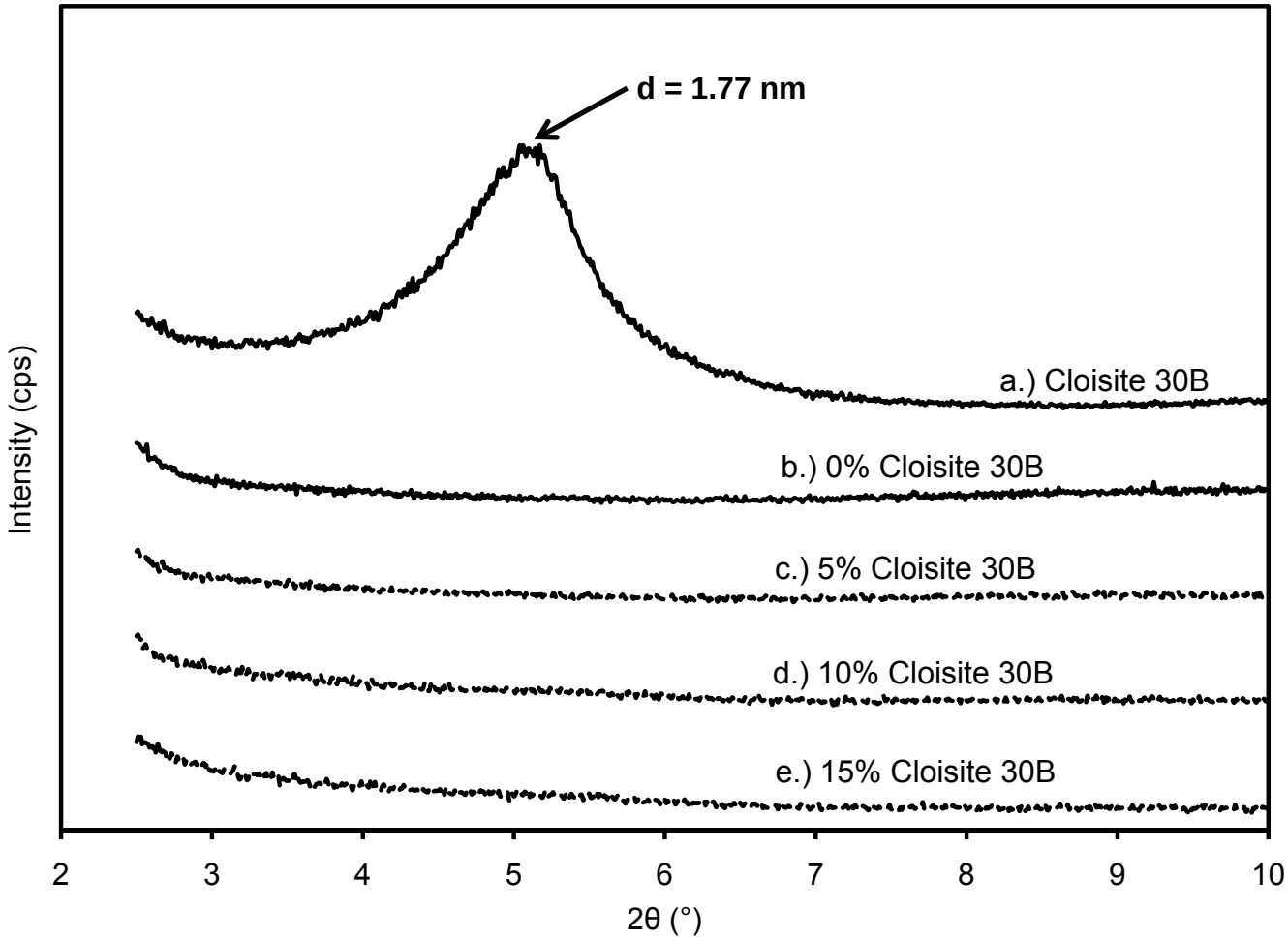

Figure 3 – XRD patterns of Cloisite 30B and SPI-Cloisite 30B bio-nanocomposites with different Cloisite 30B contents.

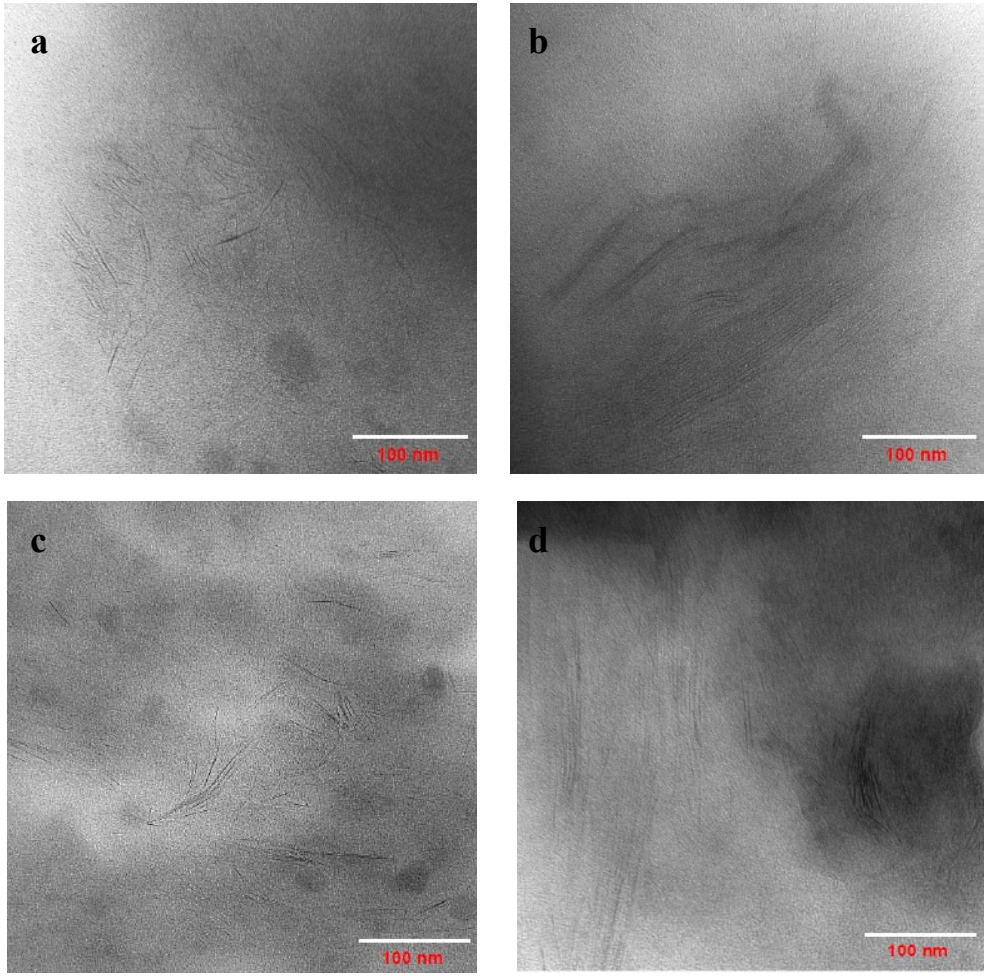

Figure 4 – TEM images of bio-nanocomposites with (a) 5% Cloisite 20A, (b) 15% Cloisite 20A, (c) 5% Cloisite 30B, and (d) 15% Cloisite 30B.

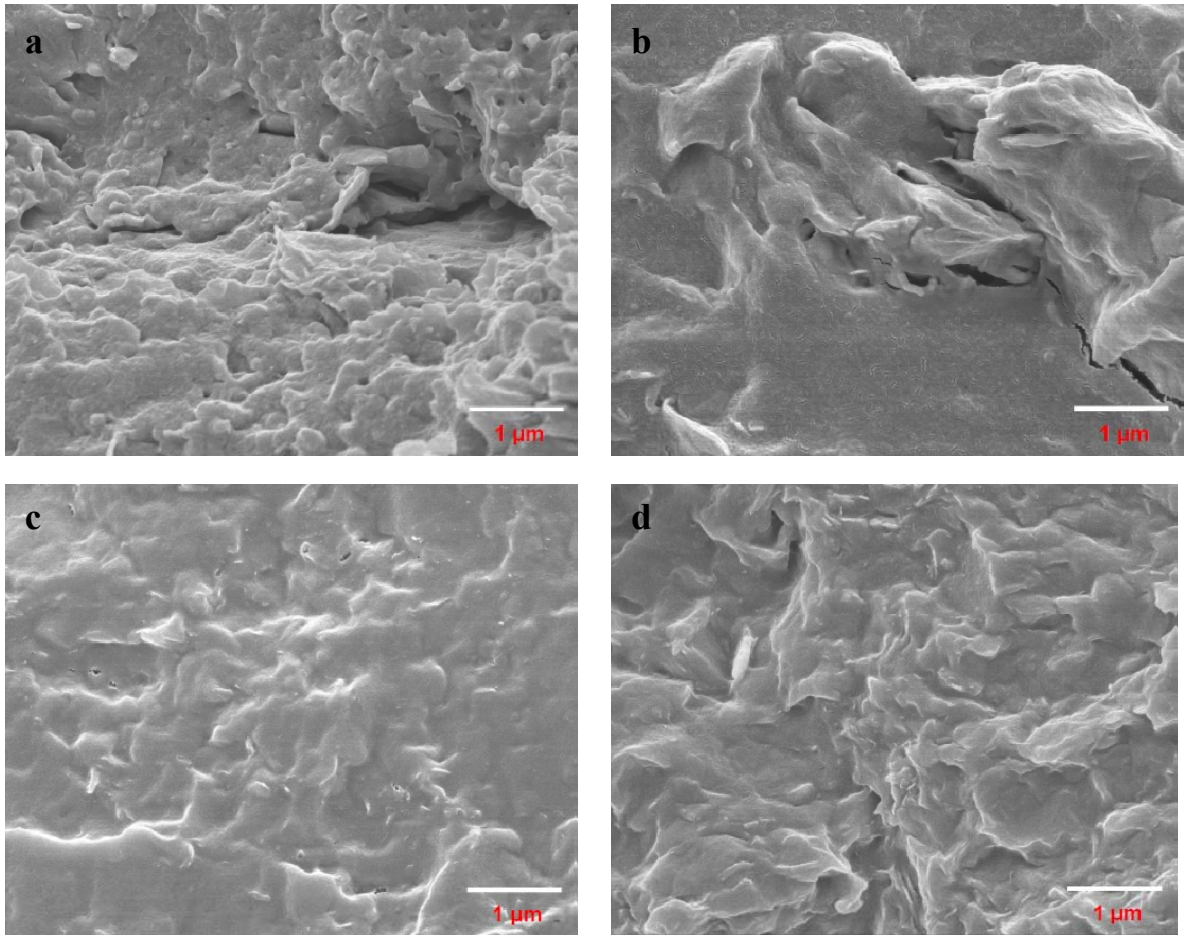

Figure 5 – SEM images of bio-nanocomposite films with (a) 5% Cloisite 20A, (b) 15% Cloisite 20A, (c) 5% Cloisite 30B, and (d) 15% Cloisite 30B.

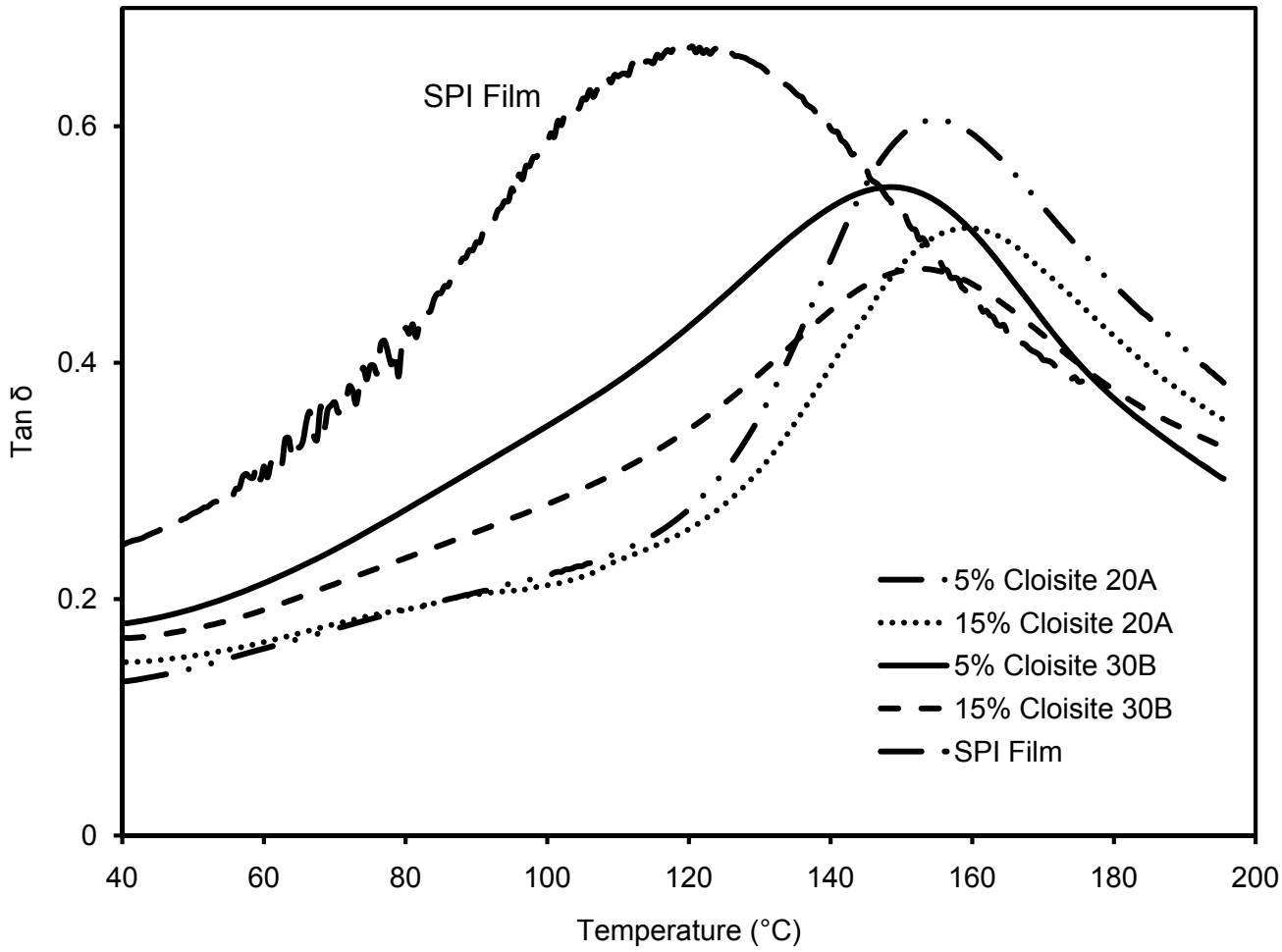

Figure 6 – Effect of temperature on tan δ of bio-nanocomposite films based on SPI and modified MMTs at different MMT contents.

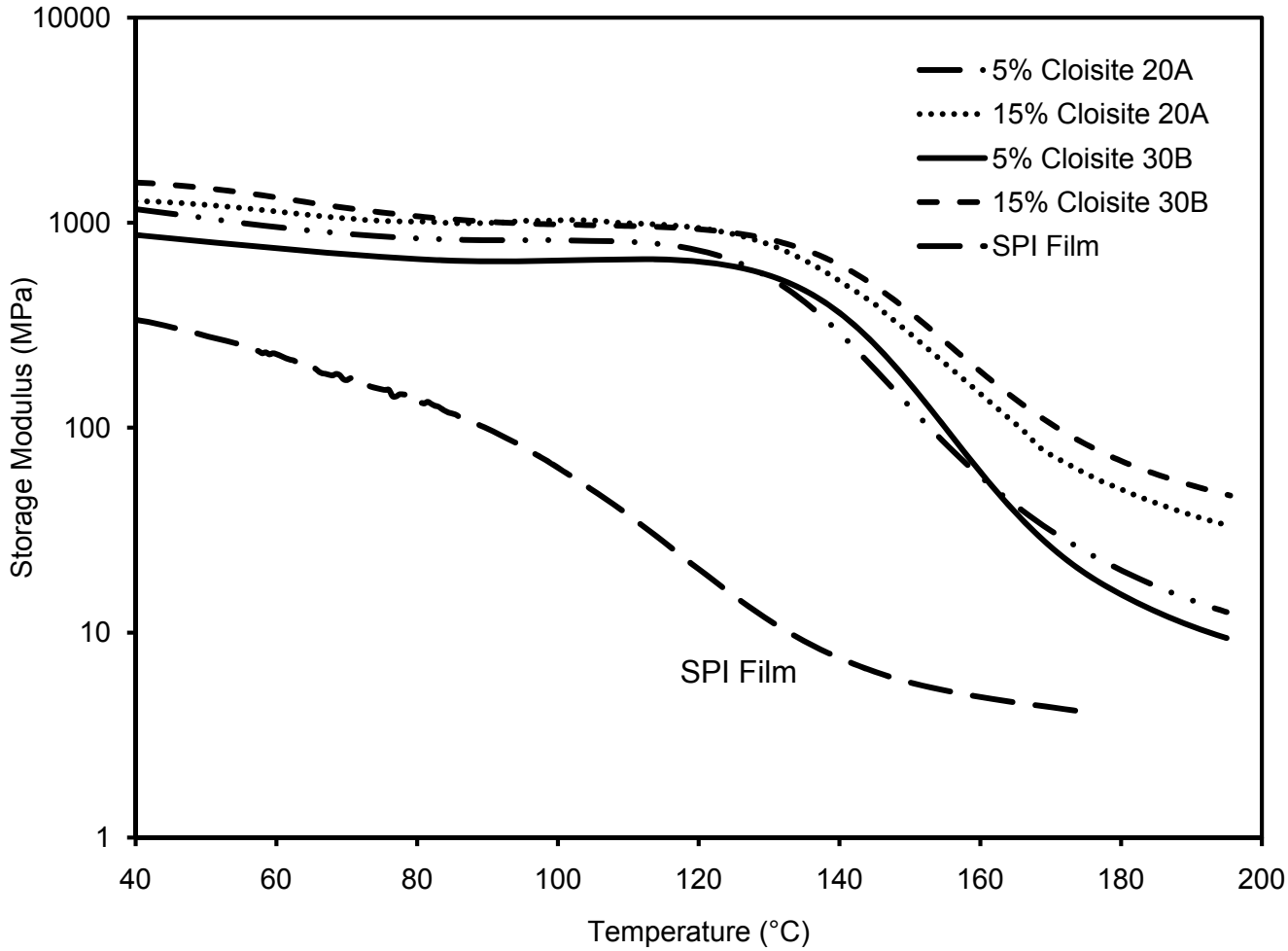

Figure 7 – Effect of temperature on storage modulus of bio-nanocomposite films based on SPI and modified MMTs at different MMT contents.

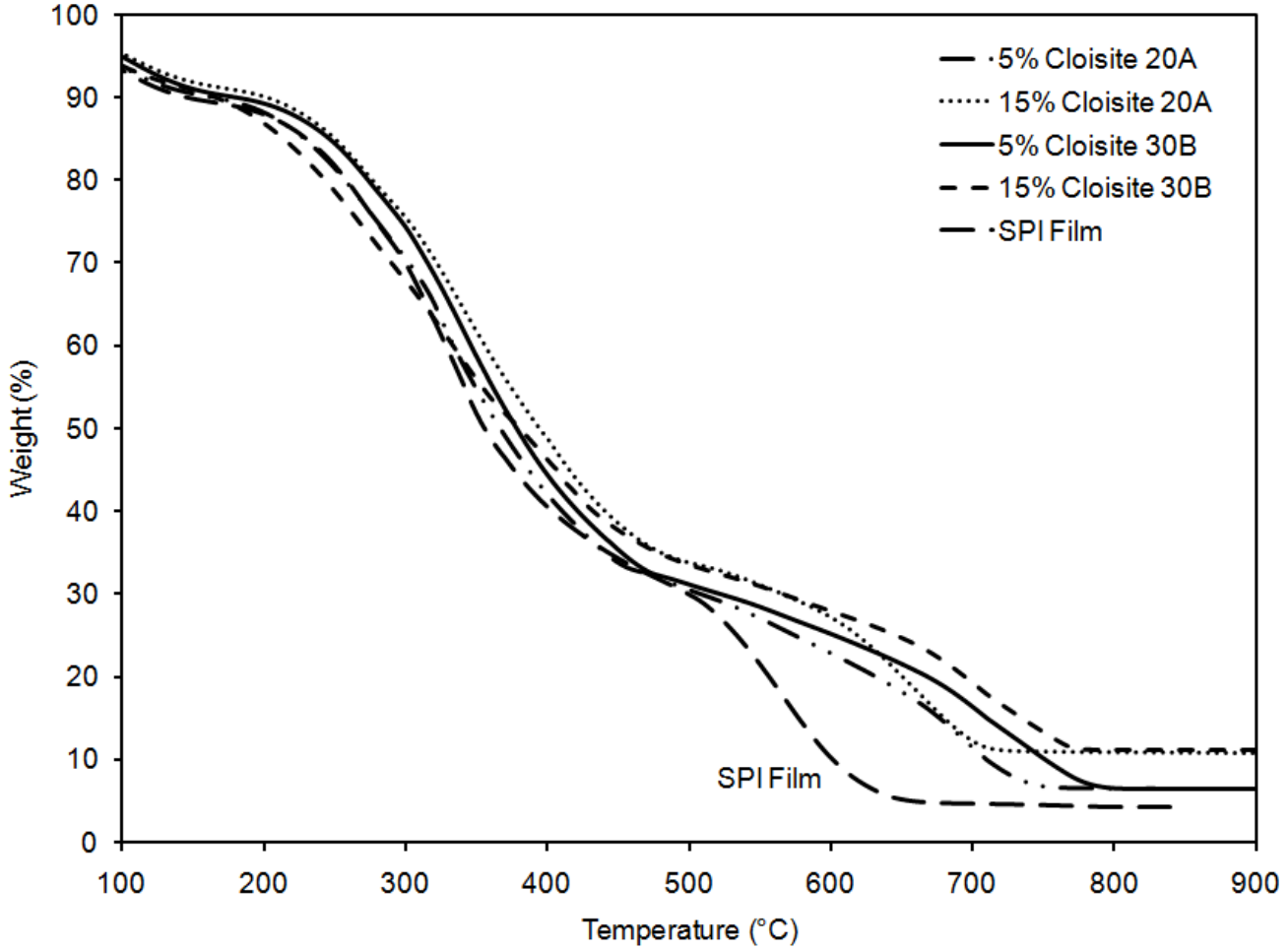

Figure 8 – TGA curves of bio-nanocomposite films based on SPI and modified MMTs at different MMT contents under air flow.

Chapter 8

CONCLUSIONS

The non-degradable and non-renewable nature of plastic packaging has led to a renewed interest in packaging materials based on biopolymers derived from renewable sources. However, materials based on biopolymers cannot meet the requirements of a cost-effective film with mechanical and barrier properties similar to those of plastics. This study has focused on bio-nanocomposites (biopolymer matrix reinforced with nanoparticles) to improve the properties of biopolymer films based on soy protein isolate (SPI).

Bio-nanocomposite films based on SPI and montmorillonite (MMT) with improved properties were prepared using melt extrusion. The arrangement of MMT in the bio-nanocomposite matrix ranged from exfoliated to intercalated depending on the type (natural and modified) and content of MMT. The results showed that extrusion of SPI and MMTs resulted in bio-nanocomposites with exfoliated structures at lower MMT content (5%) for natural (Cloisite Na^+) as well as modified MMTs (Cloisite 20A and Cloisite 30B). At higher MMT content (15%), the structure of bio-nanocomposites ranged from intercalated for Cloisite Na^+ and Cloisite 20A to disordered intercalated for Cloisite 30B.

Properties of the SPI-MMT films were significantly affected by the pH of film forming solutions, extrusion processing parameters (screw speed and barrel temperature distribution), content of MMT, and type of MMT. The results showed that pH value of 9 was the optimum pH to obtain SPI-MMT films with improved mechanical {tensile strength (TS) and percent elongation at break (%E)} and dynamic mechanical {glass transition temperature (T_g) and storage modulus (E')} properties. Higher screw speed and barrel temperature

resulted in films with improved mechanical (increase in TS from 4.63 to 9.25 and increase in %E from 11.24 to 64.60) and dynamic mechanical (increase in T_g from 134.3 °C to 158.6 °C and increase in E' from 349.6 MPa to 1265 MPa) properties. Higher screw speed also resulted in films with lower water vapor permeability (WVP). However, the effect of barrel temperature distribution on WVP was insignificant.

There was a significant improvement in mechanical and dynamic mechanical properties, thermal stability, and WVP of the films with the addition of natural and modified MMTs. For bio-nanocomposites based on Cloisite Na^+, there was a significant improvement in mechanical (increase in TS from 2.26 MPa to 15.60 MPa) and dynamic mechanical (increase in T_g from 119.7 °C to 199.5 °C and increase in E' from 337 MPa to 2064 MPa) properties as the MMT content increased from 0 to 15%. WVP reduced by as much as 42.9% as the MMT content increased from 0% to 15%. At a MMT content of 5%, bio-nanocomposite films based on modified MMTs had better mechanical, dynamic mechanical, and water barrier properties as compared to those based on natural MMT. However, films based on modified MMTs were thermally less stable at temperatures higher than 500 °C as compared to films based on natural MMT.

Bio-nanocomposite films based on 10% Cloisite 30B had mechanical properties comparable to those of LDPE and PVDC which are currently used in food packaging applications. Thus, this study shows the potential of films based on SPI and Cloisite 30B to replace some of the existing plastics such as LDPE and PVDC. However, much higher WVP values of these films as compared to those of LDPE and PVDC might limit the application of these bio-nanocomposite films to packaging of high moisture foods such as fresh fruits and

vegetables. Some of the other challenges associated with commercial application of these bio-nanocomposite films include higher cost of ingredients and complexity associated with the approval of these bio-nanocomposite films as food contact materials.

Chapter 9

RECOMMENDATIONS FOR FUTURE WORK

The results presented in this study showed the feasibility of using bio-nanocomposites to improve the properties of biopolymer based on soy protein isolate (SPI). These bio-nanocomposite films could potentially be used in food packaging to replace some of the existing plastics. Some recommendations to further improve the properties of these SPI-MMT bio-nanocomposite films for commercial application are presented below.

Properties of SPI-MMT films could further be improved by incorporating other biodegradable synthetic polymers with improved properties. One such biodegradable polymer is polyvinyl alcohol (PVOH) which has higher TS (44-64 MPa) and %E (150-400%) (Bohlmann 2005). Thus, addition of PVOH to SPI-MMT bio-nanocomposites could result in films with higher TS and %E. There is also a need to explore other biopolymers which can be used as a base material for bio-nanocomposites. A number of cellulose derivatives such as methyl cellulose and cellulose acetate possess excellent mechanical properties. However, higher cost of these cellulose derivatives prevents their use on commercial scale. One of the alternatives to reduce the cost of raw materials could be to use starch, which is cheap and easily available, as a filler material.

This study was limited to bio-nanocomposites based on nanoparticles belonging to the class of layered clay minerals (MMT). However, preliminary studies conducted with TiO_2 nanoparticles (anatase, particle size < 25 nm) have shown great potential for improvement in properties and color of these bio-nanocomposite films at a concentration as low as 0.5%. Bio-nanocomposites based on TiO_2 could also exhibit antimicrobial properties

because of the photocatalytic properties of TiO_2 (Fu and others 2005). Therefore, further studies should be conducted to prepare and characterize bio-nanocomposites based on SPI and TiO_2 nanoparticles.

This study was conducted to study the effect of two extrusion processing parameters (screw speed and barrel temperature distribution) on the structure and properties of bio-nanocomposites. However, formation of bio-nanocomposites depends not only on screw speed and barrel temperature distribution, but also on the sequence of thermal and mechanical energy received by the material along the screw of the extruder. Screw configuration of an extruder determines the sequence of energy received by the material because it changes the intensity of shear mixing. The twin-screw extruder used in this study had a 5 head barrel configuration with 5 screw elements. By adding barrel heads and different types (forward screw, kneading screw, and reverse screw elements) of screw elements, the effect of screw configuration on the structure and properties of bio-nanocomposites can be studied.

In this study, wide-angle X-ray diffraction (WA-XRD) was one of the techniques used for structural characterization of bio-nanocomposites. This technique is not useful to study intercalation once the d-spacing exceeds 6-7 nm. Small-angle X-ray diffraction (SA-XRD) in combination with WA-XRD and microscopic techniques (TEM and SEM) can be useful for characterization of intercalated structures in bio-nanocomposites. There is also a need to gain a basic understanding of molecular interaction between SPI and nanoparticles. Fourier transform infra-red (FTIR) spectroscopy can be used to determine the formation of

hydrogen bond between amide groups of SPI and polar groups of MMT. FTIR spectroscopy can also be used to determine the extent of exfoliation in the bio-nanocomposites.

The above mentioned recommendations will help in further improving the properties of bio-nanocomposite films for commercial application. Better analytical techniques such as SA-XRD and FTIR spectroscopy will give a basic understanding of the interactions between nanoparticles and biopolymer matrix.

References

Bohlmann GM. 2005. General characteristics, processability, industrial applications and market evolution of biodegradable polymers. In: Bastioli C, editor. Handbook of Biodegradable Polymers. Shropshire, UK: Rapra Technology Ltd. p 183-218.

Fu G, Vary PS, Lin CT. 2005. Anatase TiO_2 nanocomposites for antimicrobial coatings. Journal of physical chemistry B 109: 8889-8898.